ALMA MATER STUDIORUM - UNIVERSITÀ DI BOLOGNA

DIPARTIMENTO DI INGEGNERIA INDUSTRIALE

CORSO DI LAUREA MAGISTRALE IN INGEGNERIA ENERGETICA

TESI DI LAUREA

in
Energetica e Impianti Termotecnici M

Design and characterization of latent thermal energy storage systems (LTESS) using pure and metal-foam-loaded PCMs

CANDIDATO:
Alessandro Bianchini

RELATORE:
Chiar.mo Prof. Ing. Gian Luca Morini

CORRELATORI:
Dott. Matteo Dongellini
Ing. Morena Falcone
Dott. Danish Rehman
Ing. Michele Silvestrini
Ing. Federica Salvi

Anno Accademico 2019/20

Sessione II

ABSTRACT

Latent thermal energy storage systems (LTESSs) are innovative technologies to store thermal energy very useful when the heat production is decoupled by the heat request (i.e. when renewable energy is used in a thermal system).

Heat storage systems which use phase change materials (PCMs) represent an efficient solution to store thermal energy thanks to the PCMs high energy storage density.

Actually, these materials are widely used as components of building elements (walls, windows), in solar energy systems, heat exchangers and heat pumps storage systems.

This thesis follows the research purpose of the CLIWAX project which is devoted to demonstrate the effectiveness of PCM-based energy storage solutions dedicated to HVAC systems.

In this Thesis a series of experimental results are presented on the thermal behavior of PCMs.

The main goals of this Thesis can be summarized as follows:

- To achieve a deeper knowledge about PCMs thermal behaviour during both cooling and heating
- To verify the PCM thermodynamic properties as declared by the manufacturers
- to test the characteristics of PCM loaded in metal foams having high porosity values (>94%)
- to obtain repeatable and accurate experimental data on the thermal charging (heating) and discharging (cooling) of PCM-based energy storage systems,
- to compare the experimental results with those obtained with numerical simulations.

The first part of the Thesis provides an overview about all the existing kinds of PCMs. The attention is particularly focused on their physical properties and their use in thermal storage applications.

Considering small volumes, PCMs show a high latent heat storage capability. But, on the other hand, they present some undesirable properties: low thermal conductivity, incompatibility with plastic containers and a certain degree of flammability.

These effects can be partly eliminated modifying the PCM composition and/or by loading PCM in metallic foams of copper or aluminum: this aspect is deeply investigated in this Thesis.

The second part of the Thesis mainly focuses on the experimental characterization of a specific paraffin (RT35) as PCM, presenting a series of experimental results carried on at the Applied Thermal Engineering laboratory of the University of Bologna.

The first tests were simply of qualitative nature: time-lapse videos have been recorded in order to observe, under the same heat supplied and the same volumes of materials, the differences between the melting phase of pure PCM and metal-foam-loaded ones.

After this first approach, a series of experiments were made with the aim to characterize a LTESS based on RT35.

A polystyrene "Jar to Investigate the thermal behavior of Melting Materials with high Insulation" (named JIMMI in the Thesis) was built to study the melting process of a fixed volume of RT35 heated from the top thanks to an electrical heater.

With the first version of this thermal case (here named JIMMI 1), the PCM temperature homogeneity along the axial direction inside the polycarbonate case was demonstrated: the thermocouples immersed in the pure RT35 recorded the same temperature trends for a fixed height showing a homogeneous temperature distribution along horizontal planes.

Great improvements were done with the second version of the test rig (JIMMI 2), in which the external thermal insulation of the polystyrene case was enhanced thanks to a series of layers of EUROBATEX® added around the box to fill the air cavities between the polycarbonate case and the polystyrene box. EUROBATEX® was also useful to cover the external thermal bridges of the complete box (case+insulation).

Finally, with the last version of the experiment (JIMMI 3) the repeatability of the experiments has been accurately checked. Three experiments with pure RT35 PCM and two experiments with copper foam-loaded RT35 were conducted with the same starting temperature and using the same heat flux made with the heater.

Finally, the experimental results are used in order to check the values of the thermodynamic properties declared by the manufacturer of RT35.

1 PHASE CHANGE MATERIALS

1.1 INTRODUCTION ON PCMS

Phase change materials (PCMs) are latent heat accumulator materials, which exploit the phase transition phenomenon to absorb energy, storing a high amount of energy and keeping their temperature constant. The energy that is absorbed by the material acts to increase the energy of the constituent atoms or molecules, increasing their vibrational state. At the melt temperature the atomic bonds weaken, and the materials change from solid to liquid. Solidification is the reverse of this process, during which the material gives energy to its surroundings and the molecules lose energy and order themselves into their solid phase. The melting/solidification process can be seen in Fig. 1.
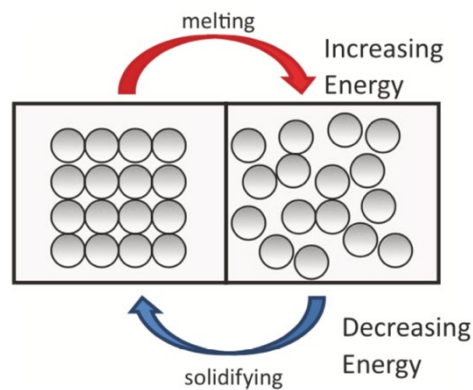
FIG. 1: MELTING/SOLIDIFICATION PROCESS [1]

The energy that is either absorbed or released during the melting-solidification cycle is known as the latent heat of fusion. Each material is characterized by a fixed value of the latent heat and this thermal energy is exchanged between the material and the environment with an isothermal process during the phase change. For example, it can be seen for the melting of an ice cube. An ice cube can be heated by exposing it to room ambient conditions or by heating it with a hair dryer, but regardless of given thermal energy, the ice cube will not increase its temperature until the melting process is complete. The latent heat absorbed during this process is called latent heat of fusion, while the transition from liquid phase to gas phase is characterized by latent heat of vaporization.

Sensible heat, on the other hand, is a heat exchange form that causes a temperature variation in the material. For example, if we consider a standard continuous heating process, when we heat a subcooled solid to its melting point, we use sensible heat. After passing from the solid phase to the liquid phase with the absorption of the latent heat of fusion, the material increases its temperature up to the boiling point. Once the boiling point is reached, the liquid elements pass to the vapor phase by absorbing the latent heat of vaporization until the phase change process is complete. This process can be seen in Fig. 2.
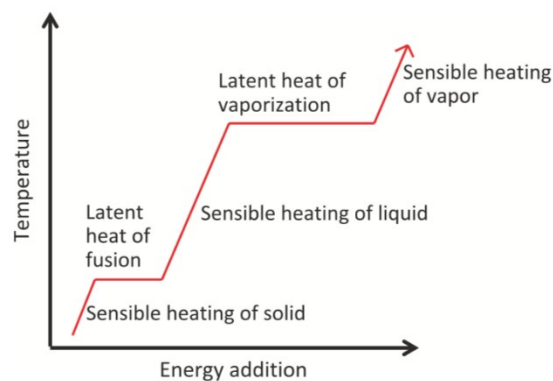
FIG. 2:STANDARD HEATING CURVE [1]

It can be seen in Fig. 2 that the latent heat of vaporization is linked a higher quantity of energy than the latent heat of fusion, but in pratical applications the focus is related to solid to liquid phase change process because the density change from a liquid to a vapor phase is large, and working with boilers and condensers often requires a significant amount of support equipment which is not always convenient. The amount of energy absorption or release during the melting-solidification cycle is governed by the value of that material's latent heat of fusion (expressed in J/g or kJ/Kg).

1.2 CLASSIFICATION OF PCMS

There are many phase change materials that are available covering a huge temperature range, but the majority fall into two main classifications: organics and inorganics

The first factor that is needed to be considered during the selection of the proper PCM is the melting point. A primary consideration is that the melting point of the PCM must be below the temperature of the heat source and at the same time above the ambient conditions to which the device will be exposed. When choosing the operating point, it is needed to know the boundary temperature to which our device will be subjected.

For systems that are designed preferentially for thermal management (maintenance of a specific operating point), the general guide is to pick a PCM with the highest possible melt point that is still below the desired thermal control point. For instance, if the desired operating point of a portable electronic system is 80° C, then it will be advantageous to select a PCM with a melt temperature range around 70–75° C. The advantage to using a high melting point material in these situations is that it leads to a longer melting time, and thus a longer effective thermal management duty cycle before the PCM is completely melted. Systems with a higher melting point will dissipate more heat to the ambient while simultaneously melting, due to the higher differential from the system to the ambient, thus extending the melt time.

The second most important criterion is generally the value of the latent heat of fusion of the material. The latent heat is the energy that can be stored in a specified mass of material (kJ/kg) during the melting transient and released during solidification. The higher the latent heat of fusion, the more energy efficient the system is, and less mass can be used, minimizing the size of the system to exchange the same amount of energy. The goal is to select a material with the highest latent heat of fusion as possible and with a melting point temperature in a range previously determined.

Materials that have a high latent heat of fusion generally have also a high specific heat. Specific heat refers to the amount of energy it takes to increase one kg of mass of the material of one Kelvin and its unit is J/kg K.

For energy storage applications, material characterized by high specific heat and a high latent heat of fusion are advantageous. This is because a considerable quantity of energy can be stored during both the sensible heating stage (when the PCM is close to the melting point) and during the latent heating phase (in correspondence of the melting transition).

There are also other important factors to consider when selecting a PCM material. The material must be stable, both chemically and physically, over repeated thermal cycling with repeatable and consistent melting/freezing cycles. It's necessary to be aware about the possibility that certain PCMs may break down over extended cycling. It should be considered the compatibility of the considered material with the casing and other materials, as some PCMs tend to be corrosive and / or chemically incompatible. It is also preferred to have a non-flammable, non-toxic and environmentally safe PCM.

Many PCMs have a different density between solid phase and liquid phase, which in most cases leads to volume contractions during the solidification also up to 15%. This density difference must be considered in the design of any containment structure.

Finally, the PCM should have a high thermal conductivity to prevent thermal bottlenecking, but actually it's difficult to find a PCM that have both high latent and specific heats as well as high thermal conductivity. Normally, we prefer to have the ability to store more energy (high latent heat) rather than high thermal conductivity. As no single material can have all the required properties for an ideal thermal-storage media, one has to use the materials available on the market and try to make up for the poor physical properties by an adequate system design. For example, metallic fins or metallic foams can be inserted within the PCM and used to increase their thermal conductivity of PCMs.

In general, inorganic compounds have almost double values of density (250–400 kg/dm3) than the organic compounds (128–200kg/dm3). Due to their different chemical and thermal behavior it will be discussed about the properties of each subgroup, which affect the design of storage systems based on PCMs.

1.2.1 ORGANIC PCMs

Organic phase change materials are likely the most popular and the most studied. They are divided in two classes: paraffin and non-paraffins. The organic PCMs tend to be abundantly available, relatively inexpensive and easy to work with. As seen in fig.3 paraffin and non-paraffin have similar physical characteristics, exhibiting a white surface which is soft and waxy in appearance.

FIG. 3: PARAFFIN WAX(LEFT) AND FATTY ACID (RIGHT) [1]

Paraffins

Paraffin wax consists of a mixture of mostly straight chain n-alkanes $CH_3–(CH_2)–CH_3$. Paraffins are mainly used for storage systems due to their high latent melting heat and their wide temperature range. Paraffin is safe, reliable, predictable, relatively cheap and non-corrosive. They are chemically inert and stable below 500° C, show little volume changes on melting and have low vapor pressure in the melt form. For these properties, system-using paraffins usually have very long freeze–melt cycle. Tab 1 shows thermal properties of some technical grade paraffins. The melting point of alkane increases when the increasing number of carbon atoms increases.

TAB 1: PHYSICAL PROPERTIES OF SOME PARAFFINS [2]

Paraffin[a]	Freezing point/ range (°C)	Heat of fusion (kJ/kg)	Group[b]
6106	42–44	189	I
P116[c]	45–48	210	I
5838	48–50	189	I
6035	58–60	189	I
6403	62–64	189	I
6499	66–68	189	I

[a] Manufacturer of technical Grade Paraffin's 6106, 5838, 6035, 6403 and 6499: Ter Hell Paraffin Hamburg, FRG.
[b] Group I, most promising; group II, promising; group III, less promising; — insufficient data.
[c] Manufacturer of Paraffin's P116: Sun Company, USA.

Paraffins show some undesirable properties such as: low thermal conductivity, it is not compatible with plastic container and moderately flammable. All these undesirable effects can be partly eliminated by slightly modifying the wax and the storage unit.

It can be seen in Tab 2 that the melting point of alkane increases with the increasing number of carbon atoms; in this table some selected paraffins are shown with their melting point, latent heat of fusion and groups (group I, most promising; group II, promising; group III less promising).

TAB 2 : MELTING POINT AND LATENT HEAT OF FUSION: PARAFFINS [2]

No. of carbon atoms	Melting point (°C)	Latent heat of fusion (kJ/kg)	Group[a]
14	5.5	228	I
15	10	205	II
16	16.7	237.1	I
17	21.7	213	II
18	28.0	244	I
19	32.0	222	II
20	36.7	246	I
21	40.2	200	II
22	44.0	249	II
23	47.5	232	II
24	50.6	255	II
25	49.4	238	II
26	56.3	256	II
27	58.8	236	II
28	61.6	253	II
29	63.4	240	II
30	65.4	251	II
31	68.0	242	II
32	69.5	170	II
33	73.9	268	II
34	75.9	269	II

[a] Group I, most promising; group II, promising; group III, less promising; — insufficient data.

Non-paraffins

The non-paraffins organic PCMs are the most numerous of the phase change materials with highly variation of physical properties. Each of these materials has its own properties unlike the paraffin's, which have very similar properties. These materials are divided into other subgroups, like fatty acids and other non-paraffin organic materials. They are flammable and they shouldn't be exposed to excessively high temperature because flames ore oxidizing agents. Some non-paraffin's PCMs are tabulated in Tab 3.

TAB 3 :MELTING POINT AND LATENT HEAT OF FUSION: NON PARAFFINS [2]

Material	Melting point (°C)	Latent heat (kJ/kg)	Group[a]
Formic acid	7.8	247	III
Caprilic acid	16.3	149	–
Glycerin	17.9	198.7	III
D-Lattic acid	26	184	I
Methyl palmitate	29	205	II
Camphenilone	39	205	II
Docasyl bromide	40	201	II
Caprylone	40	259	II
Phenol	41	120	III
Heptadecanone	41	201	II
1-Cyclohexylooctadecane	41	218	II
4-Heptadacanone	41	197	II
p-Joluidine	43.3	167	–
Cyanamide	44	209	II
Methyl eicosanate	45	230	II
3-Heptadecanone	48	218	II
2-Heptadecanone	48	218	II
Hydrocinnamic acid	48.0	118	–
Cetyl alcohol	49.3	141	–
α-Nepthylamine	50.0	93	–
Camphene	50	238	III
O-Nitroaniline	50.0	93	–
9-Heptadecanone	51	213	II
Thymol	51.5	115	–
Methyl behenate	52	234	II
Diphenyl amine	52.9	107	–
p-Dichlorobenzene	53.1	121	–
Oxolate	54.3	178	–
Hypophosphoric acid	55	213	II
O-Xylene dichloride	55.0	121	–
β-Chloroacetic acid	56.0	147	III
Chloroacetic acid	56	130	III
Nitro naphthalene	56.7	103	–
Trimyristin	33–57	201–213	I
Heptaudecanoic acid	60.6	189	II
α-Chloroacetic acid	61.2	130	–
Bee wax	61.8	177	II
Bees wax	61.8	177	II
Glyolic acid	63.0	109	–
Glycolic acid	63	109	–
p-Bromophenol	63.5	86	–
Azobenzene	67.1	121	–
Acrylic acid	68.0	115	–
Dinto toluent (2,4)	70.0	111	–
Phenylacetic acid	76.7	102	–
Thiosinamine	77.0	140	–
Bromcamphor	77	174	–
Durene	79.3	156	–
Benzylamine	78.0	174	–
Methyl brombrenzoate	81	126	–
Alpha napthol	96	163	–
Glautaric acid	97.5	156	–
p-Xylene dichloride	100	138.7	–
Catechol	104.3	207	III
Quinone	115	171	II
Acetanilide	118.9	222	II
Succinic anhydride	119	204	II
Benzoic acid	121.7	142.8	III
Stibene	124	167	–
Benzamide	127.2	169.4	III

[a] Group I, most promising; group II, promising; group III, Less promising; — insufficient data.

Some of the characteristics of these organic materials are as follows: high latent heat of fusion, flammability, low thermal conductivity, low flash points, varying level of toxicity, and instability at high temperatures. Their main disadvantage, however, is their cost, which is 2-2.5 times higher than paraffins. They are also mild corrosive. Some fatty acids used for storage system are presented in Tab 4.

Material	Formula	Melting point (°C)	Latent heat (kJ/kg)	Group[a]
Acetic acid	CH_3COOH	16.7	184	I
Polyethylene glycol 600	$H(OC_2H_2)_n·OH$	20–25	146	I
Capric acid	$CH_3(CH_2)_8·COOH$	36	152	–
Eladic acid	$C_8H_7C_9H_{16}·COOH$	47	218	I
Lauric acid	$CH_3(CH_2)_{10}·COOH$	49	178	II
Pentadecanoic acid	$CH_3(CH_2)_{13}·COOH$	52.5	178	–
Tristearin	$(C_{17}H_{35}COO)C_3H_5$	56	191	I
Myristic acid	$CH_3(CH_2)_{12}·COOH$	58	199	I
Palmatic acid	$CH_3(CH_2)_{14}·COOH$	55	163	I
Stearic acid	$CH_3(CH_2)_{16}·COOH$	69.4	199	I
Acetamide	CH_3CONH_2	81	241	I
Methyl fumarate	$(CHCO_2NH_3)_2$	102	242	I

[a] Group I, most promising; group II, promising; group III, less promising; —insufficient data.

1.2.2 INORGANIC PCMS

Inorganic PCMs are divided into two classes: salt hydrates and metallic material. These phase change materials do not supercool appreciably and their heats of fusion do not degrade with cycling.

Salt hydrates
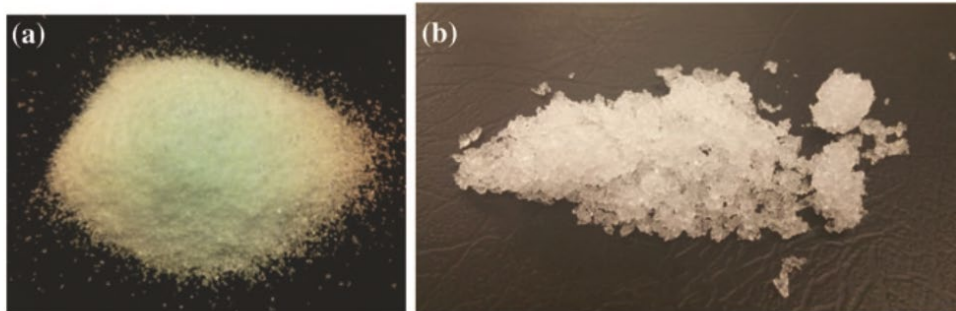
FIG. 4 (A) **SODIUM CHLORIDE,** (B) **MAGNESIUM CHLORIDE HEXAHYDRATE [1]**

Salt hydrates are combinations of elements of the inorganic salt family (oxides, carbonates, sulphates, nitrates and halides) with water molecules in a specific ratio. Salt hydrates are named using the name of the salt compound *n H_2O. During phase transformation dehydration of the salt occurs, forming either a salt hydrate that contains fewer water molecules:

$$AB \times nH_2O \longrightarrow AB \times mH_2O + (n-m)\ H_2O$$

or to its anhydrous form

$$AB \times nH_2O \longrightarrow AB + nH_2O$$

At the melting point the hydrate crystals breakup into anhydrous salt and water, or into a lower hydrate and water. One problem with most salt hydrates is that of incongruent melting caused by the fact that the released water of crystallization is not sufficient to dissolve all the solid phase present. Due to density difference, the lower hydrate (or anhydrous salt) settles down at the bottom of the container.

Salt hydrates are one of the most important group of PCM, they have been studied for their latent heat thermal energy storage systems. The most attractive properties of salt hydrates are: high latent heat of fusion per unit volume, relatively high thermal conductivity (almost double of the paraffin's), and small volume changes on melting. They are not very corrosive, compatible with plastics and only slightly toxic. Many salt hydrates are sufficiently inexpensive for the use in storage [2].

Salt hydrates can be classified in three categories, depending on the melting behaviour:

1. Congruent: salt hydrate is completely soluble in the hydration water at the melting point
2. Incongruent: the salt is not totally soluble in the hydration water at the melting temperature
3. Semi-congruent: during the during the phase transition the solid and liquid phases that are in equilibrium have different compositions because of the transformation of the salt hydrate to a salt hydrate with a lesser amount of hydration water.

The major problem in using salt hydrates for their use in thermal storages is that melt incongruently. Therefore, the amount of water released in this process is insufficient to dissolve the crystalline sale during the dehydration process. This leads to stratification problems, differences in density and phase separation causing serious technical problems during practical experiments.

Another problem common to the inorganics is that they tend to exhibit a high propensity towards supercooling, meaning that they do not begin to freeze at their solidification point, but instead can

require substantial subcooling before solidification nucleation begins. This unwanted instability makes it difficult to solidify the melted pcm. One solution to this problem is to add a nucleating agent, which provides the nucleion which crystal formation is initiated. Another possibility is to retain some crystals, in a small cold region, to serve as nuclei [2].

A list of salt hydrates is given in Tab 5.

TAB 5 :MELTING POINT AND LATENT HEAT OF FUSION: SALT HYDRATES [2]

Material	Melting point (°C)	Latent heat (kJ/kg)	Group[a]
$K_2HPO_4 \cdot 6H_2O$	14.0	109	II
$FeBr_3 \cdot 6H_2O$	21.0	105	II
$Mn(NO_3)_2 \cdot 6H_2O$	25.5	148	II
$FeBr_3 \cdot 6H_2O$	27.0	105	II
$CaCl_2 \cdot 12H_2O$	29.8	174	I
$LiNO_3 \cdot 2H_2O$	30.0	296	I
$LiNO_3 \cdot 3H_2O$	30	189	I
$Na_2CO_3 \cdot 10H_2O$	32.0	267	II
$Na_2SO_4 \cdot 10H_2O$	32.4	241	II
$KFe(SO_4)_2 \cdot 12H_2O$	33	173	I
$CaBr_2 \cdot 6H_2O$	34	138	II
$LiBr_2 \cdot 2H_2O$	34	124	I
$Zn(NO_3)_2 \cdot 6H_2O$	36.1	134	III
$FeCl_3 \cdot 6H_2O$	37.0	223	I
$Mn(NO_3)_2 \cdot 4H_2O$	37.1	115	II
$Na_2HPO_4 \cdot 12H_2O$	40.0	279	II
$CoSO_4 \cdot 7H_2O$	40.7	170	I
$KF \cdot 2H_2O$	42	162	III
$MgI_2 \cdot 8H_2O$	42	133	III
$CaI_2 \cdot 6H_2O$	42	162	III
$K_2HPO_4 \cdot 7H_2O$	45.0	145	II
$Zn(NO_3)_2 \cdot 4H_2O$	45	110	III
$Mg(NO_3) \cdot 4H_2O$	47.0	142	II
$Ca(NO_3) \cdot 4H_2O$	47.0	153	I
$Fe(NO_3)_3 \cdot 9H_2O$	47	155	I
$Na_2SiO_3 \cdot 4H_2O$	48	168	II
$K_2HPO_4 \cdot 3H_2O$	48	99	II
$Na_2S_2O_3 \cdot 5H_2O$	48.5	210	II
$MgSO_4 \cdot 7H_2O$	48.5	202	II
$Ca(NO_3)_2 \cdot 3H_2O$	51	104	I
$Zn(NO_3)_2 \cdot 2H_2O$	55	68	III
$FeCl_3 \cdot 2H_2O$	56	90	I
$Ni(NO_3)_2 \cdot 6H_2O$	57.0	169	II
$MnCl_2 \cdot 4H_2O$	58.0	151	II
$MgCl_2 \cdot 4H_2O$	58.0	178	II
$CH_3COONa \cdot 3H_2O$	58.0	265	II
$Fe(NO_3)_2 \cdot 6H_2O$	60.5	126	–
$NaAl(SO_4)_2 \cdot 10H_2O$	61.0	181	I
$NaOH \cdot H_2O$	64.3	273	I
$Na_3PO_4 \cdot 12H_2O$	65.0	190	–
$LiCH_3COO \cdot 2H_2O$	70	150	II
$Al(NO_3)_2 \cdot 9H_2O$	72	155	I
$Ba(OH)_2 \cdot 8H_2O$	78	265	II
$Mg(NO_3)_2 \cdot 6H_2O$	89.9	167	II
$KAl(SO_4)_2 \cdot 12H_2O$	91	184	II
$MgCl_2 \cdot 6H_2O$	117	167	I

[a] Group I, most promising; group II, promising; group III, less promising; — insufficient data.

Metallics [2]

This category includes the low melting metals and metal eutectics. These metallics elements have not yet been seriously considered for PCM technology because of weight penalties. However, when volume is a consideration, they are likely good candidates because of the high heat of fusion per unit volume. They have high thermal conductivity, so other elements used to enhance this physical property are not required. The use of metallics poses a number of unusual engineering problems. A major difference between the metallics and other PCMs is their high thermal conductivity. A list of some selected metallics is given in Tab 6.

Some of the features of these materials are as follows: low heat of fusion per unit weight high heat of fusion per unit volume, high thermal conductivity, low specific heat and relatively low vapor pressure.

TAB 6: MELTING POINT AND LATENT HEAT OF FUSION: METALLICS [2]

Material	Melting point (°C)	Latent heat (kJ/kg)	Group[a]
Gallium–gallium antimony eutectic	29.8	–	–
Gallium	30.0	80.3	I
Cerrolow eutectic	58	90.9	–
Bi–Cd–In eutectic	61	25	–
Cerrobend eutectic	70	32.6	I
Bi–Pb–In eutectic	70	29	–
Bi–In eutectic	72	25	–
Bi–Pb–tin eutectic	96	–	–
Bi–Pb eutectic	125	–	–

[a] Group I, most promising; group II, promising; group III, less promising; — insufficient data.

1.2.3 ENCAPSULATED PCM [5]

In most cases, except for some applications of water-ice, the PCM needs to be encapsulated. The two main reasons are to hold the liquid phase of the PCM and to avoid contact of the PCM with the environment, which might be harmed by the material, or may change the composition of the PCM. Furthermore, the surface of the encapsulation acts as heat transfer surface. In some cases,

the encapsulation also serves as a construction element, which may add mechanical stability. Encapsulations are usually classified by their size into macro and microencapsulation.

When encapsulating PCM, it is necessary to take into account several aspects. First, the material of the container wall must be compatible with the PCM. Then, once selected the wall material, the container wall has to be sufficiently thick to assure the necessary diffusion tightness. Finally, the encapsulation must be designed in a way that it is able to cope with the mechanical stress on the container walls caused by the volume change of the PCM.

Macroencapsulation

Macroencapsulation process is linked to the filling of PCM in a macroscopic containment that is characterized by a volume ranging from several millilitres up to several litres. These are often containers and bags made of metal or plastic. Macroencapsulation is very common because such containers are available in a large variety from other applications. In this case, macroencapsulation is mainly done to hold the liquid PCM and to prevent changes in its composition due to contact with the environment. If the container is rigid enough, the encapsulation can also add mechanical stability to a system.

To encapsulate salt hydrates, usually plastic containers are selected because of the proper material compatibility. Plastics are not corroded by salt hydrates; however, attention has to be paid to the water tightness of the material of the capsule wall. This is to make sure that the water content in the capsule and thus the composition of the salt hydrate does not change with time. Plastic encapsulations can also be used for organic PCM, but the combination of PCM and encapsulation material has to be chosen very carefully because organic materials may soften plastics. Fig. 5 shows several examples of macro encapsulation in plastic containers from different companies. Many manufacturers produce a selection of different encapsulations. Because plastic containers can nowadays be produced easily in a high variety of shapes, there are few restrictions on the geometry of the encapsulation.
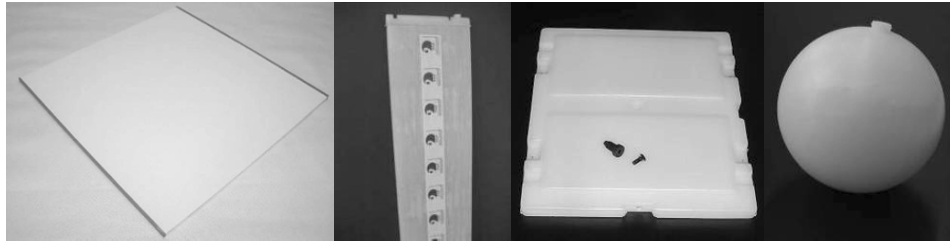
FIG. 5: MACROENCAPSULATION IN PLASTIC CONTAINERS. FROM LEFT TO RIGHT: BAR DOUBLE PANELS, PANEL, FLAT CONTAINER AND BALLS [5]

Another form of macroencapsulation is shown in Fig. 6. Here, plastic sheets form small containments for the PCM that are sealed with a plastic foil. Such encapsulations, called capsule stripes or dimple sheets, are useful to cover large surfaces and can be manufactured on a fully automated production line.
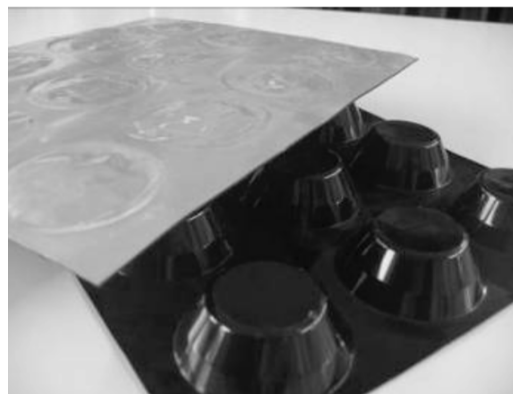
FIG. 6: MACROENCAPSULATION IN CAPSULE STRIPES FOR INORGANIC PCM [5]

Microencapsulation

Microencapsulation is the encapsulation of solid or liquid particles of 1 μm to 1000 μm diameter with a solid shell. Physical processes used in microencapsulation are spray drying, centrifugal and fluidized bed processes, or coating processes. Besides the containment of the liquid phase, other advantages of microencapsulation regarding PCM are the improvement of heat transfer to the surrounding because of the large surface to volume ratio of the capsules, and the improvement in cycling stability since phase separation is restricted to microscopic distances. Furthermore, it is also possible to integrate microencapsulated PCM into other materials. A potential drawback of

microencapsulation is however that the chance of subcooling increases. Currently, microencapsulation on a commercial scale is applied only to PCM that are not soluble in water.

Commercial products seem to use exclusively paraffins. Fig. 7 shows commercial microencapsulated paraffin, with a typical capsule diameter in the 2-20 μm range.
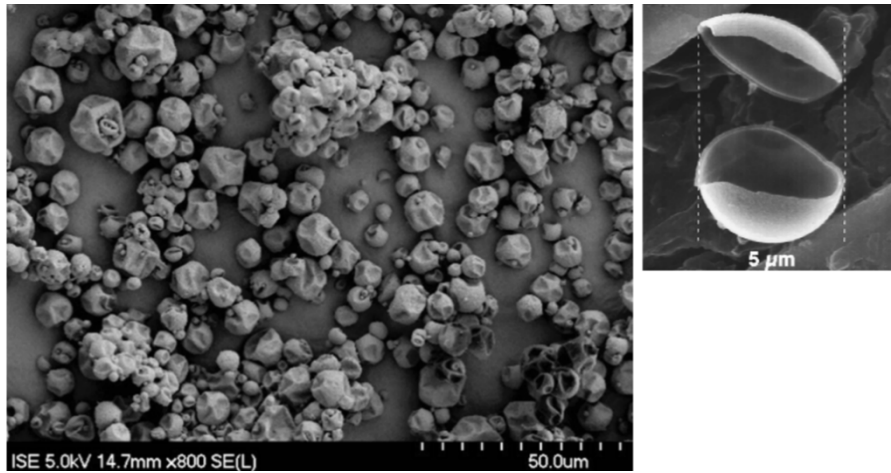
FIG. 7: ELECTRON MICROSCOPE IMAGE OF MANY CAPSULES AND AN OPENED MICROCAPSULE [5]

The microencapsulated PCM is available as fluid dispersion or as dried powder (Fig. 8)

FIG. 8: MICROENCAPSULATED PARAFFIN, ON THE LEFT AS FLUID DISPERSION, AND ON THE RIGHT AS DRY POWDER.
[5]

1.3 ENERGY STORAGE APPLICATIONS

1.3.1 BUILDING MATERIALS

The use of PCMs as building materials is the most widespread application of such materials. From the beginning, mankind wanted to design comfortable homes, able to absorb heat during the day and that retain as much heat as possible at night. One good example could be Adobe. These materials store a significant quantity of thermal energy during the day and released it slowly during the night creating a comfortable abode in desert environments. Adobe housing has been popular for millennia, and among the most famous adobe dwellings is Cliff Palace, in Mesa Verde National Park in Colorado (see Fig. 9). Adobe houses are still a popular option in the American Southwest today. [1]
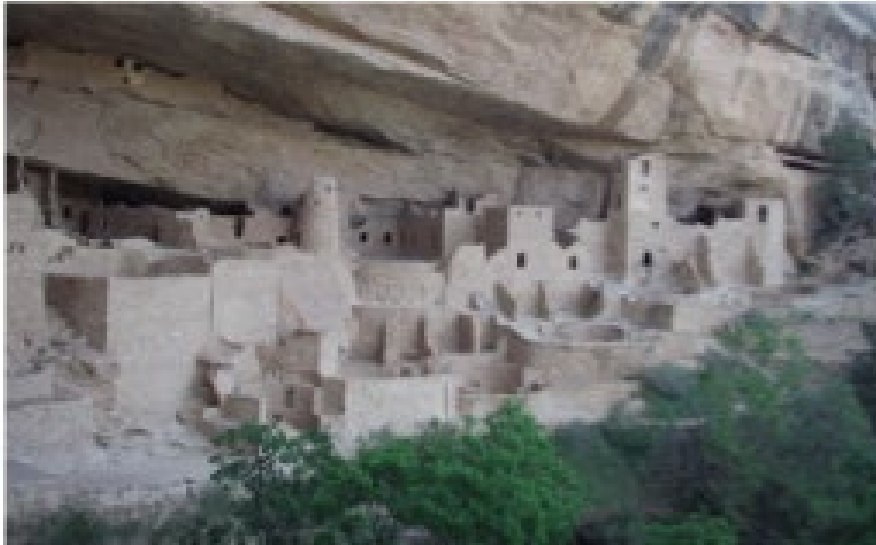
FIG. 9: MESA VERDE'S CLIFF PALACE SANDSTONE AND ADOBE DWELLING [1]

The interest on PCMs in building materials is linked to the ability to harness energy storage through the latent heat phase transition instead of through sensible heat exchange. The best advantage is the availability of a larger amount of energy during the phase change, meaning that more energy can be stored with a fixed volume. By storing energy through the phase transition, the overall thermal load of the structure to be faced by the HVAC plant can be reduced. This is related to the

constant temperature linked to the phase transition. When solar energy is incident on traditional building envelope components, characterized by sensible energy storage, the temperature of these elements rises. However, with PCM-based building envelope components, their temperature will rise until the temperature of phase transition is reached. Then, incident energy is absorbed to melt the PCM and the temperature of the panel remains constant. This works particularly well in desert environments, where it is possible to have high solar insolation during the day and cold nights where the heat is released by the PCM.

One of the main areas of implementation of the PCMs for energy storage in buildings is the gypsum board. In most cases, these products have a melting point which ranges between 20 and 30 ° C. Currently there are several commercial PCM gypsum boards available on the market, many of which use an encapsulated PCM supplied by BASF with a melting point of about 23 ° C.

As it can be seen from the examples given by Fleischer [1] PCMs are an effective way to reduce energy costs when embedded in building materials. The PCMs can be embedded by direct immersion, macroencapsulation or microencapsulation, depending on the host material and application. The primary advantages to using PCM in building materials is their ability to store energy without temperature increase, thus mitigating temperature rise and thus HVAC loading within the building. Several commercial products are now available, and the only barrier to their greater implementation currently is cost and wide scale availability. These materials can be further refined and optimized by addressing issues related to melt temperature range, to avoid situations where the PCM remains either fully liquid of fully solid for days at a time, as well as issues of weight and for concrete, structural integrity.

1.3.2 SOLAR ENERGY SYSTEMS

1.3.2.1 CONCENTRATING SOLAR POWER PLANTS

FIG. 10 :PARABOLIC THROUGH CONCENTRATING SOLAR COLLECTORS WITH HEAT TRANSFER FLUID IN THE TUBING ABSORBING THERMAL ENERGY [1]

An evident drawback of solar power systems of any type is the limitation of the effectiveness of the technology to periods with high solar irradiation. This is particularly an issue for large commercial solar power plants, as electricity demand is not limited to daylight hours. The use of phase change materials for thermal energy storage (TES) in these applications can extend the usefulness of this technology in order to provide free renewable energy even where there is low or no direct insolation. In fact, for large solar power plants, fully integrated TES is necessary for the design of economically viable plants to reduce reliance on supplemental fossil fuel burners.

Commercial solar power plants are designed using the concept of Concentrating Solar Power (CSP) technology. In these plants, sunlight is reflected and concentrated using mirrors and then used to heat a carrier fluid. There are four main types of concentrator designs: parabolic trough, linear Fresnel, power tower (helio- stat) and dish-sterling.

An example of parabolic trough technology is shown in Fig. 10. In this image, the thermal receiver is supported above the concentrating mirrors. The receiver is a black pipe encased in a vacuum tube to reduce convective losses. A high temperature, high pressure heat transfer fluid (HTF) circulates through the receiver pipes. Depending on the design of the system, the HTF fluid may serve as the heat source in an evaporator, creating steam which powers a stream turbine which drives a generator, or the HTF may directly vaporize as it passes through the solar field and then

pass straight through the turbine without an intermediate heat exchanger. In either design, during periods of high insolation, it is possible to absorb more solar thermal energy into the HTF than is necessary to power the turbine [1].
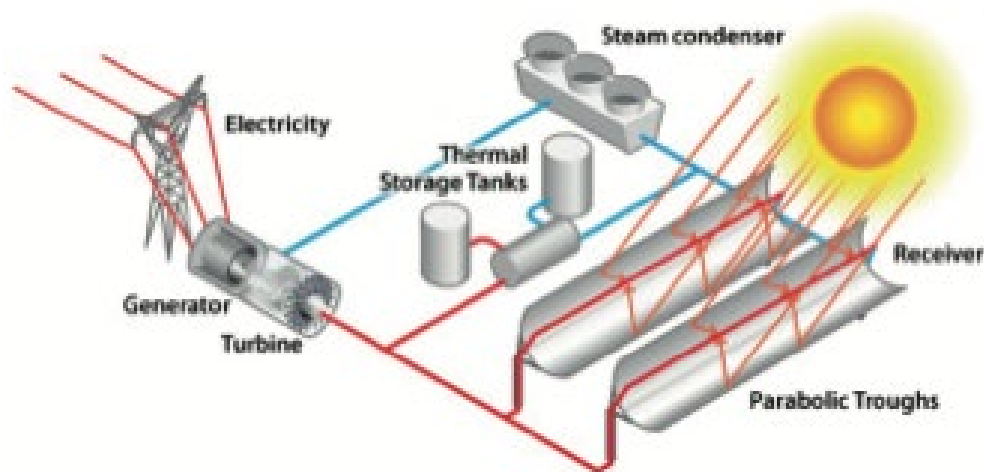
FIG. 11: AN EXAMPLE OF A DIRECT STEAM GENERATION CONCENTRATING SOLAR PLANT WITH THERMAL ENERGY STORAGE [1]

Fleischer [1] gives a review of the main applications of PCMs to TES for solar power plant applications and it is reported that the use of these materials can thus reduce tank number (to one), size and installation costs, creating an economic benefit. It can be seen from Fleischer's overview that the thermal energy storage has been shown to be necessary in the implementation of large scale concentrating solar plants. Although the existing CSP plants use sensible heat storage with a two-tank system, it is clearly shown that the use of PCMs can lead to significantly lower capital and operating costs. The typical PCMs used in these applications are inorganic salts which melt in the range between 300–800 ° C. These PCMs tend to be corrosive and have low thermal conductivity but it was shown that this can be offset with the use of embedded heat pipes or thermosyphons. In certain applications liquid metals may be used in place of inorganic salts.

1.3.2.2 DOMESTIC SOLAR THERMAL APPLICATIONS
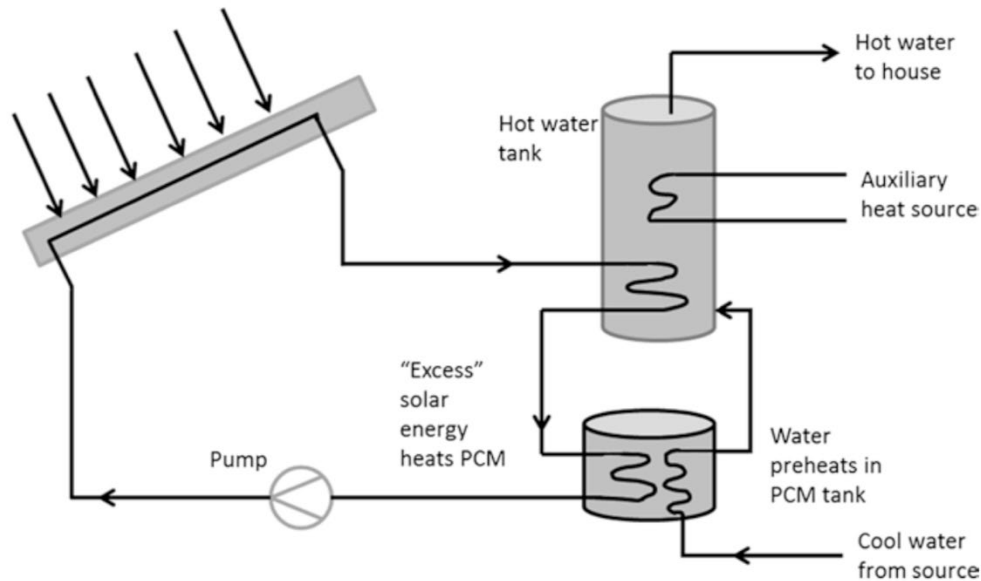
FIG. 12: DOMESTIC SOLAR HOT WATER HEATING SYSTEM WITH PCM THERMAL STORAGE [1]

While the large CSP plants certainly have significant technical and economic incentives to implement PCM thermal energy storage systems, smaller scale solar systems can also reap some benefits from TES. For example, solar thermal systems can be used by small companies and homes for domestic hot water production and for heating systems. A small scale solar hot water system with energy storage is depicted in Fig.5. These systems feature a flat plate solar collector, typically mounted on the roof, and a heat transfer fluid (HTF) passing through the receiver tubes. The receiver tubes are isolated within an enclosure with a glass cover plate. The enclosure may be evacuated to prevent convective losses. In many ways this is similar to the CSP solar field, but without the concentrators. The lack of concentrators means that the HTF will not reach the high temperatures typical of CSP applications: the fluid can't be used to create steam and drive a power system but is hot enough to provide the heat source for a domestic hot water tank. As with CSPs, the effectiveness of the system is limited to daylight hours, but the solar thermal system can be designed to store additional thermal energy using PCM in the storage tanks for the overnight hours, greatly reducing dependence on supplemental natural gas or electrical heating. Fleischer [1] gives examples of possible designs of domestic hot water tanks.

Thermal energy storage can also be used with solar thermal systems used to heat air (instead of water) in order to eliminate or reduce the size of HVAC systems. This is particularly useful for solar heating in greenhouse systems, as reported again by Fleischer.

PCM thermal energy storage can also be implemented as part of a solar-aided heat pump system to allow operation during the night and on cloudy days [1]. During times characterized by high solar insolation occurs, the thermal energy is transferred to and stored in the PCM tank and when space heating demands occur, they are met using the tank's stored energy. In this application, Fleischer [1] shows a parametric analysis that was completed to determine the effect of PCM choice on the solar energy storage time.

Finally, as it can be seen from the overview of smaller industrial and domestic thermal energy storage applications, it is shown that although the economic benefits are reduced when compared to large CSP plants, there is still a role for thermal energy storage in smaller domestic scale solar thermal heating systems. The lower temperatures for these solar applications (50–120 ° C) necessitate a different choice of PCM. The typical PCMs used in these applications are characterized by a melting point in the range between 29–55 ° C and commonly included $CaCl_2 \cdot 6H_2O$ and paraffin wax. These PCMs have been shown to be effective when used with domestic solar hot water, solar assisted heat pumps and ground source heat pump systems.

1.3.3 HEAT EXCHANGER DESIGNS

The previous section illustrated the possible benefits of PCM thermal energy storage in commercial and domestic scale solar systems. In many of these systems, the PCM is implemented in a heat exchanger where the free heat obtained from the solar field is used to charge the storage tank. In fact, PCM energy storage heat exchangers can be useful in any system in which an excess quote of thermal energy can be stored for future use through heat exchange from a heat transfer fluid to a PCM storage system.
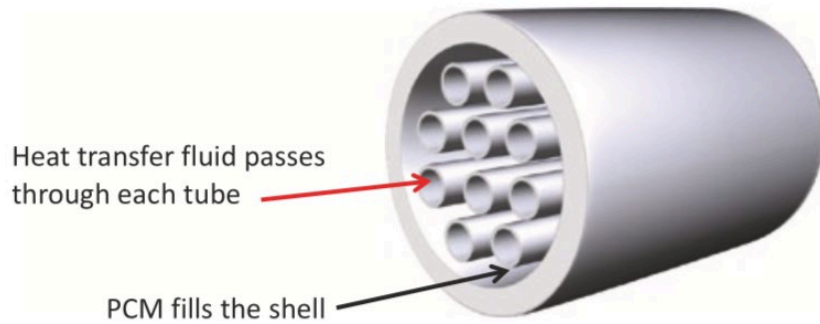
FIG. 13: PCM ON THE SHELL SIDE OF A SHELL TUBE HEAT EXCHANGER [1]

These applications often take the form of a shell and tube heat exchanger with the PCM on the shell side as seen in Fig. 13, although some devices have the PCM on the tube side. The choice of PCM material in these applications depends on the operating temperature range of the system and can include molten salts for high temperature waste heat recovery and paraffin for lower temperature domestic heating systems.

In this section, Fleischer [1] presents some of the design and application issues involved with using PCMs in heat exchangers. Al-abibi et al. [3] include a section on PCM usage in heat exchangers within the context of a review of thermal energy storage in HVAC systems (LHTES for air conditioning systems, PCMs for air conditioning applications).

The effective application of PCM in a shell and tube exchanger for thermal energy storage requires a low thermal resistance between the heat transfer fluid in the tubes and the PCM in the shell. When operating in charging flow, with hot HTF acting to melt the shell side PCM, it is desirable to transfer as much heat as possible as the fluid flows through the tubes. In this case, with melting PCM, the heat transfer will be convection dominant on the outside of the tubes, as natural convection is induced in the shell side. When operating in discharge flow, with the heat extracted from the molten PCM, the heat transfer will be conduction dominant as the PCM solidifies around each tube. Much of the design work in this application has considered methods to reduce thermal

resistance in both melting and solidification in order to most effectively transfer heat in and out of the PCM to the flowing HTF [1].

Various different shell and tube side modifications have been analyzed for their effects on thermal resistance [1]. For instance, the use of longitudinally internally finned tubes has been considered as a method to induce tube-side turbulence and create a lower total thermal resistance to the shell [3]. The design was analyzed numerically during the melting/charge phase. The addition of internal tube fins was found to significantly increase the rate of PCM melting, and thus decrease charging time. The melting volume fraction, which reflects the progression of the melt at a given point in time, increased with the fin thickness, height and number of fins [1].

Another way to optimize the thermal response of a PCM heat exchanger during charging and discharging is to design the exchanger to contain multiple PCMs with different melting ranges. Fleischer [1] gives an example of a multiple PCM exchanger for high temperature applications. In this design, the PCM with the highest melt temperature is located at the inlet to the exchanger and occupies the first 1/3 of the shell length, the second PCM with a lower melt temperature fills the middle third of the shell and the PCM with the lowest melt point fills the final 1/3 of the shell as shown in Fig. 14. In this way, as the HTF drops in temperature as it traverses the tube, the temperature difference between the HTF and the melt point of the PCM is adjusted by moving to lower melting point PCMs, maintaining a more consistent heat flux.
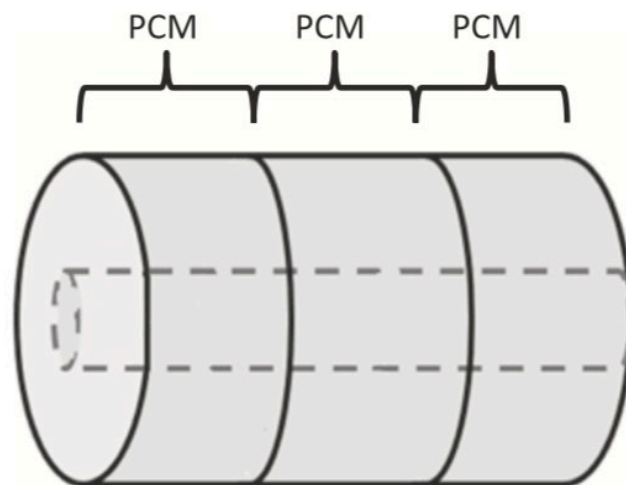
FIG. 14: CASCADED PCMS WITH DIFFERENT MELT TEMPERATURES [1]

It can be seen from the overview given by Fleischer [1] that PCMs can be implemented in heat exchanger designs for quick charge and discharge of thermal energy to/from a flowing heat transfer fluid. The PCM is typically installed on the shell side of a shell and tube exchanger and the PCM used will depend on the temperature of the application. The main design concern with PCM implementation in this manner is the reduction of thermal resistance during both melting and solidification. The thermal resistance is often reduced using both internal and external fins on the tubes, and by the use of high conductivity particles in the PCM itself.

1.3.4 PHASE CHANGE MATERIALS AND HEAT PUMPS [4]

Thermal energy can be stored as sensible heat, latent heat or chemical energy. Phase-change materials (PCMs) are included in the second storage mechanism, since they take advantage of the latent heat of the freezing and melting processes. Many different eutectics and mixtures can be potentially used as PCMs, but to be considered PCMs there are some requirements to be fulfilled. Among these requirements the most relevant are a high storage capacity, a melting point suitable with the chosen application and chemical stability.

From a theoretical point of view, the use of PCMs in storage systems leads to a higher density of thermal energy storage than systems based on sensible thermal storage only. This would yield a reduction of the storage tank size. This would be useful in buildings, especially in cities, where there is a space limitation. The thermal storage density of PCM systems is between 5 and 14 times higher than in sensible heat storage systems such as water, masonry or rock. PCM systems lead to more stable temperatures during the process of thermal energy charging and discharging.

Controlling the capacity of compressors, pumps and ventilators in heat pumps adds degrees of freedom for the control system. The ability to control the heat pump more accurately than simple on-off control leads to increased energy efficiency and possibly to a reduction of the size of the storage tank.

Combining heat pumps and PCMs has two main advantages. On the one hand, the energy stored in PCMs can be used as heat source for the evaporator. This leads to an almost constant evaporation temperature. Given that the solar radiation is not constant, and the air temperature varies so much within a normal day in a cold climate, using PCM as intermediate storage would be beneficial for the heat pump to work in more stable conditions. In addition, this prevents defrost cycles in air-source heat pumps. On the other hand, using a storage based on PCMs would reduce the required installed cooling capacity of the heat pump, reduce the compressor's start/stop cycles and simultaneously cut down the investment cost.

Heat pumps cover demands ranging from space heating or cooling to ventilation and DHW production. This applies even when the energy requirements have different temperatures depending on the demand. In high-efficiency buildings, space heating is provided at temperatures ranging between 25° C and 50° C. For space cooling, the temperature requirement varies between 12° C and 20° C depending on the country and risk of condensation. Thus, the existence of PCMs with different melting points allows optimizing PCM selection.

Pardinas et al. [4] considered different substances with different phase change temperatures for storing, heating or cooling implemented in heat pump systems for applications of space heating and domestic hot water production.

1.3.4.1 SPACE HEATING

A first possible application of PCMs for space heating could be their implementation in a storage tank heated by the heat pump condenser to store thermal energy and shift the production and consumption periods.
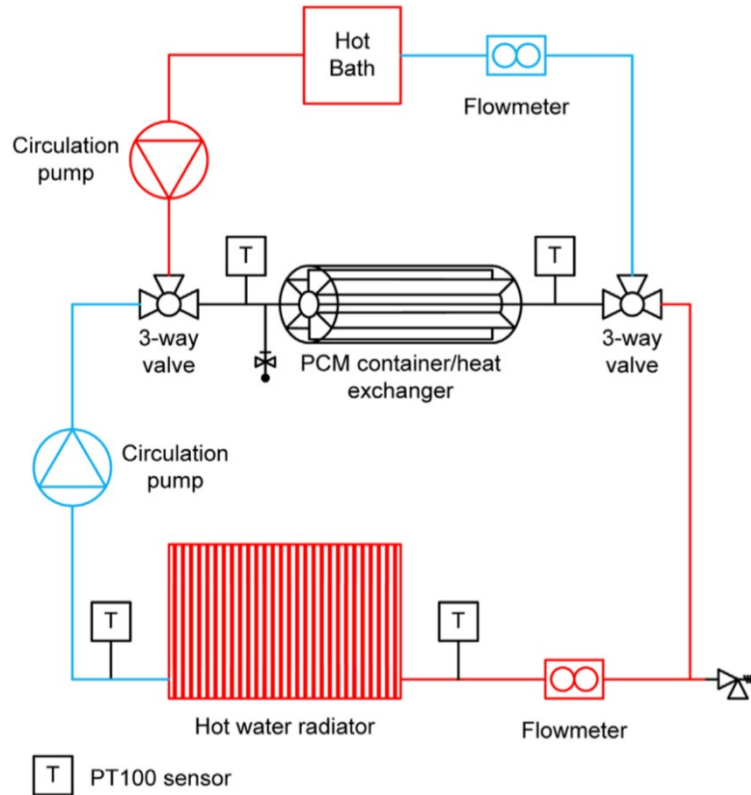
FIG. 15: SIMPLIFIED SKETCH OF THE EXPERIMENTAL FACILITY TO TEST THE PCM ENERGY STORAGE [4]

Pardinas et al. [4] shows an experimental study focused on the use of fins for enhancing the heat transfer in a PCM energy storage system. This PCM tank was planned to be used in combination with heat pumps to shift electricity demand for space heating to off-peak electricity periods. The setup is represented in Fig. 15. The main device is the PCM container/heat exchanger, which consists of a cylindrical shell (375 mm outer diameter), with a concentric tube (65 mm outer diameter) with 8 longitudinal fins braced on its surface (1.1 m long, 120 mm wide and 1 mm thick). The water of the space heating installation flows through the tube. Between the fins was placed PCM RT 58 (melting temperature range between 56° C and 63° C and solidification temperature range between 51° C and 60° C). The main result of this work is that a PCM tank of 1116 L is needed to meet the daily space heating demand of 25 kWh (in 4h) for a house of 105 m² if the heat is produced during the low-cost period for electricity (7h a day). This is due to the low thermal conductivity of RT58. The authors concluded that the tank volume can be reduced by up to 30% if the heat transfer is improved by means of enhanced heat exchangers in PCM energy storage.

Another approach for providing space heating with heat pumps and PCMs consists in using solar-assisted heat pumps to improve the evaporation conditions of the heat pump and, if possible, provide space heating directly with the solar collectors. There are three possible systems for these types of configurations:
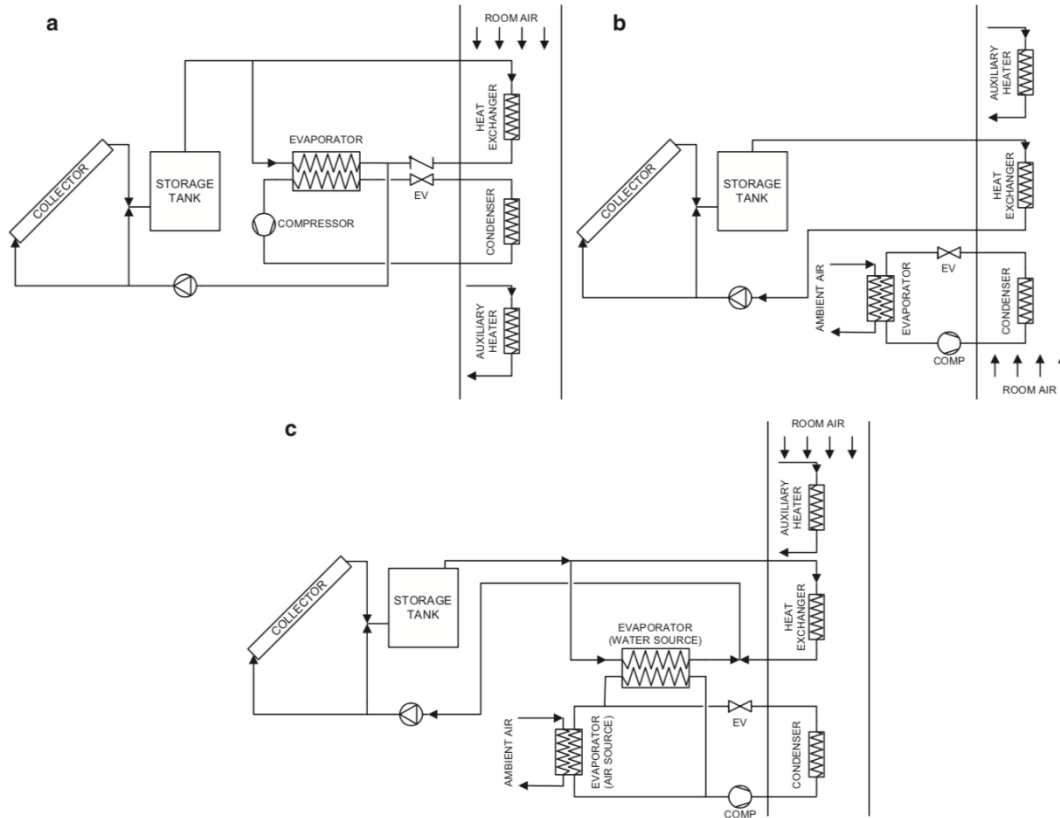
FIG. 16: SOLAR-ASSISTED HEAT PUMPS WITH PCM ENERGY STORAGE A) SERIES SYSTEM B) PARALLEL SYSTEM C) DUAL SOURCE SYSTEM. [4]

1. **Series system**: During daytime with solar radiation, the hot water from the solar collectors heats the PCM in the storage tank and this hot water is also the heat source of the heat pump (if there is a space heating demand). During night time, or under no radiation conditions, the heat pump refrigerant absorbs heat at a relatively high temperature from the PCM storage tank to improve the heat pump performance. (Fig. 16 a)

2. **Parallel system**: The heat pump uses ambient air as heat source and heats the room air by transferring heat from the condenser. In parallel, when radiation is available, the hot water from

the solar collectors heats the PCM in the storage tank and as much of the room air as possible. (Fig. 16b)

3. **Dual source system**: The heat pump has two evaporators and uses either of them depending on the ambient and tank temperatures. In addition, if the tank is warmer than a certain value, it heats the room air directly. (Fig. 16c)

Pardinas et al. [4] represented some experiments with these configurations and concluded that the seasonal performance factors (COP) for the series, parallel and dual source systems were 3.3, 3.7 and 4.2, respectively. The main conclusion of their work is that the dual source system is the optimal configuration since it makes the most out of the features of both the series and parallel systems.

1.3.4.2 WATER HEATING (DHW)
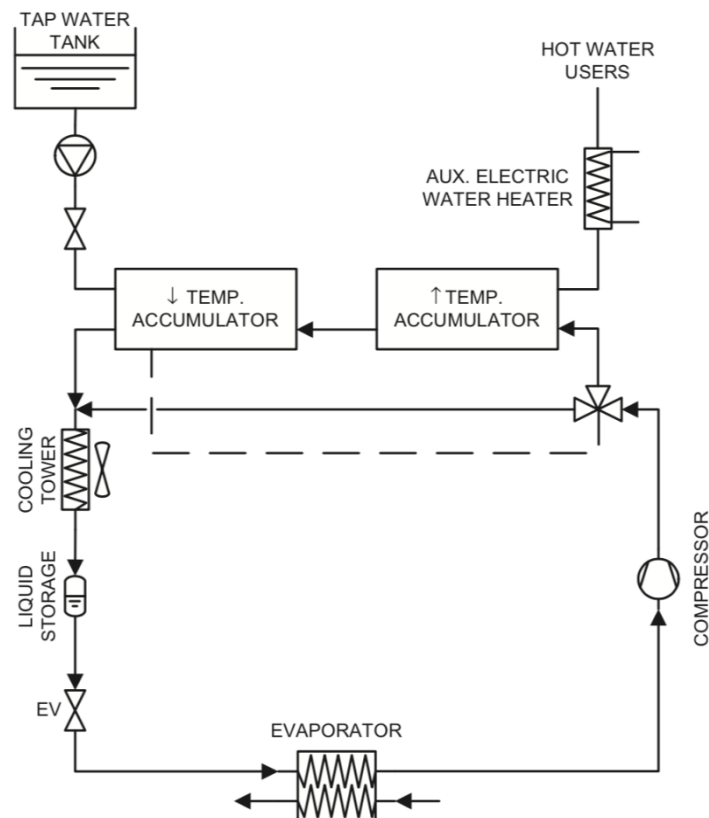
FIG. 17: AIR CONDITIONING SYSTEM WITH PCM TANKS FOR HEAT RECOVERY AND WATER HEATING [4]

PCMs seem to be a good solution for the storage of energy for the production of domestic hot water, which represents a growing share regarding the requests in homes. The system shown in Fig. 17, given by Pardinas et al. [4], consists of two PCM tanks in series with the condensing outdoor unit. Both tanks are heated by the refrigerant (R22) discharged by the compressor when there is an air conditioning demand. The three-way valve bypasses the tanks when they have achieved the tank temperature set-point and the heat produced by the air conditioning system is rejected in the cooling tower. When DHW is to be produced, it passes through both PCM tanks. If the water temperature is not sufficiently high for DHW use, it receives additional heat from an auxiliary heater. The system was modelled at different condensation temperatures and a parameter was defined in order to analyse its performance (integrative energy efficiency ratio, IEER). it was observed that the more recovered heat, the better the performance of the system.

The method of storing the heat recovered from air conditioning systems in PCM tanks was also studied. It was observed that the addition of the energy storage to recover heat from the air conditioning system increases the cooling capacity and power consumed by the air conditioning system, compared to the basic systems without PCM tank, and decreases the air conditioning condensing temperature.

In conclusion, it can be seen, from the overview given by Pardinas et al. [4], that reducing the size of the buffer tanks used with heat pumps, avoiding the oversizing of heat pumps or detaching thermal energy production and consumption are among the benefits that could result from the combination of heat pumps and latent heat thermal energy storage. In addition, this form of thermal energy storage allows enhancing the use of renewable energy sources as heat sources for heat pump systems.

1.4 EXAMPLES OF EXPERIMENTAL SETUP TO STUDY PCMS

In this section an overview of papers, dealing with some experimental set up and design to study PCMs in thermal energy storage, is given.

1.4.1 EXPERIMENTAL INVESTIGATIONS ON PHASE CHANGE MATERIAL BASED THERMAL ENERGY STORAGE UNIT [6]

Kabbara et al. [6] experimentally investigated the performance of a thermal storage unit with phase change material encapsulated in cylinders. A schematic representation of the storage system is shown in Fig. 18. Air was the heat transfer fluid, flowing across the tube banks to charge and discharging the storage system. The investigation analysed the storage capacity and the heat transfer rate to the phase change material.
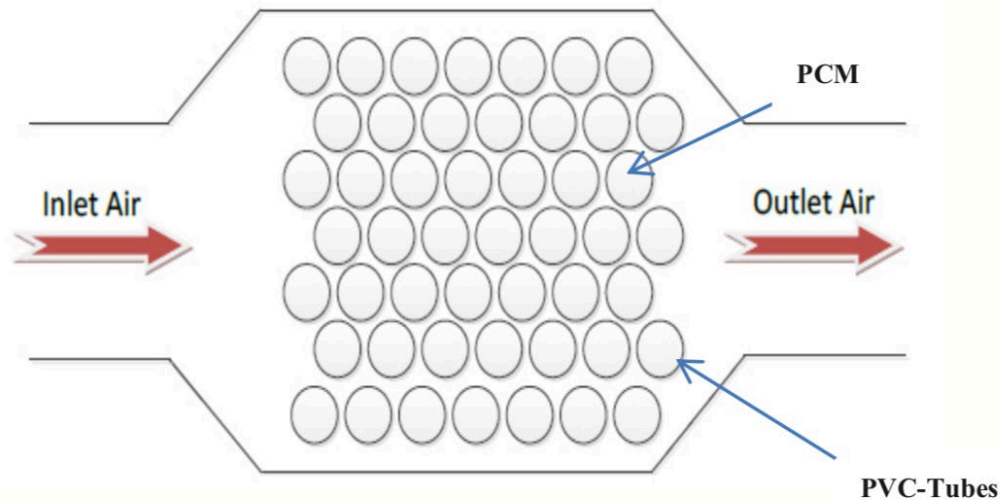
FIG. 18: GENERAL LAYOUT OF THE THERMAL STORAGE UNIT [6]

The unit consists of 49 staggered tubes (6 cm in diameter and 61 cm in length) filled with the phase change material with air flowing across the tube bank. The total PCM (Calcium Chloride Hydrate) mass in the system is 121.30 kg encapsulated and distributed equally in the cylinders. The material has a freezing point of 27-28 ° C, and a latent heat of fusion 170 kJ/kg. The maximum latent heat storage capacity of the unit is 20.6 MJ. The volume occupied by the thermal energy storage unit is 0.18 m³ giving an energy storage density equal to 110.17 MJ/m3. The tank has 1.9 cm plywood

siding from the sides and it is well insulated from the environment with 5 cm of Styrofoam (Re=1.76 m^2 K/W). The charging cycle of the storage unit is accomplished when the PCM is at room temperature, with inlet air temperature set constant at 42 ° C. For the discharging cycle, two different inlet temperatures were used during two separate experiments while keeping the inlet temperature of the charging cycle constant during both of those experiments. The inlet temperatures used during the discharging cycles are 22° C and 7° C, respectively.

The overall process is shown in Fig. 19; the experimental setup consists of a heater, a temperature controller, a variable speed fan, a gate valve, thermocouples, a pressure meter and a computer based data logger. The indoor/outside air is circulated using the variable speed fan and heated up to the desired constant inlet temperature by the heaters and it is controlled using the temperature controller that has a temperature sensor connected to the entrance of the storage tank.

The gate valve is opened when the air reaches the desired constant temperatures and presents a steady-state behavior; during the period when the air is heating up or cooling down the air flowrate is diverted to another duct. The thermocouples used in the experiments are type T devices, which have a measure uncertainty of 0.75-1° C. Five thermocouples are placed in the system in order to measure the inlet air temperature, outlet air temperature, PCM temperature closer to the inlet, PCM temperature closer to the outlet, and the ambient room temperature. The time interval between measurements is 1 minute. The duration of the melting/freezing process was determined by observing the temperature profiles of the PCM and the air.
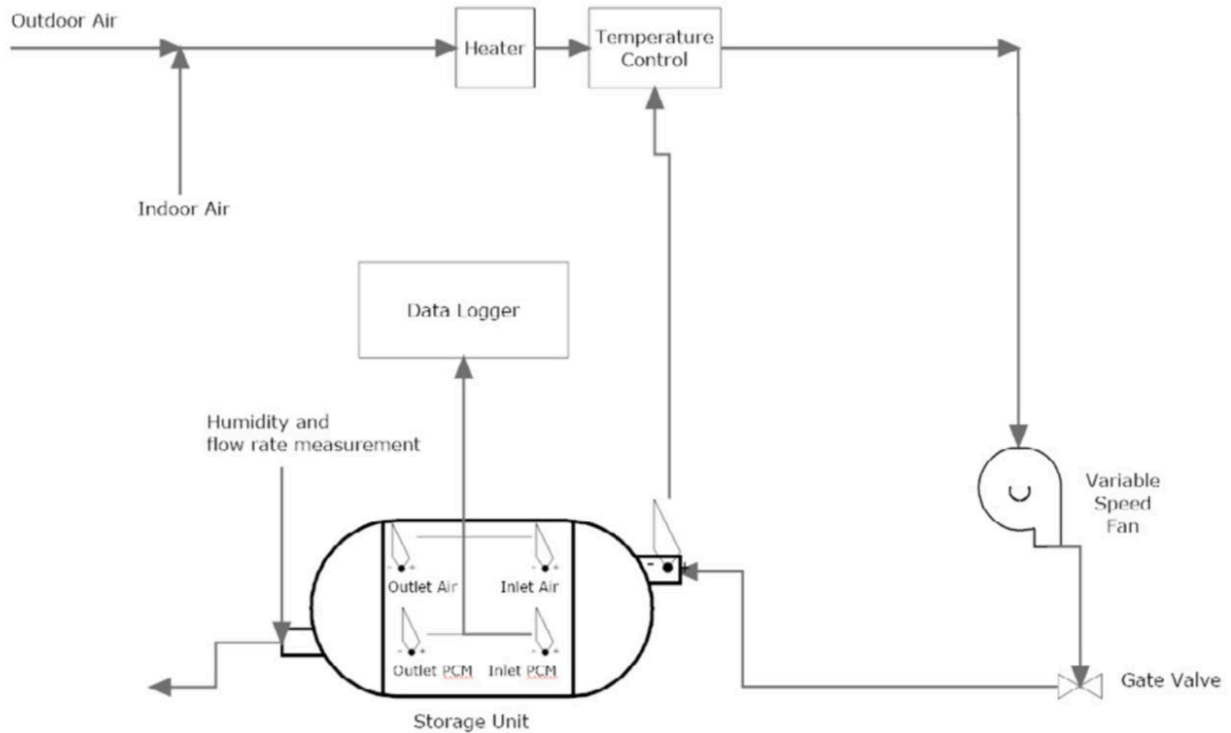
FIG. 19: GENERAL SCHEMATIC OF THE EXPERIMENTAL SETUP

The temperature profiles during the melting and freezing processes for flow rates of 0.182 kg/s is represented in Fig.20. Each process took around 10 hours, making the full cycle around 20 hours.

The most significant parameter monitored in the experiment was the inlet temperature during the freezing cycle which almost doubled the heat flux from the previous temperature used. This could mean that the data and results displayed could be utilized for further investigation in heat transfer rate enhancement or used for scaling up and design purposes in solar energy applications that could utilize such a low inlet temperature (e.g. solar energy recovery in greenhouses, solar assisted heat pumps).
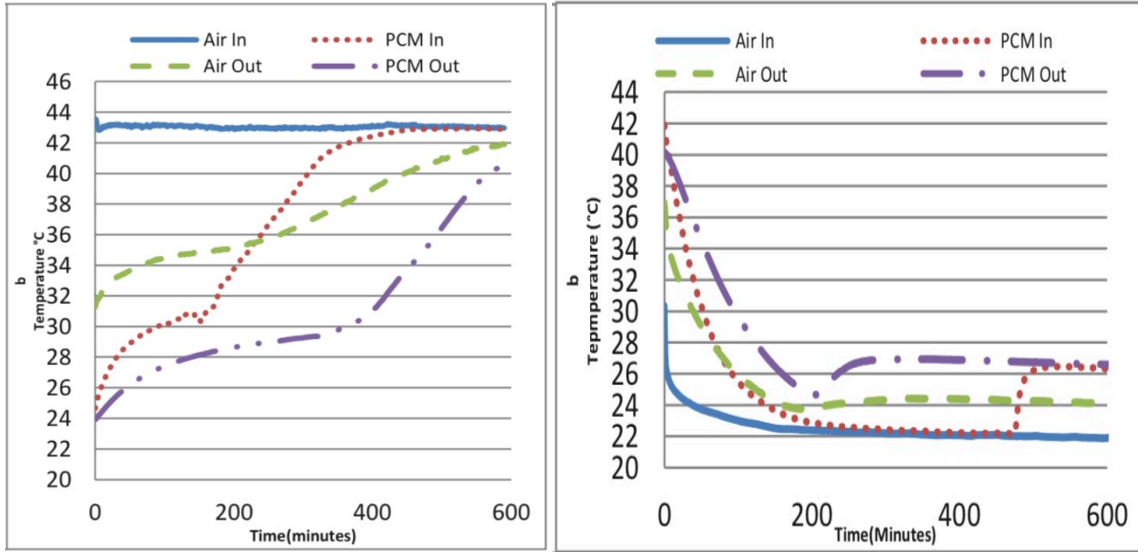
FIG. 20: TEMPERATURE PROFILES DURING THE MELTING/FREEZING PROCESSES [6]

1.4.2 EXPERIMENTAL AND NUMERICAL INVESTIGATION OF THE STEADY PERIODIC SOLID–LIQUID PHASE-CHANGE HEAT TRANSFER *[7]*
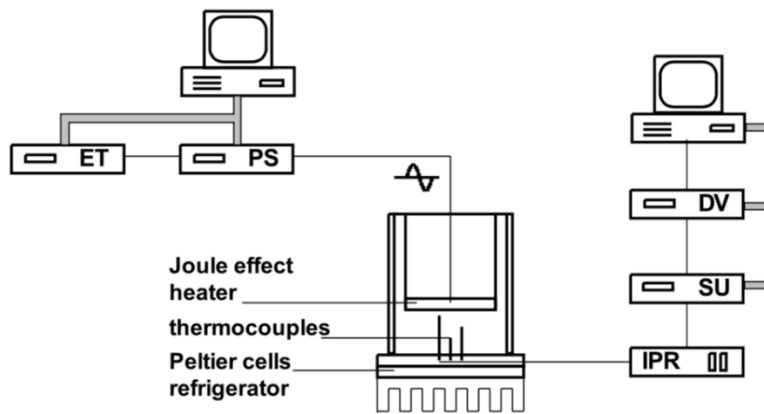
FIG. 21: SCHEMATIC DIAGRAM OF THE EXPERIMENTAL EQUIPMENT: ET, EXTERNAL TRIGGER; PS, POWER SUPPLY; IPR, ICE POINT REFERENCE; SU, SWITCH CONTROL UNIT; DV, DIGITAL VOLTMETER. [7]

Casano and Piva [7] presented a numerical and experimental investigation of a periodic phase-change process dominated by heat conduction. In the experimental arrangement a plane slab of

PCM was periodically heated from above. The comparison between numerical predictions and experimental data shows good agreement.

Fig. 21 shows a schematic diagram of their experimental equipment. The test cell consists of a polycarbonate round duct (outer diameter 150 mm, inner diameter 140 mm and height 210 mm) filled with the phase-change medium. Its bottom extremity is glued on a circular aluminum plate, used as the base. Such a base is kept at a temperature lower than the melting point of the test material by means of a refrigeration system. The uniform contact between the base and the refrigerator is enhanced by a thin layer of thermal conductive paste.

To remove easily the heat flow during the experiment, the refrigeration system uses Peltier cells. Nine thermoelectric modules (dimension 40x40x4 mm3) connected in series allow a uniform distribution of temperature over the whole surface of the bottom wall. They are sandwiched between a square plate of aluminum (2 mm of thickness) and a finned one (40 mm high fins). In order to reduce the heat transfer to the environment, the wall of the cylinder is insulated with a 20 mm thick layer of foam rubber surrounded by a 100 mm thick layer of expanded polystyrene.

The heat flow is obtained by dissipating via the Joule effect an assigned power in a resistor (450 W of nominal power at 220 V). Such a resistor is placed inside a copper disk soldered at the end of a cylindrical copper container (outer diameter 135 mm, inner diameter 133 mm and height 112 mm). This copper cylinder is placed coaxially inside the polycarbonate container. The air space between the two cylindrical surfaces is used as an auxiliary volume of expansion, allowing the volume of the liquid phase to change during the melting process.

The temperature inside the specimen is measured by copper–constantan thermocouples distributed at different heights. The positions of the thermocouples are shown in Tab 7. The first and last thermocouples are in contact, respectively, with the hot and cold walls. The hot junctions of the thermocouples are supported by polycarbonate stands.

TAB 7: POSITION OF THE THERMOCOUPLES [7]

TC no.	1	2	3	4	5	6	7	8
x (mm)	0	6.6	14.4	20.8	25.7	35	44.9	51.1

The origin is placed on the top of the specimen.

The data acquisition system was managed through a personal computer and the time was measured with the inner clock of the personal computer.

The PCM used for this experiment was 99% pure n-octadecane, because it is non-corrosive and non-toxic, chemically inert and stable, with low vapour pressure, small volume changes during melting process and large enthalpy release during the phase transition. The melting temperature of the PCM has been measured to be $T_f = 28\,°$ C.

The experimental tests were carried out to obtain cyclic processes of melting and freezing in a sample of n-octadecane. The experiments always included a preliminary settling period when the sample, previously frozen in a refrigerator, was kept solid. When the measured temperature of the sample became practically uniform, enabling the reaching of steady-state conditions to be assured, the heating system was activated, and the periodic heating process started.

The results of the comparison are reported for three experimental tests. The runs differ according to the period of the sinusoidal power dissipated in the heater (4, 8 and 16 h for Test a, b and c respectively). The temperature was sampled every 4 min, the experiments lasting for 24 h in the case of Test a and 48 h for Tests b and c.

In Fig. 22, for the selected runs, the measured and computed temperature distributions are compared. Results for the three tests show that only Test b reaches steady periodic conditions; Tests a and c are too short to achieve steady state conditions.

For all the tests reported in Fig. 22, the presence of an interface separating an upper zone, where the material is liquid, from a lower zone at the solid state, is clearly evidenced. The liquid zone is characterised by wide oscillations of temperature, reaching the maximum amplitude at the heated

surface (equal to 5, 8 and 15 ° C for Tests a, b and c respectively). The solid region is characterised by moderate oscillations of temperature.

In Fig. 22 the oscillations of temperature seem to be sinusoidal when completely included in the liquid or in the solid phase, they change from this shape when intersecting the phase-change surface. In fact, they are clearly distorted, as particularly evident in Test b.

In conclusion, the comparison among the numerical and the experimental data is very good. The start of the melting process, and of the following freezing and melting cycles, appears clearly and the wide oscillations of temperature in the liquid are also well evident.

The decision to neglect all phenomena apart the conduction is confirmed by the excellent results. The prevailing role, therefore, is played by the conduction.
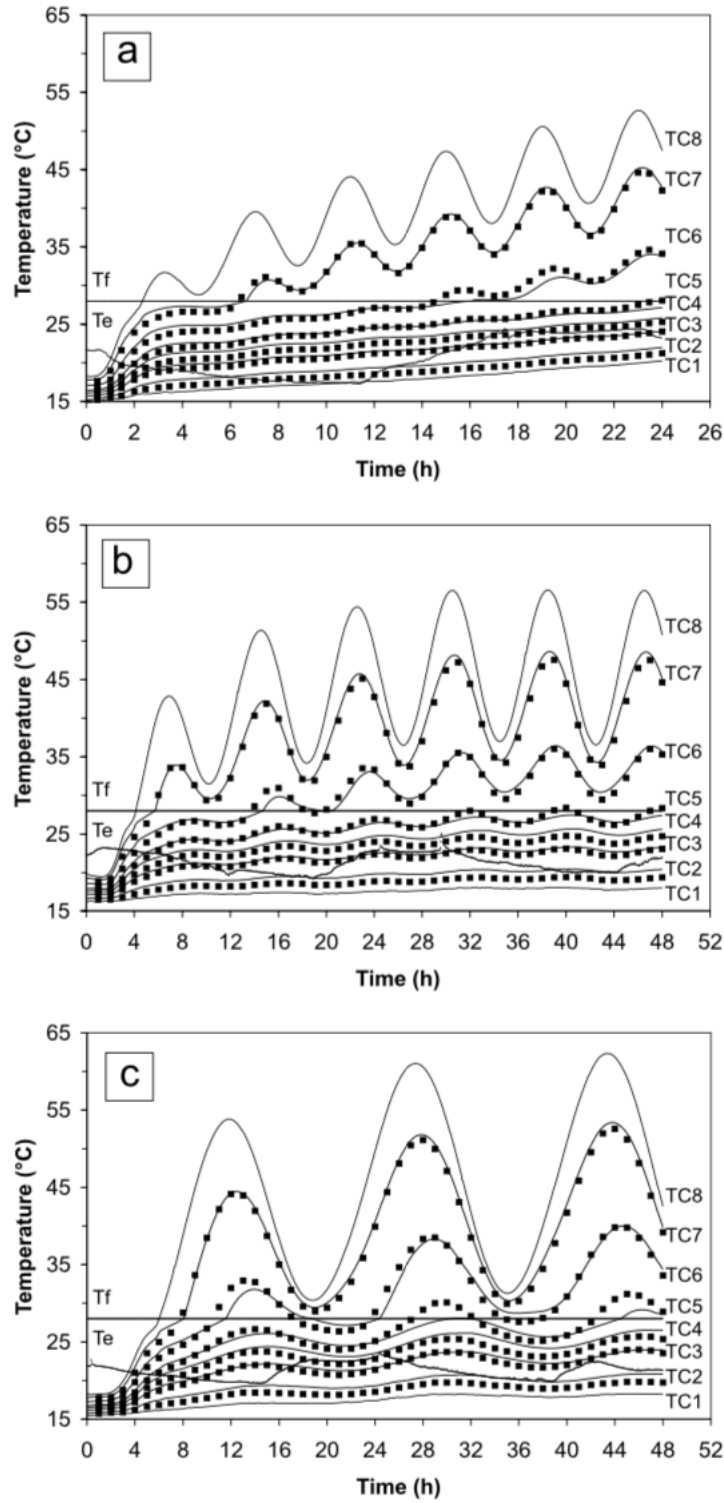
FIG. 22: COMPARISON BETWEEN COMPUTED (LINES) AND MEASURED(SYMBOLS) TEMPERATURES DISTRIBUTIONS FORT TESTS OF DIFFERENT PERIODS (A: 4 H, B: 8 H, C: 16 H). [7]
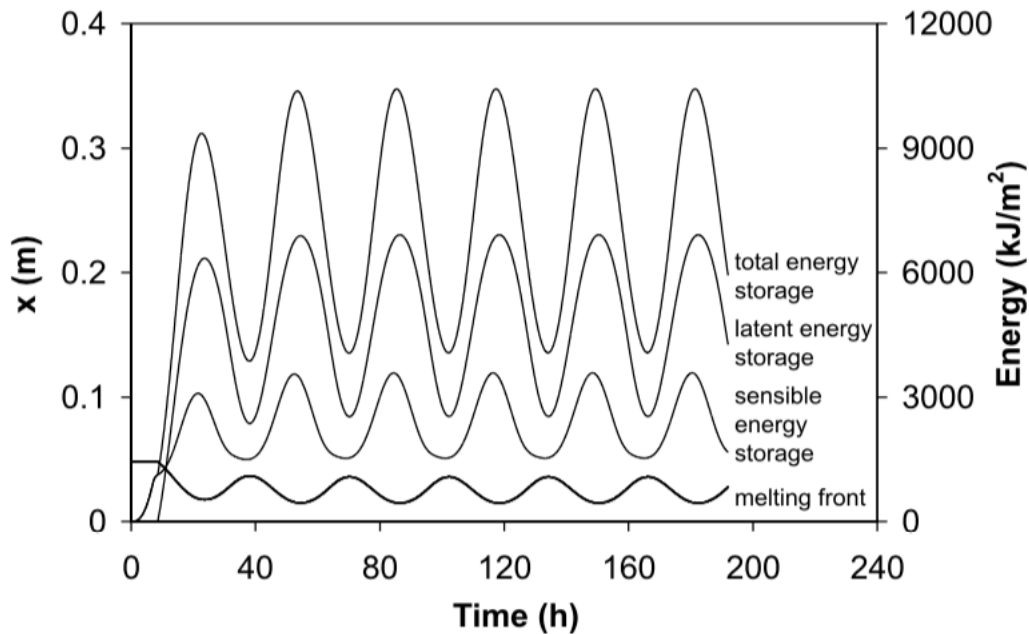
FIG. 23: ENERGY STORAGE AND INTERFACE POSITION IN THE STEADY PERIODIC HEATING [7]

Finally, the analysis of the energy behaviour of the system also gives interesting results. It can be seen that, after an initial phase of sensible heating, the melting front moves until it oscillates steadily around a constant mean value.

Unlike the total storage, the sensible and latent heat storage show trends periodic but clearly not sinusoidal, lagging each other in time. A significant contribution to this phase shift is due to the preliminary sensible heating of the slab. This delays the beginning of the phase-change phenomenon, which starts only when the top surface reaches the phase-change temperature.

1.4.3 PERFORMANCE ANALYSIS OF INDUSTRIAL PCM HEAT STORAGE LAB PROTOTYPE *[8]*

Zondag et al. [8] built and tested a 140 L lab scale shell-and-tube PCM heat storage and compared the experimental results to a numerical model. In this paper, it is shown that natural convection in the PCM has a significantly influence on the local temperature distribution in the storage vessel. Experimentally, it can be noticed that a horizontal orientation can give benefits due to increased heat exchange during melting. Two PCMs were used in the testing (RT70 and $MgCl_2 \cdot 6H_2O$, Tab

8), it was found that the RT70 had stable performance while the salt hydrate showed a reduced melting enthalpy which was ascribed to phase separation.
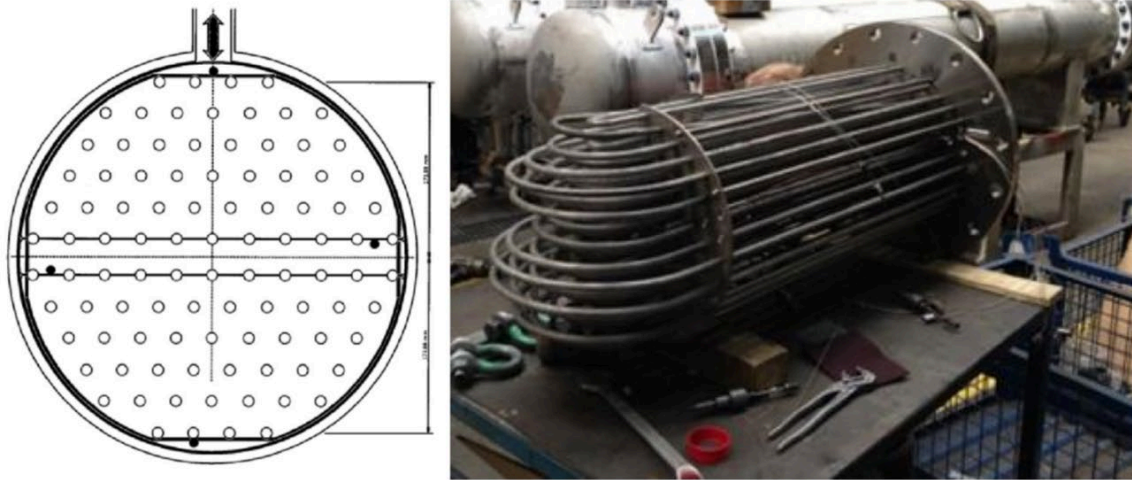
FIG. 24: (A) HEAT EXCHANGER DESIGN, (B) HEAT EXCHANGER (BEFORE INTEGRATION IN STORAGE VESSEL) [8]

TAB 8: PROPERTIES FOR RT70 AND MGCL$_2$·6H$_2$O AS USED IN THE SIMULATIONS [8]

material	T $_{phasechange}$ (°C)	ΔH$_{melt}$ (kJ/kg)	ρ (kg/m^3)	Cp (J/kgK)	k (W/m K)
RT70	70	230	770 (l), 880 (s)	2000	0.20
MgCl$_2$·6H$_2$O	117	167	1450 (l), 1570 (s)	2000	0.57 (l), 0.70 (s)

The PCM storage design is based on a shell and tube heat exchanger, being an industrial standard solution, in which the shell side is filled with the PCM. This introduces a number of design parameters, such as pitch and number of tubes, depending on the effective conductivity of the PCM [8]. Fig. 24 shows the heat exchanger. It contains 49 U-tubes for heat transfer, with an outside diameter of 12 mm and a triangular pitch of 36 mm. Fig. 25 shows the full prototype. The vessel, with this design, can be placed in either horizontal or vertical position, to investigate the effect of vessel orientation on thermal performance of the PCM (related to the direction of natural convection in the molten PCM). The vessel was connected to a heating/cooling infrastructure. Two different types of PCM materials have been tested in the vessel; Rubitherm paraffin PCM RT70

(an organic PCM with a melting temperature of 70 ° C) and pure MgCl2·6H2O (a salt hydrate PCM with a melting temperature of 117 ° C). In horizontal orientation, the prototype could be filled with 103 kg of Rubitherm paraffin PCM RT70 (in vertical orientation, a slightly lower PCM content of 85 kg was realized, due to limitations caused by the position of the filling valve). The inflow temperature to the vessel was controlled by a thermostatic bath, with sufficient cooling/heating power to have an inlet temperature stable within 0.5 K of the setpoint value.

FIG. 25: LARGE SCALE PROTOTYPE (A) HORIZONTAL CONFIGURATION (B) VERTICAL CONFIGURATION (AFTER INSULATION) [8]

The thermocouple distribution is shown in Fig. 26. Temperature measurements are carried out both along the reference tube, and in between two tubes, as shown Fig. 27.
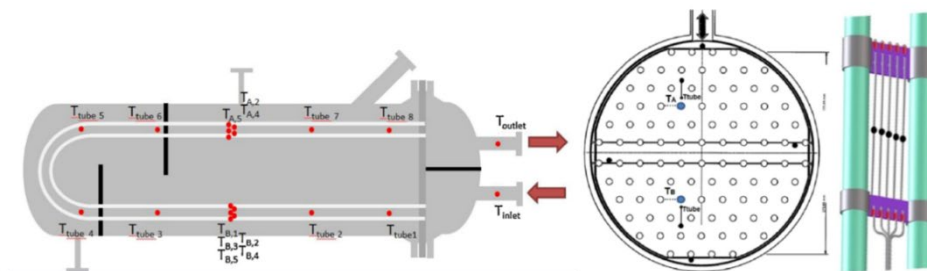
FIG. 26: POSITIONING OF THERMOCOUPLES IN VESSEL [8]

The temperatures inside the vessel were measured as a function of time over a complete charging-discharging cycle of about 8 h. Detailed results are shown in Fig. 27(along the tube) and Fig. 28 (perpendicular to flow between two tubes). Both figures show the effect of melting and solidification around the melting temperature of 70 ° C. Along the tube, a good qualitative match is found between experiments (solid lines) and model results (dotted lines). However, quantitatively, the melting in the PCM occurs faster than indicated by the model, which is ascribed to natural convection in the molten PCM.
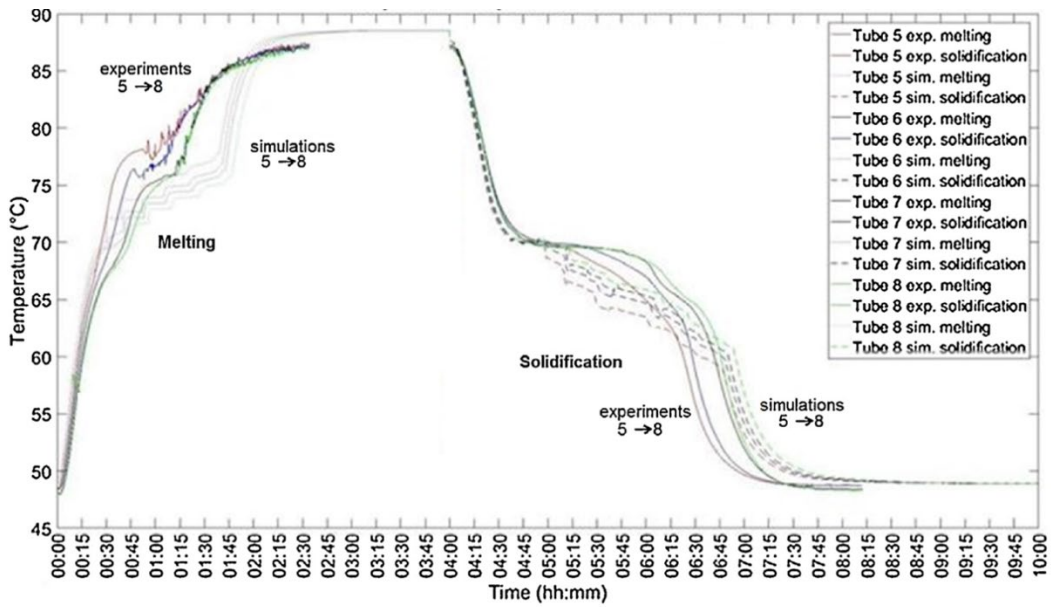
FIG. 27: TEMPERATURE MEASUREMENTS ALONG A TUBE (RT70, HORIZONTAL ORIENTATION VESSEL, ΔT = 20 ° C, MASS FLOW 20 KG/MIN) [8].
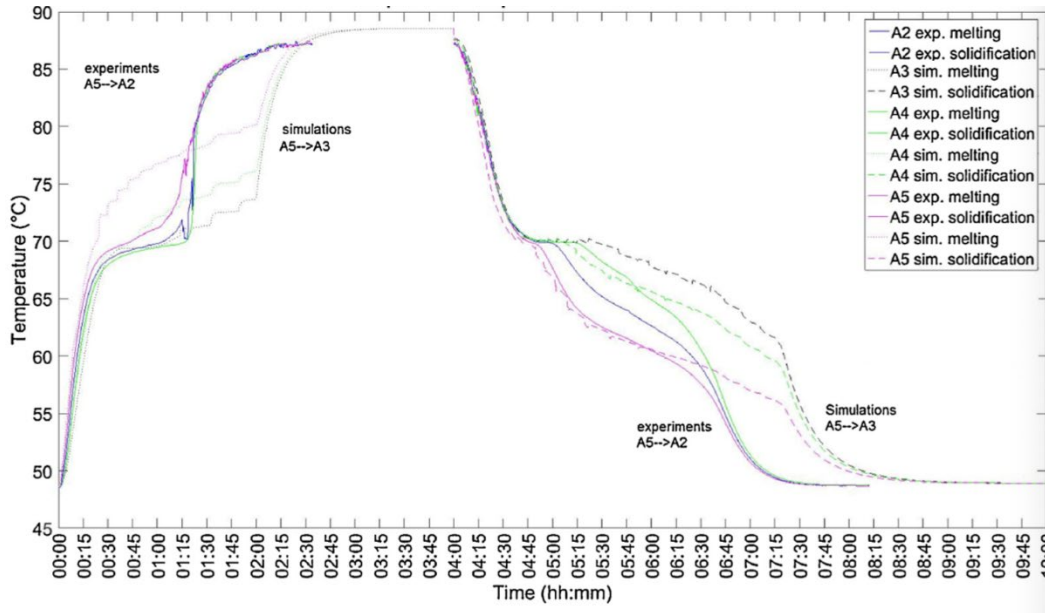
FIG. 28: TEMPERATURE MEASUREMENTS BETWEEN THE TUBES (TOP SECTION OF THE TANK) (RT70, HORIZONTAL ORIENTATION VESSEL, ΔT = 20 ° C, MASS FLOW 20 KG/MIN) [8].

In the direction perpendicular to the tube (Fig. 28), in the melting phase, the experimental temperature differences in radial direction are much smaller than expected based on the model, indicating an almost instantaneous change in temperature. One possible reason is that the thermocouples perpendicular to the tube are positioned horizontally, as shown in Fig. 26. The experiments show that the melting front from the tube underneath rises up much faster than the mathematical model and intercepts all the horizontally distances thermocouples at about the same time, as shown in the experimental results.

In the solidification phase, the model is too slow compared to the experiments as shown in Fig. 28. This may be caused by an underestimation of the PCM thermal conductivity. In the model, this was set to 0.25 W/m·K, to stay within the range indicated by the manufacturer (manufacturer value for the PCM conductivity is 0.2 W/m K). However, increasing this to 0.3 W/m·K significantly reduces the mismatch in the solidification phase between simulation results and experiments, as shown in Fig. 29.
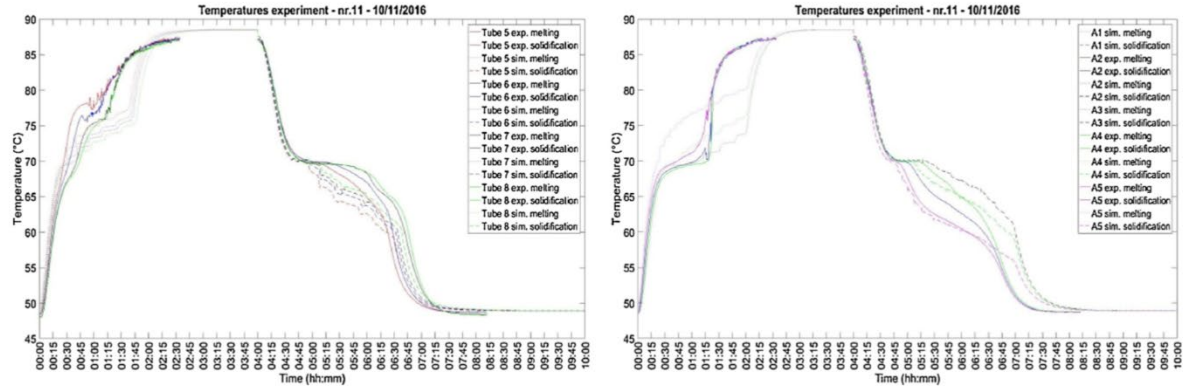
FIG. 29: SAME MEASUREMENTS AS FIGS 29 AND 29, BUT NOW COMPARED TO SIMULATION RESULTS FOR A PCM THERMAL CONDUCTIVITY OF 0.3 W/MK [8]

Fig. 30 shows a comparison between the thermal power as calculated by the model and the measurements. The figure shows that on discharge (solidification), the match between model and experiments is good. However, on charging (melting), the experimental storage is charged faster than that predicted by the model. This is attributed to the effect of natural convection in the molten PCM, which affects the melting phase much more strongly than the solidification phase. To correct for this, a high effective heat transfer of 150 W/m²K was assumed in the numerical model for the heat transfer between all adjacent shells, for the case that these shells were both containing molten PCM (replacing the conductive heat transfer calculated from h= k/d$_{shell}$, where h is the heat transfer coefficient (W/m² K) and d$_{shell}$ is the distance between shells. This gives a much better match with the experimental data in the charging phase (as shown in Fig. 30), while having almost no effect in the discharging phase (as expected).
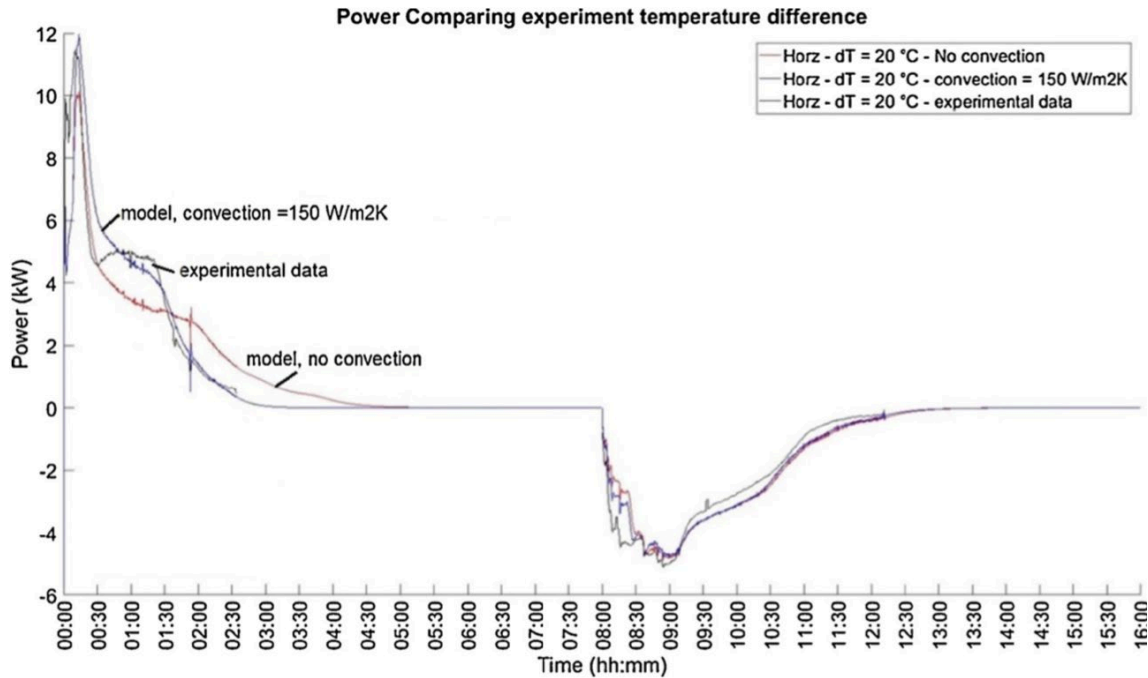
FIG. 30: COMPARISON OF POWER IN NUMERICAL MODEL WITH AND WITHOUT CORRECTION FOR PCM CONVECTION.

[8]
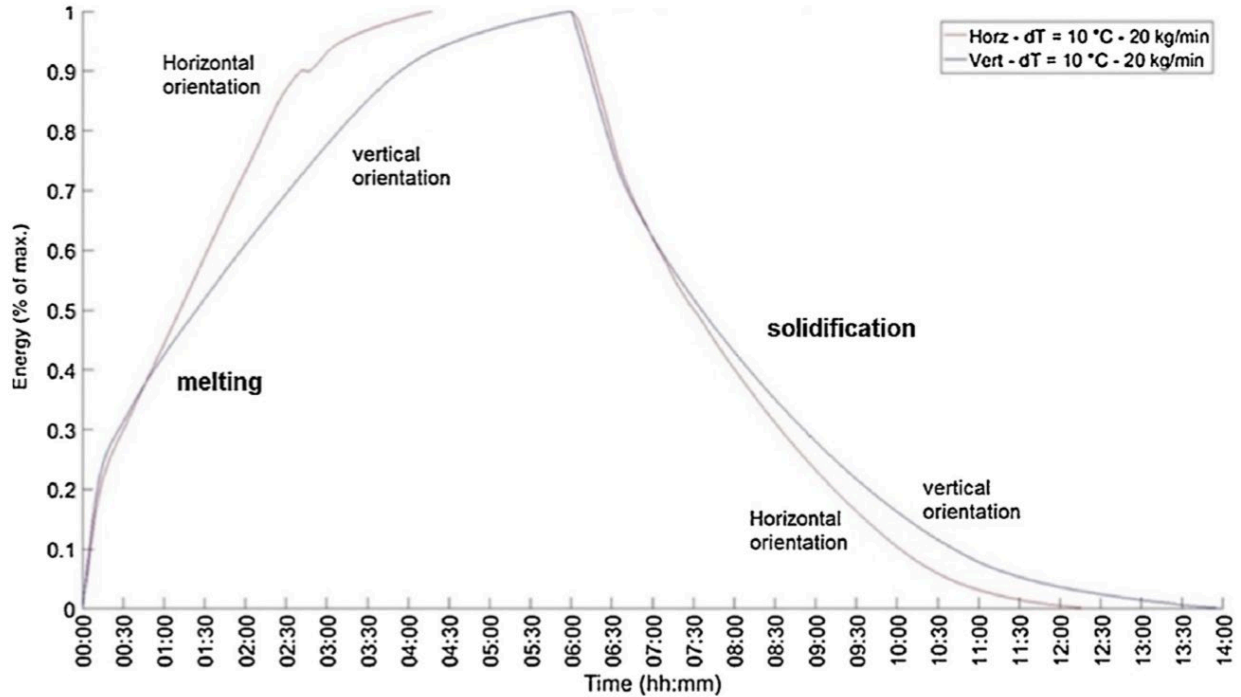
FIG. 31: EFFECT OF ORIENTATION ON ENERGY CONTENT OF THE STORAGE. TEMPERATURE DIFFERENCE IS 10 ° C, MASS FLOW IS 20 KG/MIN. [8]

Finally, Fig. 31 shows the effect of the vessel orientation. In the measurements, a significantly higher thermal power was found for the horizontal configuration than for the vertical configuration, which is consistent with the faster charging of the storage as shown in the figure. The effect is particularly important for charging (melting), while for discharging (solidification) the difference between the configurations is lower. This indicates that the effect is probably due to natural convection in the molten PCM. It is concluded that the horizontal orientation promotes effects of natural convection much more than the vertical orientation, which can be ascribed to the fact that in horizontal orientation, more and smaller convection cells will appear than in vertical orientation, and in addition, the convective flow is perpendicular to the tubes, instead of parallel to the tubes. Both these effects tend to increase the effectiveness of the natural convection heat transfer.

1.4.4 HEAT TRANSFER ENHANCEMENT IN A LATENT HEAT STORAGE SYSTEM *[9]*

Velraj et al. [9] investigated on various heat transfer enhancement methods for Latent heat thermal storage (LHTS) systems. Three different experiments to increase heat transfer were conducted and the findings are here reported. (Fig. 32)
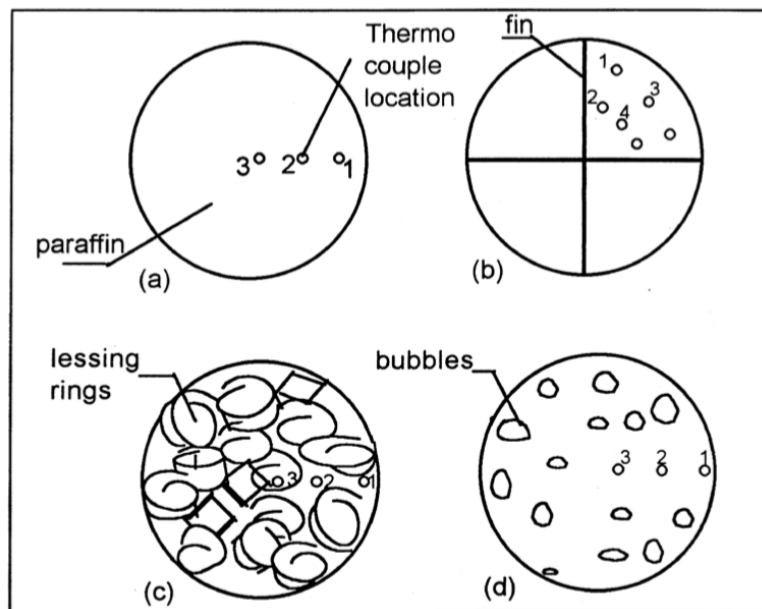
FIG. 32: PARAFFIN STORAGE TUBE CROSS SECTION AND THERMOCOUPLE LOCATIONS FOR THE CONFIGURATIONS (A) PLAIN TUBE (B) WITH FINS (C) WITH LESSING RINGS (D) WITH BUBBLE AGITATION. [9]

The first enhancement technique uses internal longitudinal fins inside a cylindrical vertical storage tube containing paraffin. In the second method, the tube is filled with lessing rings of 1 cm diameter which are commonly used in the chemical reactors to enhance the surface contact, and the molten paraffin is poured into the tube. These lessing rings are made of steel and have a thin- walled hollow cylindrical structure with a partition. Without partition these rings are known as Raschig-rings. A photographic view of the lessing rings is shown in Fig. 33. The molten paraffin occupies 80% of the storage volume. In the third method a very small amount of water is poured into the tube. Molten paraffin is then added and the tube is evacuated by a vacuum pump. The vacuum is maintained such that the saturation temperature of the water inside the tube is nearly equal to the phase change temperature of the PCM. The intention is to create steam bubbles inside the PCM during the phase change that would promote the heat transfer.

FIG. 33: A PHOTOGRAPHIC VIEW OF THE LESSING RINGS. [9]

Fig. 34 shows the experimental setup of the storage unit. It consists of a vertical cylindrical storage tube made of aluminum, with an outside diameter of 6 cm, an inside diameter of 5.4 cm and an active length of 60 cm. The tube is placed inside another cylindrical vessel with 25 cm diameter and having the same height as the tube, containing water. The vessel is well insulated. The temperature of the water bath is controlled by a thermostat, having a variable heating coil capacity

of 500, 1000 and 2000 W. A magnetic stirrer is provided at the bottom of the trough to have a uniform temperature in the axial direction of the cylindrical vessel. A small top portion of the tube unit is kept above the water level to provide convenient thermocouple connections and for easy handling of the tube from outside. While conducting experiments with fins, an assembly of four aluminum fins with the dimensions of 0.15 cm thickness, 2.7 cm height and 50 cm length each, and forming a cross shaped cross-section is placed inside the tube and welded at the top and bottom of the tube. The intermediate length of the fin was thermally bonded to the tube by solder. [9]

For all the experiments, thermocouples were placed in two different horizontal planes, at a distance of 20 cm and 35 cm from the bottom of the tube as shown in Fig. 35. The position of the thermocouples in one plane for all the configurations is shown in Fig. 33. Three thermocouples are located in the surrounding water bath at different heights to monitor and ensure that there is minimum temperature variation in the axial direction. The thermocouples are connected to a data acquisition system, which can provide instantaneous analog and digital outputs. The system has a precision of ±0.05% of the reading of +0,5° C and a resolution of 0.1° C for the measurements with K type thermocouples. Molten paraffin is poured into the tube carefully avoiding cavities. For the experiments with the plain tube, paraffin RT 58 was used and for the experiments with heat transfer enhancement methods, paraffin RT 60 was used. Both paraffins have the same thermophysical properties except for the phase change temperature. RT 60 has a phase change temperature range of 58 to 60° C and RT 58 has a phase change range of 58 to 59° C. Tab 9 summarizes the thermophysical properties of paraffin RT 58 and RT 60.
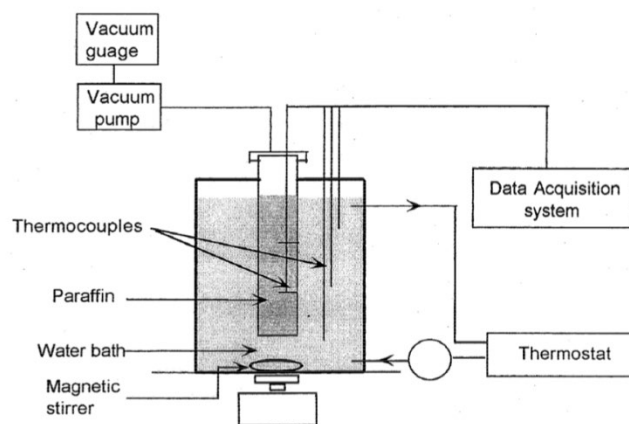
FIG. 34: EXPERIMENTAL SETUP [9]

Velraj et al. [9] performed several experimental runs to find the temperature distribution within the paraffin during solidification. At first, the experiments were conducted without fins (plain tube configuration). Subsequently, the authors conducted experiments for heat transfer improvement configurations, following the same procedure.

TAB 9: THERMOPHYSICAL PROPERTIES OF PARAFFIN RT 60 AND RT 58 [9]

Property	Value
Latent heat of fusion	214.4 kJ kg^{-1}
Specific heat capacity	900 J kg^{-1} K^{-1}
Thermal conductivity	0.2 W m^{-1} K^{-1}
Density	
Solid	850 kg m^{-3}
Liquid	775 kg m^{-3}

Initially, the water temperature was kept constant above the solidification temperature. Subsequently, the water temperature was decreased to a value lower than solidification temperature and kept constant. That was possible by removing part of the hot water and adding cold water.

The thermostat was then set to the new surrounding water temperature and the acquisition system was also switched on. The water bath was maintained at a constant temperature (within a range of $\pm 0.2°$ C) throughout the experiment by thermostat control. The transfer of fusion heat from the PCM increases the temperature of the surrounding water.

As the solidification proceeded, the temperature and time readings were recorded and monitored. The experimental readings were obtained till all the thermocouples showed temperatures well below the solidification temperature.

Fig. 35(a) shows the experimental and simulated temperature variation for the value of h=400 W/m^2 K (heat transfer coefficient), at the locations of the thermocouples shown in Fig. 32(a), where h is the heat transfer coefficient. The numerical and simulated temperature variation are in close agreement with each other.

Fig. 35(b) shows the experimental and predicted temperature variation within the paraffin for the fin configuration at the locations of the thermocouples shown in Fig. 32(b). The predicted

temperature variation at the above locations is obtained from the numerical model. The theoretical and the experimental curves are in rather close agreement one another. In the theoretical curves, the rate of temperature drop is slower during phase change and faster after phase change is completed at any location. In the experimental curves, there is not much change in the rate of temperature drop even after the lower extremity of the phase change temperature range is reached. This could be due to the solidified paraffin, that may still have some amount of latent heat even after the lower limit of the phase change temperature range is reached.
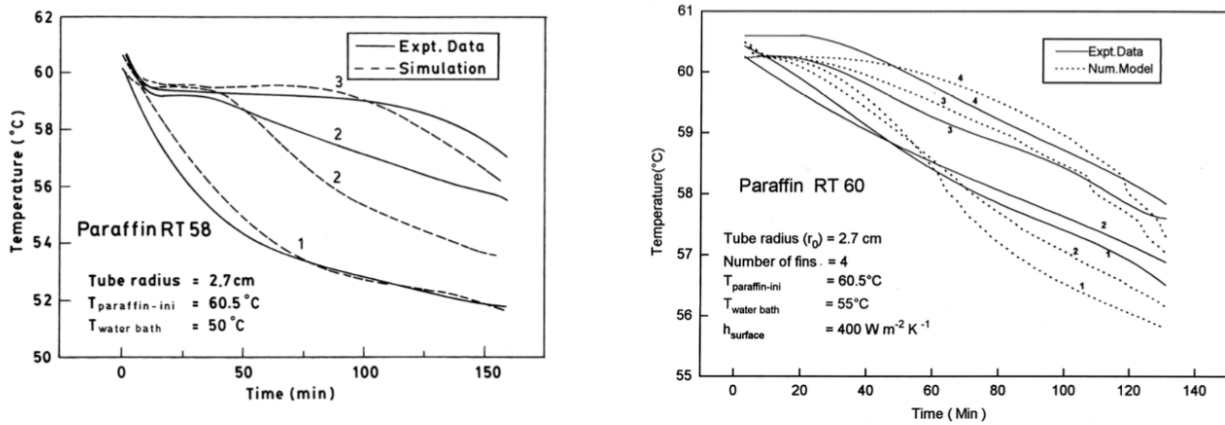
FIG. 35: (A) EXPERIMENTAL AND SIMULATED (WITH H=400 W/M^2 K) TEMPERATURE VARIATION WITHIN THE PARAFFIN FOR THE PLAIN TUBE CONFIGURATION AT THE THERMOCOUPLE LOCATIONS IN FIG 33(A); (B) EXPERIMENTAL AND PREDICTED TEMPERATURE VARIATION WITHIN THE PARAFFIN FOR THE TUBE WITH FIN AT FOUR THERMOCOUPLE LOCATIONS SHOWN IN FIG. 33 (B). [9]
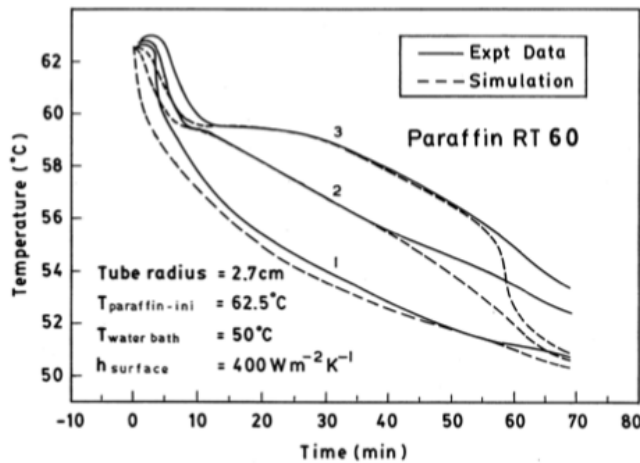
FIG. 36: EXPERIMENTAL AND SIMULATED TEMPERATURE VARIATION WITHIN THE PARAFFIN FOR THE TUBE WITH LESSING RINGS AT THREE THERMOCOUPLE LOCATIONS SHOWN IN FIG. 33(C). [9]

Fig. 36 shows both the experimental and simulated (with a value of conductivity k= 2 W/mK) temperature distribution within the paraffin for the enhancement technique employing paraffin-lessing ring mixture at the thermocouple locations shown in Fig. 32(c). So, the value of the thermal conductivity was founded to be ten times higher than the original conductivity of paraffin. This enhancement is achieved with a loss of 20% volume of paraffin for the particular tube diameter of 5.4 cm and lessing ring diameter of 1 cm. The increase in effective thermal conductivity depends on the ratio of the diameter of the tube and the dimensions of the ring and it is well known that for larger tube diameter this enhancement is much higher.
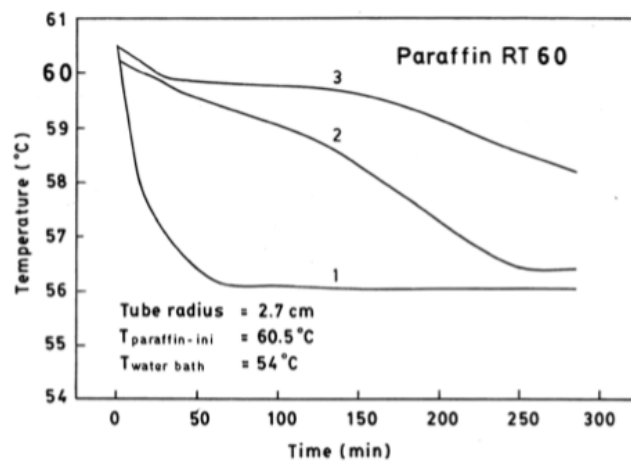
FIG. 37: EXPERIMENTAL TEMPERATURE VARIATION WITHIN THE PARAFFIN FOR THE TUBE WITH ENHANCEMENT THROUGH BUBBLE AGITATION AT THREE THERMOCOUPLE LOCATIONS SHOWN IN FIG. 32(D).[9]

Fig. 37 shows the experimental temperature distribution within the paraffin for the case employing bubble agitation at the thermocouple locations shown in Fig. 32(d). It was found that there is not much increase in heat transfer during solidification. Though the movement of bubbles induces convection during melting, the vapor pocket enters within the solid paraffin during solidification reduces the conduction heat transfer as the vapor is a poor conductor of heat.

In conclusion, it can be seen that the heat transfer enhancement with fin configuration for storage tubes and by using lessing rings in storage tanks was appreciable, and these two methods are highly suitable for solidification enhancement. The storage configuration employing bubble agitation may be suitable for applications where heat transfer enhancement for melting is required.

1.4.5 AN EXPERIMENTAL INVESTIGATION OF THE MELTING OF RT44HC INSIDE A HORIZONTAL RECTANGULAR TEST CELL SUBJECT TO UNIFORM WALL HEAT FLUX [10]

This study experimentally investigates the effect of different values of wall heat flux intensity on the melting of RT44HC (Tab 10). Experiments were performed for three constant uniform wall heat flux values (q"wall = 675, 960 and 1295 W/m^2) applied to both left and right sides of the test cell. An imaging technique was used to visualize and record the movement of the solid-liquid interface using a Canon EOS DSLR Camera. The obtained results show a strong correlation between the magnitude of wall heat flux which drives the convective heat transfer and melt fraction development in the PCM. The results also show that increasing the input power from 675 W/m^2 to 960 W/m^2 to 1295 W/m^2 reduces the total time for the melting process by 26.3% and 42.10% respectively.

This aim of this research was to experimentally investigate the effect of input wall heat flux intensity on the transient melting process in a horizontal rectangular test cell and measure the transient temperature distribution within the PCM. A horizontal test cell with a rectangular cross-section filled with organic PCM RT44HC which can be subjected to a uniform wall heat flux from both left and right horizontal sides was designed and fabricated.
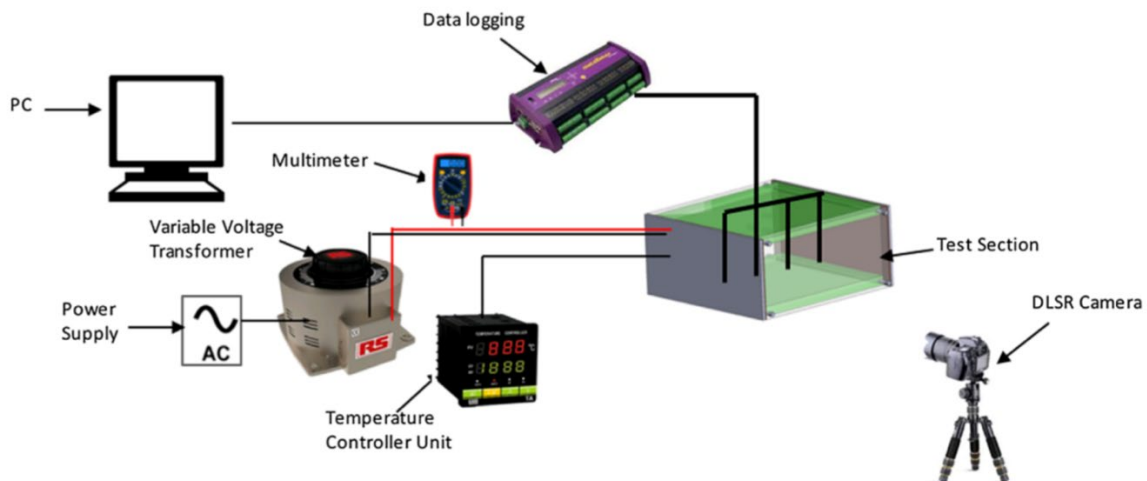
FIG. 38: A SCHEMATIC DIAGRAM OF THE DEVELOPED EXPERIMENTAL APPARATUS [10]

A schematic of the experimental setup is presented in Fig. 38. It consists of a rectangular cross section horizontally oriented PCM test cell, insulation, electric heaters, data acquisition system, DSLR camera, thermocouples, power supply and voltage transformer. The rectangular test cell was fabricated from 12mm thick transparent polycarbonate sheet (Thermal conductivity of 0.2 W/m K) with a maximum operating temperature of 150° C and density of 1190 kg/m^3 to allow observation of the development of the melt fraction of the RT44HC with time. The interior dimensions of the test cell were 200 mm width, 76 mm height and 176 mm depth as shown in Fig. 39.

Four holes in the upper side of the test cell were drilled and used to introduce the liquid PCM into the store and to provide space for thermal expansion of the liquid PCM that occurs during the melting process. Thin 2 mm copper plates with an area of 100 x 200 mm from the right and left horizontal sides of the test cell on which heating pads are mounted to provide uniform wall heat flux to the plates. The heater which could operate up to a maximum voltage of 240 VAC was connected to an adjustable AC power supply to allow heat input rate to be varied.
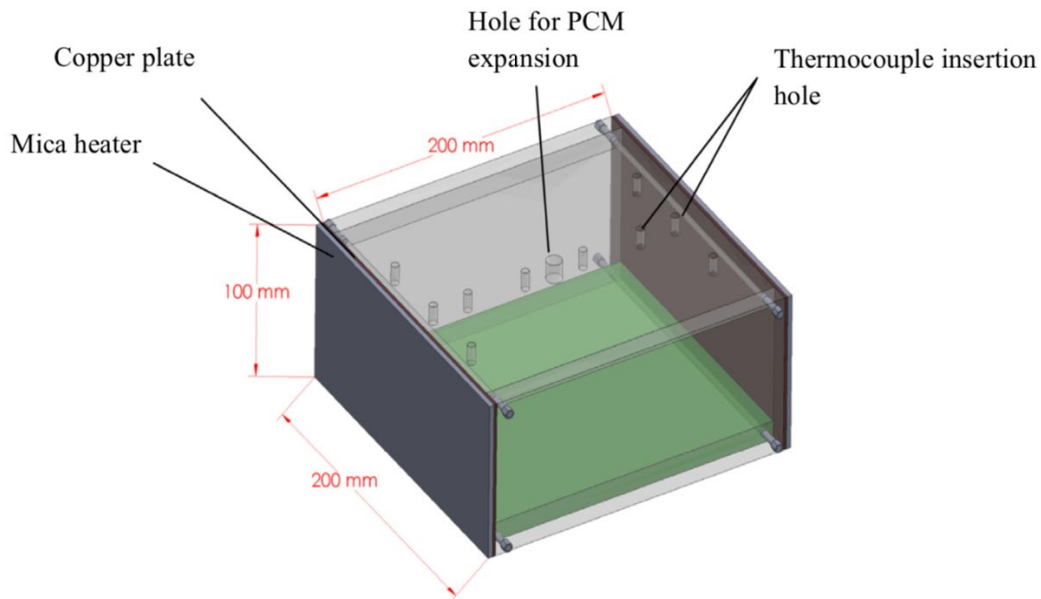
FIG. 39: SCHEMATIC DIAGRAM OF THE RECTANGULAR CROSS-SECTION TEST CELL.[10]

In the experiments, the vertical middle plane of the test cell was chosen to monitor the temperature of the PCM. 21 T-type thermocouples formed from 0.26 mm diameter wire with a calibrated

accuracy of ±0.3 ° C were placed in seven columns and three rows as shown in Fig. 40. These were connected to a data logger and temperatures were recorded during the melting process.
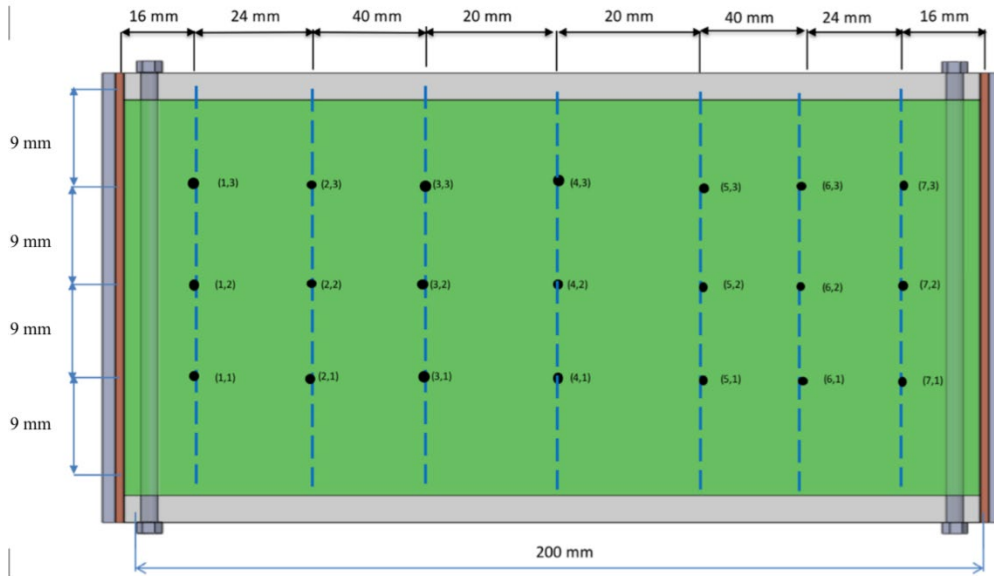
FIG. 40: THERMOCOUPLE LOCATIONS IN THE VERTICAL MID-PLANE OF THE PCM TEST CELL. [10]

TAB 10: THERMOPHYSICAL PROPERTIES OF PARAFFIN WAX RT44HC [10]

Thermal conductivity (k_s)	0.2 W/m K
Thermal conductivity (k_{liq})	0.2 W/m K
Specific heat of solid phase $(C_p)_s$	2000 J/kg K
Specific heat of liquid phase $(C_p)_{liq}$	2000 J/kg K
Density: solid phase (ρ_s)	800 kg/m^3
Density: liquid phase (ρ_{liq})	700 kg/m^3
Volumetric expansion coefficient (β)	0.00259 K^{-1}
Dynamic viscosity (μ_{liq})	0.008 kg/m s

Fig. 41 presents the temperatures measured by the thermocouples on the heated wall with a constant heat input of 27 W (corresponding to a heat flux of 675 W/m^2) applied to the left and right sides of the enclosure. It can be seen from the Fig. 41 that the process is divided into 3 phases: I) conduction phase, the heated surface temperatures in the vertical direction are similar and show a nearly linear increase with time; II) Transient Convection phase, natural convection starts to drive the hot liquid

PCM upwards due to the density difference between the hotter and cooler liquid PCM, the temperature of the hot wall remains almost constant because of onset of natural convection in the liquid PCM; III) Quasi-Steady Convection phase, as melting progress (t > 360 min) the fluid circulation continues to grow increasing the melt fraction. Natural convection becomes dominant and the heat transfer coefficient from the heated surface to the PCM increases meaning that the power input is transferred from the wall to the PCM for a smaller temperature difference, therefore, the rate of increase of local wall surface temperature slows down.

The temperatures measured with the thermocouples inside the test cell are presented in Fig. 42 for a heat flux q" = 675 W/m^2. Fig. 42(a) shows that when the PCM melting temperature is achieved the rate of temperature increase in the first column of thermocouples is much higher than those of second and third columns (Fig. 42 b and c). This can be explained by the fact that the heat transfer to the solid PCM surrounding the first column of thermocouples is high due to convection in the melt phase and heat conduction through a thin layer of solid PCM surrounding the thermocouples.
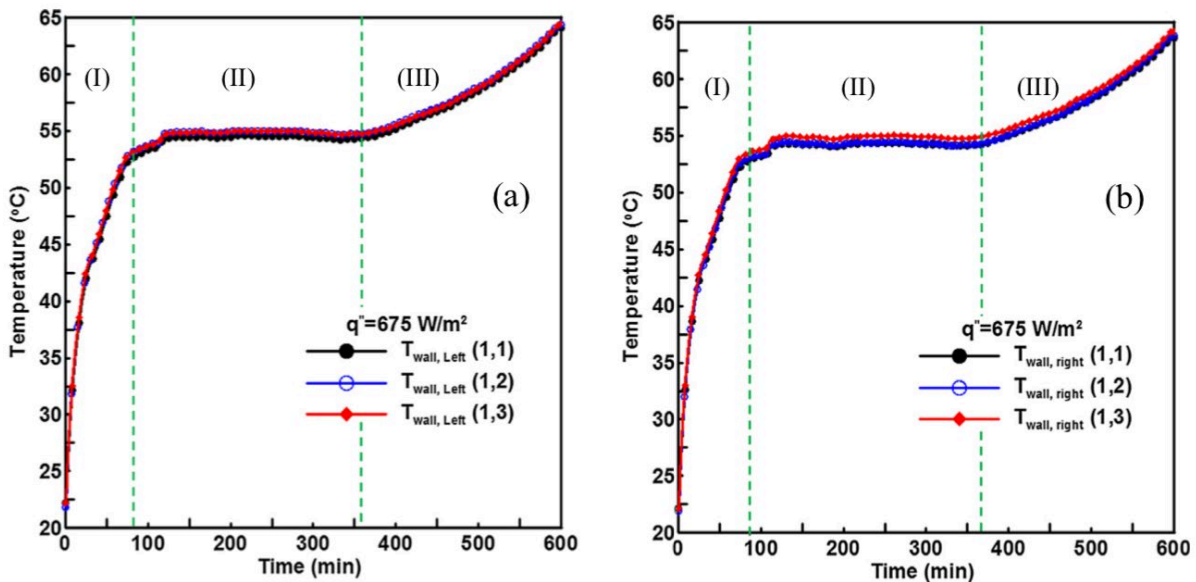
FIG. 41: MEASURED HEATED WALL SURFACE TEMPERATURES IN THE VERTICAL DIRECTION FOR A HEAT FLUX, Q" = 675 W/M^2, (A) LEFT WALL. (B) RIGHT WALL. (I) CONDUCTION PHASE (II) TRANSIENT CONVECTION PHASE AND (III) QUASI-STEADY CONVECTION PHASE. [10]
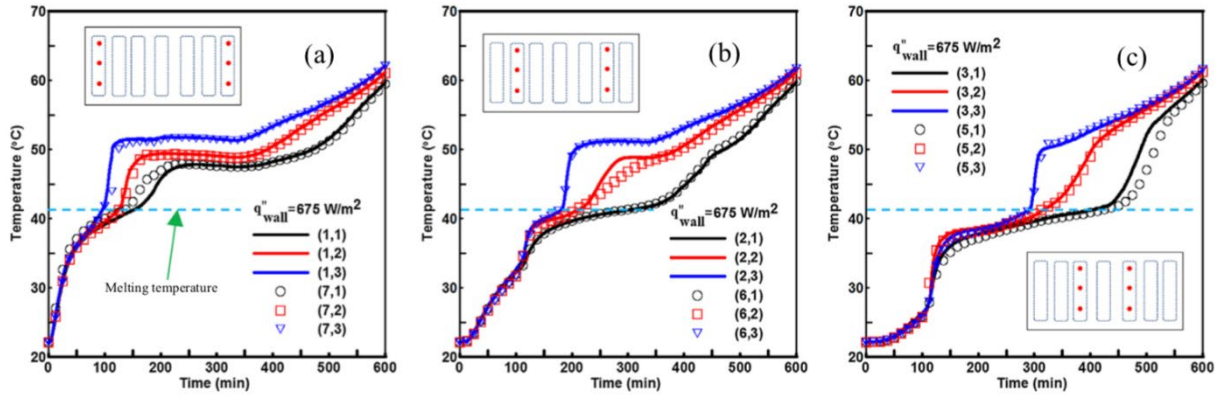
FIG. 42: MEASURED TEMPERATURES AT THE 18 THERMOCOUPLE LOCATIONS WITHIN THE TEST CELL WITH TIME FOR A WALL HEAT FLUX OF Q" = 675 W/M². [10]

From Fig. 43(a) it can be seen that as the wall flux increases, the time for total melting decreases, this is expected due to the increased rate of heat transfer to the enclosure. The increase in power input also led to an increase in the average temperature of both the PCM and the heating surface. Increasing the input power from 675 W/m2 to 960 W/m2 to 1295 W/m reduces the total time for the melting process by 26.3% and 42.10% respectively.

Fig. 43(b)shows the temperature history along the hot wall at the three constant heat flux values. It can be observed from Fig. 43(b) that the hot wall temperature rises linearly with time following the initial start-up. This shows that melting is determined by conduction in the early stages. The conduction dominated period lasts for 50 min, 75 min and 100 min for heat fluxes of 1295, 960 and 675 W/m², respectively. The wall temperatures rise to 63° C, 57° C and 53° C during conduction dominated phases. Afterwards, the temperature of the hot wall remains almost constant because of the onset of natural convection in the melting PCM. As time progresses, the temperature of the hot wall starts to increase slowly until the end of the melting process.
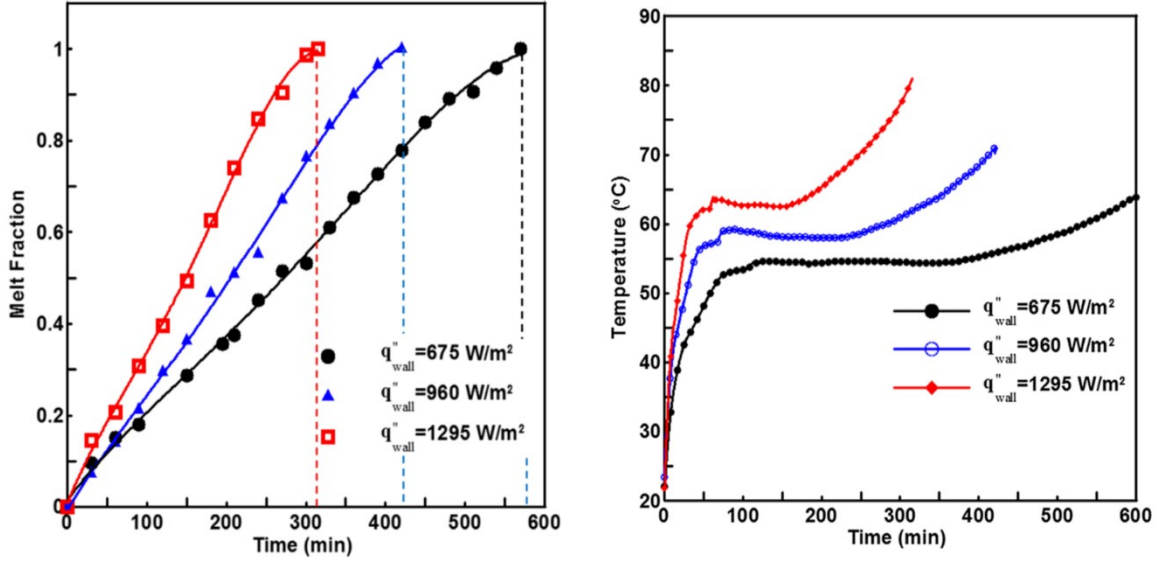
FIG. 43: (A) MELT FRACTION VERSUS TIME FOR THREE DIFFERENT WALL HEAT FLUXES. (B) THE TEMPERATURE HISTORY ALONG THE HOT WALL FOR THREE DIFFERENT WALL HEAT FLUXES. [10]

Fig. 44 shows the calculated increase in sensible, latent and total stored energy within the test cell at every 30 min for different wall heat flux values. As can be seen in Fig. 44, the contribution of latent heat to the total heat absorbed is much greater than sensible heat. As expected for all values of wall heat flux, the maximum values of absorbed latent heat are equal since they are a function of the test cell volume which is constant for all experiments. It can be observed that the values of the maximum total energy absorbed change slightly due to the change of hot wall temperature which is the result of different values of heat flux.

The authors calculated sensible and latent heats at every data acquisition period, in order to determine the amount of energy absorbed. The used the following equations:

$$Q_{sensible,PCM}(t) = \int_{V_{liq}(t)} \rho_s C_s (T_{m1} - T_i) dV_{liq} + \int_{V_{liq}(t)} \rho_{liq} C_{liq} (T_{mean\ liq} - T_{m2}) dV_{liq} + \int_{V_{liq}(t)} \rho_s C_s (T_{mean\ s} - T_i) dV_s \quad (1)$$

Where T_{m1} is the onset of melting temperature [° C] T_{m2} the endset of melting temperature [° C], ρ is the density [kg/m³], C is the specific heat at constant pressure [kJ/kg K]; $T_{mean\ liq}(t)$ and $T_{mean,s}(t)$ represent the instantaneous mean temperatures of liquid and solid phases, respectively which were calculated by averaging the temperatures of thermocouples located in each region as follow:

$$T_{mean\ liq}(t) = \frac{1}{n_l(t)}\sum_{i=1}^{n_{liq}(t)} T_i \tag{2}$$

$$T_{mean\ s}(t) = \frac{1}{n_s(t)}\sum_{i=1}^{n_s(t)} T_i \tag{3}$$

where n_l and n_s are the numbers of thermocouples located in each of the liquid and solid regions of the PCM at each measurements time, respectively. The latent heat linked to the thermocouple is given by the following equation:

$$Q_{latent}(t) = f\, M_{PCM} h_{latent} \tag{4}$$

where f is the value of the liquid fraction percentage, M_{PCM} is the mass of PCM [kg], h_{latent} is the latent heat [kJ/kg]

The total absorbed energy by the PCM for each thermocouple region is calculated by the sum of the latent and sensible heats which have been estimated by Eq (1) and (4):

$$Q_{total,PCM}(t) = Q_{sensible,PCM}(t) + Q_{latent,PCM}(t) \tag{5}$$
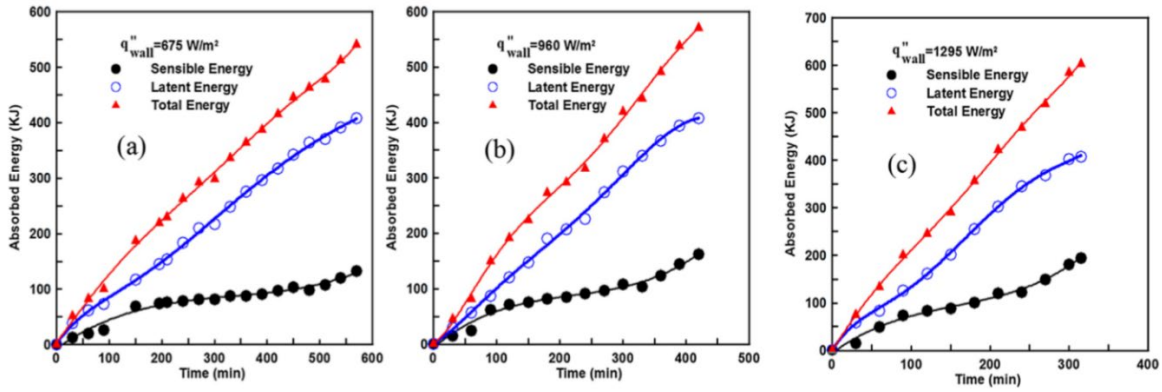
FIG. 44: CALCULATED SENSIBLE HEAT, LATENT HEAT AND TOTAL HEAT ABSORBED WITH TIME IN THE PCM TEST CELL FOR WALL HEAT FLUX VALUES OF (A) Q" = 675 W/M², (B) Q" = 960 W/M², AND (C) Q" = 1295 W/M². [10]

In conclusion, it can be seen from this study, that:

1) At higher values of wall heat flux, the average temperature of the heater's surface and the PCM increased and the total melting time reduced.

2) Conduction is the dominant mode of heat transfer during the early stage of melting which is followed by a short transition period before convection dominates the remainder of the melting process.

3) Increasing the input power from 675 W/m^2 to 960 W/m^2 to 1295 W/m^2 reduces the total time for the melting process by 26.3% and 42.10% respectively.

2 EXPERIMENTAL CHARACTERIZATION OF PCM RT35

2.1 EXPERIMENTAL EQUIPMENT

In this chapter it is given the list of the materials, tools and softwares used in the experiments, so that it is possible to understand the work that done, whose aim was the characterization of a precise PCM.

2.1.1 PCM RT 35

FIG. 45 RUBITHERM PARAFFIN RT 35 [18].

The thermal energy storage (TES) is a proven efficient way to smooth the discrepancy between the energy supply and the demand and it is becoming increasingly significant in the heating and cooling of buildings. Latent heat thermal energy storage (LHTES) is a promising way to store thermal energy. As a matter of fact, using a phase change material (PCM) is quite attractive due to high storage density and the relatively constant heat transfer fluid (HTF) temperature. Several PCMs have been identified as latent heat storage means to low and increase the temperature. Paraffin is one of most interesting PCM which can be used for LHTES because it is safe, reliable, relatively cheap, and non-corrosive.

The following study shows is an experimental investigation of the melting process on the RT35 paraffin-based PCM melting process, with the aim of creating a set up useful to characterize other kind of PCMs, too. RT35 paraffin-based (Fig. 45) is made by Rubitherm., its properties are shown in Fig. 46.

FIG. 46 RT35 PCM DATASHEET PROPERTIES [18].

RT35 main properties are: the high thermal energy storage capacity, the heat storage and release of heat which take place at a relatively constant temperature, no supercooling effects. Further, thy are chemically inert, and they have a long-lives with stable performance during the phase change cycles.

Paraffins show some undesirable properties such as: low thermal conductivity, they are not compatible with plastic container and they are also moderately flammable. All these undesirable effects can be partly eliminated by modifying the wax and the storage unit. For instance, the thermal conductivity can be increased adding metal foams to the PCMs.

Measured with 3-layer-calorimeter.
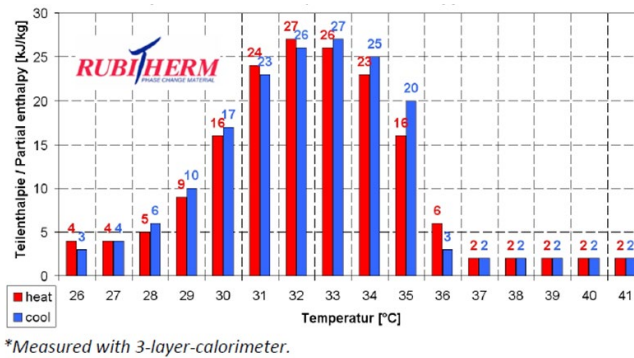
FIG. 47 HEAT STORAGE CAPACITY GIVEN BY RUBITHERM DATASHEET [18].

Looking at the Rubitherm datasheet (Fig. 46) it is possible to compare the stored thermal energy of PCM with water. Considering a volume of 135.4 mm x 80 mm x 70 mm = 0.758 liters, the variation of c_p in Fig. 47, and a range of temperature between 20° C and 50° C it is possible to calculate the thermal energy stored:

- Thermal energy stored with PCM: $\rho\, V\, c_p\, \Delta T = (0{,}758/1000) * 860 * (4 * (27\text{-}20) + 5 + 9 + 16 + \dots + 2\,(50\text{-}36) = 134{,}6$ kJ

- Thermal energy stored with water: $\rho\, V\, c_p\, \Delta T = 997 * 0{,}758 * 4{,}186 * (50\text{-}20) = 94{,}9$ kJ

Using PCM it is possible to increase the stored thermal energy by around 42% considering the same volume. To store the same amount of thermal energy the volume is reduced by 30%: this is another observation that is another observation which can convince about the usefulness of PCMs.
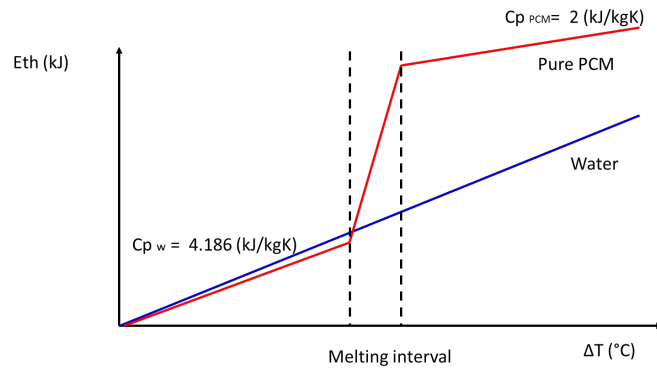
FIG. 48 PCM AND WATER HEAT CAPACITY VALUES.

2.1.2   METAL FOAMS

Aluminum and copper foams

Metal foams are a class of cellular structured materials with open cells randomly oriented and mostly homogeneous in size and shape. Aluminum and copper foams are used with the aim of increasing the conductivity of PCM and to see the differences between them. The characteristics of the aluminum and copper foams are shown in Tab 11[16].

TAB 11: RACEMAT BV DATASHEET OF ALUMINUM AND COPPER FOAMS [16].

	Aluminum	Copper
Range of pores [mm]	152-254	279-406
Estimated average pore [mm]	2,4	1,4
Average Density [g/cm³]	0,14	0,3-0,5
Relative Density	5%	5%
Porosity	95%	95%
Estimated average specific surface [m²/m³]	500	500
Thermal conductivity [W/mK]	170	385

2.1.3 ROLAND MDX-40A

Roland MDX-40A is a milling machine, which is a machine that works removing chip. The cutting motion is given by the multi-cutting tool called cutter, while the feed motion is given by the workpiece holder table. By milling it is possible to carry out various processes such as cutting of gears, grooves, and face milling. This type of milling machine (Fig. 49) was used to build the polycarbonate box inside which the PCM RT35 was studied and characterized.

FIG. 49 THE ROLAND MDX40-A MILLING MACHINE.

To ensure that the machine receives information from the PC, the SRP and VPanel software must be installed.

2.1.4 SRP PLAYER

SRP software is the software that the user needs to generate an STL file from a 3D CAD drawing and then to convert it into a PRN file software (a printer which will be later used with the software

VPanel). With SRP Player there are five steps that the user has to satisfy to ensure the export of the project in the STL format:

1. Model size and orientation: in this first step the user can view the model of the piece to be machined, he can decide to change its size and how orient it in the space.

2. Type of milling: it is possible to choose whether to use a type of cut that favors the surface finishing, (while lengthening the processing time) or a cut which lasts less and gives out a lower surface quality than the previous cut. The user is then asked to indicate whether the model on which he intends to work is mostly made up of flat or curved surfaces. The last step is the choice to cut the surface only at the top or both at the top and at the bottom.

3. Create a tool path: you can indicate the material you are working with, the dimensions of the starting piece and where the model is positioned. After satisfying the previous requests, the software will create the path that the tool will follow to complete the machining. It is also possible to choose whether roughing or finishing the piece and the type of tip to for these processes.

4. Results preview: this section let the user know the time the process will take.

5. Run cut: the last step allows the user to export the file in the PNG format, by the software VPanel. The user is also required to specify where he wants the cutting of the piece to start.

2.1.5   V-PANEL

VPanel is a software used to center the piece which is going to be machined: it gives a 3D reference to the milling machine and, subsequently, it imports the PRN file previously created with SRP Player.

2.1.6   AUTODESK FUSION 360

Autodesk Fusion 360 is a 3D CAD / CAM cloud-based software for designing, developing and producing. It combines industrial and mechanical design, collaboration and sharing of project data, and CAM tools all in a single package. It was used to draw the polycarbonate cases for the experiments presented in this thesis. In Fig. 50 it is shown the draw of the first case. [23]
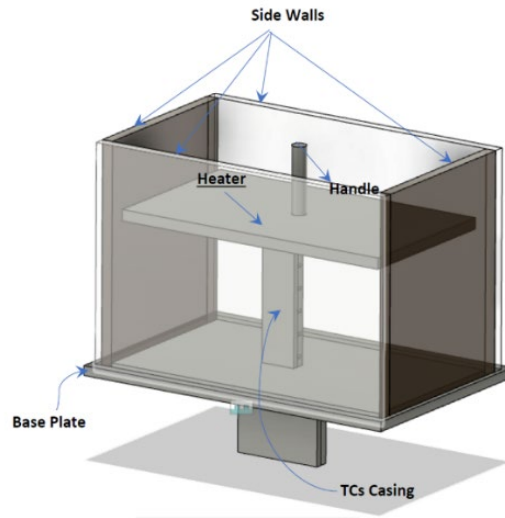
FIG. 50 CASE USED TO STUDY THE MELTING OF PCMS.

2.1.7 AUTOTRANSFORMER

FIG. 51 SINGLE-PHASE TRANSFORMER.

The autotransformer, shown in Fig. 51, is an electrical transformer with only one winding. A very handy and compact single-phase autotransformer, with continuous variation of the transformation ratio, was used in the laboratory. It consists of a toroidal ferromagnetic core on which the conductor that constitutes the winding is arranged in a helix in a single layer; the ends of the winding lead to

two terminals, while a movable brush in contact with the conductor leads to a separate terminal. This single winding is "tapped" at various points along its length to provide a percentage of the primary voltage supply across its secondary load. Then, the autotransformer has the usual magnetic core but there is only one winding, which is common both to the primary and to the secondary circuits. [21]

Therefore, in an autotransformer the primary and the secondary windings are linked together both electrically and magnetically. The main advantage of this type of transformer design is that, for the same VA rating, it is cheaper, but the biggest disadvantage is that it does not have the primary/secondary winding insulation of a conventional double wound transformer. [21]

This tool was used as power supply to the system, to heat an electrical resistance used 220 V.

2.1.8 AMMETER
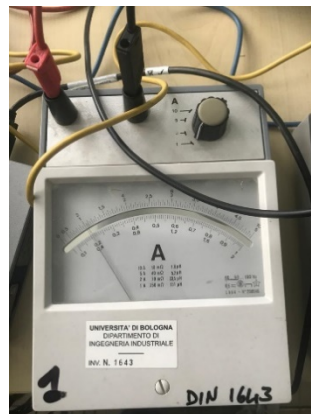
FIG. 52 AMMETER.

The ammeter is an instrument to measure either direct or alternating electric current, in amperes. An ammeter can measure a wide range of current values because at high values only a small portion of the current is directed through the meter mechanism; a shunt resistance put in parallel with the meter carries the major portion of current. [21]

2.1.9 Voltmeter

FIG. 53 VOLTMETER.

When analyzing the operations of the electrical and electronic circuits or trying to understand why a circuit does not work as expected, it could be necessary to use a voltmeter to measure the voltage levels. The voltmeters come in many shapes and sizes, they can be analogue or digital devices or parts of digital multimeters more commonly used today.

Voltmeters can be also used to measure DC voltage as well as sinusoidal AC voltages but the introduction of a voltmeter into a circuit as a measuring instrument can interfere with its steady state conditions.

As its name implies, a "voltmeter" is an instrument used to measure the voltage (V), that is the potential difference present between any two points within a circuit. To measure a voltage, the voltmeter must be connected in parallel with the component whose voltage you wish to measure. Voltmeters can be used to measure the voltage drop across a single component, or the sum of voltage drops across two or more components within a single circuit.

In the following experiments it was used to better control the voltage supplied to the system. [21]

2.1.10 T-TYPE THERMOCOUPLES [20]

A thermocouple (TC) is a sensor that measures temperature. It is made of two different types of metals, joined together at one end. When the junction of the two metals is heated or cooled, a voltage is generated and can be correlated to a temperature value. A TC is a simple, robust and cost-effective tool used in a wide range of temperature measurement processes. TCs are manufactured in a variety of styles, such as TC probes, TC probes with connectors, transition joint TC probes, infrared TCs, bare wire TCs or even just TC wires.

TCs are commonly used in a wide range of applications. Thanks to the several existing models and technical specifications, but it is extremely important to understand their base structure, functionality, working ranges to better determine the proper type of TC for the precise application we are going to approach.

TCs are available in different combinations of metals or calibrations. The most common are the "*base metal*" thermocouples known as J, K, T, E and N-type TCs. There are also high temperature calibrated TCs – the noble metal TCs –known as Types R, S, C and GB. Each calibration has different temperature ranges and environments and, furthermore, the maximum temperature varies with the diameter of the wires used in the TC: a very thin TC may not reach the full temperature range. All types of thermocouples available on the market are shown in Fig. 54, as it can be seen, T-type thermocouples result to be the proper ones for the experiments proposed below.

Common Thermocouple Temperature Ranges

Calibration	Temperature Range	Standard Limits Of Error
J	0° to 750°C (32° to 1382°F)	Greater of 2.2°C or 0.75%
K	-200° to 1250°C (-328° to 2282°F)	Greater of 2.2°C or 0.75%
E	-200° to 900°C (-328° to 1652°F)	Greater of 1.7°C or 0.5%
T	-250° to 350°C (-418° to 662°F)	Greater of 1.0°C or 0.75%

FIG. 54 DATA SHEET OF J, K, E, T THERMOCOUPLES [20].

2.1.11 LabVIEW and DAQ Device

LabVIEW is a systems engineering software for applications that require test, measurement, and control with rapid access to the hardware and data insights. In the Thesis experiments LabVIEW was used with the data acquisition (DAQ), shown in Fig. 55, this tool let the user acquire analogical or digital signals such as voltage, current, temperature, pressure, vibrations or sounds. A DAQ system consists of sensors, a DAQ measurement hardware, and a computer with the application software. [22]

FIG. 55 THE NATIONAL INSTRUMENTS DAQ DEVICE.
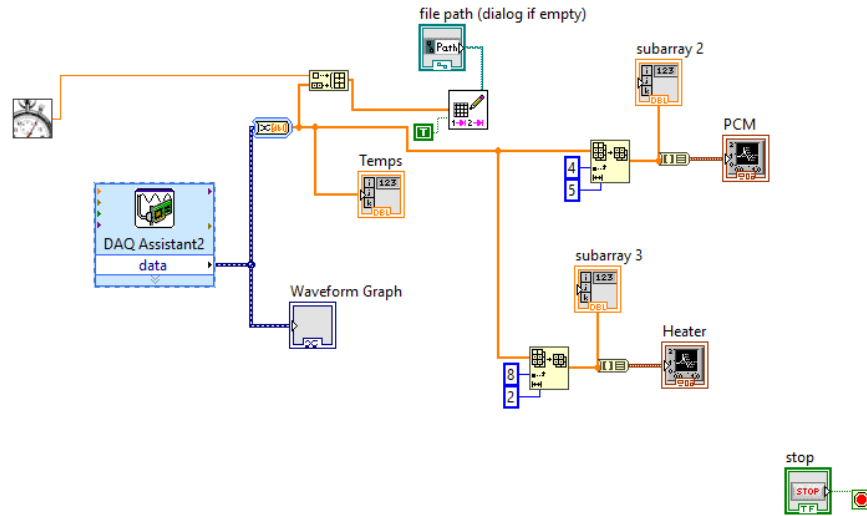
FIG. 56 LABVIEW BLOCK DIAGRAM USED TO ACQUIRE DATA.

LabVIEW was used to acquire the temperature values from the TCs and to create text files the values of which would have subsequently been plotted with Matlab. Fig. 56shows the LabVIiEW block diagram designed to acquire the temperature data: using the DAQ Assistant function, it is possible to add the number of TCs that the user needs for the test. Fig. 56illustrates the test for which there were needed 5 TCs to record the temperatures inside the PCM, and 2 TCs for the heater temperature. The *high solution relative seconds* function, indicated with the clock block in Fig. 56, is a millisecond time counter. A vector with all the time and temperature values is created in a text file with "*write delimited spreadsheet*" function and then saved in a folder.

2.1.12 MATLAB

MATLAB (MATrix LABoratory) is a programming environment for scientific applications, numerical analysis and simulation of dynamic systems; MATLAB was used to postprocess THE text files generated with LabVIEW. The *filepath* function, shown in Fig. 57, indicates to the software where to find the text files to read (where the experimental data have been saved). The *filename* function communicates to MATLAB the name of the text file to process. With the code "*time*" data(:,1) the user considers all the elements present in the first column of the text file named above, "*T_tc*" (TCs temperature) refers to all of the elements from the second to the sixth columns in the text file, "*T_heat*" (heater temperature) refers to all of the elements of the seventh and eighth columns, "*T_air*" refers to nineth column.

75

```matlab
 filepath = 'C:\Users\ADMIN\Desktop\PCM_Morena\Jimmy\'; %questo è il

%    filename = 'RT35_281020_Jimmy_3.0.txt';        %JIMMY 3.0
%    filename = 'RT35_281020_Jimmy_3.0_cool.txt';   %JIMMY 3.0 cool
%    filename = 'RT35_11120_Jimmy_3.1_cool.txt';    %JIMMY 3.1
     filename = 'RT35_11120_Jimmy_3.1.txt';    %JIMMY 3.1

data = Mat_tc(strcat(filepath,filename), [1, Inf]); %così richiamo l
% Strcat mi serve a combinare due stringhe di testo che sono quelle

time = data(:,1); %in secondi
eff_time = (time-time(1))./3600; %sottraggo il T_tc n-esimo al T_tco

T_tc = data(:,2:6);


T_heat = data(:,7:8);
T_air = data(:,9);
T_melt = 35;
```

FIG. 57 EXTRACT OF MATLAB FILE.

RT35_281020_Jimmy_3.0 - Blocco note di Windows

File   Modifica   Formato   Visualizza   ?

781518.985	23.266	23.444	23.373	23.403	23.178	23.124	23.128	20.536
781521.059	23.256	23.429	23.360	23.401	23.168	23.127	23.124	20.518
781522.817	23.267	23.439	23.370	23.405	23.185	23.128	23.133	20.519
781524.584	23.257	23.422	23.356	23.385	23.165	23.123	23.130	20.504
781526.347	23.257	23.418	23.367	23.388	23.168	23.129	23.118	20.510
781528.108	23.265	23.440	23.367	23.409	23.174	23.124	23.136	20.523
781529.862	23.260	23.428	23.370	23.401	23.168	23.117	23.122	20.509
781531.627	23.266	23.425	23.375	23.398	23.180	23.119	23.140	20.515
781533.393	23.272	23.419	23.367	23.395	23.174	23.116	23.122	20.516
781535.160	23.257	23.420	23.362	23.397	23.173	23.111	23.123	20.511
781536.925	23.259	23.429	23.367	23.404	23.179	23.123	23.131	20.519
781538.693	23.254	23.428	23.372	23.401	23.171	23.119	23.128	20.525
781540.457	23.276	23.450	23.374	23.414	23.183	23.135	23.138	20.534
781542.223	23.260	23.422	23.368	23.390	23.163	23.117	23.119	20.522
781543.990	23.264	23.438	23.366	23.405	23.168	23.120	23.132	20.528
781545.752	23.269	23.429	23.375	23.402	23.176	23.121	23.130	20.527
781547.520	23.251	23.431	23.369	23.399	23.174	23.131	23.127	20.526
781549.286	23.269	23.426	23.364	23.397	23.172	23.125	23.134	20.517
781551.051	23.273	23.436	23.374	23.416	23.176	23.138	23.132	20.537
781552.817	23.267	23.440	23.377	23.415	23.186	23.135	23.136	20.535
781554.583	23.260	23.432	23.368	23.399	23.180	23.122	23.127	20.532
781556.347	23.266	23.440	23.366	23.399	23.168	23.131	23.140	20.526
781558.112	23.262	23.427	23.364	23.394	23.170	23.118	23.122	20.517
781559.877	23.247	23.425	23.361	23.401	23.172	23.116	23.115	20.508
781561.643	23.272	23.439	23.371	23.410	23.184	23.131	23.149	20.529
781563.409	23.247	23.428	23.358	23.396	23.162	23.113	23.120	20.520

FIG. 58 EXTRACT OF TEXT FILE WHERE ALL TEMPERATURES ARE SHOWN.

The command plot (x, y), in Fig. 59, was used to plot the time and the temperature respectively as x and y. What is interesting to identify is the melting point and was put in evidence with the find function these temperature conditions: ind=(find(T_tc(:,i)>34,9 & T_tc(:,i)<35,1)). When a TC reached 35° C, the reaching of the melting point would have been represented with a vertical dashed line in the graph.

```matlab
%% *** PLOT ***

[r c] = size(T_tc); %specifico che le dimensioni della nuova matrice devono esse
pc={'r.','g.','b.','c.','k.','m.','r*','g*','b*','c*','k*','m*'}; %colori e simb
pc_l={'r--','g--','b--','c--','k--','m--','r--','g--','b--','c--','k--','m--'};
figure('DefaultAxesFontSize',16); %è la funzione con cui creo l'immagine finale

% subplot(2,1,1)%per creare un plot sotto il mio plot principale


for i = 1:(c)
plot(eff_time,T_tc(:,i),pc{i},'DisplayName',strcat('T',num2str(i))); %uso il com
%delle tc prendendo tutte le righe da ogni colonna (una colonna per iterazione),
%Il nome sarà una combinazione di stringhe che sono i nomi delle tc e i
%numeri di riferimento (perciò uso strcat) ma i numeri devono essere
%convertiti in stringhe, ecco perché uso num2str(i).
hold on %per visualizzare le curve che vengono fuori da ogni iterazione su un un

ind = (find(T_tc(:,i)>34.9 & T_tc(:,i)<35.1)); %ciò che mi interessa individuare
%una riga che raccoglie gli indici degli elementi presenti nella matrice delle t
time_melt = min(eff_time(ind)); %individuo i tempi corrispondenti agli indici ap
    if (time_melt~=0) %serve inserirlo perché in alcuni test non si ragiunge la
        plot(time_melt.*ones(100,1),0:1:99,pc_l{i}) %voglio un plot che mi mostr
        %(perché ho deciso di far arrivare la linea fino a 100), la mia y
        %deve essere una riga della stessa dimensione di x, quindi dico che
        %deve andare da 0 a 99 con passo di 1. Poi arricchisco alla
        %funzione plot la definizione di come voglio graficamente le linee.
    end


end

legend('show');
plot(eff_time,T_heat(:,1),'DisplayName','T_{heat}');
plot(eff_time,T_melt.*ones(1,length(eff_time)),'DisplayName','T_{melt}'); %non p
%di x moltiplicando il valore costante che ho di y per una riga di 1 con il
%comando ones e a questa riga do la lunghezza (length) del valore di x.
plot(eff_time,T_air,'DisplayName','T_{air}');
```

FIG. 59 EXTRACT OF MATLAB FILE, PLOT FUNCTION.

2.1.13 ARDUINO

```
relayonoff
int inl = 7;
int thour=24;
int tmsec=thour*60*60*1000;
void setup() {
  pinMode(inl, OUTPUT);
  digitalWrite(inl,LOW);
}
void loop() {
  //digitalWrite(inl, LOW);
  //delay(3000);
  //digitalWrite(inl, HIGH);
  //delay(tmsec);
}
```

FIG. 60 EXTRACT OF ARDUINO CODE.

Arduino was used to control a relay, by remote switching on and off the autotransformer. In this way, if the temperatures were too high and it was possible to face risky situation, the user could turn off the system from home.

The *pin mode* function configures the specified pin to behave either as input or as output.

The *digital Write* command write a HIGH or a LOW value in a digital pin. If the pin has been configured as an OUTPUT with pinMode(), its voltage will be set to the corresponding value: 5V (or 3.3V on 3.3V boards) for HIGH, 0V (ground) for LOW.

If the pin is configured as an INPUT, digitalWrite() will enable (HIGH) or disable (LOW) the internal pullup on the input pin. It is recommended to set the pinMode() to INPUT_PULLUP to enable the internal pull-up resistor.

If you do not set the pinMode() to OUTPUT, and connect an LED to a pin, when calling digitalWrite(HIGH), the LED may appear dim. Without explicitly setting pinMode(), digitalWrite() will enabled the internal pull-up resistor, which acts like a large current-limiting resistor [17].

2.2 Melting of pure RT35 PCM with no insulation

2.2.1 Experimental setup

A schematic diagram of the experimental equipment is shown in Fig. 61. The test case consists of a polycarbonate container with a rectangular base, filled with the paraffin phase change material made by Rubitherm, the RT35 PCM: the data sheet of this material is given in Tab 11. The temperature inside the specimen is measured by T-type TCs distributed at different heights. The positions of the TCs are shown in Tab 13, 6 TCs were placed along the central axis of the case, 2 TCs (T_{h1} and T_{h2}) close to the heater and 1 TC was used to record the air temperature in the room. TCs data were acquired by the National Instruments acquisition equipment already discussed. An Ammeter was connected to the system (as can be seen in Fig. 62 to control the power supply of the Variac (the autotransformer).
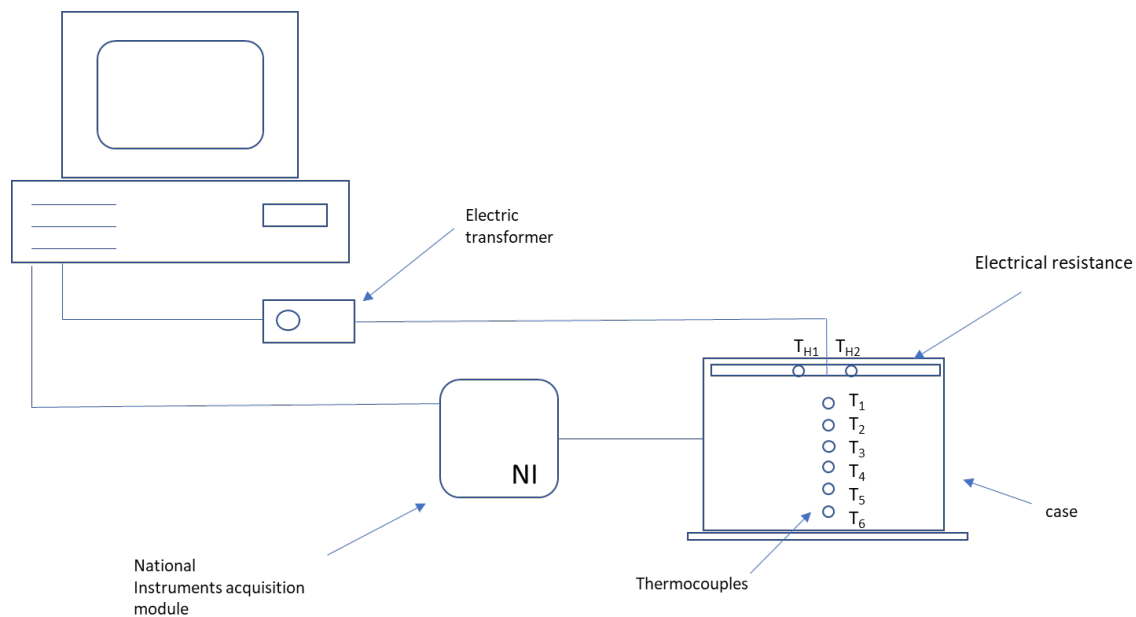
FIG. 61 SCHEMATIC DIAGRAM OF EXPERIMENTAL SETUP.
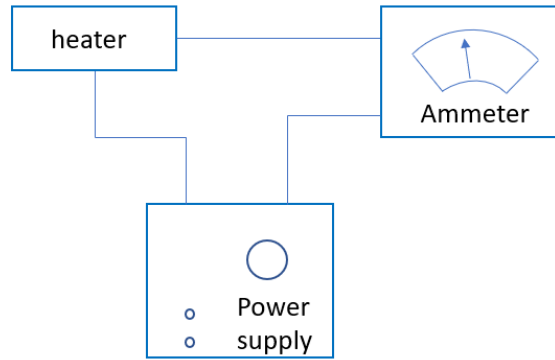
FIG. 62 POSITION OF AMMETER.

TAB 12: DATA SHEET VALUES OF THE RUBITHERM RT35 PCM.

Properties	Values
ρ_{liq} [kg/l]	0,77
ρ_{sol} [kg/l]	0,86
Heat storage capacity [kJ/kg]	0,2
Volume expansion [%]	12,5
Melting Area [° C]	29-36
C_p [kJ/kg K]	2
Heat conductivity [W/m K]	0,2

TAB 13: POSITIONS OF THERMOCOUPLES

Tc	H1	H2	1	2	3	4	5	6
x (mm)	70	70	49	40	31	20	11	2
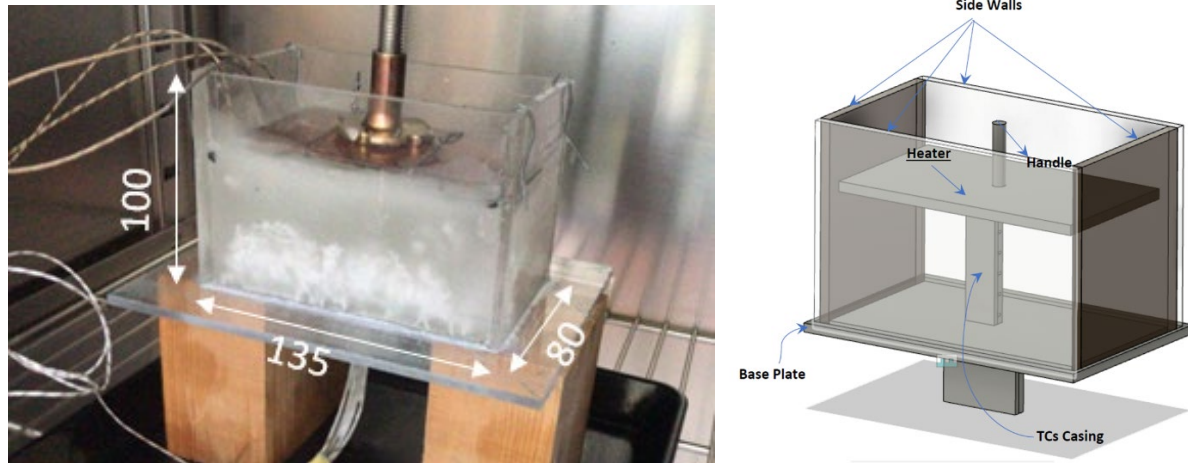
FIG. 63 (A) CASE FILLED WITH SOLID PCM (B), CAD DRAW OF THE CASE.

The case was 135 mm high, 100 mm wide and 80 mm deep, as shown in Fig. 63(a). The voltage was set to 40 V with the Variac and an electrical resistance, above the PCM, supplied heat for 8 hours (pure conduction experiment) with a constant heat flux. In 5h 30 min the melting front reached the third TC with a temperature of the heater which arrived at 80° C, as can be seen in Fig. 65. The temperatures recorded are shown in Fig. 65. The y-axis indicates the temperature, the x-axis indicates the time, the recordings of heater TCs are shown by a thin light blue line at the top, the results of the first TC under the heater is the red one, for the second it's the green one, for the third it's the blue one, for the third the light blue one and for the fifth it's the black one, that remain all time nearly constant. Fig. 65 also shows the trend of the heat flux, calculated as:

$$q = -k\frac{\partial T}{\partial x} \qquad (6)$$

Where k is the conductivity of PCM, $\partial T/\partial x$ is the infinitesimal variation of temperature with space. Fig. 65(b) shows that the heat flux results to follow the same trend for all the TCs, and it is almost constant for the whole duration of the experiment. The vertical dashed lines in Fig. 65 (a) show that the TC has reached the melting temperature of 35° C.
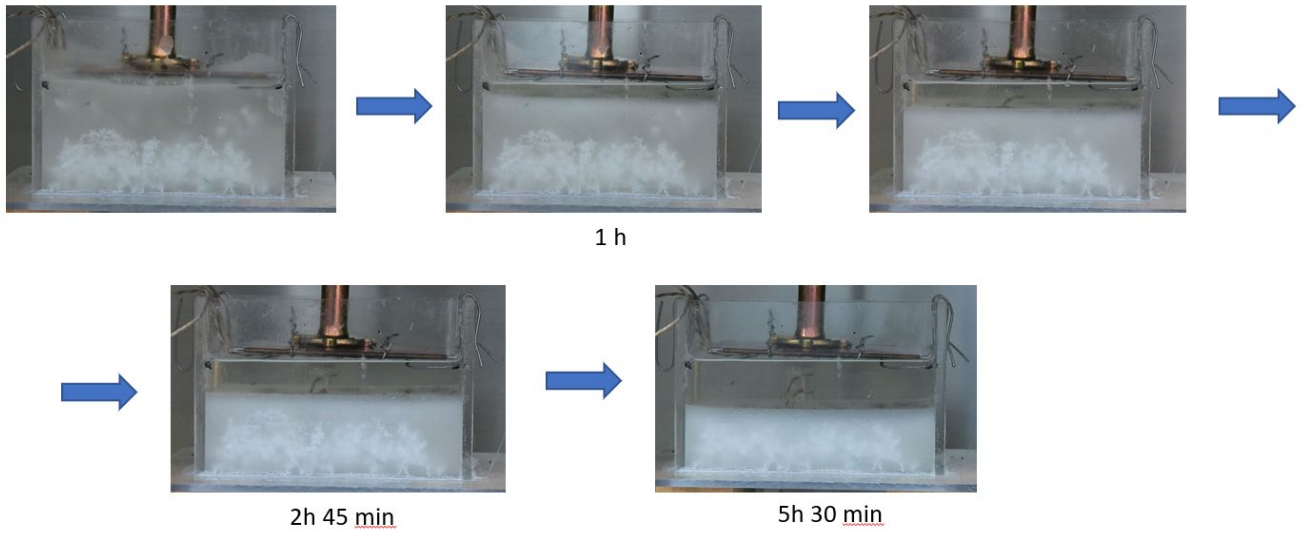
FIG. 64 THE PROGRESS OF THE PCM MELTING FRONT.
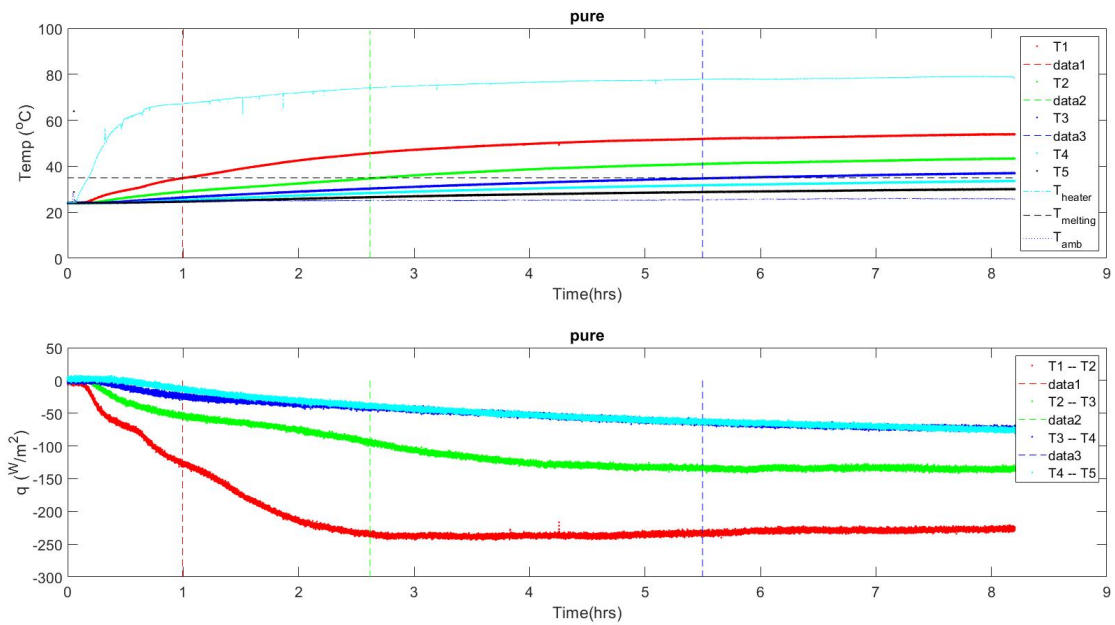
FIG. 65 (A) VARIATION OF TEMPERATURES ACQUIRED BY THERMOCOUPLES (B) TREND OF THE HEAT FLUX FOR THE WHOLE DURATION OF EXPERIMENT.

Another observation is that the melting front reached the first TC very quickly (1 hour), the second one in 1h 30 min, the third one in 3 hours. It could be observed that the losses in this experiment were very high and the heat flux was not enough to melt all the PCM. The melting front arrived at

a point where the heat provided balanced the losses. This is due to the very low conductivity of the PCM (0.2 W/m K) and the very high value of the global heat transfer coefficient (U $\approx$ 2 [W/m^2 K]). It can be calculated with an energy balance inside the case:

$$\rho c_p \frac{\partial T}{\partial \tau} = q'' - U\Delta T \tag{7}$$

Where ΔT is the difference between the temperature inside the case and the ambient temperature. When the melting front arrived at the third TC, the time to melt the remaining PCM tends to infinite and a difference of temperature inside the case could not be seen.

2.2.2 MELTING OF RT35 PCM WITH METAL FOAM

2.2.2.1 PCM WITH METAL FOAMS: LONGITUDINAL BLOCKS

The same setup of the previous experiment was used, metal foams (aluminum, 96% bulk porosity of the foam) were arranged longitudinally and added to the PCM-filled case, with the goal to increase the conductivity of PCM as shown in Fig. 66.
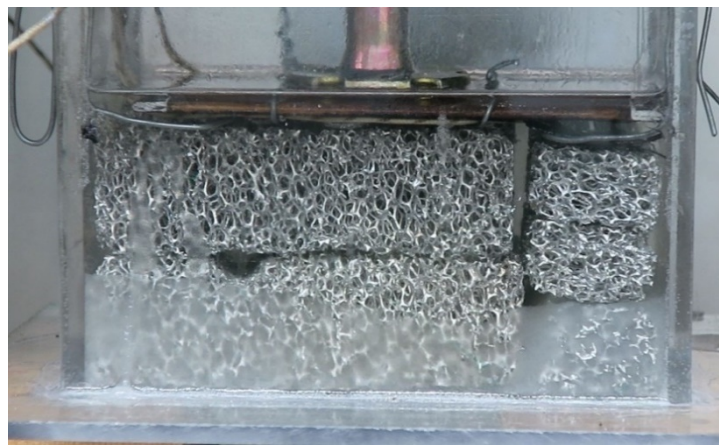
FIG. 66 CASE FILLED WITH PCM AND ALUMINUM FOAM.

The experiment was conducted in the same way than the previous one. The goal was to see in a quantitative and qualitative manner the difference in terms of melting time between the two experiments. Fig. 67 shows the progress of the melting front over time. The time needed to completely melt the PCM greatly decrease (less than 5 hours), but there was a strange different trend of the heat flux, probably due to the non-homogeneous disposition of metal foam. Actually, it was put in the case in a longitudinal way and there were several holes between the single pieces of metal foam.

Another experiment with the same setup and voltage but with transversal pieces of metal foam was needed to verify the trend of the heat flux for the heating of PCM with aluminum foams.
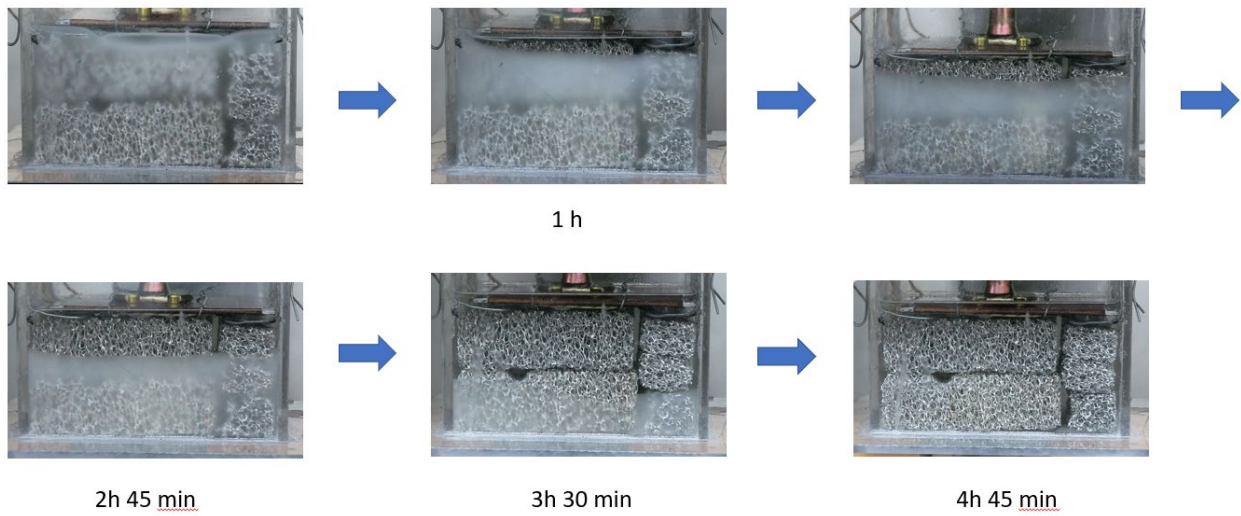
FIG. 67 THE PROGRESS OF THE PCM MELTING FRONT.
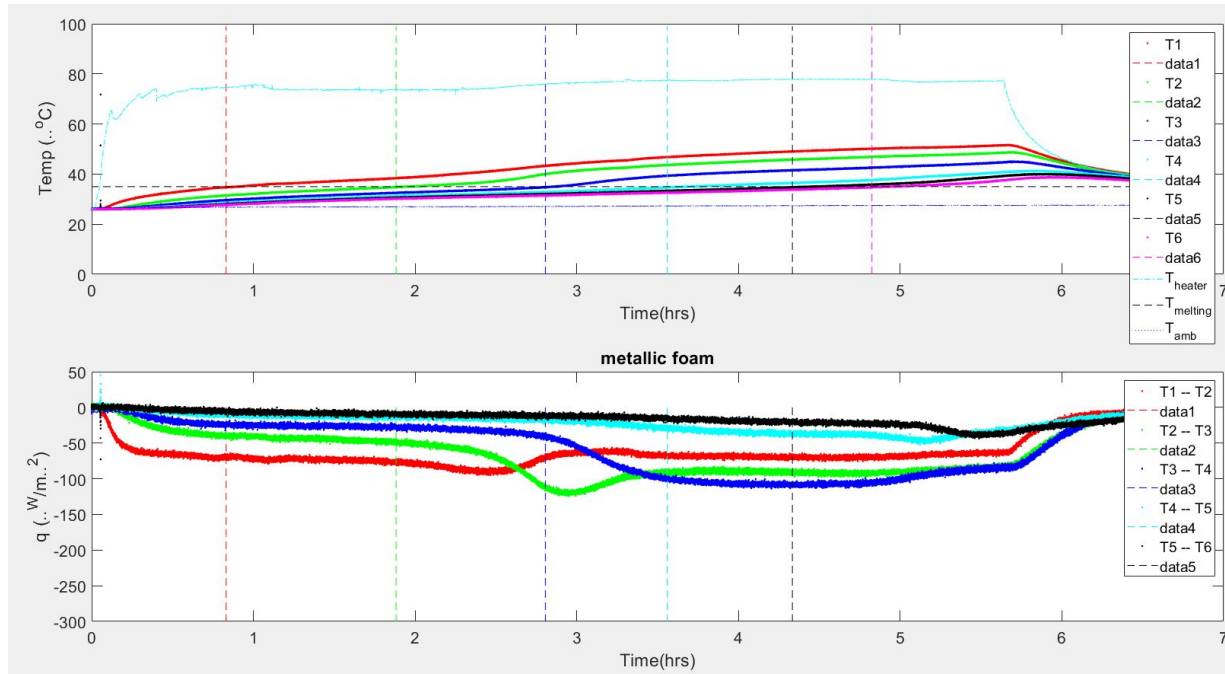
FIG. 68 (A) TEMPERATURE VARIATION ACQUIRED BY THE THERMOCOUPLES OVER TIME (B) TREND OF THE HEAT FLUX FOR THE WHOLE DURATION OF EXPERIMENT.

2.2.2.2 **PCM** WITH METAL FOAMS: TRANSVERSAL BLOCKS

In the second experiment metal foams were disposed in vertical way as shown in Fig. 69⌷In the graph in Fig. 70(b) in can be seen that the trend of heat flux was more constant than in the previous experiment. From this test it has been understood that it is better to use metal foams in a transversal way and the problem of the previous experiment was the non-homogeneous arrangement of the metal foam pieces.
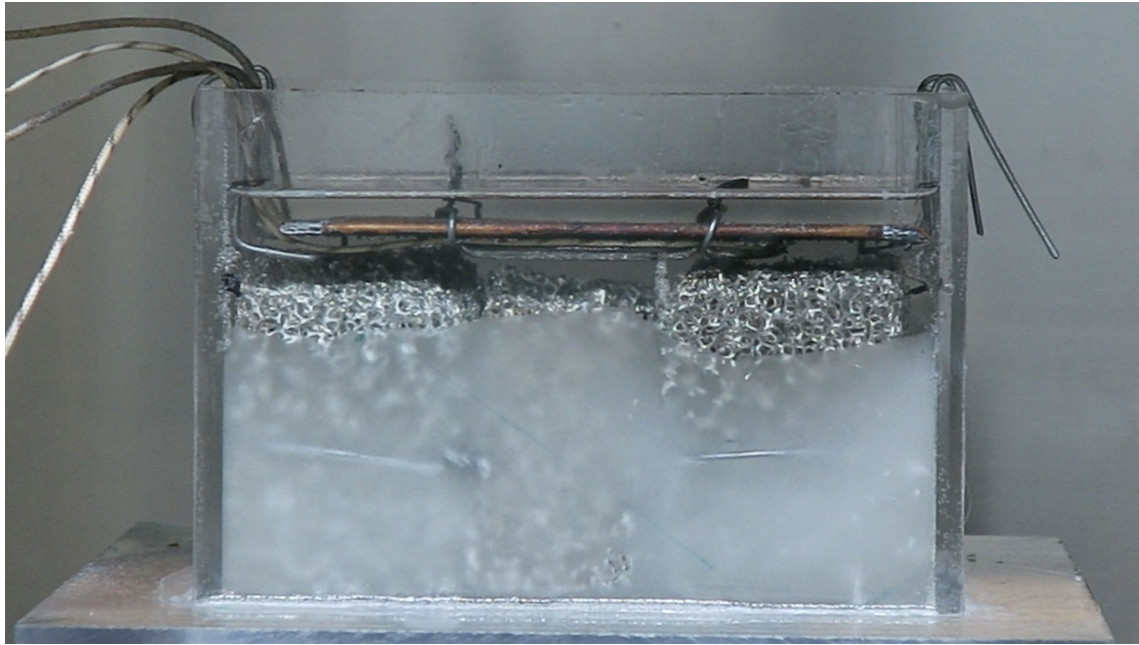
FIG. 69 CASE FILLED WITH PCM AND TRANSVERSAL METAL FOAM BLOCKS
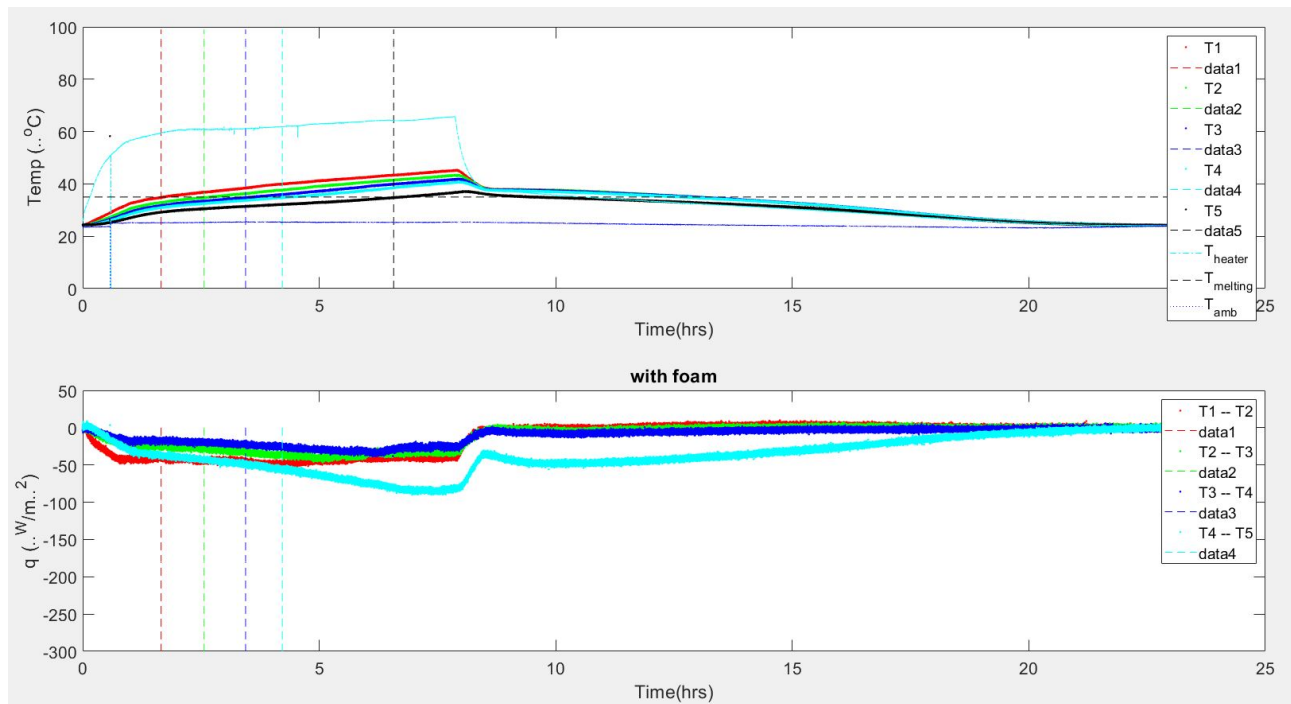
FIG. 70 (A) TEMPERATURE VARIATIONS ACQUIRED BY THE THERMOCOUPLES OVER TIME (B) TREND OF THE HEAT FLUX FOR THE WHOLE DURATION OF EXPERIMENT.
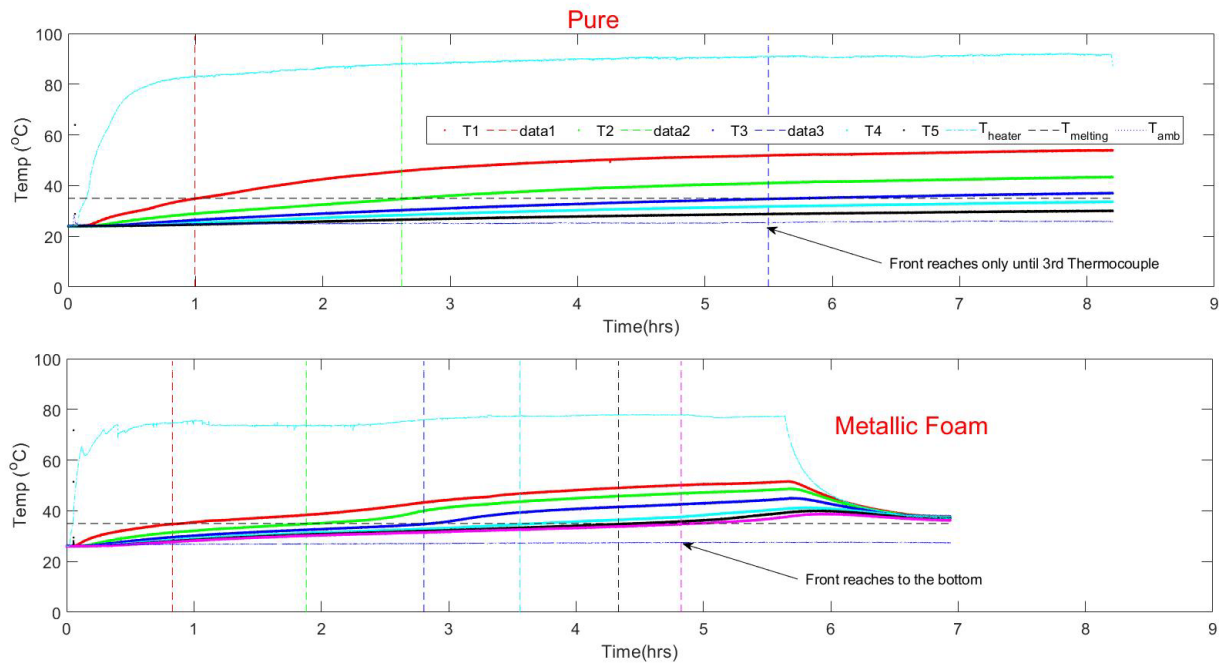
FIG. 71 COMPARISON BETWEEN THE HEATING WITH PURE PCM (A) AND THE PCM WITH METAL FOAMS (B).

The goal of increasing the conductivity of the system was reached and the differences in terms of time between the two experiments are evident: the whole PCM melted in only 5 hours, while in the first experiment the front reached only the third TC at the same time.

2.3 DESIGN AND CHARACTERIZATION OF A LATENT THERMAL ENERGY STORAGE SYSTEM (LTESS)

This chapter is focused on the study of the temperature trend inside the case (filled with same PCM of the previous experiments) and on the characterization of an insulation box, trying to reduce the losses as much as possible in order to low the heat exchange coefficient, aiming to adiabatic (ideal) conditions. The insulation box, JIMMI (Jar to Investigate on Melting Materials Insulation), was made of polystyrene. It will be also presented a comparison between the numerical simulation and the real experiment.

2.3.1 DEMONSTRATION OF TEMPERATURE HOMOGENEITY ALONG THE AXIAL DIRECTION

2.3.1.1 TEST 1: MELTING OF PURE PCM WITH POLYSTYRENE INSULATION, JIMMI 1.0

At this point, given the high duration of the heating experiments, Arduino was introduced in the system in order to control the heater by remote.

The arrangement of TCs was changed: 6 TCs were soldered onto 3 iron wires in the top part of the case (on a plane 45 mm distant from the bottom) and 6 TCs were in the bottom part of the case (on a plane 5 mm distant from the bottom) disposed as shown in Fig. 72(b), 1 TC was used to record the air temperature in the room. The heater temperature was not recorded in this experiment. The purpose of this experiment was to see the temperature trend over the entire volume of PCM and to demonstrate that the temperature values were the same in each point of the melting front. Such a resultwould have meant that this was really a pure conduction problem.
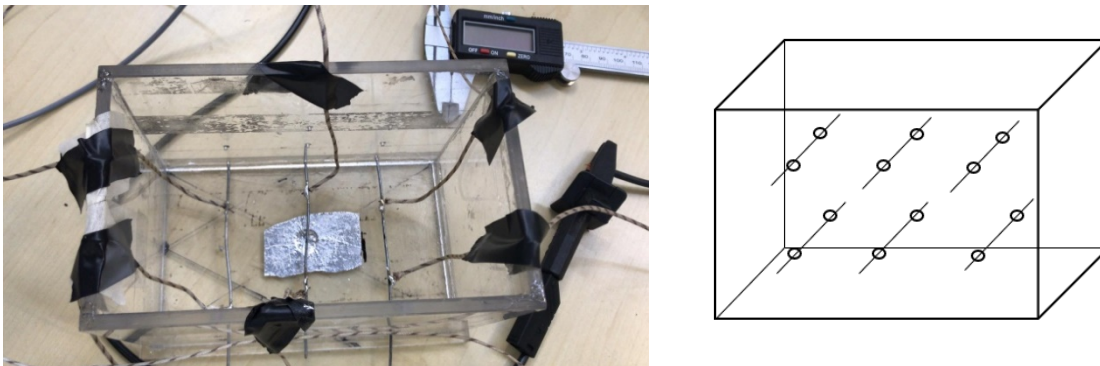
FIG. 72 (A) THE NEW CASE DURING CONSTRUCTION (B) FRONT VIEW OF NEW CASE.
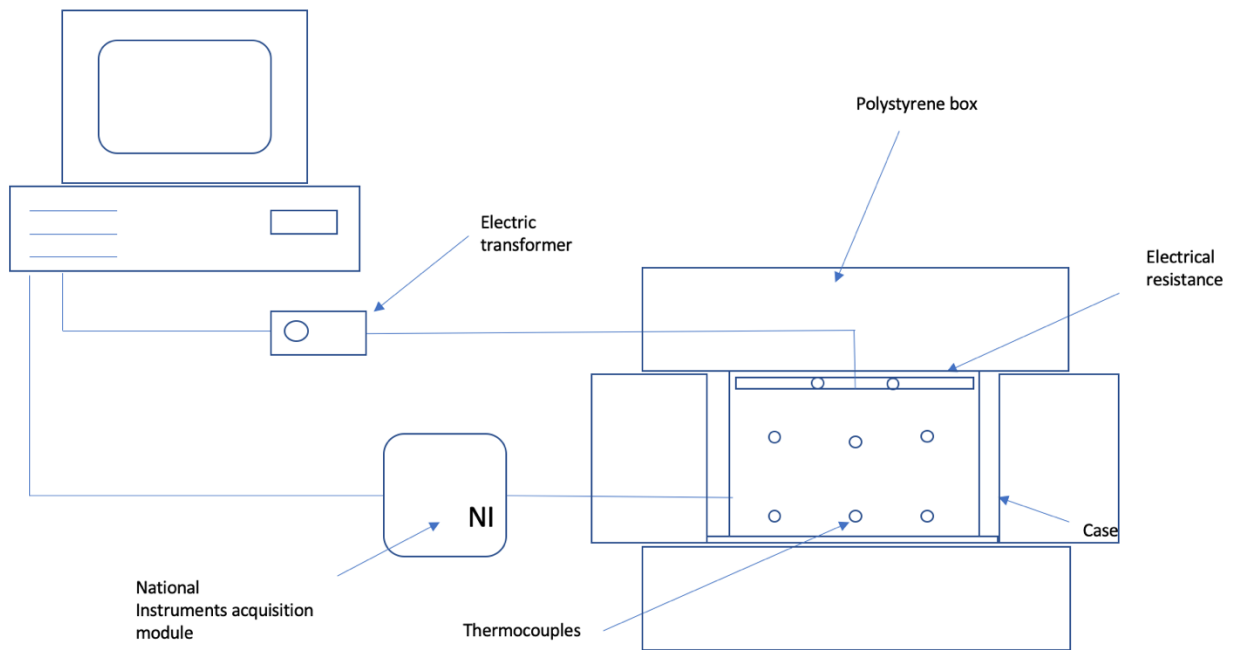
FIG. 73 SCHEMATIC DIAGRAM OF THE EXPERIMENTAL SETUP.

After the construction of the case, a 10 cm thick polystyrene box was built as hyper insulated chamber. The case was put in the centre of the box (Fig. 72): in this way the losses should have been lowerand the whole experiment should have been closer to an ideal adiabatic condition.

Fig. 73 shows the whole set-up of the experiment.

FIG. 74 THE POLYSTYRENE BOX JIMMI 1.0.
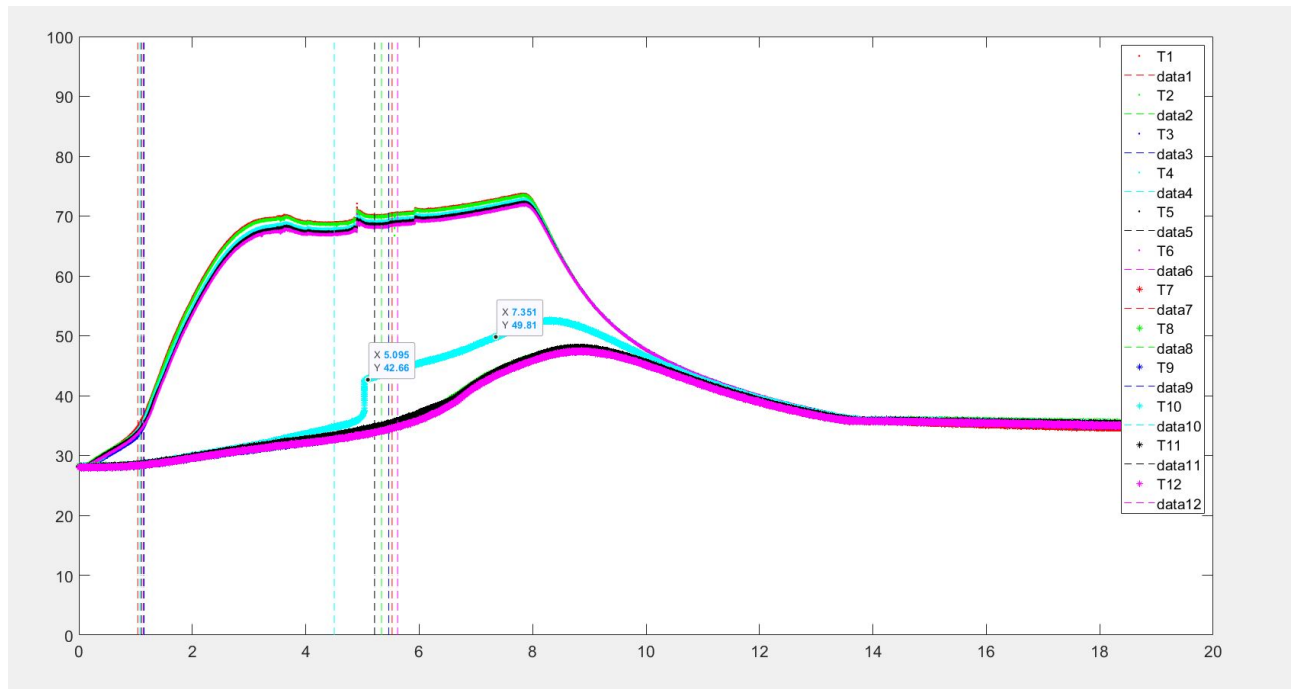
FIG. 75 TREND OF TEMPERATURES RECORDED BY THE THERMOCOUPLES.

The first experiment with JIMMI 1.0 was conducted with the same voltage as the previous ones (40 V): the resultsin Fig. 75 are interesting but they also showsome errors. The light blue line has a totally different temperature compared to the other lines under it (the temperatures recorded on the bottom plane) and this is due to an unsoldered TC:that temperature trend has been neglectedbecause it showed the temperature of a different point of the melting front (at a different value of z).

Fig. 76 shows the results without the trend of temperature given by the unsoldered TC.
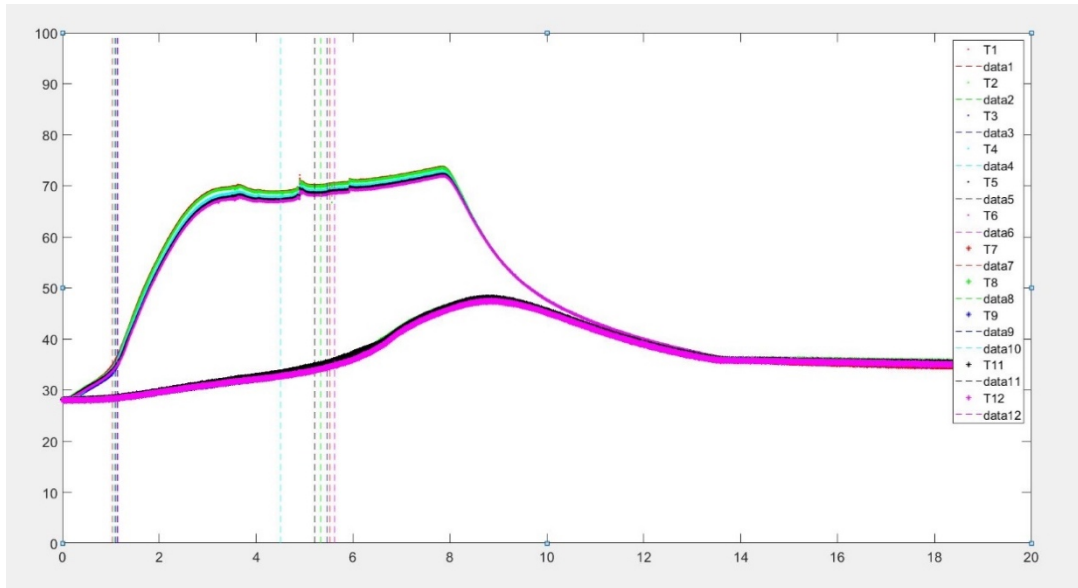
FIG. 76 EXPERIMENTAL RESULTS WITHOUT THE TREND OF TEMPERATURE GIVEN BY THE UNSOLDERED THERMOCOUPLE.

From this experiment it can be seen that, with a good insulation, the trend of the temperature is almost the same for all the TCs at the same distance from the bottom and that all the PCM melted at almost 75° C in 6 hours (the reaching of the melting temperature is shown by the vertical dashed lines). The temperature between the TCs put on the same plane has a maximum difference of maximum 2° C on the top plane and 1° C on the bottom plane. Another good result is the time that the TCs at the bottom took to reach the melting temperature:it is defintely lower than the experiment with pure PCM without insulation ($t_{melting}$ = 6 hours) thanks to the losses that, in this case, were almost insignificant compared to previous experiments.

2.3.1.2 MAIN PROBLEMS FACED

The temperature reached by the case was so high that melted the top part of the insulation box and deformed the lateral walls of the polycarbonate case itself, as shown rispectively in Fig. 77 and Fig. 78.

FIG. 77 TOP PART OF INSULATION BOX (A) BEFORE HEATING (B) AND AFTER HEATING.

FIG. 78 POLYCARBONATE CASE (A) BEFORE HEATING (B) AND AFTER HEATING.

After this experiment, the top part in polystyrene was replaced by another one completely identical. The experiment was repeated with same setup, adding 2 TCs to record the temperature of the heater which reached 120° C (Fig. 79), a much higher temperature value high than the experiments without insulation, proving that the insulation worked. However, this value of temperature was too high both for the polycarbonate and for the polystyrene that couldn't resist, and they were deformed.
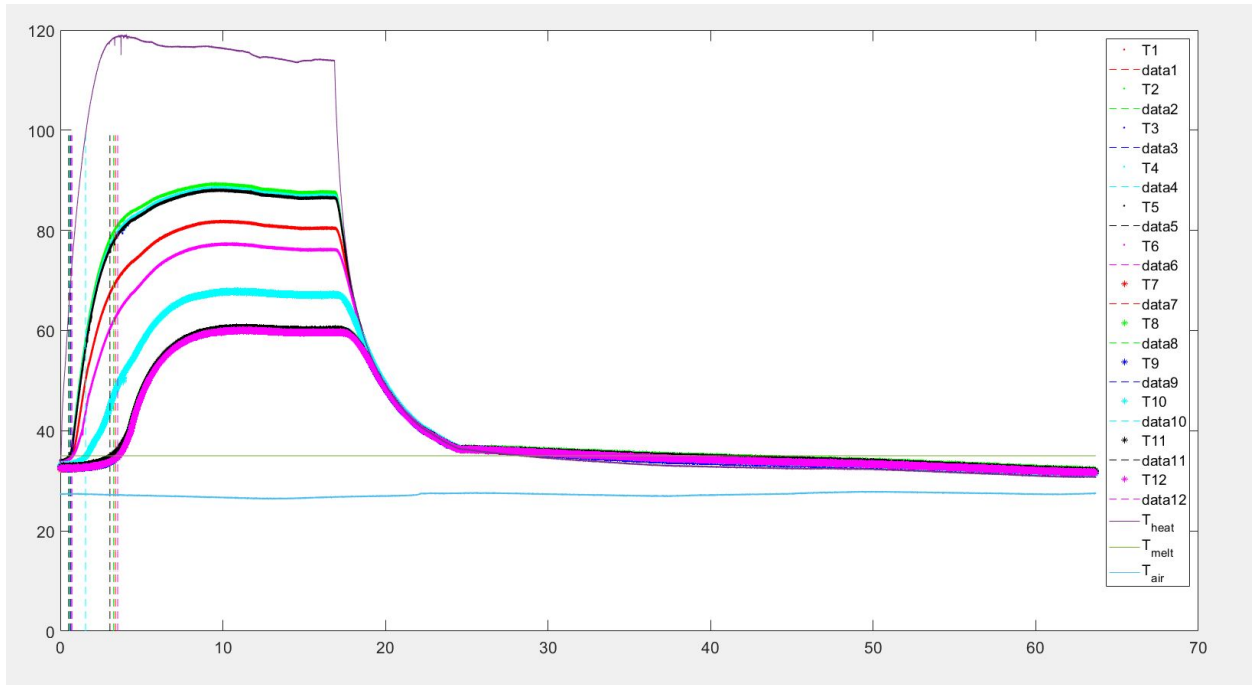
FIG. 79 TREND OF TEMPERATURES RECORDED BY THE THERMOCOUPLES.
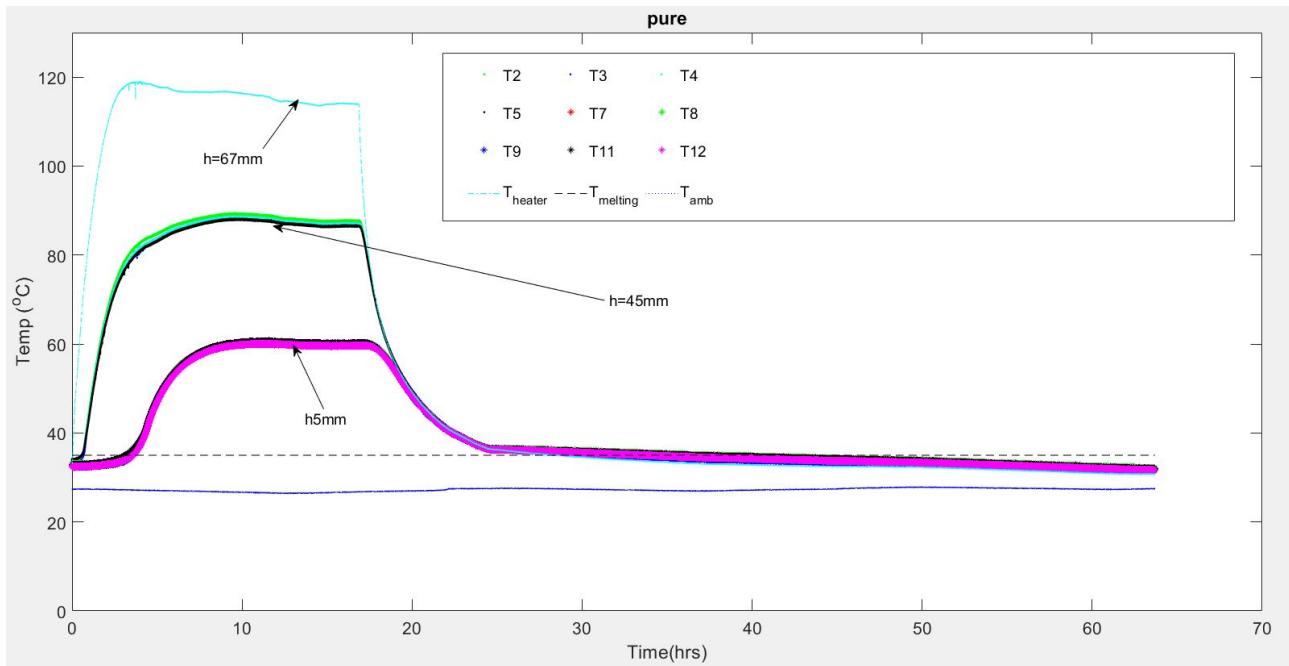
FIG. 80 TEMPERATURE TRENDS WITHOUT DETACHED THERMOCOUPLES.

The red, purple and light blue lines shown in Fig. 79 have been neglected because they represent temperature trends recorded by unsoldered TCs, so they were not at same heights of the others. Fig. 80 shows the trend of TCs that were at the same distance from the bottom.

93

A calculation with Excel, comparing the temperature differences recorded in the upper and lower parts of the box has been made. The TC that recorded the highest temperatures was compared to the one which recorded the lowest ones and this was repeated both for the TCs on the top and for those on the bottom of the case. In Fig. 81(b) the results of ΔT for TCs on the top plan are shown: the ΔT range considered acceptable was 2° C, because each TC has the precision of 1° C. It was found that, in a complete charging and discharging (melting and cooling) cycle of 65 hours, only 1,1% of values are out of the acceptable range and the maximum value of temperature difference was 2,4° C. Same calculations are illustrated in Fig. 82(b), where there were not values out of the range selected before and the highest temperature difference was 1,47° C. The results can be considered good, the temperature was homogenus in the whole plan of melting front.
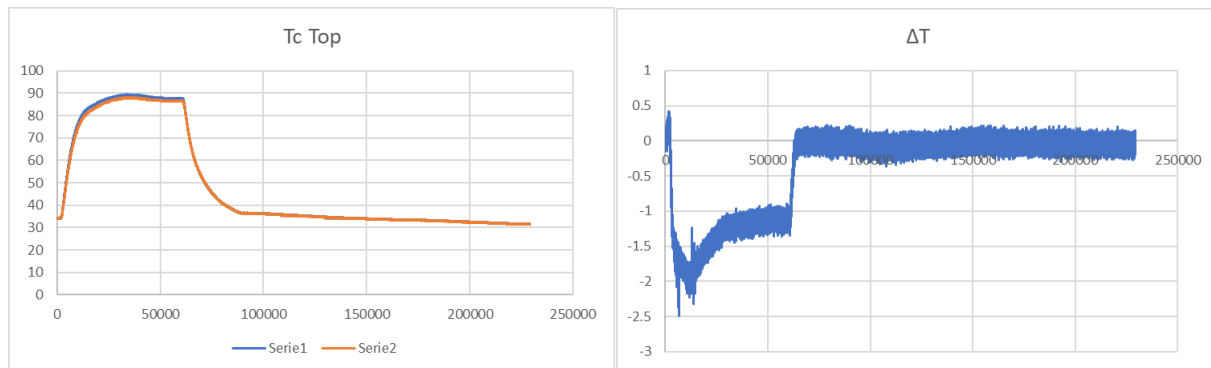
FIG. 81 (A) TRENDS OF THE HIGHEST AND LOWEST TEMPERATURES RECORDED BY THE THERMOCOUPLES AT THE TOP (B) ΔT CALCULATED WITH EXCEL.
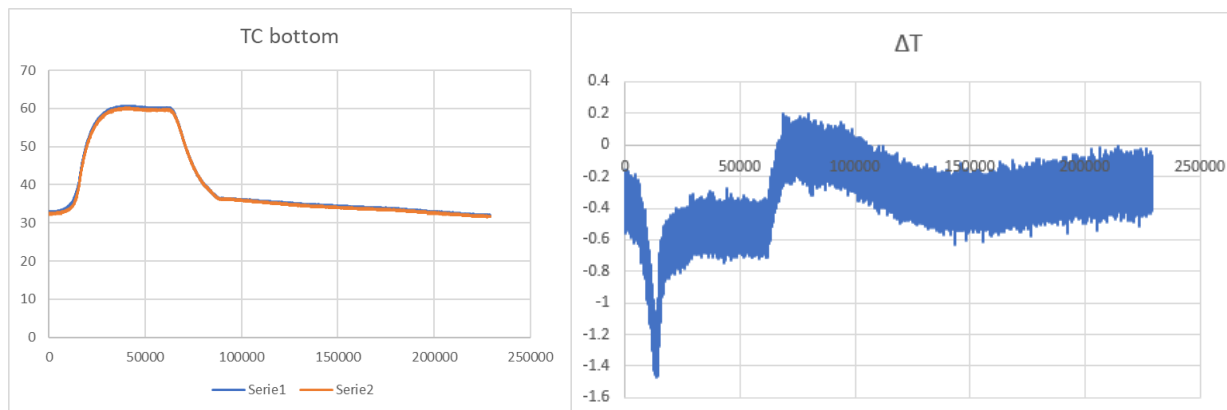
FIG. 82 (A) TRENDS OF THE HIGHEST AND LOWEST TEMPERATURES RECORDED BY THE THERMOCOUPLES AT THE BOTTOM (B) ΔT CALCULATED WITH EXCEL.

It was found that the temperature of the heater was too high (120°) causing again the partial melting of the top andlateral walls of JIMMI 1.0 and deformation problems on the lateral walls of the case

(Fig. 83). This high temperature was due to the reduction of the losses. Another experiment with a new insulation box, a new caseand a lower voltage was needed.
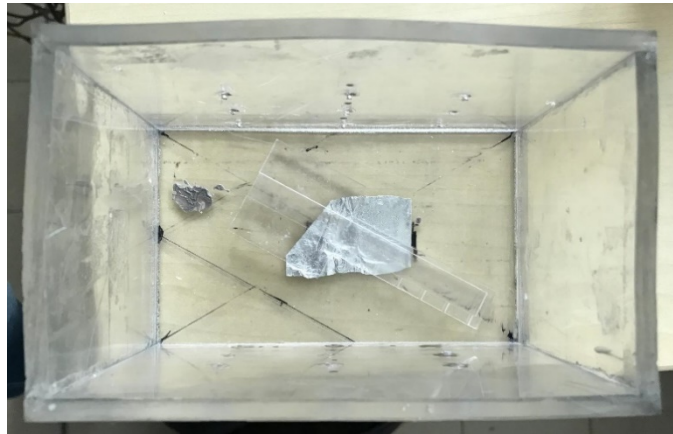
FIG. 83 LATERAL WALLS OF THE CASE DEFORMED DUE TO THE HIGH TEMPERATURES REACHED.

Parallel to this test, , a numerical simulation concerning this type of experiment and considering no losses was done at the University of Parma. The simulation revealed different results in terms of temperature trends: they were much higher compared to the last experiment (Fig. 84). This was probably due to the holes in the the polystyrene topthrough which there were losses.

FIG. 84 COMPARISON BETWEEN THE NUMERICAL SIMULATION AND THE EXPERIMENTAL RESULTS.

2.3.1.3 HEAT TRANSFER COEFFICIENT – CALCULATION

For the calculation of the heat transfer coefficient, all the data from the previous cooling experiment were considered and written on a Excel file, as can be seen in Fig. 85

time	tc1	tc2	tc3	tc4	tc5	tmed1	tc6	tc7	tc8	tc9	tc10	tmed2	t h1	t h2	tmed tot	t air	θ
29763.79	33.679	34.061	33.97	33.854	34.093	33.82542	32.374	32.893	32.57	32.828	32.533	32.6396	33.23	33.361	33.33133	27.343	5.988326
29764.39	33.709	34.111	34.01	34.02	34.064	33.87025	32.486	33.032	32.62	32.926	32.568	32.7264	33.222	33.393	33.39365	27.419	5.974646
29764.99	33.673	33.995	33.86	33.867	34.056	33.77633	32.407	32.991	32.479	32.86	32.373	32.622	33.149	33.265	33.29536	27.402	5.893361
29765.59	33.669	34.139	33.989	33.96	34.052	33.85325	32.451	33.005	32.548	32.859	32.609	32.6944	33.249	33.372	33.3704	27.411	5.959396
29766.19	33.752	34.179	34.036	33.976	34.167	33.92333	32.491	33.048	32.659	32.972	32.606	32.7552	33.395	33.465	33.43661	27.504	5.932611
29766.79	33.726	34.154	33.957	33.966	34.141	33.88908	32.47	32.964	32.577	32.85	32.571	32.6864	33.277	33.504	33.38797	27.418	5.969965
29767.39	33.567	34.006	33.939	33.864	33.952	33.75008	32.352	32.922	32.43	32.782	32.426	32.5824	33.098	33.247	33.26355	27.353	5.910549
29767.99	33.716	34.036	33.968	33.9	34.077	33.83183	32.363	33.002	32.559	32.891	32.491	32.6612	33.214	33.374	33.34407	27.434	5.910069
29768.59	33.709	34.051	33.947	33.952	34.121	33.8425	32.488	33.052	32.516	32.844	32.491	32.6782	33.172	33.378	33.35738	27.391	5.966375
29769.19	33.681	34.041	34.037	33.922	34.127	33.84308	32.343	32.964	32.578	32.848	32.538	32.6542	33.103	33.398	33.34772	27.419	5.928715
29769.79	33.662	34.025	33.915	33.863	34.069	33.79358	32.318	32.965	32.494	32.859	32.496	32.6264	33.168	33.287	33.30726	27.358	5.949257
29770.39	33.666	34.043	33.9	33.874	34.02	33.80833	32.407	32.974	32.562	32.874	32.535	32.6704	33.23	33.464	33.33419	27.412	5.922194
29770.99	33.697	34.086	33.922	33.849	34.079	33.81958	32.408	32.954	32.497	32.797	32.519	32.635	33.212	33.357	33.32601	27.389	5.937007
29771.59	33.733	34.015	33.881	33.925	34.029	33.81658	32.385	32.946	32.549	32.873	32.487	32.648	33.277	33.356	33.32967	27.413	5.916674
29772.19	33.631	34.067	33.83	33.837	34.005	33.76917	32.427	32.909	32.455	32.848	32.508	32.6294	33.13	33.36	33.29426	27.365	5.929264
29772.79	33.657	34.043	33.867	33.842	34.072	33.80175	32.421	32.928	32.475	32.894	32.581	32.6598	33.226	33.433	33.32594	27.326	5.999937
29773.39	33.752	34.051	33.898	33.815	34.064	33.81342	32.439	32.951	32.553	32.905	32.622	32.694	33.18	33.421	33.34699	27.395	5.951993
29773.99	33.586	34.033	33.928	33.88	33.954	33.7745	32.357	32.925	32.492	32.851	32.471	32.6192	33.201	33.331	33.29313	27.309	5.984125
29774.59	33.73	34.013	33.908	33.951	34.091	33.84058	32.447	33.013	32.524	32.953	32.541	32.6956	33.263	33.438	33.36351	27.413	5.950507
29775.19	33.692	34.068	33.932	33.89	34.044	33.82092	32.4	32.972	32.516	32.866	32.484	32.6476	33.181	33.418	33.33203	27.414	5.918035
29775.79	33.62	34.074	33.913	33.796	33.996	33.78158	32.406	32.909	32.49	32.885	32.488	32.6356	33.222	33.359	33.30409	27.457	5.84709
29776.39	33.698	34.11	33.982	33.905	34.15	33.88158	32.506	33.038	32.498	32.952	32.612	32.7212	33.352	33.537	33.39809	27.475	5.92309
29776.99	33.67	34.063	33.886	33.87	33.976	33.79467	32.43	32.949	32.524	32.807	32.533	32.6486	33.23	33.376	33.31714	27.416	5.901139
29777.59	33.659	34.014	33.924	33.881	34.042	33.79825	32.343	32.893	32.433	32.774	32.521	32.5928	33.178	33.361	33.29598	27.304	5.991979
29778.19	33.628	34.014	33.904	33.819	33.979	33.77475	32.283	32.885	32.493	32.814	32.46	32.587	33.251	33.358	33.27985	27.351	5.928854
29778.79	33.793	34.083	34.012	33.935	34.106	33.88875	32.479	33.128	32.637	32.926	32.618	32.7576	33.346	33.461	33.41744	27.432	5.985438
29779.39	33.572	33.93	33.773	33.744	33.996	33.7105	32.309	32.834	32.411	32.739	32.398	32.5382	33.176	33.32	33.22204	27.267	5.955042
29779.99	33.657	33.982	33.953	33.881	34.025	33.79467	32.43	32.897	32.46	32.77	32.448	32.601	33.21	33.33	33.29731	27.366	5.931306
29780.59	33.458	33.748	33.711	33.64	33.771	33.57192	32.234	32.819	32.388	32.66	32.342	32.4886	33.027	33.18	33.12053	27.173	5.947535

Vtot	0.000648
Vtop	0.000378
Vbot	0.00027
cp liq	2
RO	770
M cp	0.99792

Tmed tot

FIG. 85 EXTRACT OF AN EXCEL FILE WITH CALCULATION OF T AVERAGE.

The data for RT35 PCM are shown in Tab 14.

TAB 14: DENSITY AND HEAT CAPACITY OF RT35 PCM FOR SOLID AND LIQUID PHASE.

	Solid phase	Liquid phase
ρ [kg/m³]	860	770
c_p [kJ/kg K]	3	2

The goal was to calculate the heat transfer coefficient k which comes from:

$$M\,c_p\,\frac{d\theta}{dt} = -k\,\theta \tag{8}$$

In this equation M is the mass of the PCM in the case calculated as the product of density and volume of PCM, $\theta = (T - T_{air})$, c_p is the specific heat capacity of the PCM, and t is the time. In Fig. 85 are presented some data about the time, the temperature and the first calculations to find the average temperatures inside the case.

Considering that θ (t = 0) = θ_0 = 45,28° C, as can be seen in Fig. 90, integrating the previous equation it can be deduced:

$$\int_{\theta_0}^{\theta} \frac{d\theta'}{\theta'} = -\int_0^t \left(\frac{k}{Mc_p}\right) \cdot dt' \qquad \rightarrow \qquad (\ln\theta - \ln 45{,}28) = -B\,t \qquad \rightarrow$$

$$\rightarrow \qquad \ln\theta = \ln 45{,}28 - B\,t \qquad \rightarrow \qquad -\ln\frac{\theta}{45{,}28} = B\,t$$

With $B = \left(\dfrac{k}{Mc_p}\right)$ which is the slope of the resulting line.

To find the value of k it was necessary to calculate the temperature difference θ which, in the experiment, reasonably comes out from aweighted average calculated considering 5 sub-volumes at 5 different temperatures (the ones recorded by the 5 TCs). The distances between the TCs were the following, as can be seen in Fig. 86:

- $d_{BOTTOM-1} = 5$

- $d_{central} = 40$ mm

- $d_{5\text{-}heater} = 15$ mm
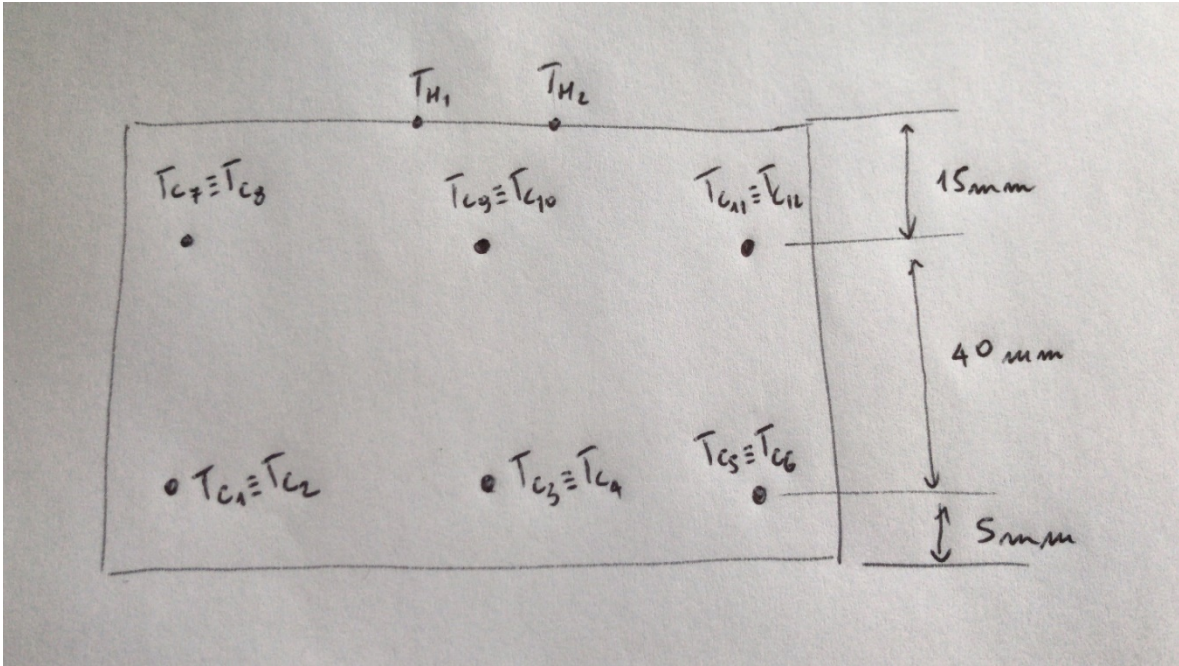
FIG. 86 POSITIONS OF THERMOCOUPLES.

The whole volume of the PCM in the case (whose base measures $135 * 80 = 1,08 * 10^4$ mm^2) was divided in 2 sub-volumes, shown in Fig. 87:
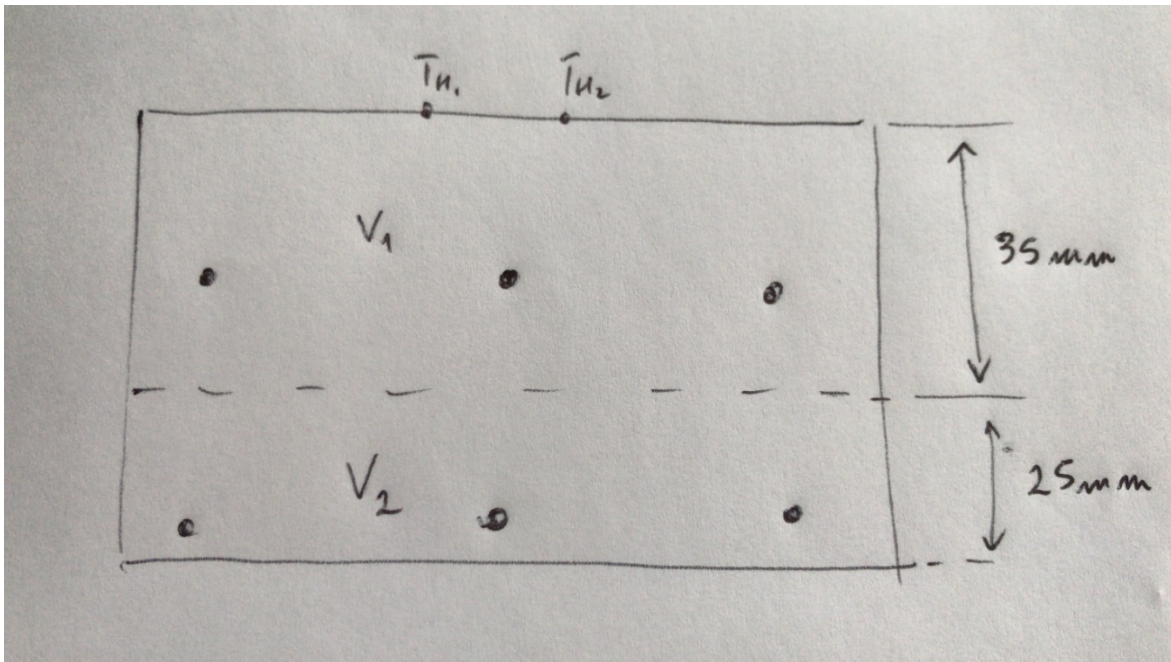
FIG. 87 VOLUMES CONSIDERED FOR THE CALCULATION OF THE AVERAGE TEMPERATURES.

Each sub-volume has a "thermal weight" depending from its mass (the c_p is constant for each phase, liquid or solid). The average temperature of all the PCM had been calculated considering these weights . One TC at the top and one at the bottom were not considedered for uncertainties about their positions.

$$\bar{T} = \frac{m_1 c_{p_1}((T_{H1}+T_{H2})/2)+(T_1+T_2+T_3+T_4+T_5)/5)+m_2 c_{p_2}((T_6+T_7+T_8+T_9+T_{10})/5)}{\sum_1^2 m_i c_{p_i}} \tag{9}$$

$\bar{T}$ is represented in Fig. 85 as T_{med}. $\bar{T}$ would have had the same value if calculated considering ρ and c_p for liquid or solid, because both the density and the c_p can be collected in the numerator and simplified, obtaining the following equation:

$$\bar{T} = \frac{\rho c_p V_1(((T_{H1}+T_{H2})/2)+(T_1+T_2+T_3+T_4+T_5)/5))+\rho c_p V_2((T_6+T_7+T_8+T_9+T_{10})/5)}{\rho c_p (V_{tot})} \tag{10}$$

With this equation $\bar{T}$ can be calculated for each instant of time, consequently, all the temperature differences θ were calculated as can be seen in extract of the Excel file in Fig. 85

From this point on it wasconsidered only a precise interval of time: it could not be taken into account the period during which the PCM presents both solid and liquid phases because its physical characteristics (density, specific heat) change, so it was decided to focus the attention on the cooling process, when the whole mass of PCM is still liquid and the solidification has not begun yet.

At the beginning of the experiment we set a certain $T_{phase\ change}$ accordingly to the PCM used but, in reality, the phase change temperature of PCMs is not a precise value as the phase change happens in a temperature range of about $5\div7°$. To be sure of not to examine the PCM when the solidification process already began, it has been also excluded the interval of time just before the reaching of the set $T_{phase\ change}$. In Fig. 88 it is shown a graph which represents the average of the recorded temperatures in the cooling experiment:the red circle puts in evidence the range of temperature that was chosen for the calculations.
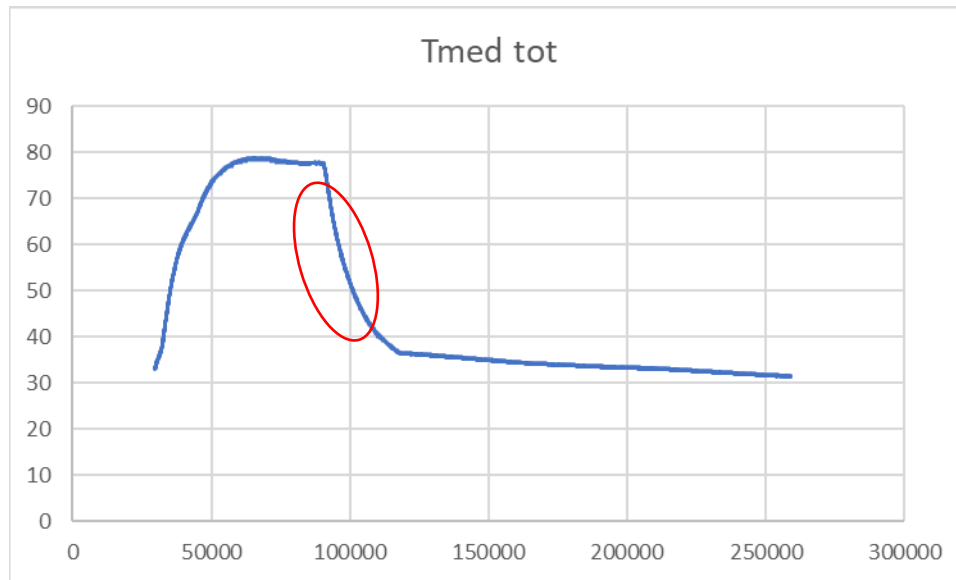
FIG. 88 RANGE OF TEMPERATURE CHOSEN FOR THE CALCULATIONS.

As it has already been said, $-\ln\dfrac{\theta}{45{,}28} = B\,t$, is the equation of a line whose slope is B

($y = -\ln\dfrac{\theta}{45{,}28}$ and x = t): using all the values of y and x obtained from $-\ln\dfrac{\theta}{\theta_0}$ in function of time (blue points in the graph in Fig. 89 below), the slope (B) of the regression line can be calculated (SLOPE Excel function).

Once obtained B, the interpolating line can be plotted (the red one in the graph in Fig. 89 below), which has the classical equation y = mx + q (q has been chosen in order to better matches the experimental curve).
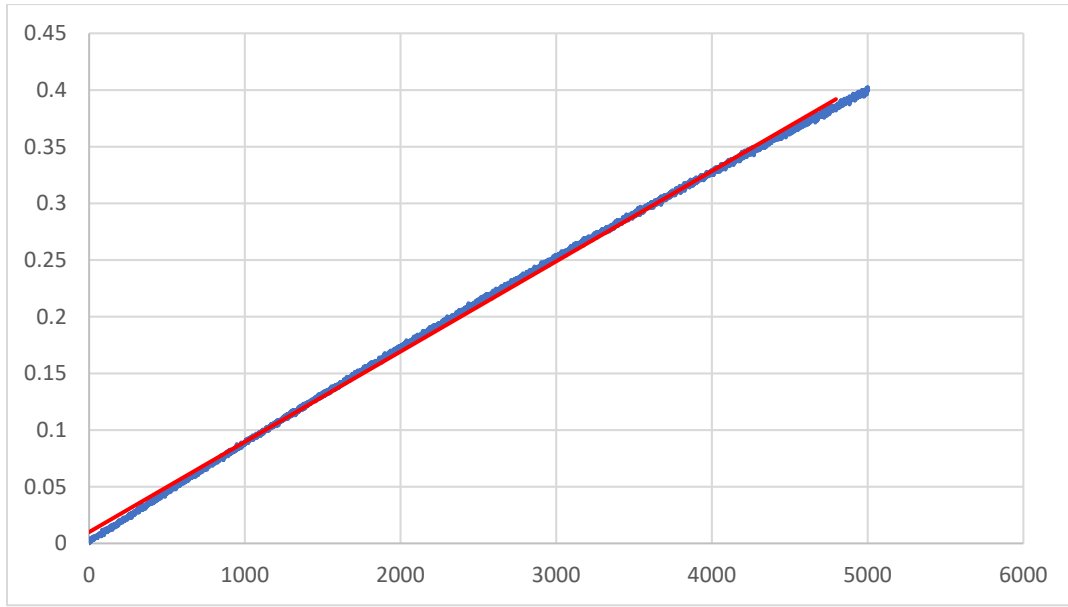
FIG. 89 REAL LINE AND INTERPOLATING LINE.

				LabVIEW Time	θ	Absolute Time	$\ln((\theta)/(\theta_0))$	Interpolating line
				92123.222	45.28884	0	0	0.01
Σ (M*cp) [J/K]	997.92			92123.821	45.16663	0.599	0.002702068	0.010047698
				92124.421	45.27713	1.199	0.000258559	0.010095476
B [s⁻¹]	7.96297E-05			92125.022	45.16794	1.8	0.002673009	0.010143333
C	0.01			92125.621	45.21793	2.399	0.001566949	0.010191032
K [W/K]	0.079464041			92126.22	45.189	2.998	0.002206956	0.01023873
				92126.821	45.20197	3.599	0.001919932	0.010286587
				92127.421	45.09448	4.199	0.004300825	0.010334365
				92128.022	45.16852	4.8	0.002660248	0.010382222
External heat exchanging surface [m²]		U [W/m² K]		92128.62	45.21185	5.398	0.001701491	0.010429841
0.6		0.132440069		92129.22	45.09363	5.998	0.004319613	0.010477619
				92129.821	45.20037	6.599	0.001955421	0.010525476
				92130.421	45.14224	7.199	0.003242343	0.010573254

FIG. 90 EXTRACT OF THE EXCEL FILE WITH THE CALCULATIONS OF THE HEAT TRANSFER COEFFICIENT AND THE GLOBAL HEAT EXCHANGE COEFFICIENT.

Finally, it can be calculated the heat transfer coefficient k with the inverse equation of B, as can be seen in Fig. 90:

$$k = B \, M \, c_p \qquad (11)$$

The value obtained by the first cooling experiment was: k = 0,079 W/K.

Knowing k, it can also be calculated the global heat exchange coefficient simply using the formula:

$$U = \frac{k}{A} \tag{12}$$

with A as the total external heat exchanging area.

In the experiment the values obtained for the area and for the global heat exchange coefficient were: $A = 0,6$ m^2 and $U = 0,1324$ W/m^2 K, as can be seen in Fig. 90.

2.3.2 THERMAL INSULATION ENHANCEMENT

2.3.2.1 TEST 2: MELTING OF PURE RT35 PCM IN AN EUROBATEX ® AND POLYSTYRENE BOX, JIMMI 2.0

A new box with an insulation of polystyrene and EUROBATEX ® on the top part was realized to prevent damages to the upper polystyrene part and to obtain a better insulation. The voltage was reduced to 20 V (from 40 V), in order to have a lower heater temperature and to prevent damages to the case. A new polycarbonate case, with the same dimention of the previous one but different holes locations for the TCs, was designed and built, . Tab 15 shows the distances of the central TCs from the bottom.

TAB 15: POSITIONS OF CENTRAL THERMOCOUPLES.

Central Tc	1	2	3	4	5
x (mm)	55	42	29	16	3

.
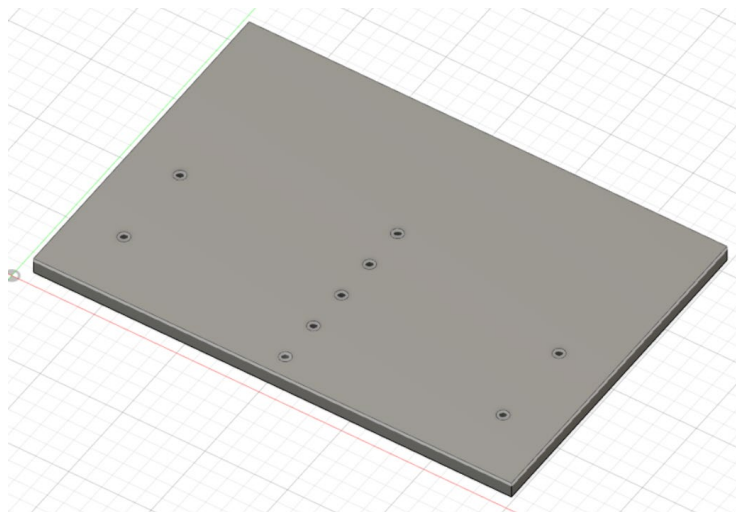
FIG. 91 HOLES MADE IN EACH SIDE OF THE CASE.

Fig. 91 shows the holes that were made on both of the two bigger lateral walls the case: as can be seen, in this case there were 2 holes on each side of the lateral walls, at the same height of the second and the fourth holes. In this way the temperature trend on the lateral walls could be monitored.

Fig. 92 shows the new case, with 5 TCs in the central part and 2 TCs close to the left side wall, 2 TCs on the rightside wall. The TCs were welded on iron wires and the holes in the walls were filled with epoxy glue,.

In this in this test there was no possibility to control the system remotely, because the Arduino relay burnt due to a short circuit.
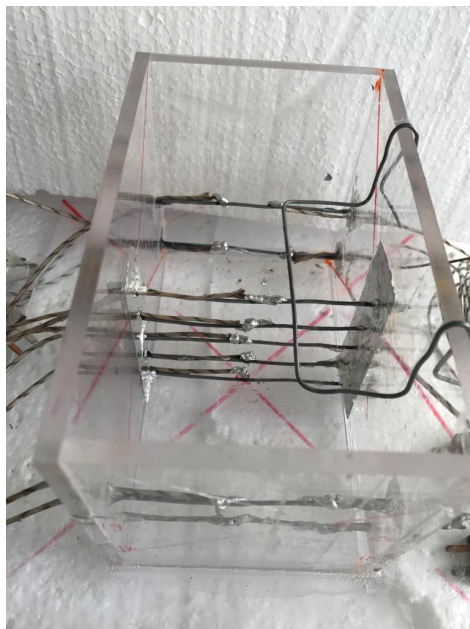
FIG. 92 NEW POLYCARBONATE CASE.
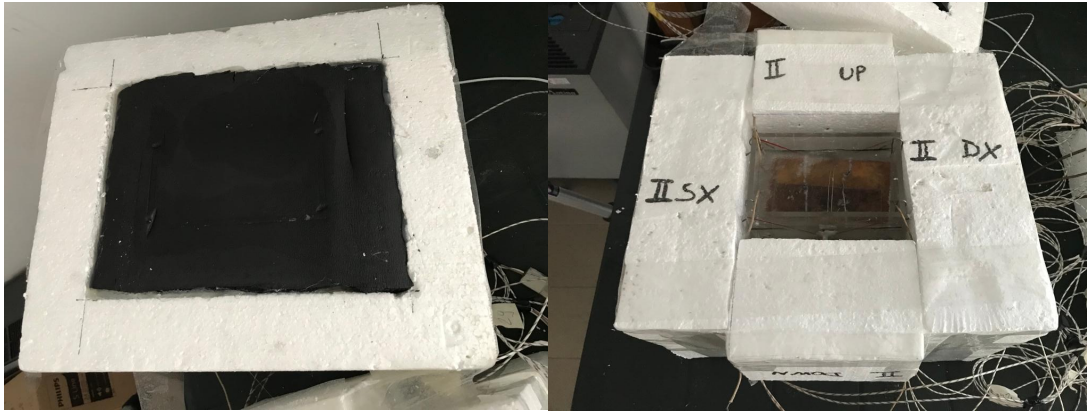
FIG. 93 THE NEW BOX BETTER INSULATED WITH POLYSTYRENE AND EUROBATEX® : (A) UPPER PART (B) LATERAL WALLS.

Fig. 93 shows the new insulation box made with polystyrene and Eurobatex ®. It could be seen that there were no dameges on the upper part and lateral part of the box. A little air gap between the polycarbonate and the polystyrene walls was left empty.. The polystyrene box and the polycarbonate case didn't show any problem and the whole system resisted at the heating.

Fig. 94 shows the final set-up with higher insulation.
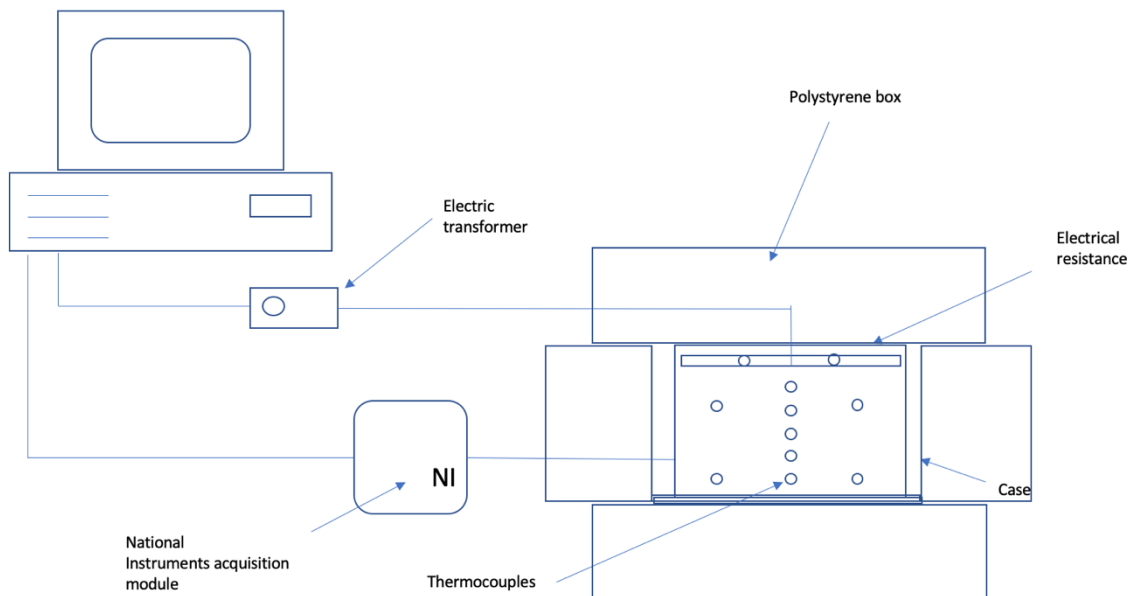
FIG. 94 SCHEMATIC DIAGRAM OF THE EXPERIMENTAL EQUIPMENT.

Fig. 95 (a) shows the trend of the temperature related over time recorded by the two TCs at the bottom of each side of the case, Fig. 95(b) shows the trend of the temperature at the top part. From these two graphs it could be deduced that, considering the same distance from the bottom, the temperature was the same in all of the surface of the case..
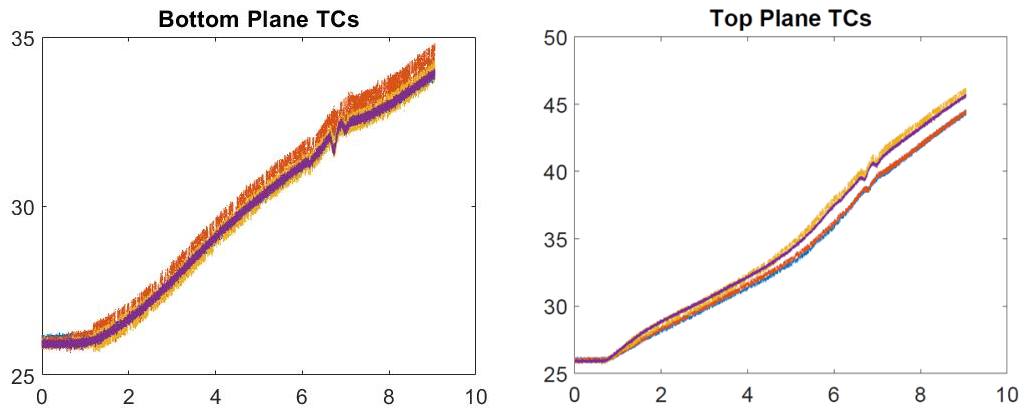
FIG. 95 (A) TREND OF THE TEMPERATURES CLOSE TO THE LATERAL WALLS, AT THE BOTTOM PART OF THE CASE (B) TREND OF THE TEMPERATURES CLOSE TO THE LATERAL WALLS AT THE TOP OF THE CASE.
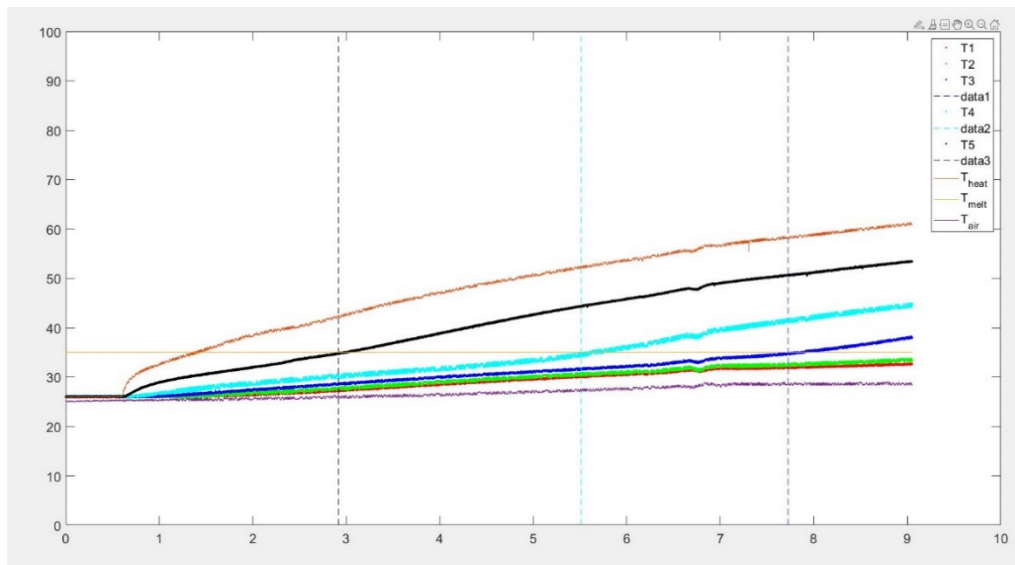
FIG. 96 TEMPERATURE TREND RECORDED BY THERMOCOUPLES.

Fig. 96 describes the development of the temperature over time recorded by TCs at the center of the case: a decrease in temperature can be appreciate compared to previous experiment ($T_{max, \, heater}$

= 60° C). The heater temperature is given by the first orange line in the upper part of the graph and the lines below show the temperature trend over time of the other TCs, starting from the top.

Fig. 96 also reveals the same trend for all the temperatures. The melting front reached the third TC in less than 8 hours, then the experiment was stopped due to the impossibility to control the system by remote.
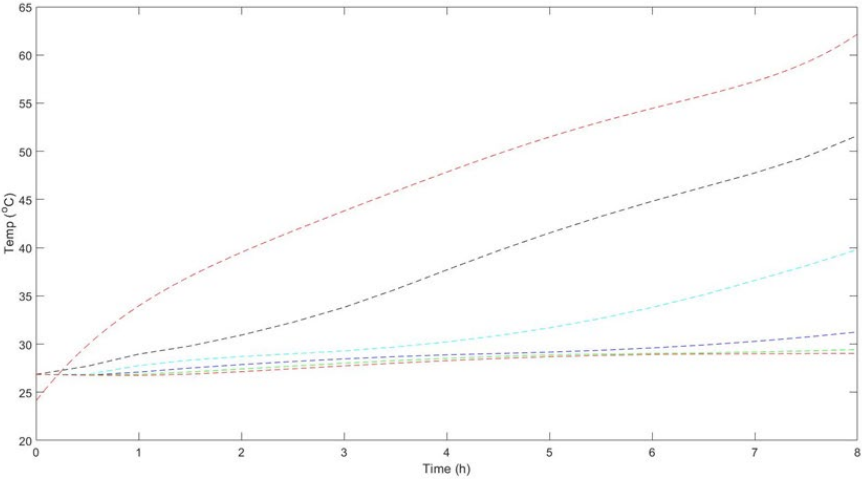
FIG. 97 NUMERICAL SIMULATION.

A numerical simulation was made, as can be seen in Fig. 97, considering 5 W/m^2 of losses.
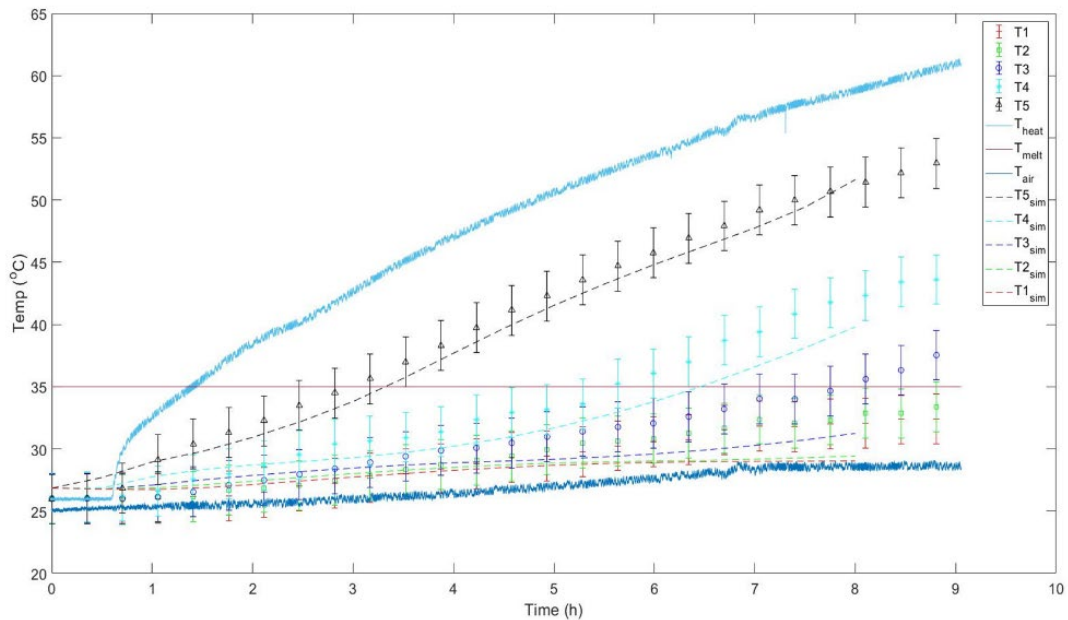
FIG. 98 COMPARISON BETWEEN NUMERICAL AND EXPERIMENTAL RESULTS.

Fig. 98 shows a comparison between numerical (T_{sim}) and experimental (T_{exp}) results. Experimental results were plotted considering an acceptable temperature range of 2° C in which the match with T_{sim} can be found. Comparing the experimental results with the simulation ones, it is evident that T_{sim} are lower than T_{exp}. There could be three possible reasons:

- The heater was too clos to the TCs respect what has been simulated;
- The losses were overestimated in the simulation;
- There was the influence of heat capacity which changes with the phase change of the PCM;

To check if the first hypothesis was correct, T_{sim} were considered at greater heights (as if the heater was placed at a lower distance from the bottom) so there could be a match betweeen T_{sim} and T_{exp} but, at the end, the results showed that the temperatures of the simulation at the bottom were still lower than in theexperiment. Further the modified heights were not realistic.

A numerical simulation with adiabatic conditions was made, in order to verify the second hypothesis but the temperatures of the simulation at the bottom still remained lower than the experimental ones.

The third hypothesis was still to be verified. Another experiment is needed to monitor the trend of T_{exp} for a longer time.

2.3.2.2 TEST 3: MELTING OF PURE RT35 PCM IN AN EUROBATEX ® AND POLYSTYRENE BOX

The experiment was repeated using the same setup and the same voltage (20 V) but adding some improvements: there was the possibility to control the experiment by remote, so the experiment could be longer in terms of time and the temperature could be better monitored.
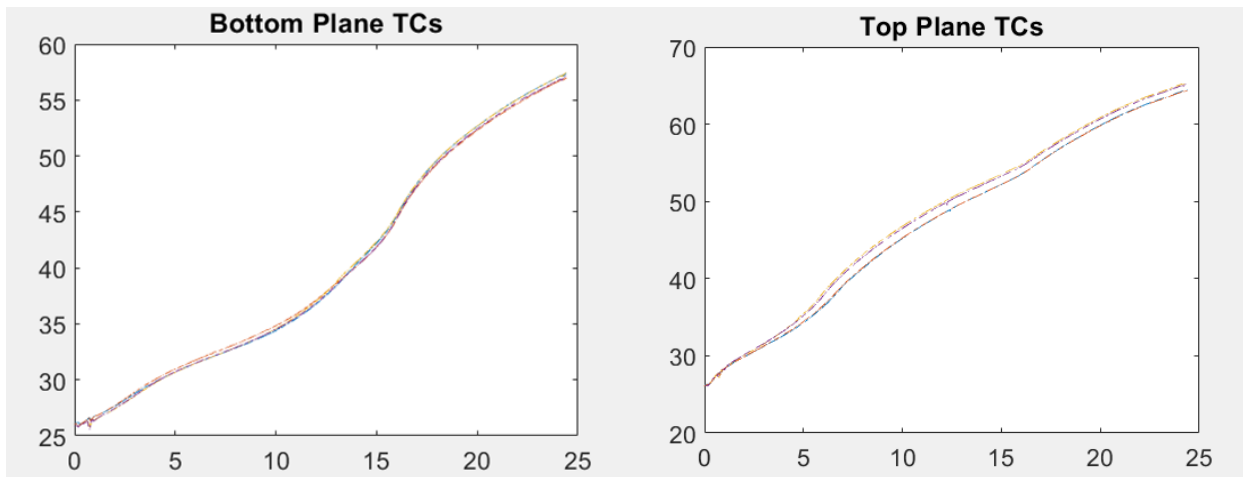
FIG. 99 (A) TREND OF THE TEMPERATURES CLOSE TO THE LATERAL WALLS AT THE BOTTOM PART OF THE CASE (B) TREND OF THE TEMPERATURES CLOSE TO THE LATERAL WALLS AT THE TOP OF THE CASE.
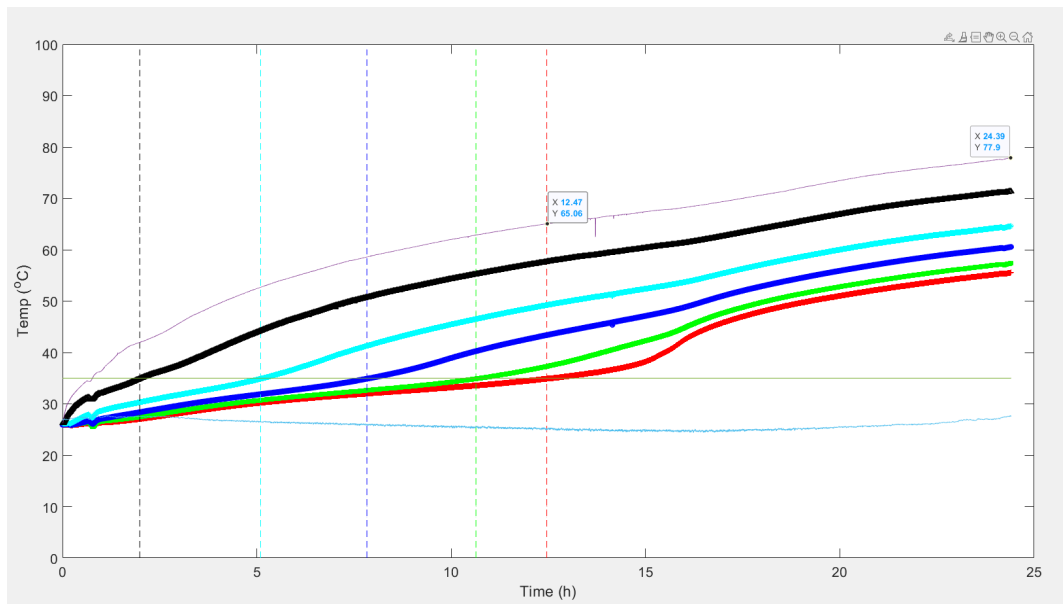
FIG. 100 TEMPERATURES TREND RECORDED BY THE THERMOCOUPLES.

108

Fig. 99 and Fig. 100 show the experimental results of the temperature with the same setup of previous the exemperiment. The first upper line shows the trend of the heater temperature, and the temperatures recorded by the five TCs, starting from the top, are given respectively by the black, the light blue, the blue, the green and the red line. The highest value of the recorded temperatures is $T_{heater, max} = 78°$ C: even in this experiment the temperature of the heater did notdamage the polystyrene box. All the PCM melted in about 12,5 hours (at that time $T_{heater} \approx 65°$ C). Even in this case the results given by the TCs close to the side walls were good: the temperatures remained the same in each point of the melting front.

In Fig. 101 Fluent simulation results are shown:the trend of all the curves has an increasement after a certain time: the deeper is the TC, the steeper is the increasement. With the previous shorter simulation it was impossible to see this trend changing.
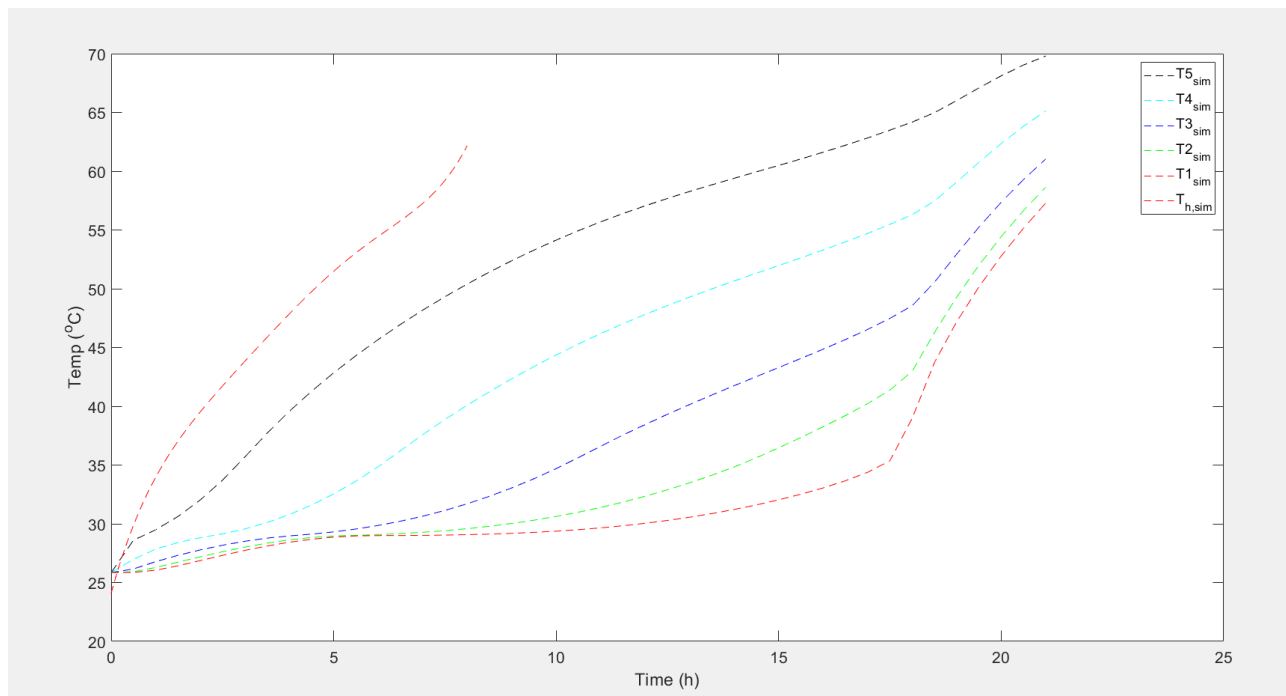
FIG. 101 FLUENT NUMERICAL SIMULATION RESULTS.

Fig. 102 shows a comparison between the experimental and numerical results. There is a good match between T_{sim} and T_{exp} trends considering the first two TCs, but T_{sim} still lower than T_{exp} for the last three TCs.
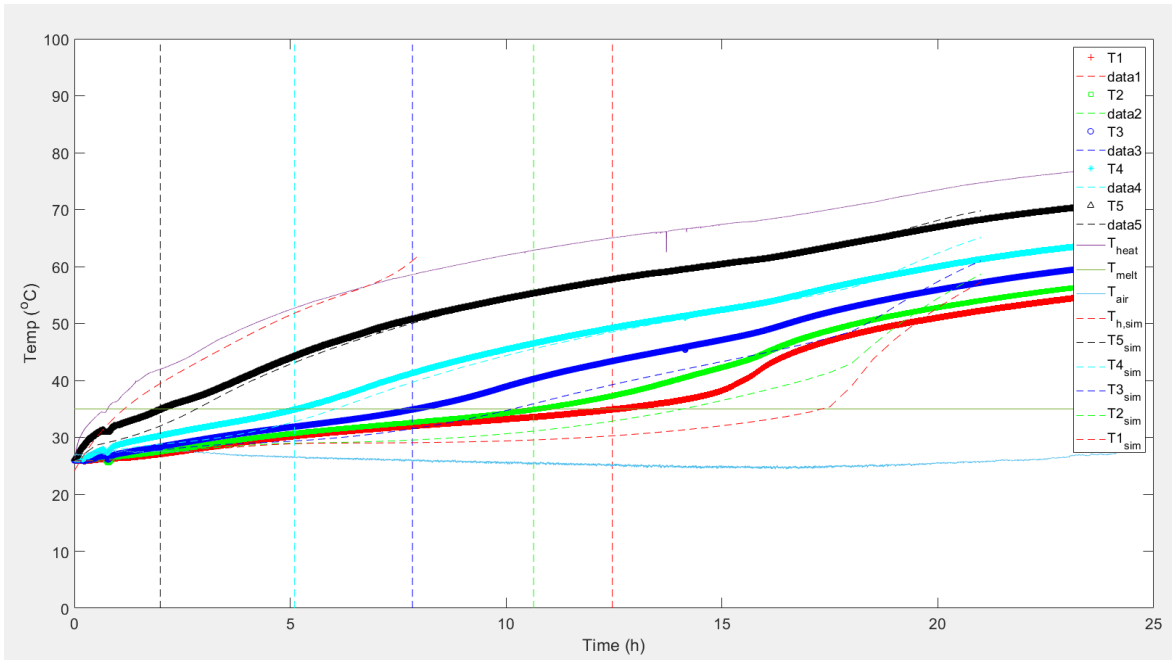
FIG. 102 COMPARISON BETWEEN NUMERICAL AND EXPERIMENTAL RESULTS.

There can be two reasons for these results:

- There could be a mistakes in Fluent simulation or some input data could be wrong, so a simulation with manifacturer input data was needed;
- The $c_{P,\ PCM}$ is not constant in both phases as the manufacturer declares but it increases with temperature, hence a simulation with a higher $c_{P,\ PCM,\ liq}$ is needed.

A numerical simulation consideringwith the manifacturer input data, was done and compared to the experimental results, as shown in Fig. 103. There is a very good match between the trends of the simulation and the experimental temperatures considering the first TCs, then the match starts to worse for TCs 3 and 4 (for which $T_{sim} < T_{exp}$); the worst match is obtained for the TC 5. It could be seen that in an ideal situation, at a certain time (17 hours), in the numerical simulation the temperature tends to grow dramatically, instead in the experimental results this is difficult to reach because there is a moment when the losses balance the heat flux given by the heater and the temperature tends to be almost constant.
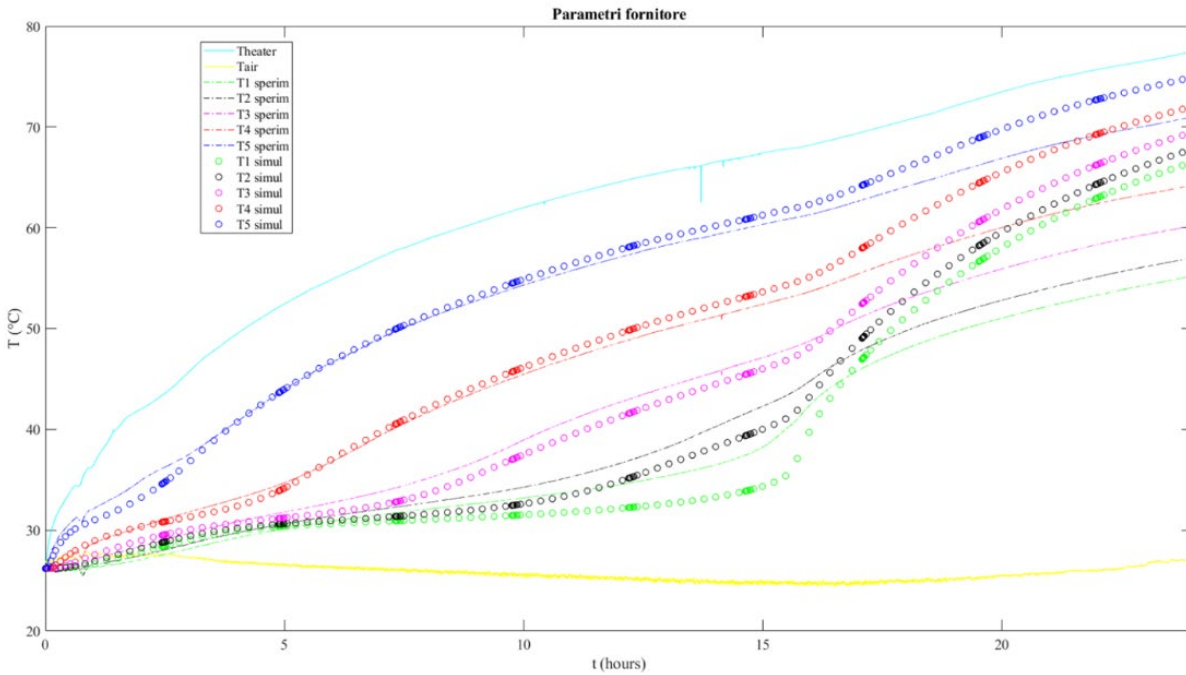
FIG. 103 NUMERICAL SIMULATION RESULTS, MADE BY THE UNIVERSITY OF PARMA, OBTAINED WITH THE MANUFACTURER INPUT DATA AND COMPARED WITH THE EXPERIMENTAL RESULTS.

Fig. 104 shows a comparison between two simulations: the one made with Fluent and that obtained with the manifacturer input data (made by the University of Parma). It can be seen that Fluent results follow a trend similar to those obtainedwith the manifacturer input data but the first simulation was more accurate. In both of the comparisons it is evident that, after the melting of all the PCM (about 15 hours), all the T_{exp} begin to tend towards a constant value as if the supplied heat was balanced by the losses: another experiment was needed to improve the set-up of the experiment achieving a better insulation.

(A)

(B)
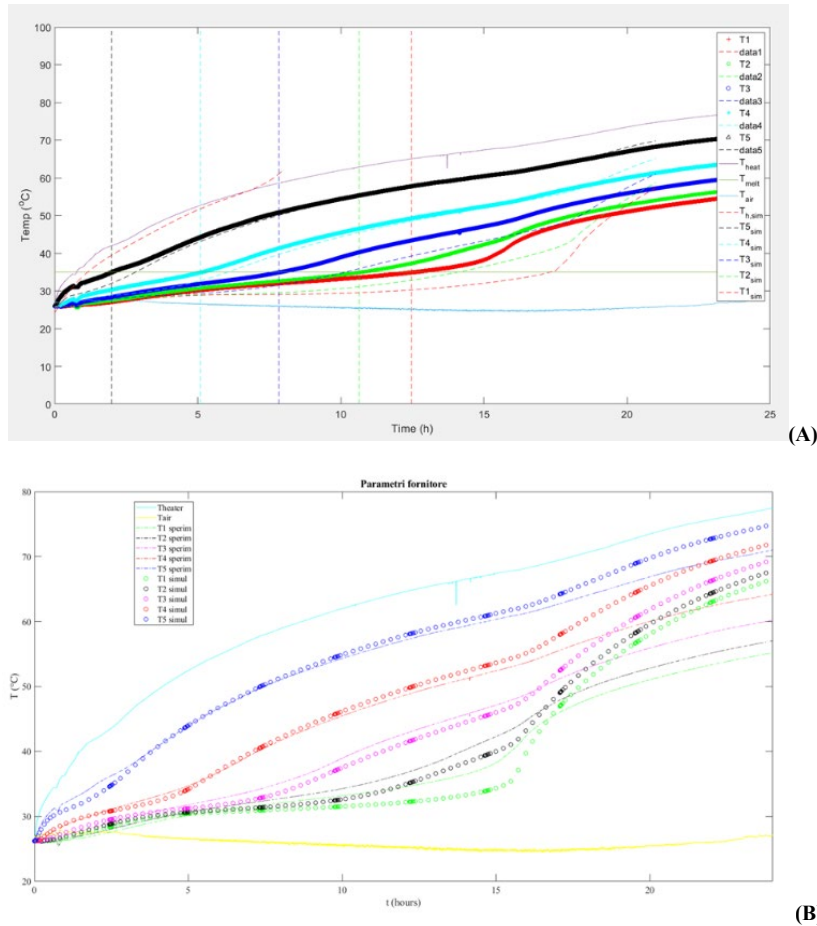
FIG. 104 COMPARISON BETWEEN FLUENT SIMULATION RESULTS AND NUMERICAL SIMULATION WITH MANUFACTURER INPUT DATA.

2.3.2.2.1 EFFECTIVE THERMAL POWER GIVEN TO THE SYSTEM

The heat is defined as that form of energy which is transferred between two systems due to a temperature difference: it follows, therefore, that no heat transmission can exist between two systems at the same temperature. The thermal power $\dot{Q}$ is the quantity of heat transmitted per unit of time (J/s = W).

In the experiments described in this thesis project the heat was transmitted by conduction. Conduction is the energy transfer which occurs as a result of the interaction of particles inside a substance with greater energy with the those inside an adjacent substance with less energy. In the laboratory experiments, the electrical heater represents the more energetic element and PCM is the

less energetic one. The theoretical electric power given to the whole system was found to be 4 W (V = 20 V, I = 0,2 A). The goal of the next calculation is to understand how much thermal power was given to the pure PCM in the experiment. The thermal power transmitted by conduction ($\dot{Q}_{cond}$) through a flat plate of constant thickness Δx is proportional to the temperature difference ΔT across the layer, to the surface A of the section normal to the direction of heat transmission and it is inversely proportional to the thickness of the layer. Hence, from the Fourier law:

$$\dot{Q}_{cond} = \lambda\, A\, \frac{\Delta T}{\Delta x} \tag{13}$$

where λ is thermal conductivity of the material equal to 0,2 W/m K for the RT35 PCM. This formula was used considering a heat transmission by conduction from the first to the second TC at the top, when the PCM is in the liquid phase, Δx is the distance between the TCs (Δx = 13 mm) and A is the area ($135*80 = 1,08*10^4$ mm^2) on which the thermal flow orthogonally impacts ⬚Fig. 105 ⬚$\dot{Q}_{tot}$⬚:

$$\dot{Q}_{tot} = \dot{Q} + \dot{Q}_{cond} \quad [\text{W}] \tag{14}$$

where $\dot{Q}$ is the thermal power given by the heater to the first layer of PCM. Hence, the formula becomes:

$$\dot{Q}_{tot} = \rho\, V\, c_p\, \frac{T_1 - T_1{}'}{\Delta t} + \lambda\, A\, \frac{\Delta T}{\Delta x} \quad [\text{W}] \tag{15}$$

where V is the volume shown in Fig. 105 between the heater and the half of the distance between the TCs (V = $18,5*80*135$ = 199800 mm^3). The whole volume is considered to have the same temperature T_1, calculated as an average between the heater temperature and the temperature of the first TC at the top (TC$_1$). $T_1{}'$ is the temperature recorded after a determined instant of time (in the calculation was 3 seconds). To avoid the values in which the temperature is lower than that measured later, a moving average with a 10 values range was used. Finally, there had been selected the values of temperatures higher than 40° C to be sure of considering only the liquid phase; in this way it was possible to use only one value both of density and of specific heat capacity. It could be seen, from Fig. 106, that the average power transmitted from the heater to PCM in the whole liquid phase was $\dot{Q}_{tot}$ = 1,37 W in a range between 1,2 W and 1,7 W. It can be deduced that, from the whole electrical power of 4 W, only 34,5% was actually transmitted to PCM. It could be seen, from

the graph in Fig. 106, that the power transmitted by the heater to PCM tends to drop as the system temperature increases. This may be due to the fact that when the system is at a very high temperature value it tends to exchange more heat with the external environment and, therefore, it is plausible that the thermal power decreases.
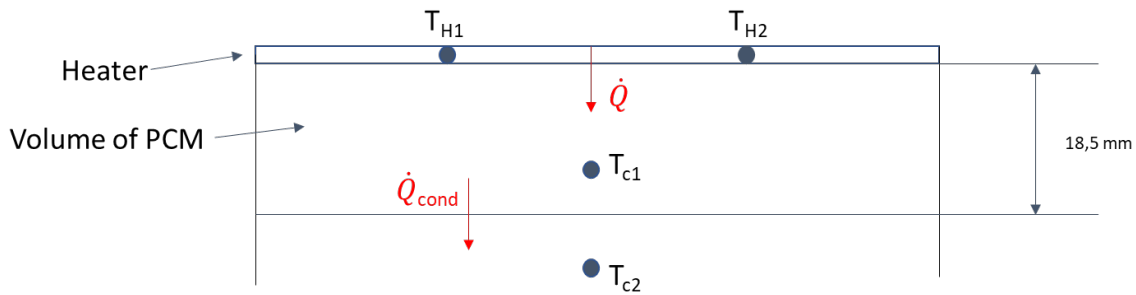
FIG. 105 GEOMETRY OF THE SYSTEM.

time	power
0	1.674676
3	1.739075
6	1.75443
9	1.729031
12	1.639304
15	1.764625
18	1.699599
21	1.739153
24	1.709443
27	1.684424
30	1.65393
33	1.679103
36	1.703895
39	1.694278
42	1.718254
45	1.709098
48	1.713545
51	1.683913
54	1.628722

Power Average
1.37997
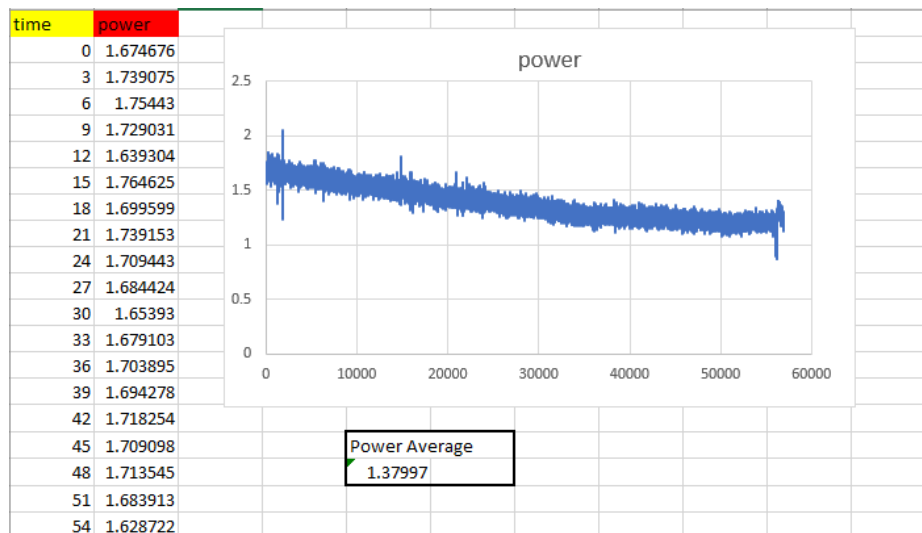
FIG. 106 EXTRACT OF EXCEL FILE OF THERMAL POWER CALCULATION.

2.3.2.3 TEST 4: MELTING OF PURE RT35 PCM IN AN EUROBATEX ® AND POLYSTYRENE BOX WITHOUT AIR CAVITY, JIMMI 2.1

In this experiment the insulation was improved. The air cavity between the polycarbonate case and the polystyrene box was filled with EUROBATEX®, as it can be seen in Fig. 107(b). Another improvement was the addition of a further piece of EUROBATEX® on the exterior part of JIMMI, in order to seal better the junction between the top and the central part of it.

Fig. 107 shows the final set-up insulation.

FIG. 107 NEW POLYSTYRENE BOX: (A) AIR CAVITY FILLED WITH EUROBATEX ®, (B) EXTERNAL PART.
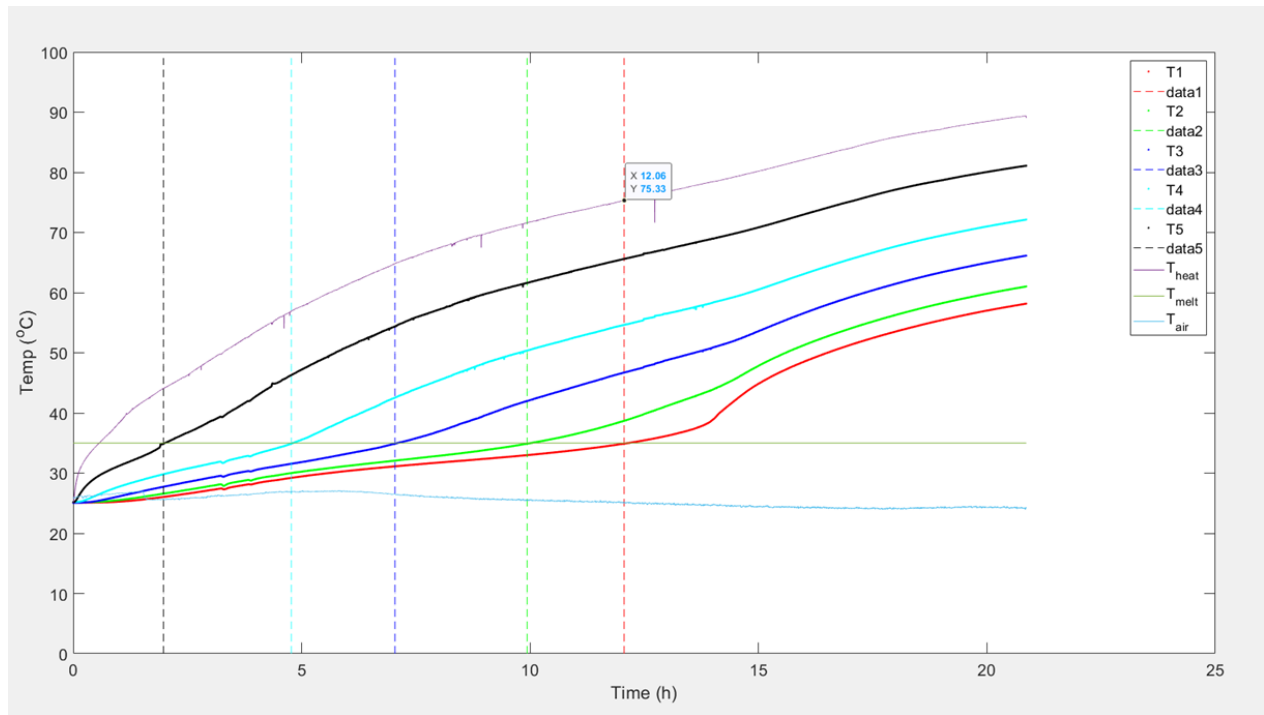
FIG. 108 EXPERIMENTAL RESULTS WITH A VOLTAGE OF 20 V.

Fig. 108 shows the experimental results obtained with the new configuration and the same voltage (V = 20 V). It can be seen that all the PCM melted in about 12 hours (at that time $T_{heater} \approx 75°$ C) and the temperature of the heater is quite higher than in the previous experiment. Therefore, it can be concluded that there have been fewer losses and the box was more insulated. The aim was to get closer to the curves made by the numerical simulation.
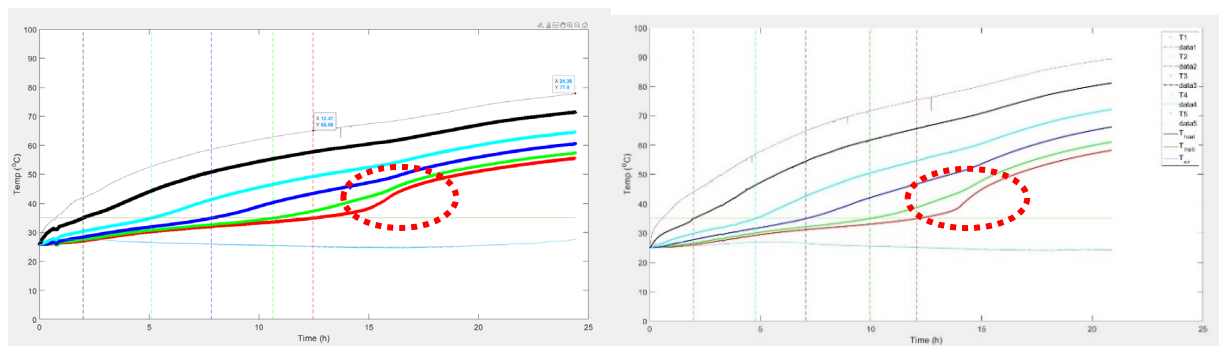
FIG. 109 COMPARISON BETWEEN TEST 3 AND TEST 4.

Fig. 109 shows a comparison between Test 3 and Test 4. There was a steep temperature increasement in both cases, but it is more evident in Test 4: this is another observation about the increase of the insulationinsulation.

116
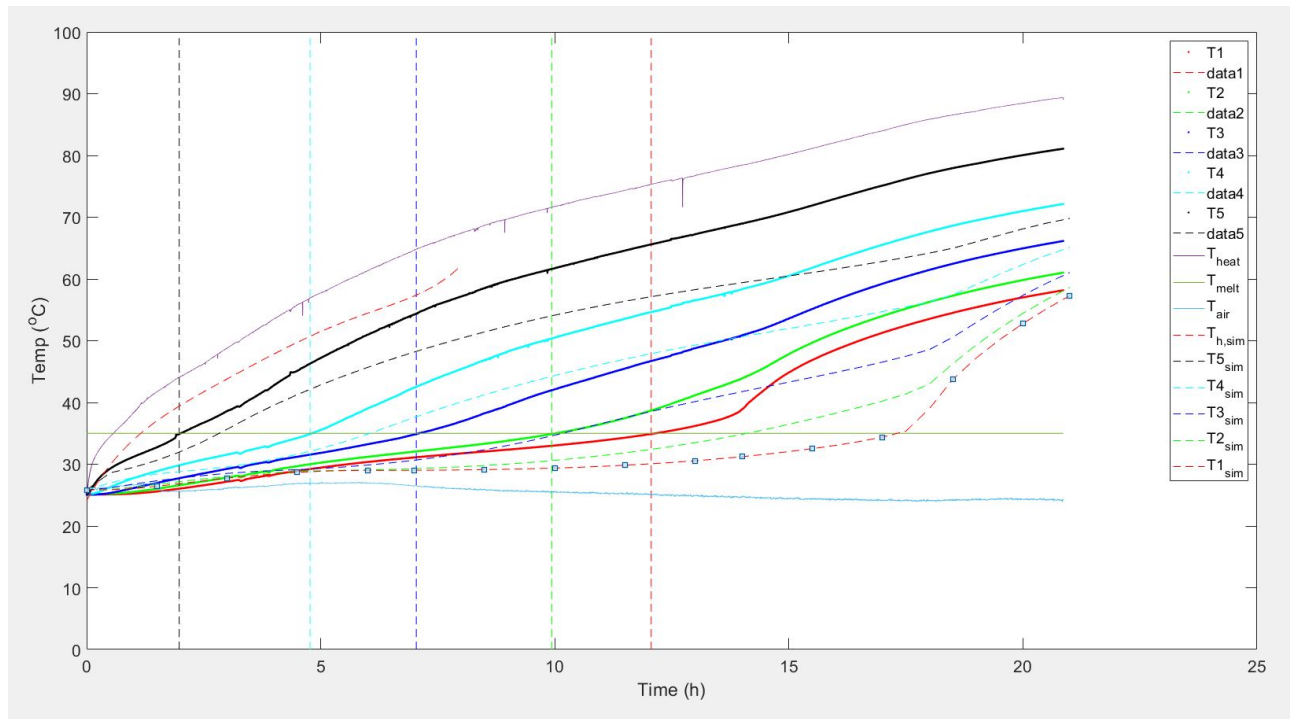
FIG. 110 COMPARISON BETWEEN NUMERICAL SIMULATION AND EXPERIMENTAL RESULTS.

Fig. 110 shows a comparison between the numerical simulation and the experimental results. As with Test 3, it is visible a steep temperature increasement, after that the temperature trends tend to go towards a constant value, as if the heat supplied was balanced by the losses: this means that the losses were not completely eliminated. About the comparison between the experimental results and the simulation ones, it seems that the experimental curves are further away from the right direction than before, but now the temperature of the heater is higher than in simulation, so another experiment with a reduced voltage is needed.

2.3.2.4 TEST 5: MELTING PURE RT35 PCM - 15 V

This experiment had the goal of reducing the temperature of the heater in order to get closer to the temperature in the numerical simulation. As with Test 4 the losses were less, the temperatures were higher and it was not possible to compare the experimental results with the simulation ones obtained using $T_{heater, test 3} < T_{heater, Test 4}$ as input. Therefore, the voltage was reduced to 15 V.
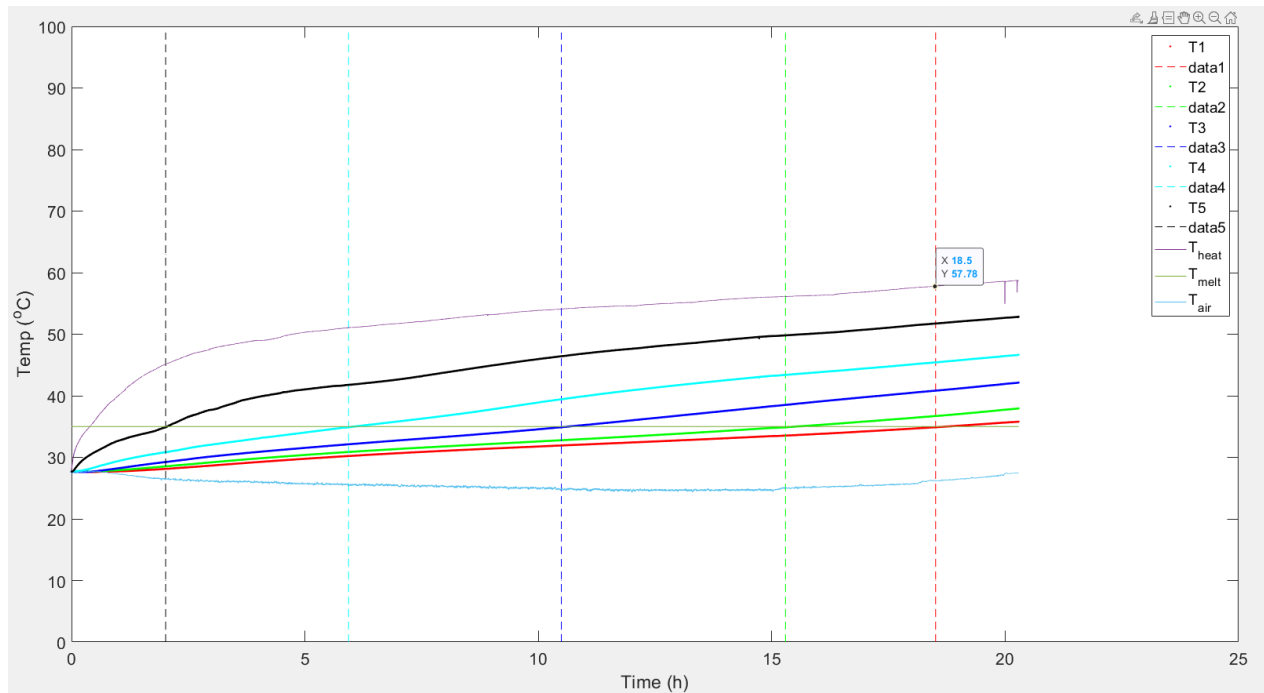
FIG. 111 EXPERIMENTAL RESULTS OBTAINED WITH A VOLTAGE OF 15 V.

Fig. 111 shows the experimental results of the new experiment: it can be noticed that the entire volume of PCM melted in about 18 h, with a heater temperature of of 58° C.
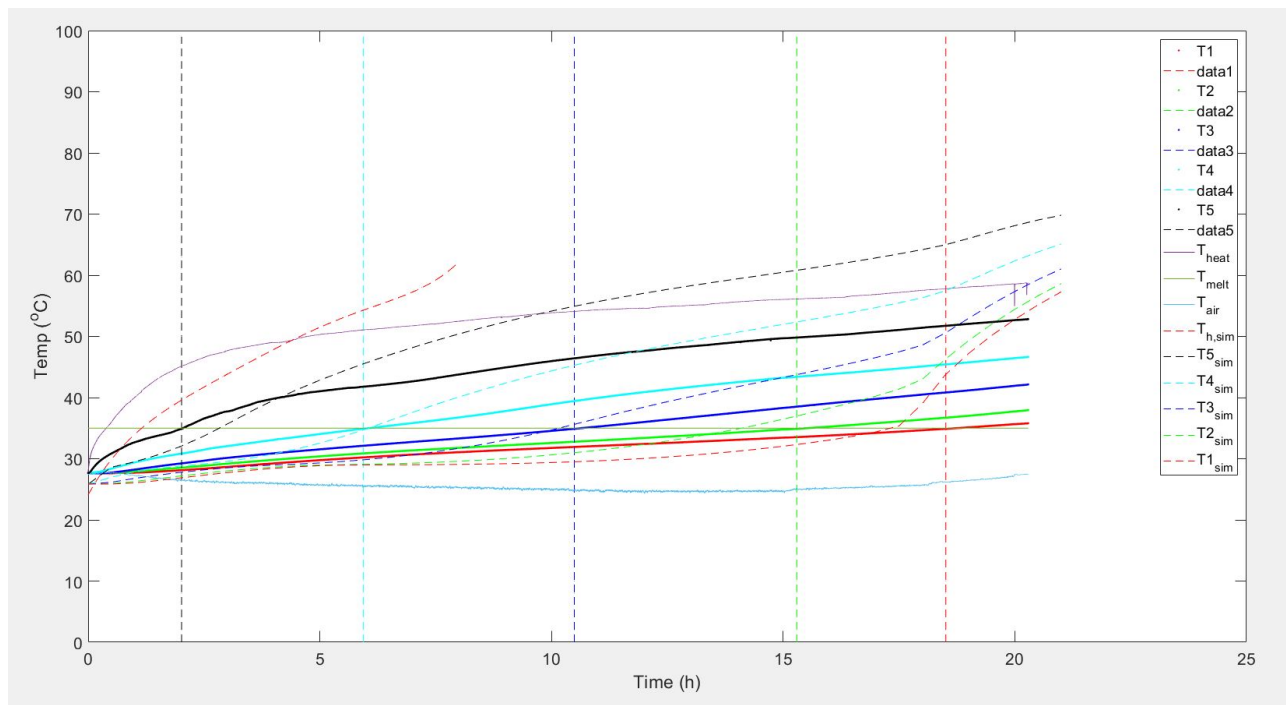
FIG. 112 COMPARISON BETWEEN NUMERICAL SIMULATION AND EXPERIMENTAL RESULTS.

Comparing the experimental results with the simulation onces (Fig. 112), it could be seen that there wasn't a very good match, yet, because of the lower heater temperature of the experiments. To obtain a T_{heater} as closer as possible to the simulated one, it was necessary to adjust better the starting voltage: in this way, the comparison between T_{exp} and T_{sim} would be reasonable.

2.3.2.5 TEST 6

2.3.2.5.1 MELTING PURE RT35 PCM - 17.5 V

In this experiment a little bit higher voltage than before was used with the aim to achieve $T_{heater,\ Test\ 5} < T_{heater,\ Test\ 6} < T_{heater,\ Test\ 4}$. A voltage of 17,5 V was used, with the goal of following the same heater temperature trend compared to the simulation results. The temperature of the TC at the bottom of the case reached the melting point (35° C) in almost 13 hours, with a heater temperature of 66 ° C, as shown in Fig. 113 by the last vertical line.
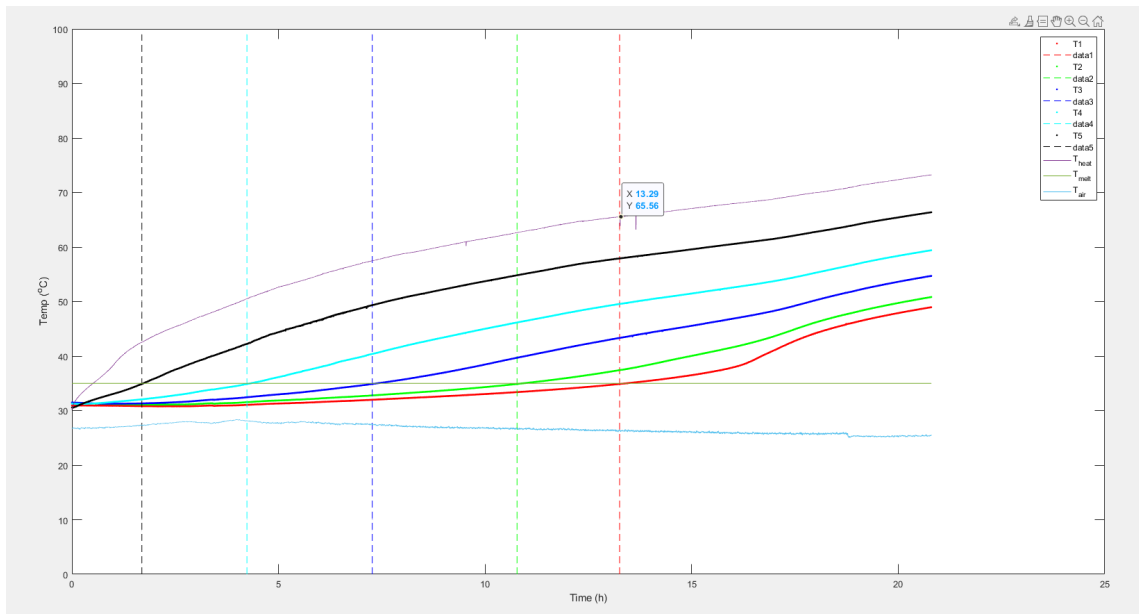
FIG. 113 EXPERIMENTAL RESULTS WITH 17.5 V.
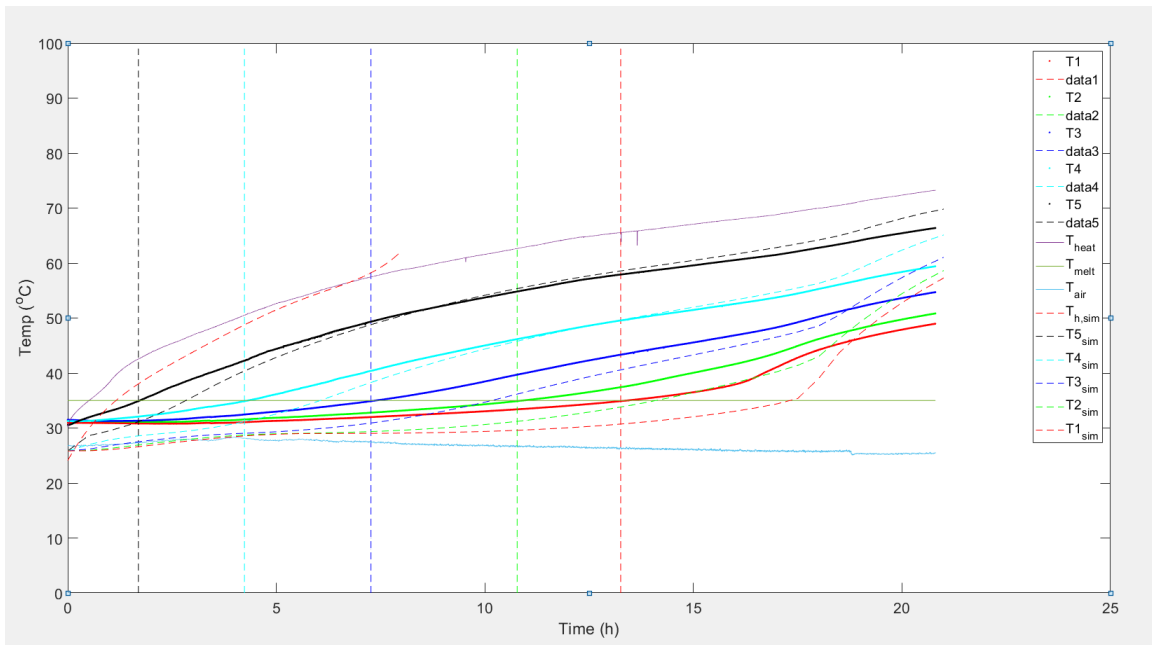
FIG. 114 COMPARISON BETWEEN THE NUMERICAL AND THE SIMULATION RESULTS.

Fig. 114. shows the comparison between the numerical and the experimental results. It could be seen that the temperature of the heater in this experiment is not lower compared to Test 4. The starting temperature (T_0) is higher than in previous test due to the high room temperature (the PCM could not be cooled before the experiment). If $T_{0,exp}$ were shifted in $T_{0,sim}$ it would be possible to see a quite good match between them. However, a new simulation, with the same input data, needs to be done to have a better and more realistic match between the numerical and the simulation results.

2.3.2.6 HEAT TRANSFER COEFFICIENT – CALCULATION

2.3.2.6.1 COOLING OF PURE RT35 PCM IN A EUROBATEX ® AND POLYSTYRENE BOX

In order to obtain realistic simulation results, it is necessary to calculate the dispersion coefficient of JIMMI (made of polystyrene and EUROBATEX ®) and run a new numerical simulation using the real heat transfer coefficient. To do this, it is necessary to carry out PCM cooling experiments (with the same geometry and set-up of the heating tests), consider an energy balance, calculate the dispersion coefficient and compare the different experiments to see the changes. TCs temperatures had been monitored while PCM was getting cold.

The experimental results are illustrated in Fig. 115 . The power supply was turned off at a temperature of 71° C and then the system was allowed to cool: the polycarbonate case was inside the polystyrene box which was at the room temperature. All the PCM reached the air temperature in almost 70 hours. It can be seen that the temperatures of the TCs drop dramatically until the solidification process started, at the temperature of 35° C: from that point on, the temperature tends to be almost constant during the whole solidification process, until the temperature reached 30° C. After that it drops more steeply, again. When the temperature tends to remain constant, the PCM is in the temperature range where the solidification occurs and this is the point where the latent heat is released. Then, there is the presence of the sensible heat and the PCM would be in a situation with a single-phase.
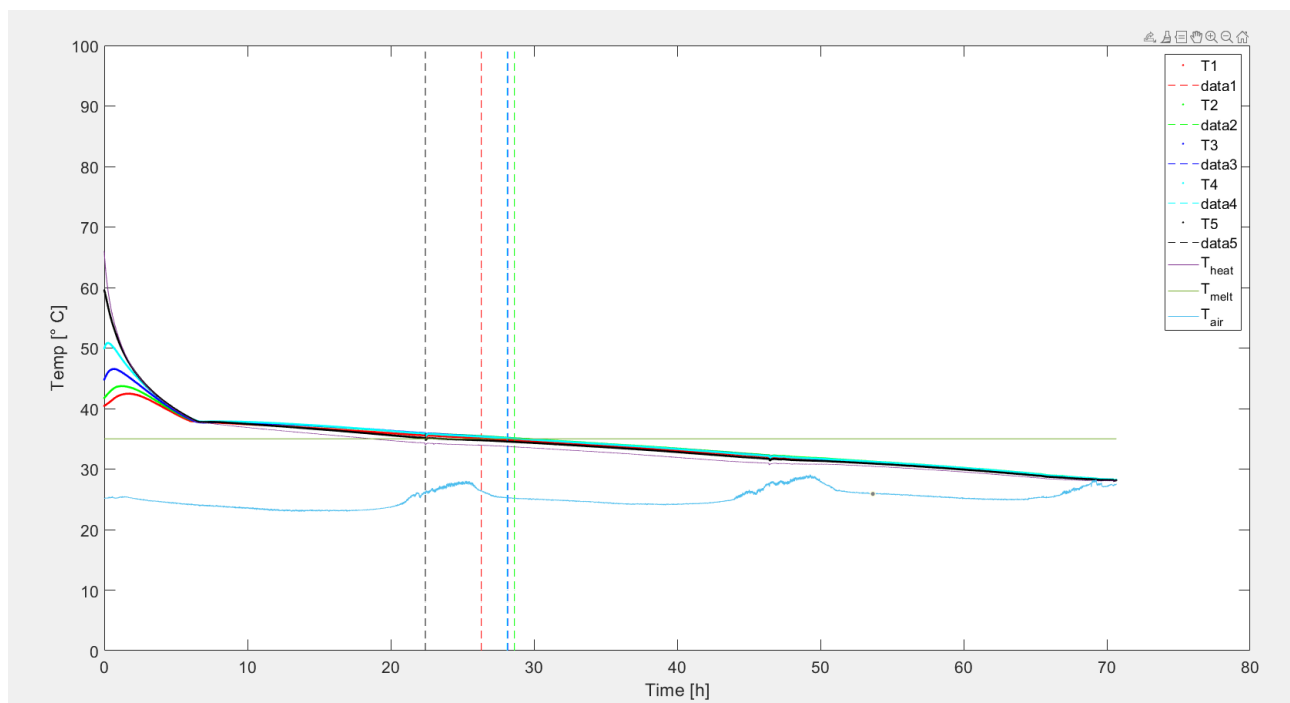
FIG. 115 COOLING TEST EXPERIMENTAL RESULTS.

For the calculation of the heat transfer coefficient it is not possible to consider the period during which the PCM presents both solid and liquid phases (29÷36° C) because its physical characteristics (density, specific heat) change from solid to liquid: the cooling process was chosen for analysis, when the whole mass of PCM is still liquid and the solidification has not begun yet.

For the calculation of the heat transfer coefficient, there were considered all the data from the previous cooling experiment (Fig. 116[OBJ].

LabVIEW Time	Absolute Time	TC_1 = TC_top	TC_2	TC_3	TC_4	TC_5 = TC_bot	TC_heat1	TC_heat2	TC_air	T_med	θ
711159,438	0	42,192	42,189	41,908	41,692	41,38	42,324	42,436	25,434	41,9501194	16,5161194
711162,809	3,371	42,19	42,187	41,907	41,685	41,385	42,393	42,491	25,427	41,9571716	16,53017164
711165,906	6,468	42,189	42,179	41,909	41,681	41,386	42,426	42,538	25,406	41,9607575	16,55475746
711168,994	9,556	42,17	42,172	41,902	41,682	41,367	42,462	42,604	25,409	41,959959	16,55095896
711172,089	12,651	42,183	42,176	41,895	41,683	41,383	42,5	42,654	25,403	41,969709	16,56670896
711175,186	15,748	42,173	42,166	41,886	41,674	41,365	42,547	42,697	25,366	41,966556	16,60055597
711178,279	18,841	42,172	42,176	41,896	41,671	41,366	42,59	42,75	25,389	41,9764851	16,58748507
711181,373	21,935	42,176	42,17	41,897	41,678	41,376	42,633	42,804	25,387	41,9855392	16,59853918
711184,469	25,031	42,168	42,168	41,89	41,664	41,362	42,672	42,855	25,368	41,9841996	16,61619963
711187,547	28,109	42,162	42,166	41,891	41,666	41,352	42,712	42,897	25,339	41,9878078	16,64880784
711190,638	31,2	42,171	42,164	41,887	41,669	41,368	42,764	42,956	25,369	41,9983993	16,62939925
711193,735	34,297	42,167	42,165	41,884	41,669	41,364	42,802	42,994	25,407	42,0021381	16,59513806
711196,806	37,368	42,161	42,16	41,886	41,668	41,357	42,841	43,044	25,426	42,0056847	16,5796847
711199,89	40,452	42,168	42,165	41,878	41,665	41,362	42,881	43,088	25,404	42,0119944	16,6079944
711202,971	43,533	42,16	42,152	41,886	41,659	41,356	42,918	43,136	25,354	42,0137724	16,65977239
711206,062	46,624	42,169	42,153	41,885	41,66	41,355	42,952	43,187	25,346	42,0209347	16,6749347
711209,134	49,696	42,158	42,157	41,88	41,651	41,353	42,996	43,231	25,321	42,0232668	16,70226679
711212,218	52,78	42,152	42,151	41,869	41,649	41,345	43,023	43,271	25,344	42,0222425	16,67824254
711215,298	55,86	42,169	42,167	41,875	41,668	41,359	43,073	43,321	25,363	42,0414328	16,67843284
711218,388	58,95	42,164	42,162	41,883	41,658	41,35	43,105	43,368	25,36	42,0435616	16,68356157
711221,483	62,045	42,152	42,151	41,871	41,656	41,351	43,138	43,405	25,352	42,042028	16,69002799
711224,563	65,125	42,157	42,152	41,867	41,65	41,342	43,178	43,441	25,338	42,0449422	16,70694216
711227,653	68,215	42,159	42,148	41,868	41,65	41,349	43,229	43,493	25,364	42,0527388	16,68873881
711230,749	71,311	42,159	42,152	41,872	41,656	41,352	43,255	43,537	25,358	42,0607127	16,70271269
711233,842	74,404	42,155	42,145	41,873	41,653	41,349	43,284	43,571	25,356	42,0623377	16,70633769
711236,939	77,501	42,146	42,138	41,868	41,644	41,334	43,32	43,613	25,337	42,060278	16,72327799
711240,028	80,59	42,156	42,144	41,869	41,66	41,344	43,369	43,651	25,33	42,0735448	16,74354478
711243,126	83,688	42,139	42,139	41,855	41,642	41,337	43,381	43,7	25,344	42,0672369	16,72323694
711246,217	86,779	42,163	42,157	41,869	41,651	41,341	43,427	43,734	25,378	42,0845951	16,70659515
711249,294	89,856	42,154	42,14	41,856	41,64	41,334	43,463	43,772	25,375	42,0795131	16,70451306
711252,389	92,951	42,153	42,138	41,858	41,644	41,334	43,492	43,817	25,395	42,0852593	16,69025933
711255,488	96,05	42,141	42,132	41,861	41,639	41,33	43,53	43,846	25,384	42,0861082	16,70210821
711258,578	99,14	42,158	42,131	41,859	41,634	41,336	43,568	43,9	25,407	42,0941045	16,68710448
711261,668	102,23	42,147	42,138	41,86	41,642	41,334	43,595	43,928	25,403	42,0992034	16,69620336
711264,764	105,326	42,15	42,132	41,849	41,633	41,324	43,625	43,966	25,401	42,0978489	16,69684888
711267,862	108,424	42,146	42,132	41,847	41,623	41,323	43,658	44,007	25,377	42,0999347	16,7229347
711270,934	111,496	42,159	42,145	41,857	41,644	41,334	43,702	44,055	25,389	42,1181772	16,72917724
711274,028	114,59	42,144	42,122	41,85	41,633	41,317	43,725	44,076	25,374	42,108778	16,73477799
711277,123	117,685	42,153	42,131	41,845	41,636	41,329	43,767	44,112	25,399	42,1184646	16,71946455

Side calculation tables:

	Solid		Liquid	
	[l]	[m³]	[l]	[m³]
V_top	174825	0,0001748	199800	0,0001998
V_TC	122850	0,0001229	140400	0,0001404
V_bot	89775	8,978E-05	102600	0,0001026

ρ_{sol} [kg/m³]	860	
ρ_{liq} [kg/m³]	770	
$c_{p,sol}$ [kJ/kg K]	3	
$c_{p,liq}$ [kJ/kg K]	2	

	Solid		Liquid	
	(M*c_p)	Weights	(M*c_p)	Weights
TC_1	0,451049	0,2761194	0,307692	0,2761194
TC_2	0,316953	0,1940299	0,216216	0,1940299
TC_3	0,316953	0,1940299	0,216216	0,1940299
TC_4	0,316953	0,1940299	0,216216	0,1940299
TC_5	0,23162	0,141791	0,158004	0,141791
Tot	1,633527		1,114344	

FIG. 116 EXTRACT OF THE EXCEL FILE WITH PART OF THE HEAT TRANSFER COEFFICIENT CALCULATIONS.

RT35 PCM data are shown in Tab 16.

TAB 16: RT35 PCM DENSITY AND HEAT CAPACITY FOR SOLID AND LIQUID PHASES.

	Solid phase	Liquid phase
ρ [kg/m³]	860	770
c_p [kJ/kg K]	3	2

Considering the energy balance shown in Eq. 8 it is possible to calculate the global heat transfer coefficient, considering $\theta\,(t = 0) = \theta_0 = 21.69°$ C, as can be seen in Fig. 122, the value of the slope B could be calculated by Eq. 9.

$$\int_{\theta_0}^{\theta} \frac{d\theta'}{\theta'} = -\int_0^t \left(\frac{k}{Mc_p}\right)\cdot dt' \qquad \rightarrow \qquad (\ln\theta - \ln 21.69) = -B\,t \rightarrow$$

$$\rightarrow \qquad \ln\theta = \ln 21.69 - B\,t \qquad \rightarrow \qquad -\ln\frac{\theta}{21.69} = B\,t$$

122

The distances between the TCs, in this case, were the following, as can be seen in Fig. 117:

- $d_{BOTTOM-1} = 3$ mm
- $d_{1-2} = d_{2-3} = d_{3-4} = d_{4-5} = 13$ mm
- $d_{5-heater} = 12$ mm
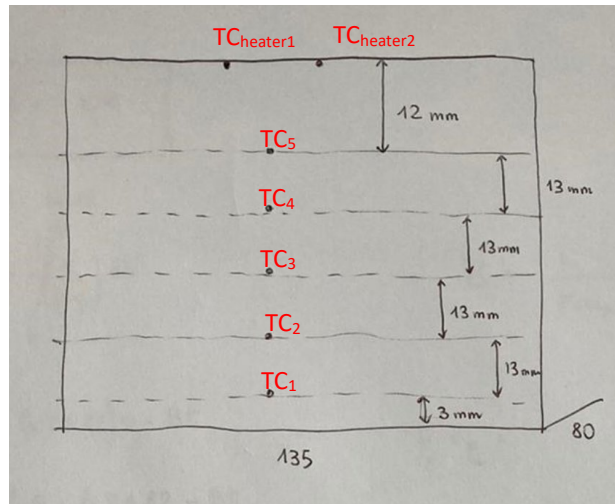
FIG. 117 POSITIONS AND DISTANCE OF THERMOCOUPLES.

The whole volume of the PCM in the case (whose base measures $135 * 80 = 1,08 * 10^4 \, mm^2$) was divided in 5 sub-volumes, shown in Fig. 118:

- $V_1 = V_{BOTTOM}$
- $V_2 = V_3 = V_4$
- $V_5 = V_{TOP}$
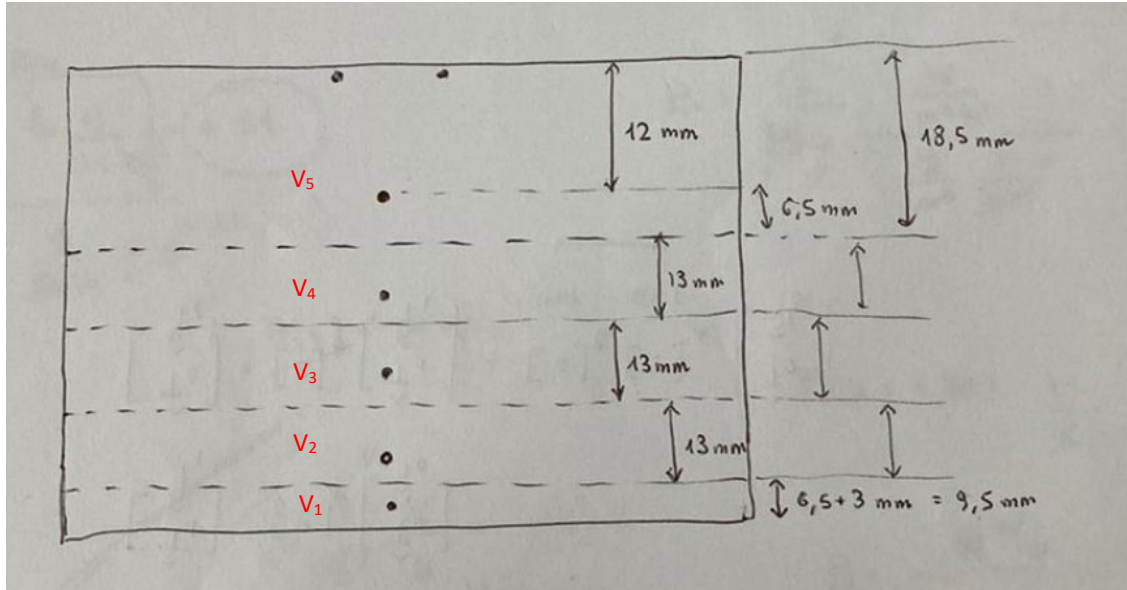
FIG. 118 VOLUMES CONSIDERED FOR THE CALCULATION.

$$\bar{T} = \frac{m_1 c_{p_1} T_1 + m_2 c_{p_2} T_2 + m_3 c_{p_3} T_3 + m_4 c_{p_4} T_4 + m_5 c_{p_5} T_5}{\sum_1^5 m_i c_{p_i}} \qquad (16)$$

T_5 is the average among the temperatures recorded by TC$_5$, TC$_{heater1}$ and TC$_{heater2}$, that are the TCs included in V$_5$. $\bar{T}$ is represented in Fig. 116 as T$_{med}$. It was calculated in the same way as before, considering the new positions of TCs.

$\bar{T}$ would have the same value if it was calculated considering ρ and c$_p$ both for liquid and for the solid phase because the density and the c$_p$ can be collected in the numerator and simplified, obtaining the following equation:

$$\bar{T} = \frac{\rho c_p (V_1 T_1 + V_2 T_2 + V_3 T_3 + V_4 T_4 + V_5 T_5)}{\rho c_p (V_{tot})} \qquad (17)$$

With this equation $\bar{T}$ was calculated for each instant of time and all the temperature differences θ were calculated and plotted in the graph below (Fig. 119).
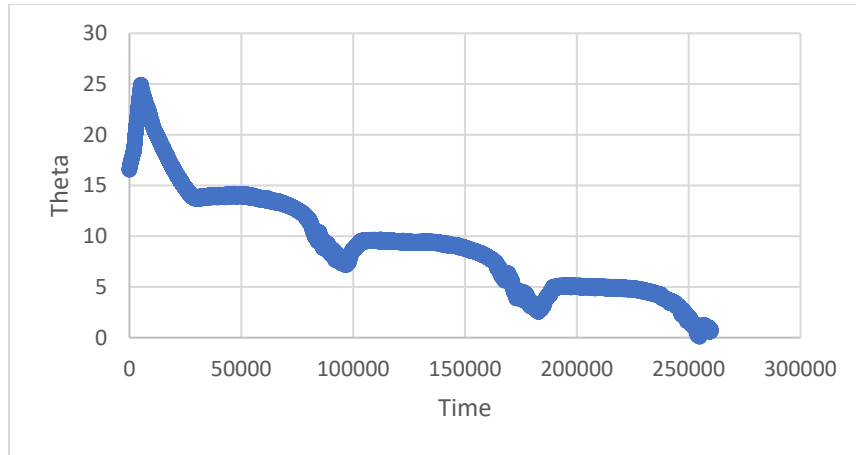
FIG. 119 TEMPERATURE DIFFERENCES OVER TIME.

To be sure of not to examine the PCM when the solidification process already began, it has been also excluded the interval of time just before the reaching of the set $T_{phase\ change}$, in Fig. 120 it is shown a graph which represent the average of the recorded temperature in cooling experiment, the red circle represents the range of temperature used to calculate the heat transfer coefficient.
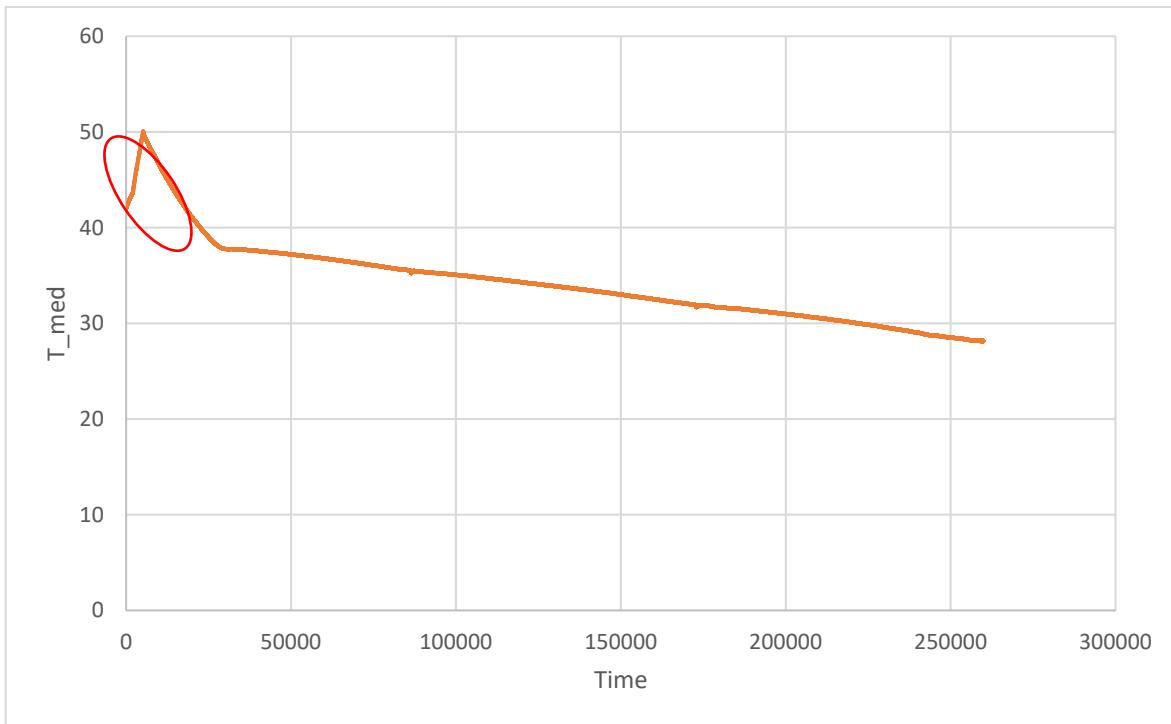
FIG. 120 RANGE OF TEMPERATURE CHOSEN FOR THE CALCULATION.

As it has already been said, $-\ln\frac{\theta}{21.69} = B\,t$, is the equation of a line whose slope is B

$(y = -\ln\frac{\theta}{21.69}$ and x = t): using all the values of y and x obtained from $-\ln\frac{\theta}{\theta_0}$ in function of time

(blue points in the graph in Fig. 121 below), the slope (B) of the regression line can be calculated (SLOPE Excel function).

Once obtained B, the interpolating line can be plotted (the red one in the graph in Fig. 121 below), which has the classical equation y = mx + q (q has been chosen in order to better matches the experimental curve).
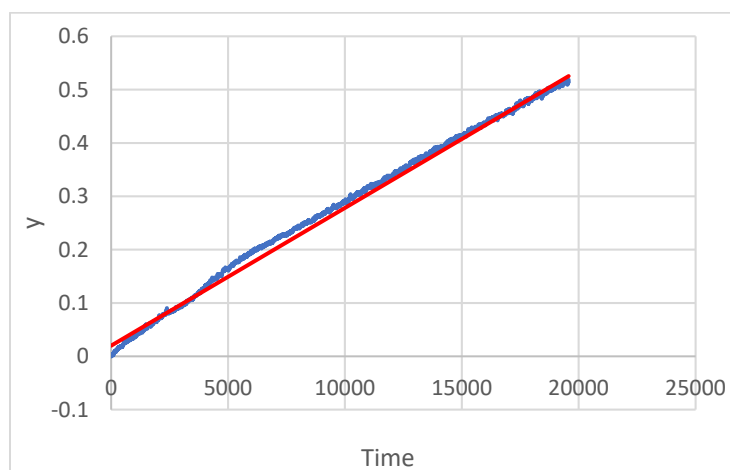
FIG. 121 REAL LINE AND INTERPOLATING LINE.

		LabVIEW Time	θ	Absolute Time	$\ln((\theta)/(\theta_0))$	Interpolating line
		720419.578	21.69303	0	0	0.01
Σ (M*cp) [J/K]	1114.344	720422.658	21.69335	3.08	-1.48785E-05	0.010073137
		720425.75	21.70137	6.172	-0.000384361	0.01014656
B [s^{-1}]	2.37459E-05	720428.842	21.69018	9.264	0.000131422	0.010219982
C	0.01	720431.924	21.71607	12.346	-0.001061405	0.010293167
K [W/K]	0.026461076	720435.012	21.69906	15.434	-0.00027801	0.010366494
		720438.109	21.69515	18.531	-9.7695E-05	0.010440035
		720441.182	21.69401	21.604	-4.51507E-05	0.010513006
External heat exchanging surface [m^2]	U [W/m^2 K]	720444.266	21.6877	24.688	0.000245484	0.010586238
0.6	0.044101793	720447.358	21.68777	27.78	0.000242473	0.01065966
		720450.44	21.68099	30.862	0.000554875	0.010732845
		720453.517	21.69012	33.939	0.000134088	0.010805911
		720456.611	21.69344	37.033	-1.89205E-05	0.010879381
		720459.701	21.68627	40.123	0.000311466	0.010952756
		720462.777	21.67992	43.199	0.000604614	0.011025798
		720465.871	21.66714	46.293	0.001194094	0.011099268
		720468.966	21.66384	49.388	0.0013466	0.011172761
		720472.063	21.66232	52.485	0.001416789	0.011246302
		720475.152	21.6536	55.574	0.001819247	0.011319653
		720478.247	21.6954	58.669	-0.000109132	0.011393147
		720481.343	21.70815	61.765	-0.000696642	0.011466664
		720484.423	21.70119	64.845	-0.000376022	0.011539801

FIG. 122 EXTRACT OF EXCEL FILE WITH CALCULATION OF HEAT TRANSFER COEFFICIENT AND GLOBAL HEAT EXCHANGE COEFFICIENT.

Finally, it can be calculated the heat transfer coefficient k with the inverse equation of B, as can be seen in Fig. 122, with the use of Eq. 11, and the global heat transfer coefficient can be calculated with Eq. 12

In the experiment the values obtained for area and global heat exchange coefficient were: A = 0,6 m^2 and U = 0,0442 W/m^2 K, as can be seen in Fig. 122.

2.3.2.7 EFFECTIVE THERMAL POWER GIVEN TO THE SYSTEM

Effective thermal power transmitted by the heater to PCM was calculated, with the same calculation of Test 3 with Eq. 15. The electrical power given to the whole system was 3.5 W (V = 17.5 V, I = 0,2 A). An average of thermal power in the whole process of melting was calculated, as can be seen in Fig. 123. The value of effective power is 1,48 W, 42,2% of the whole electrical power supplied by the autotransformer. It could be seen, comparing this result with the one obtained in Test 3 (34,5% of total electrical power), that the value of effective power transmitted to PCM is increased. This is another demonstration of the efficiency of improvements of this insulation box.

time		Power
26096.03	0	1.637481
26099.11	3.082	1.713812
26102.19	6.162	1.650246
26105.27	9.241	1.790076
26108.35	12.32	1.713269
26111.44	15.407	1.687646
26114.52	18.486	1.717617
26117.61	21.583	1.635283
26120.7	24.664	1.648866
26123.78	27.75	1.739004
26126.86	30.831	1.719072
26129.94	33.912	1.696951
26133.02	36.989	1.735473
26136.1	40.069	1.703646
26139.19	43.159	1.752989
26142.27	46.239	1.573173
26145.35	49.32	1.605392
26148.44	52.408	1.669372
26151.52	55.488	1.679379
26154.6	58.568	1.587897
26157.69	61.658	1.673013
26160.77	64.74	1.68229
26163.84	67.813	1.710785
26166.92	70.891	1.602101
26170	73.972	1.66628
26173.1	77.066	1.65715
26176.18	80.146	1.661056

Power

Power average
1.480124

FIG. 123 CALCULATION OF THE EFFECTIVE THERMAL POWER GIVEN TO PCM.

2.3.2.8 TEST 7: COOLING OF PURE RT35 PCM AND HEAT TRANSFER CALCULATION

Another cooling experiment with the same set-up and the same starting conditions was conducted to verify the values of k and U that were found in Test 1. In Fig. 124 can be seen that the trend of all the temperatures was almost the same of Test 1, the whole volume of PCM solidified and reached the room temperature in about 75 hours. Considering the first rapid curve indicated with a red circle in the graph below, new calculations of the heat transfer coefficient and global heat exchange coefficient were done.
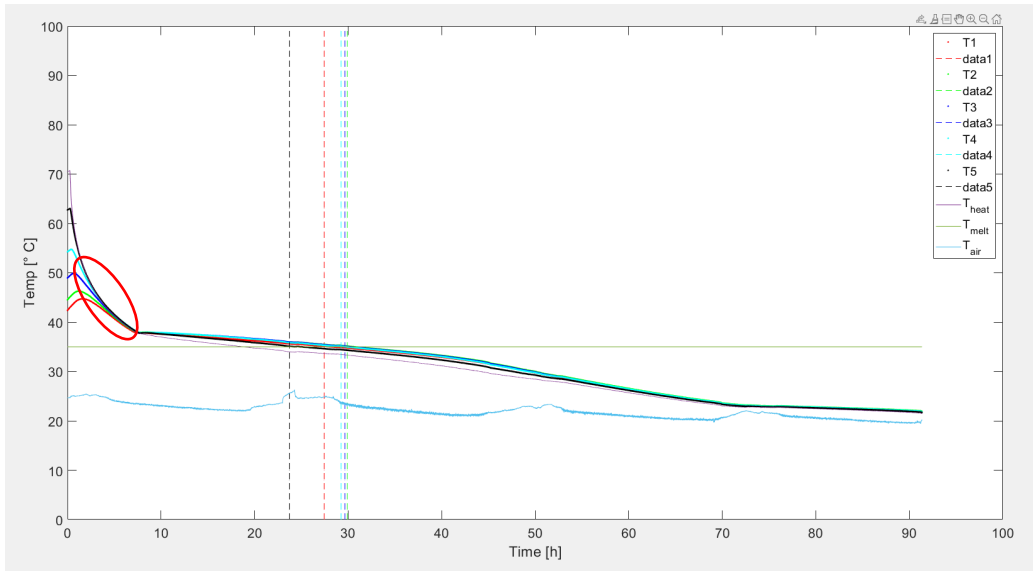
FIG. 124 COOLING EXPERIMENT WITH SAME CONDITIONS OF TEST 1.

$\bar{T}$ and θ were calculated and compared to the values obtained in previous experiment: the graph in Fig. 125 shows the values of $-\ln\frac{\theta}{\theta_0}$ in function of time (blue line) and the interpolating line. Just below the graph there are the values of k = 0,028 W/K and U = 0,046 W/m^2 K which are in agreement with the previous ones.

External heat exchanging surface [m^2]	U [W/m^2 K]
0.6	0.04645336

Σ (M*cp) [J/K	1114.344

B [s^{-1}]	2.5E-05
C	0.02
K [W/K]	0.027872
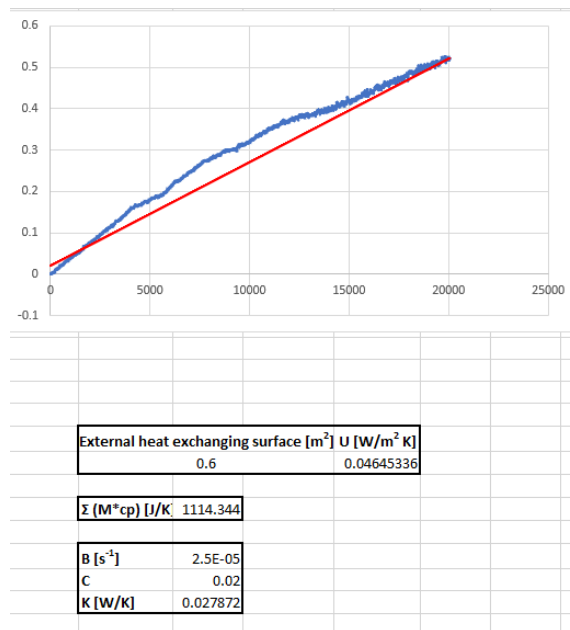
FIG. 125 EXTRACT OF THE EXCEL FILE: COMPARISON BETWEEN THE REAL CURVE AND THEINTERPOLATING LINE AND CALCULATION OF THE HEAT TRANSFER COEFFICIENT.

To have another proof that these results were correct, same calculations were done considering the decrease of temperature when the PCM was already solid. The temperature range considered is shown in the graph below, with a blue circle (Fig. 126).
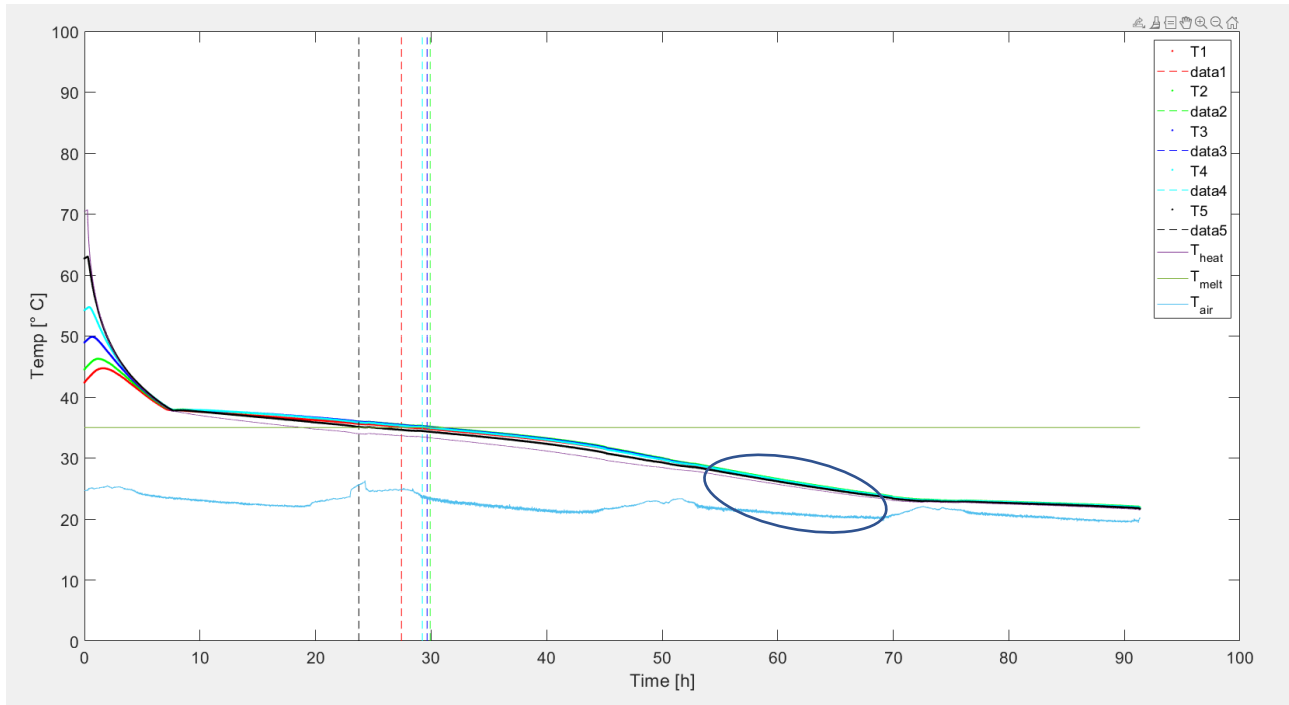
FIG. 126 COOLING EXPERIMENT WITH SAME CONDITIONS OF TEST 1.

External heat exchanging surface [m²]		U [W/m² K]	
0.6		0.030115071	
	New U		0

Σ (M*cp) [J/K]	1633.527	B [s⁻¹]	1.10614E-05
		C	0
		K [W/K]	0.018069043
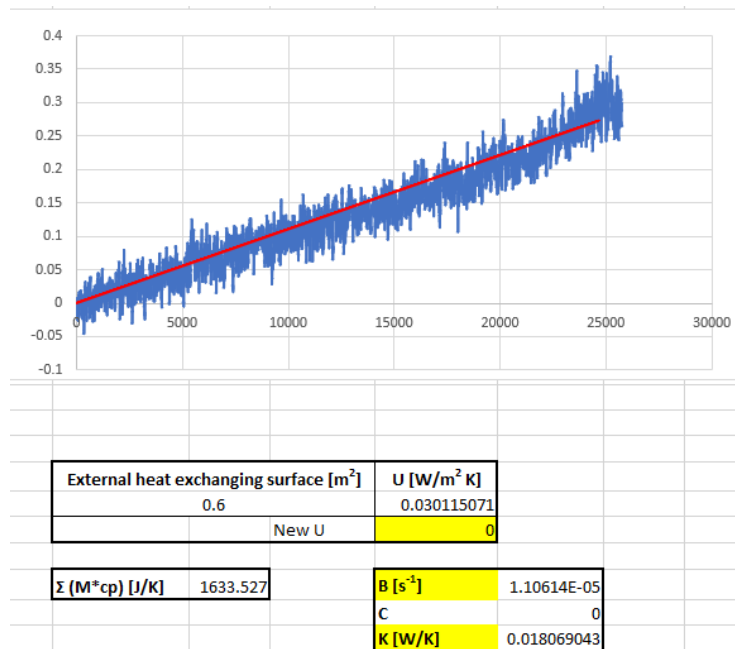
FIG. 127 FIRST RESULT OF HEAT TRANSFER COEFFICIENT IN SOLID PART.

The results initially appeared not to be in good agreement with the previous ones, the consideration was done: the temperature differences (θ) in this chosen temperature range were very small and variable, therefore the calculation uncertainty increased. Actually, the new value of k was almost 30% smaller than previous one. Hence, it was calculated new slope considering the maximum and minimum values of $-\ln\frac{\theta}{\theta_0}$ and the new values of k and U were k = 0,027 W/K and U = 0,045 W/m^2 K (Fig. 128⏎. The results were agreement with previous ones.

	Absolute Time	ln((θ)/(θ_0))
max	25730.066	0.369056154
min	355.004	-0.04595003
New B[s^{-1}]		1.63549E-05
New K		0.026716144
New U		0.044526906
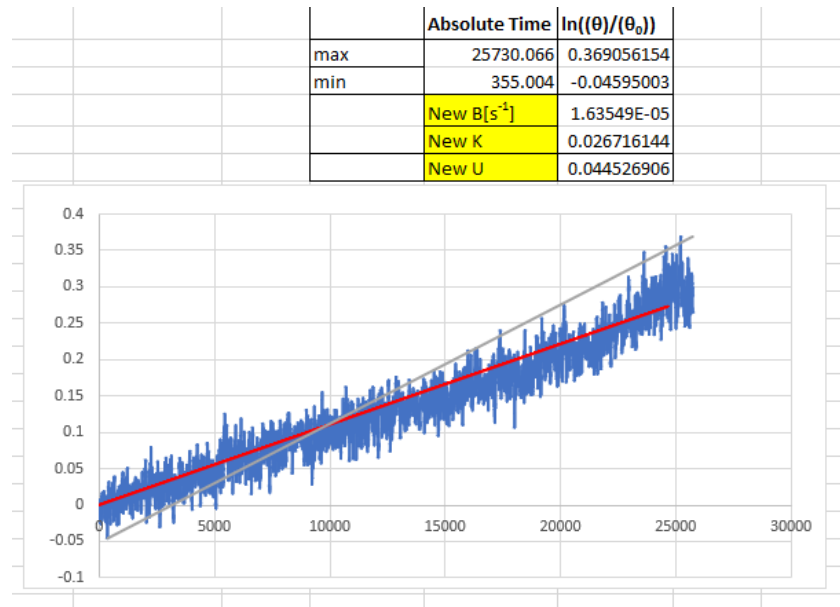
FIG. 128 NEW INTERPOLATING LINE.

2.3.2.9 TEST 8: MELTING OF RT35 PCM WITH ALUMINUM FOAM, JIMMI 2.1

The case was opened, and the aluminum foam was immersed into the PCM (Fig. 129⏎. It was used the same set up of previous experiments to test and compare the influence of metal foams in the melting process of the RT35 PCM.
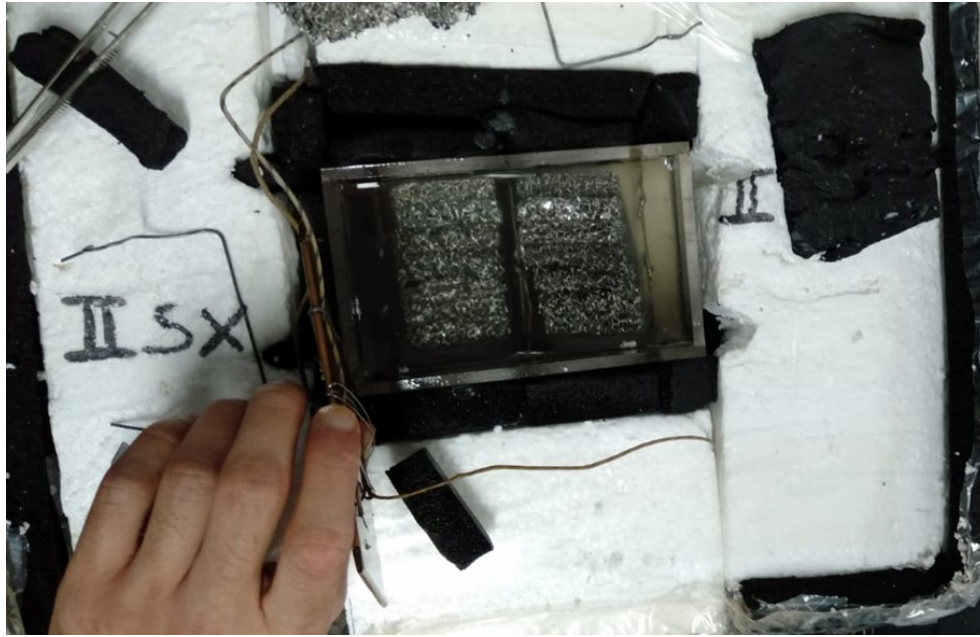
FIG. 129 INSERTION OF THE METAL FOAM INTO THE CASE

The experiment was launched with 17,5 V and 0,2 A and an improvement was added to set-up: a voltmeter was put in parallel in the system (the new set-up is described in Fig. 130: voltage set would be more accurate. The melting results are shown in Fig. 131. All the PCM melted in about 13 hours (at that time $T_{heater} \approx 48°$ C) and reached the melting area (29°÷36° C) in t ≈ 5,5 h. The trend of temperatures in all the PCM is almost the same for the experiment when the metal foams are used: the heating process is more homogeneous.
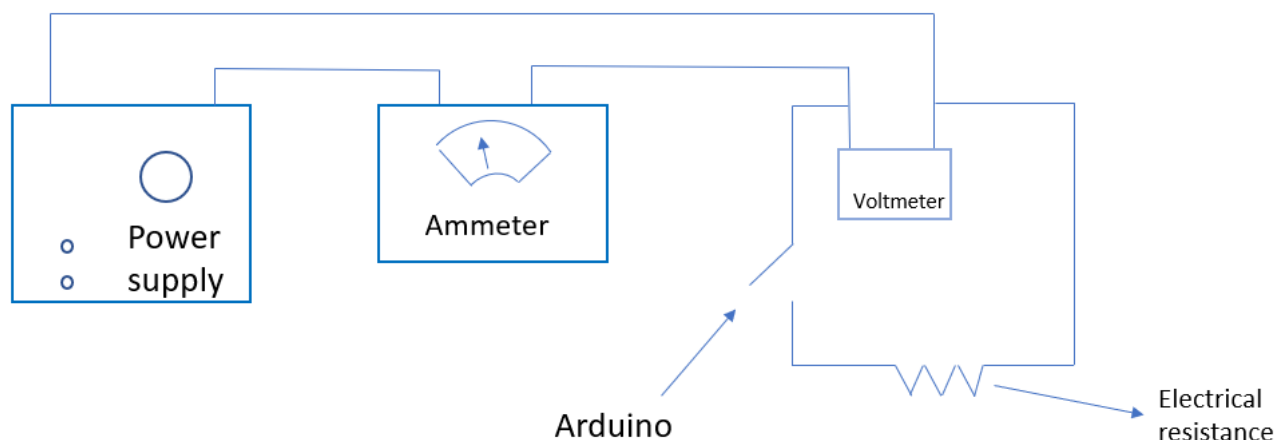
FIG. 130 NEW EXPERIMENTAL SET-UP.
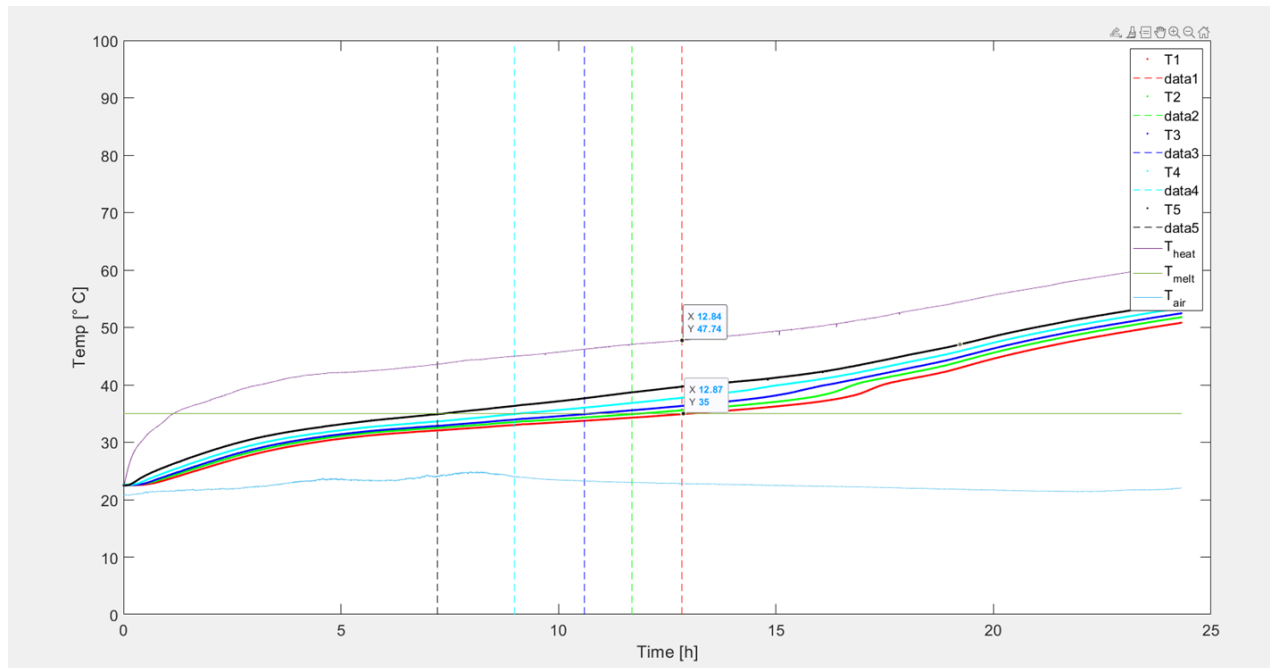
FIG. 131 EXPERIMENTAL RESULTS OF THE MELTING PROCESS WITH METAL FOAMS.

2.3.2.9.1 COOLING WITH ALUMINUM FOAM

After the whole PCM melted, a cooling experiment was conducted. The experimental results of cooling with metal foams are shown in Fig. 132. The whole volume of PCM solidified and reached the room temperature in 110 hours, a much higher value than the one obtained with pure PCM. It was expected that the cooling time was longer with metal foams because with pure PCM there was the influence of the natural convection. Therefore, metal foams forbid the natural convection due to their porous structure: the convection motus are not able to develop inside the pores and the time to solidify increases.
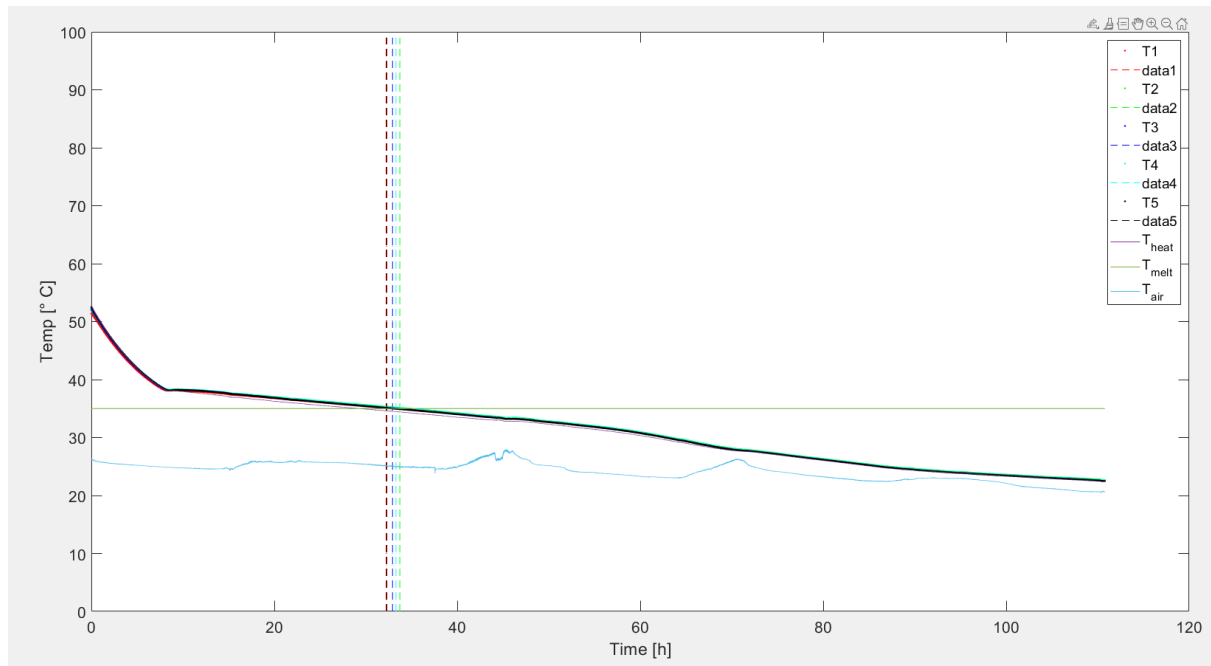
FIG. 132 EXPERIMENTAL RESULTS OF COOLING WITH METAL FOAMS.

The experiment was repeated and compared with the previous one. In the graph showed in Fig. 133 there is the comparison between the two cooling experiments with all the curves of the two graphs overlapped.
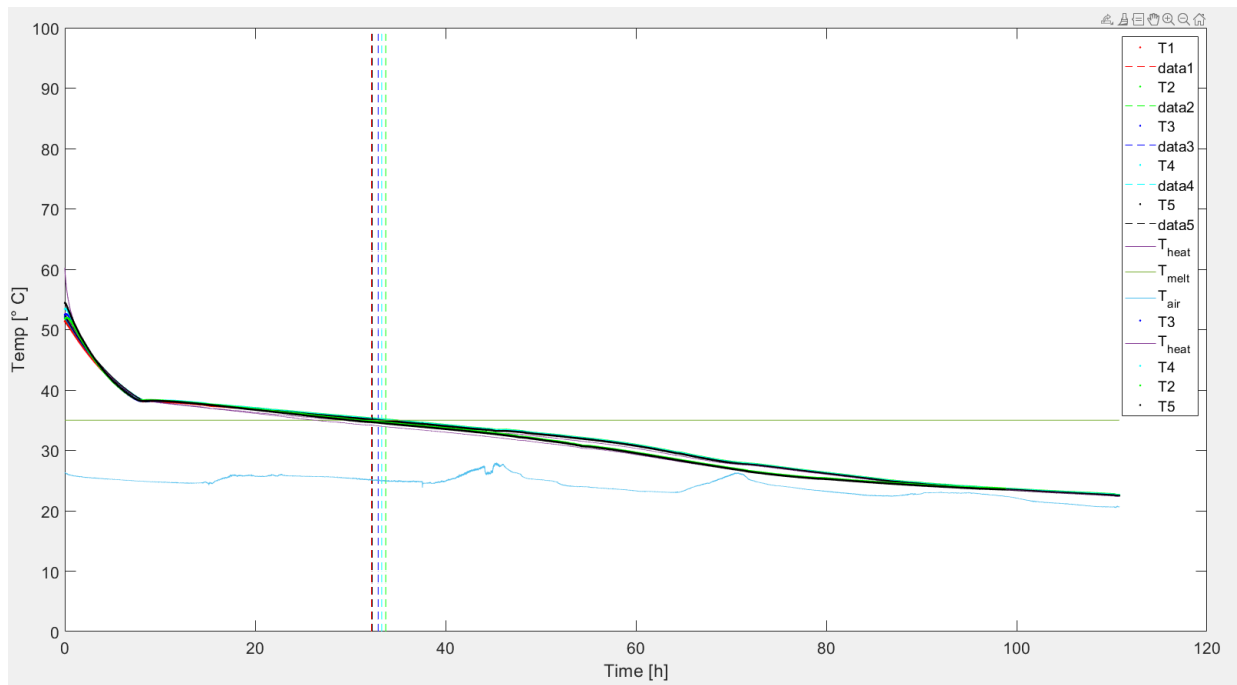
FIG. 133 COMPARISON BETWEEN THE TWO COOLING EXPERIMENT WITH METAL FOAMS.

The experiment was compared even with the cooling with pure RT35 PCM: as shown in Fig. 134, the cooling process is more homogeneous with the metal foam, all the TCs measurements tend to have almost the same values over time since the moment to the energy supply was stopped.
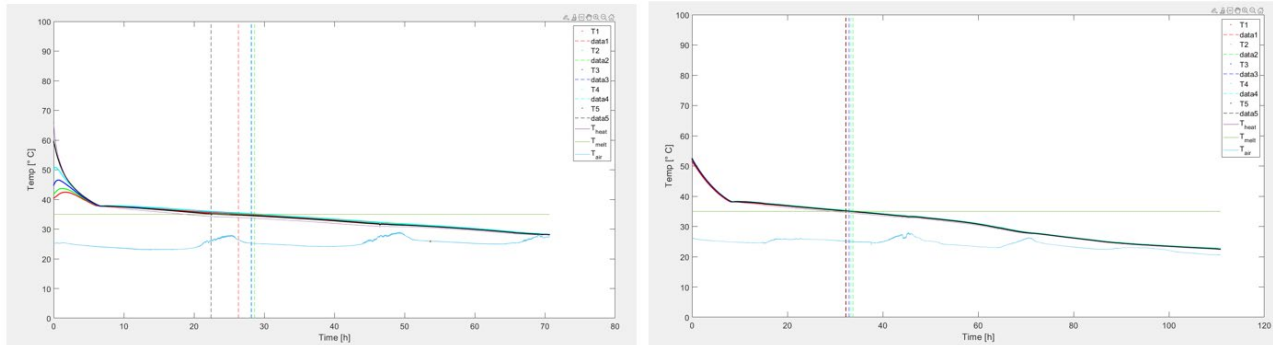
FIG. 134 COMPARISON BETWEEN PURE RT35 PCM (A) AND METAL FOAM (B) COOLING EXPERIMENTS.

2.3.2.10 LUMPED-ELEMENT MODEL

Studying the heat transmission, it is observed that some bodies behave as a "concentrated whole" presenting a uniform internal temperature during the entire heat exchange process and this temperature is only a function of time (T (t)). The study of the heat transmission based on this idealization considers the lumped parameter system, which greatly simplifies certain types of heat exchange problems, without sacrificing the precision too much.

Introducing the lumped-element model in one of the previous cooling test, the case can be seen as a body with the internal temperature T_i (T_a Will be the air temperature). If $T_i > T_a$ there will be transmission of heat from the body to the external environment with a global heat transfer coefficient U, as shown in Fig. 135. If the approximation of the lumped parameter system is valid, the temperature inside the case always remains uniform and varies only with time, so that $T = T(t)$ [13].
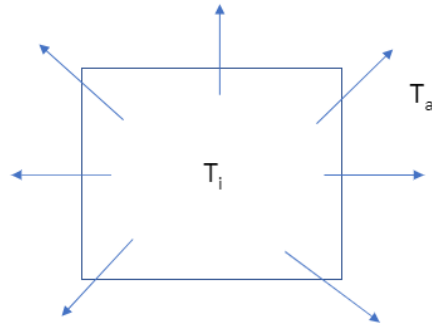
FIG. 135 LUMPED-ELEMENT MODEL SCHEME.

In the study of a lumped-parameter model it is necessary first to define the characteristic length, given by the relation:

$$L_c = \frac{V}{A} \tag{18}$$

where V is the volume occupied by the RT35 PCM, and A is the sum of walls surfaces of the polycarbonate case.

It is also needed to define the Biot number:

$$Bi = \frac{U * L_c}{\lambda} \tag{19}$$

where U is the global heat transfer coefficient calculated in the previous experiments and λ is the conductivity coefficient of the material in the case. The Biot number is the ratio between the internal resistance of a body to the heat conduction and its external resistance to the heat convection: a low value of the Biot number corresponds to a small resistance to thermal conduction and, therefore, to small temperature gradients inside the body. In general, if $Bi \leq 0,1$ the whole body can be considered at the same temperature.

Among the calculation models of effective thermal conductivity, series-parallel models of metal and the filler ones is relatively simple and available [15].

Fig. 136 shows two kinds of the idealized model used for dealing with the effective thermal conductivity. As shown in Fig. 136 (a), metals and fillers are alternately parallel and vertical arranged and the heat flux direction is parallel to the main dimension of the materials: the Eq 20 shows the calculation of the heat flux in this case [15]:

$$\dot{Q} = \dot{Q}_{PCM} + \dot{Q}_{Al} = -\lambda_{PCM} \, A \, \varepsilon \, \frac{\Delta T}{L} - \lambda_{Al} \, A \, (1-\varepsilon) \, \frac{\Delta T}{L} = -\left(A\frac{\Delta T}{L}\right)(\varepsilon \, \lambda_{PCM} + \lambda_{Al} \, (1-\varepsilon)) \quad (20)$$

The effective thermal conductivity of the composite PCM is the maximum and it is given by Eq. 24.

$$\lambda_{max} = (\varepsilon \, \lambda_{PCM} + \lambda_{Al} \, (1-\varepsilon)) \tag{21}$$

As shown in Fig. 136 (b), when the heat flux direction is orthogonal to the main dimension of the materials, it is considered that the metal and the filler are in series. Eq 22 shows the calculation of the heat flux in this case [15]:

$$\dot{Q} = \dot{Q}_{PCM} + \dot{Q}_{Al} = -\lambda_{PCM} \, A \, \frac{\Delta T}{\varepsilon \, L} - \lambda_{Al} \, A \, \frac{\Delta T}{(1-\varepsilon) \, L} = -\left(A \, \frac{\Delta T}{L}\right)\left(\frac{1}{\frac{\varepsilon}{\lambda_{PCM}} + \frac{1-\varepsilon}{\lambda_{Al}}}\right) \tag{22}$$

The effective thermal conductivity of the composite PCM is the minimum and it is given by Eq. 23 [15].

$$\lambda_{min} = \frac{1}{\frac{\varepsilon}{\lambda_{PCM}} + \frac{1-\varepsilon}{\lambda_{Al}}} \tag{23}$$
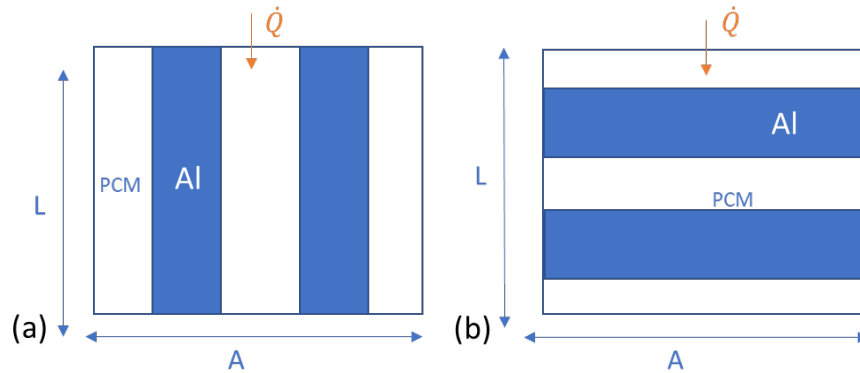
FIG. 136 EFFECTIVE THERMAL CONDUCTIVITY MODEL: (A) PARALLEL MODEL (B) SERIES MODEL [15].

For the calculation of L_c, it was considered the volume of PCM and the heat transfer surface of the case indicated in Fig. 137⌷ The conductivity of the system PCM+metal foams was calculated as a weighted average with Eq. 24:

$$\lambda_{PCM+foams} = A\lambda_{max} + (1 - A)\,\lambda_{min} \tag{24}$$

where A is a correlation coefficient found in literature [12], ε is the porosity of metal foams considered and $\lambda = 2{,}58$ W/m K is the thermal conductivity which increased about 13 times compared to RT35 PCM.

	λ[W/mK]	ε [%]	Biot Number			Data	
	λ[W/mK]	ε [%]	Biot Number			A: Corralation coefficient [0.905<ε<0.978]	0.35
Aluminum	170	0.04					
PCM RT35	0.2	0.96	0.006177761			Volume PCM [m³]	0.000724
						Heat Transfer Surface [m²]	0.0259
PCM+Aluminum (media pesata)	2.58261		0.000478412			Heat Transfer Coefficient [W/m² K]	0.0442
						Characteristic length	0.027954

FIG. 137 EXTRACT OF THE EXCEL FILE WITH THE BIOT NUMBER CALCULATION.

Fig. 137 shows an extract of the Excel file in which all the calculations have been done. The Biot number was finally calculated: it was found $Bi_{PCM} = 0.006$ and $Bi_{PCM+foams} = 0.00048$, so $Bi_{PCM+foams} \ll Bi_{PCM} < 0.1$. This means that the whole system satisfies the criteria for the lumped-parameter study, therefore a uniform temperature distribution throughout the volume can be assumed for the cooling experiment. As Bi is much lower for PCM+metal foam, this justifies the fact that all the TCs record exactly the same temperature trend: looking at the comparison between the cooling processes of Test 7 and Test 8 (with metal foams), it is clear that in the second experiment the system presents a homogeneous temperature distribution since the precise moment the energy supplied was stopped (Fig. 138⌷.

Test 1 Pure PCM RT 35

Test PCM+Metal foams
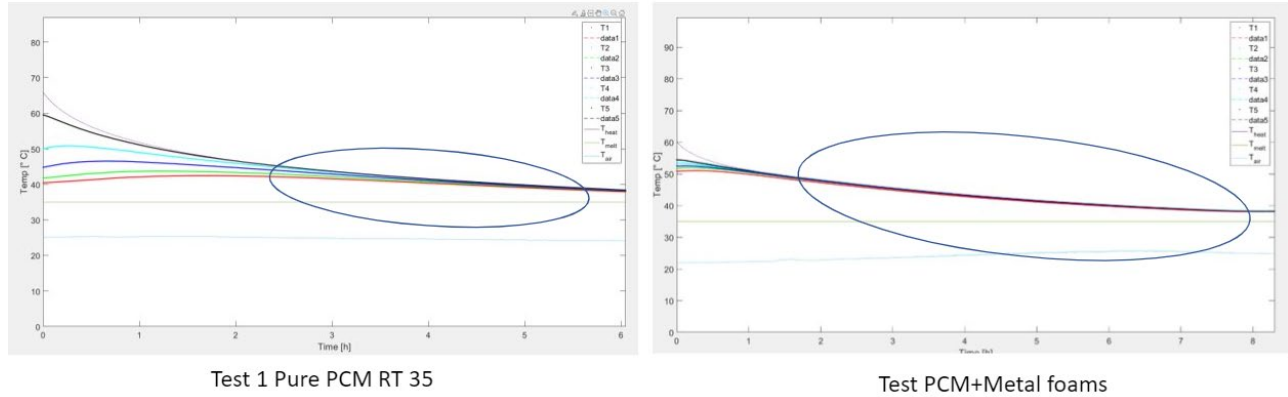
FIG. 138 COMPARISON BETWEEN COOLING PURE PCM AND COOLING WITH PCM+METAL FOAMS.

Another formula for the calculation of the thermal conductivity of metal-foam-loaded PCM is given by Wang et al. [15]: in this paper it is assumed that there is an angle β between the heat flux direction and the arrangement of the materials. The effective thermal conductivity $\lambda_{PCM+foams}$ can be written as in Eq 25. and the angle β can be determined from the unified equation shown in Eq. 26:

$$\lambda_{PCM+foams} = \sqrt{\lambda_{max}^2 (\sin \beta)^2 + \lambda_{min}^2 (\cos \beta)^2} \qquad (25)$$

$$\tan \beta^2 = 16 (1 - \varepsilon) \varepsilon^3 \frac{\ln(\lambda_{Al}/\lambda_{PCM})}{(\frac{\lambda_{Al}}{\lambda_{PCM}} - 1)^2} \qquad (26)$$

	λ[W/mK]	ε [%]	Biot Number		Data		
					$\lambda_{Al}/\lambda_{PCM}$		850
Aluminum	170	0.04			$\ln(\lambda_{Al}/\lambda_{PCM})$		6.745236349
PCM RT35	0.2	0.96	0.006177761		$Tan^2 \beta$		5.29877E-06
					β		0.002301903
PCM+Aluminum (heat flux angle)	6.991981		0.00017671		λ_{max}		6.992
					λ_{min}		0.208323121

FIG. 139 EXTRACT OF EXCEL FILE WITH THE BIOT NUMBER CALCULATION.

The theoretical effective thermal conductivity $\lambda_{PCM+foams}$ (calculated with the method proposed in Fig. 139 was $\lambda_{PCM+foams}$ = 6,99 W/m K. In this case, the thermal conductivity of the composite PCM was considered 63% higher than the one calculated in Eq. 27, almost 35 times higher than

139

thermal conductivity of the pure RT35 PCM. The Biot number was much lower than 0,1 even in this case.

From the two different equations given by the literature, it can be observed that there is no certainty regarding the right equation to use in the effective thermal conductivity calculation when PCMs are filled with metal foams.

2.3.2.11 HEAT TRANSFER COEFFICIENT CALCULATION WITHOUT INSULATING BOX

A cooling experiment was conducted starting with the whole PCM meltedand without the insulation box (Fig. 140) in order to calculate the global heat transfer coefficient of the polycarbonate test rig. From the graph in Fig. 141, it can be deducted that the phase change process from liquid to solid started at almost 39° C, and the whole PCM solidified and reached the room temperature in almost 16 hours.

To calculate the heat exchange coefficient, the temperatures average trend considered was that before the phase change happened (the area in Fig. 141) In Fig. 142 it is shown an extract of the Excel file in which the value of heat transfer coefficient was calculated: the insulation increment worked and it greatly influenced the U which passed from 2,07 $W/m^2 K$ to 0.046 $W/m^2 K$.
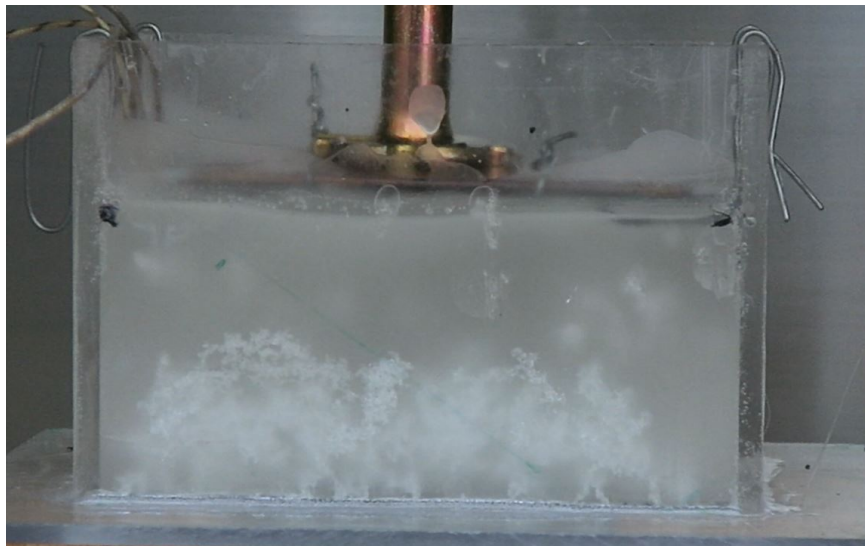
FIG. 140 RT35 PCM COOLING EXPERIMENT WITHOUT INSULATION.
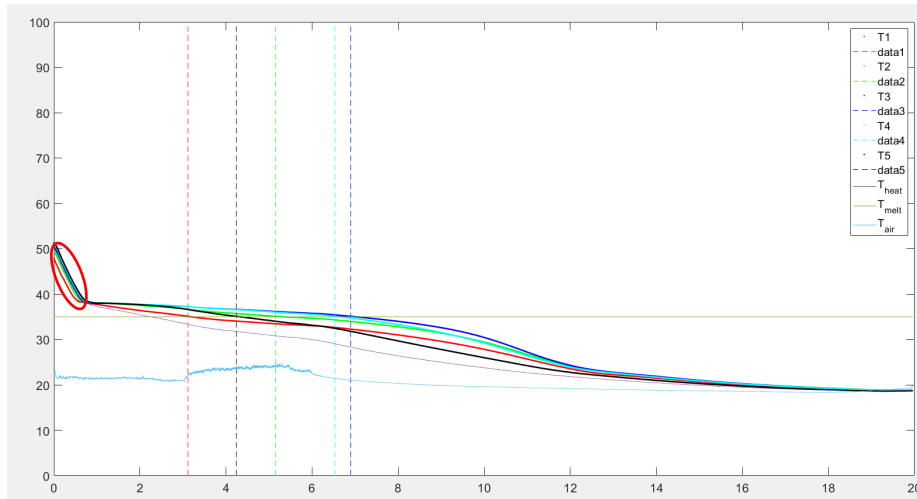
FIG. 141 COOLING EXPERIMENT RESULTS WITHOUT INSULATION.

External heat exchanging surface [m^2]	U [W/m^2 K]
0.0646	2.07383127
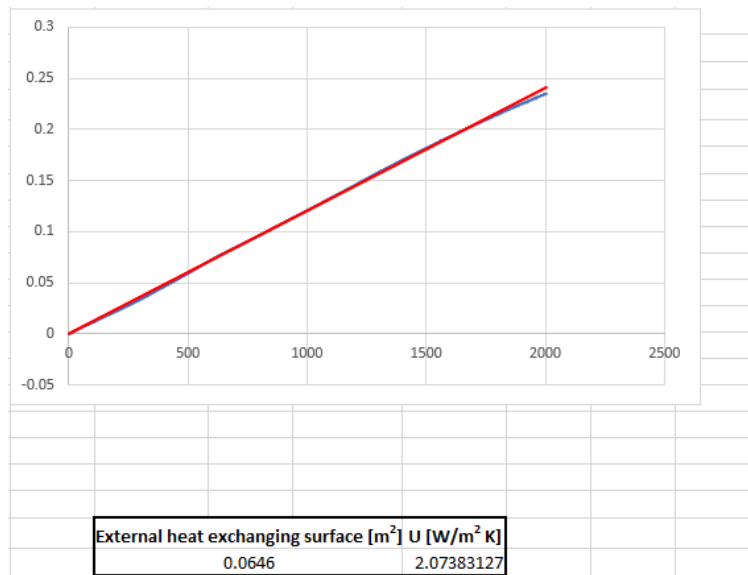
FIG. 142 HEAT TRANSFER COEFFICIENT CALCULATION.

2.3.2.11.1 BIOT NUMBER CALCULATION WITHOUT INSULATION

The calculation of the Biot number in the previous experiments gave extremely low values both for the case of pure PCM and for the composite PCM . This was for two reasons: the high insulation of the box and the high conductivity that was reached with the addition of metal foams. Therefore, there were not big differences, in terms of Biot number, between pure and metal-foam-loaded PCM: in both cases Bi was much lower than 0,1, therefore the PCM temperature could be

considered uniform throughout the polycarbonate box. Once the heat exchange coefficient of the case was obtained, it was possible to calculate Biot both for pure PCM and for the composite PCM. The results are shown in Fig. 143: $Bi_{PCM+Al} = 0,022$ and $Bi_{PCM} = 0,29$. From these results it can be deduced that, with the use of metal foams in a polycarbonate case, the composite material satisfies the study of the lumped-parameter model so it is possible to consider he same temperature in any point of the volume, when the system is at a constant temperature . Regarding the pure PCM, as $Bi_{PCM} > 0,1$, it is not proper to applicate the lumped-parameter model is not .

	λ[W/mK]	ε [%]	Biot Number
Aluminum	170	0.04	
PCM RT35	0.2	0.96	0.289320463
PCM+Aluminum	2.58261		0.022405277

FIG. 143 BIOT NUMBER FOR PURE AND METAL-FOAM-LOADED PCM.

2.3.2.12 TEST 9

2.3.2.12.1 MELTING PURE RT35 PCM - 17.5 V

A melting experiment was conducted using the same voltage and setup of the previous experiment, but a different starting temperature (the room temperature changed and it was almost 24° C). As can be seen from the Fig. 140, the whole PCM melted in about 18 hours which is a different melting time compared to previous experiment, but it is due to the different starting temperature of this experiment. In Test 6 the starting conditions were not realistic because the whole PCM was already in the melting temperature range (29° C÷36° C). From this heater temperature trend, a new numerical simulation could be done and compared with these experimental results but, to be sure

about the repeatability of the tests, three experiments with same temperature trends are needed.
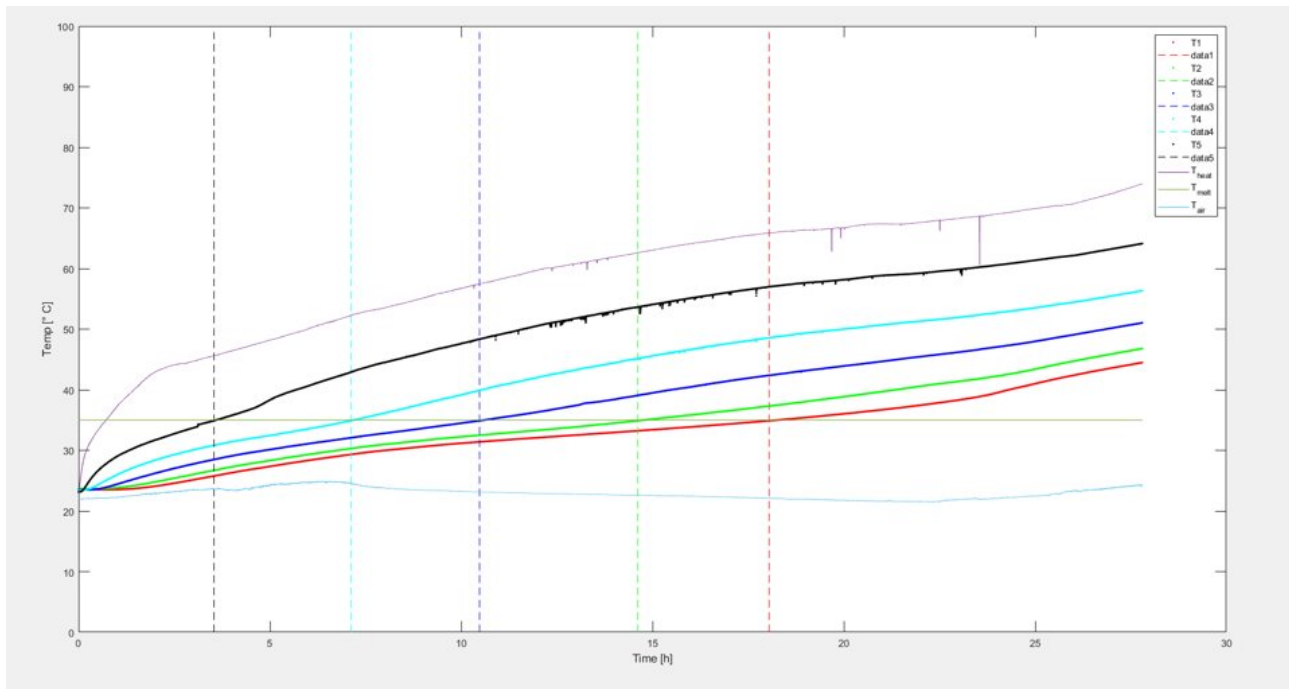
FIG. 144 EXPERIMENTAL RESULTS WITH V = 17.5 V.

2.3.2.12.2 COMPARISON BETWEEN MELTING PROCESSES: PURE RT35 PCM AND METAL-FOAM-LOADED RT35 PCM

It was done a comparison between Test 8 and Test 9 experimental results (the starting temperatures were the same for both experiments): in Test 9 the pure PCM melted in 18 hours at a heater temperature of 65 ° C, while in Test 8 the whole PCM melted in 12,5 hours at a heater temperature of 47° C. In Test 8 all the PCM took 5 hours less to melt, at temperature of 18° below.
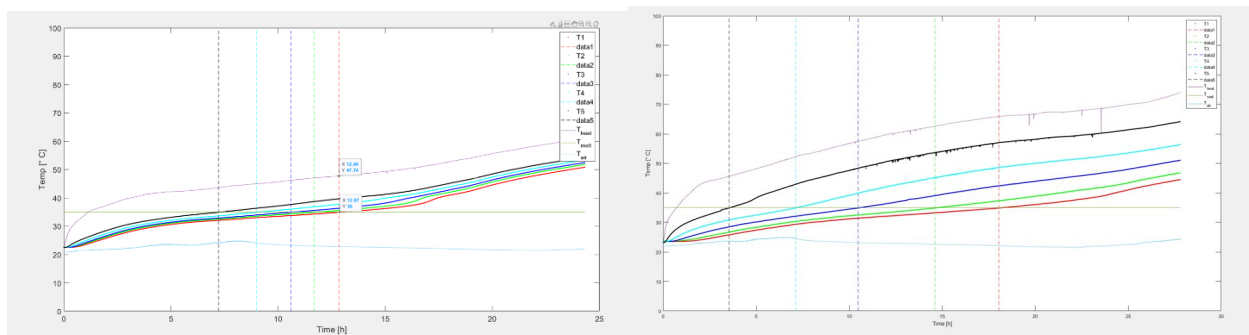
FIG. 145 COMPARISON BETWEEN MELTING WITH PURE RT35 PCM (B) AND METAL-FOAM-LOADED RT35 PCM(A).

2.3.2.12.3 COOLING WITH PURE RT35 PCM

Another cooling experiment with pure RT35 PCM was conducted with the same set-up, after opening and sealing again the polystyrene box, to verify if something changed in term of heat transfer coefficient. The graph of the cooling results is shown in Fig. 146. The whole volume of PCM solidified and reached the room temperature in about 75 hours, as in previous experiment, and new values of k and U were calculated as done before: k = 0,027 W/K and U = 0,045 W/m^2 K. Last experimental results are in agreement with previous ones.
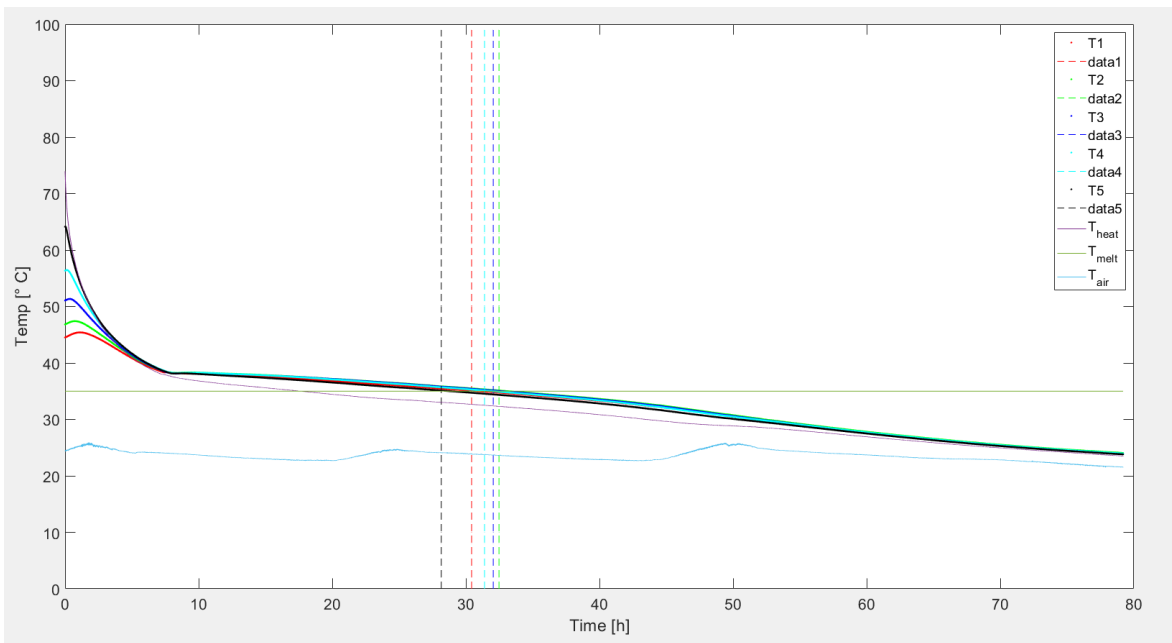
FIG. 146 EXPERIMENTAL RESULTS OF THE COOLING EXPERIMENT.
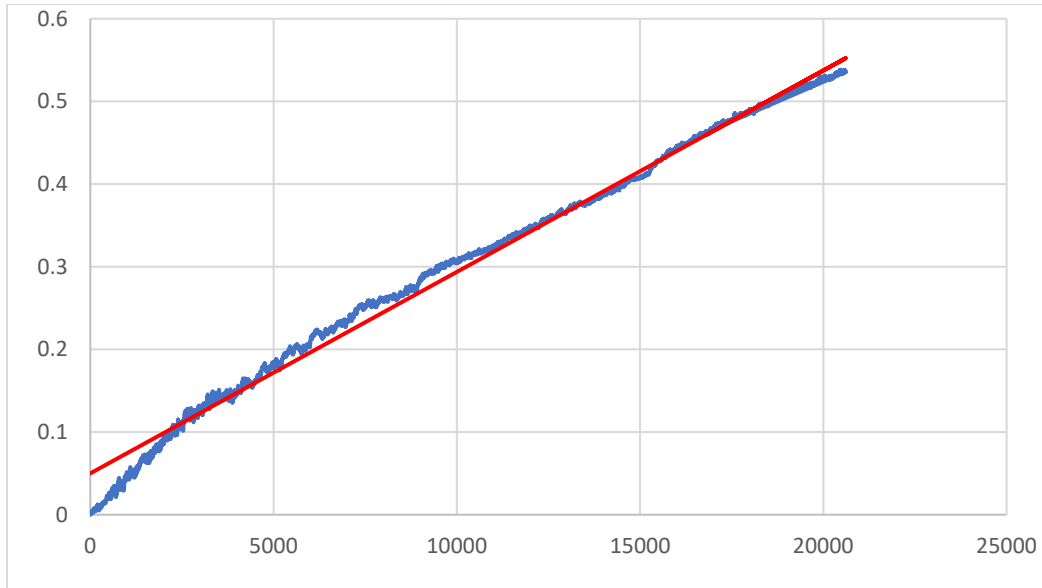
FIG. 147 REAL DATA (BLUE) AND INTERPOLATING LINE (RED).

2.3.3 DEMONSTRATION OF THE EXPERIMENTS REPEATABILITY

2.3.3.1 TEST 10: REPETITION OF TEST 9

2.3.3.1.1 MELTING OF PURE RT35 PCM - 17.5 V

Test 9 was repeated with the same starting conditions, in order to verify its correctness and repeatability. The results are shown in Fig. 148. T_{heater} was much higher than the previous experiment and after 2 hours $T_{heater} \simeq 64°$ C $>> T_{heater,Test\ 7} \simeq 43°$ C (Fig. 149. The whole volume of PCM melted in $t_{test\ 10} \simeq 21$ hours $> t_{test\ 7} \simeq 18$ h, although the heater temperatures were higher. Another observation that can be made is that all the TCs in this experiment reached lower temperatures than before. The possible reason for these problems could be the presence of an air cavity between the heater and the PCM: the polystyrene box needed to be opened and it was necessary to verify if there was this kind of problems.
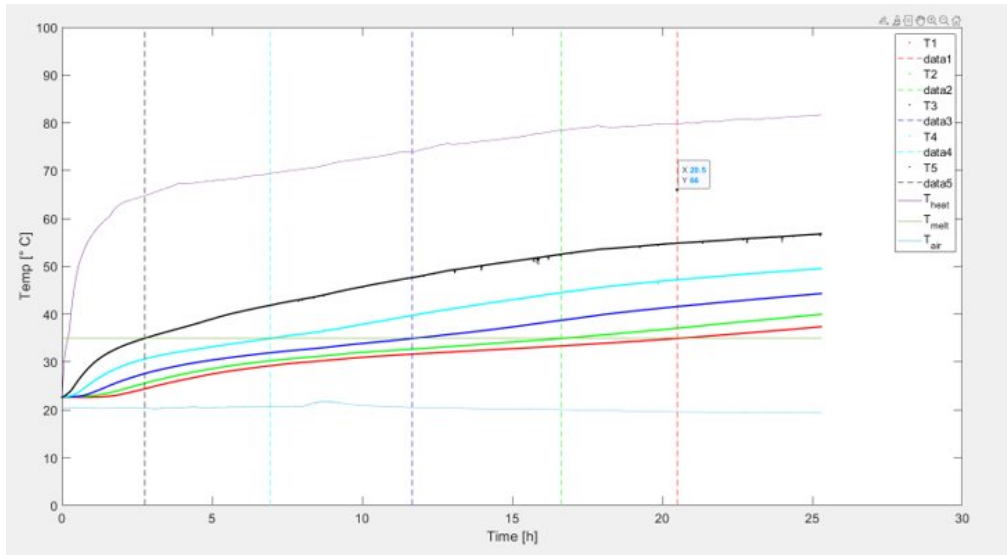
FIG. 148 EXPERIMENTAL RESULTS WITH 17.5.
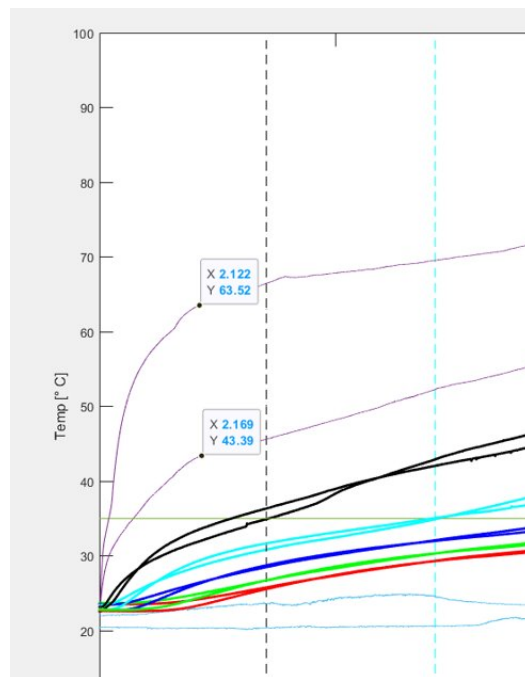
FIG. 149 COMPARISON BETWEEN TEST 9 AND TEST 10.

After two experiments the whole polystyrene box was opened and the previous consideration about the problems described before was confirmed (Fig. 150). PCM leaks were found (it flew from the holes through which the TCs had been inserted). As a result of the leaks, an air volume remained between the heater and the PCM. Air is a bad conductor so T_{heater} was

higher because the air subtracted less heat from the heater respect to the PCM and, at the same time, the PCM under the air received less heat due to the air cavity.

The leaks problem needed to be solved and the polycarbonate case needed to be refilled with PCM, the polystyrene box needed to be repaired and rebuilt because the polystyrene pieces were impregnated with some solidified PCM.
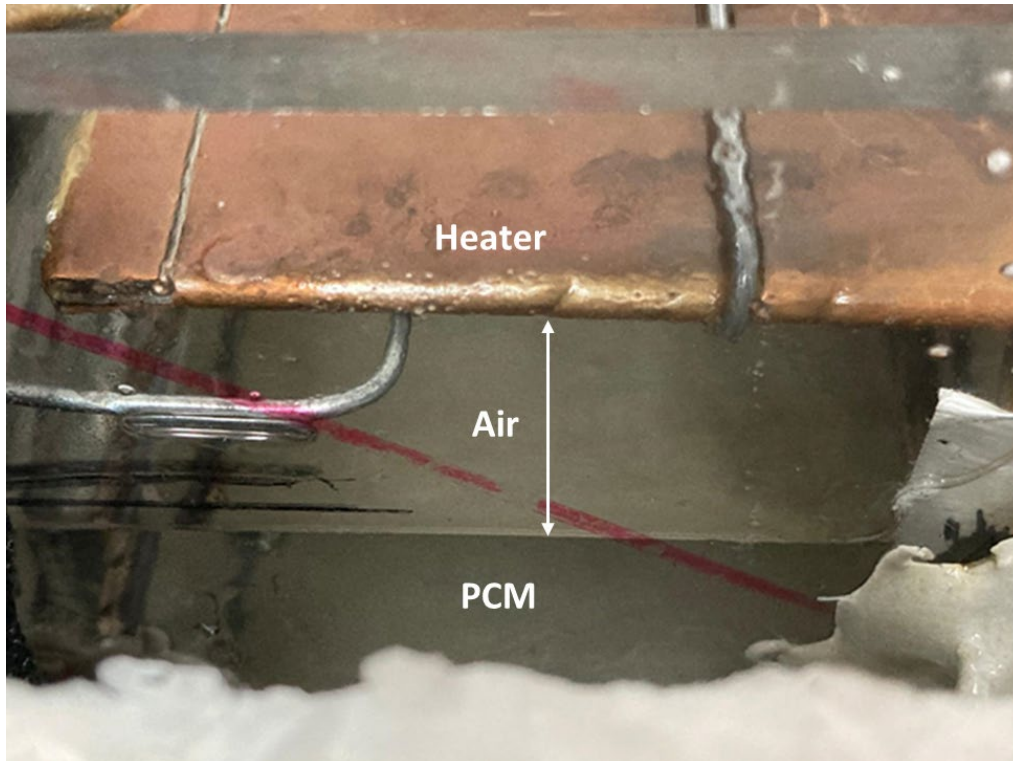
FIG. 150 AIR CAVITY IN THE POLYCARBONATE CASE DUE TO THE PCM LEAKS.

2.3.3.2 TEST 11: DEMONSTRATION OF EXPERIMENTS REPEATABILITY, JIMMI 3.0

2.3.3.2.1 MELTING OF PURE RT35 PCM - 17.5 V

The leaking spots were filled with a single component adhesive liquid solvent (specific for polycarbonate), EUROBATEX ® was put around the case, as can be seen in Fig. 151 then the new polystyrene box was assembled and EUROBATEX ® was also attached to external part of the box (Fig. 152). The main goals of these experiments were:

- Obtain a box with almost the same insulation of the previous experiments;
- Ddemonstrate the repeatability of the experiments with 3 tests with the same starting conditions (T and V);
- Calculate the heat transfer coefficient for the new box and validate the experiments with a numerical simulation.
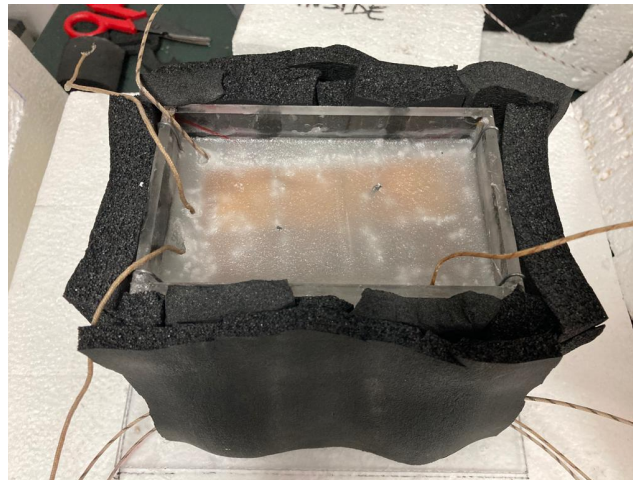
FIG. 151 REPAIRED CASE.

FIG. 152 NEW POLYSTYRENE AND EUROBATEX INSULATED BOX.

As can be seen from the Fig. 153, the whole PCM melted in about 22,2 hours at a $T_{heater} = 65°$ C. Another two experiments needed to be conducted to join the goal that was explained.
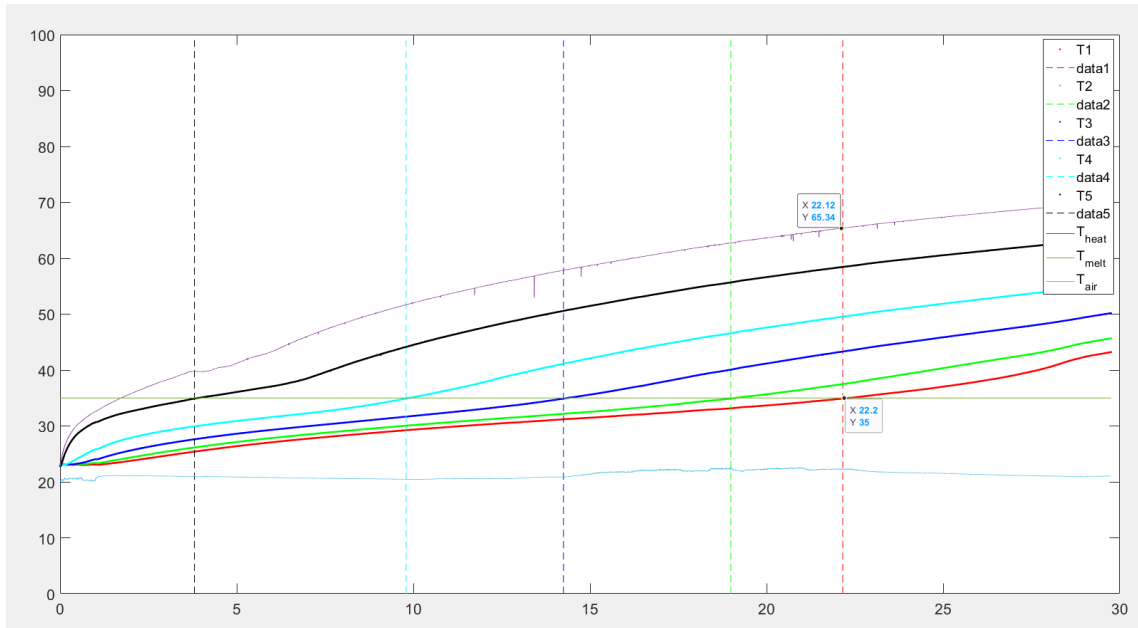
FIG. 153 EXPERIMENTAL RESULTS WITH 17.5 V.

2.3.3.2.2 COOLING WITH PURE RT35 PCM

Fig. 154 shows the temperature trends recorded by the TCs in the cooling experiment: the whole PCM reached the room temperature in almost 70 hours. The trend of temperatures chosen to calculate the heat exchange coefficient is indicated in Fig. 154 with a red circle.

FIG. 154 EXPERIMENTAL RESULTS OF COOLING EXPERIMENT.

		LabVIEW Time	θ	Absolute Time	ln((θ)/(θ₀))	Interpolating line
		892.131	35,57706	0	0	0
Σ (M*cp) [J/K]	1114,344	892.133	35,56445	1,835	0,000354664	4,89473E-05
		892.135	35,55732	3,589	0,000554972	9,5734E-05
B [s⁻¹]	2,66743E-05	892.137	35,6066	5,353	-0,000829995	0,000142787
C	0	892.138	35,60091	7,107	-0,000670067	0,000189574
K [W/K]	0,029724333	892.140	35,60543	8,871	-0,000797194	0,000236628
		892.142	35,59421	10,637	-0,000481967	0,000283734
		892.144	35,57906	12,404	-5,6162E-05	0,000330868
		892.145	35,56892	14,164	0,000228981	0,000377815
		892.147	35,56867	15,917	0,000235904	0,000424575
		892.149	35,58558	17,681	-0,000239466	0,000471628
		892.151	35,63543	19,429	-0,001639355	0,000518255
		892.152	35,58204	21,179	-0,000139848	0,000564935
		892.154	35,5599	22,931	0,00048241	0,000611668
		892.156	35,58304	24,698	-0,000168005	0,000658802
		892.158	35,56576	26,464	0,000317786	0,000705908
		892.159	35,54987	28,232	0,00076461	0,000753068
		892.161	35,61376	29,998	-0,001031021	0,000800175
		892.163	35,60299	31,761	-0,000728393	0,000847202
		892.165	35,61175	33,54	-0,000974547	0,000894656
		892.167	35,53526	35,306	0,001175616	0,000941762
		892.168	35,55614	37,074	0,000588343	0,000988923
		892.170	35,55917	38,84	0,000503134	0,001036029

External heat exchanging surface [m²]	U [W/m² K]
0,6	0,04954055

FIG. 155 EXCTRACT OF THE EXCEL FILE WITH THE CALCULATION OF THE HEAT TRANSFER COEFFICIENT.

Fig. 155 shows the extract of the Excel file: the value of the heat exchange coefficient $U = 0,049$ $W/m^2 K$ was similar to the coefficient calculated for the previous EUROBATEX ® and polystyrene box (in Test 7), when $U = 0,045 W/m^2 K$. The temperatures of the cooling experiment will be also acquired in the next experiments to confirm the obtained values. In this way it would be possible to use this value for the numerical simulations.

2.3.3.3 TEST 12: DEMONSTRATION OF EXPERIMENTS REPEATABILITY

2.3.3.3.1 MELTING OF PURE RT35 PCM - 17.5 V

The second experiment to demonstrate the experiments repeatability (with the same starting conditions of Test 11) gave the results shown in Fig. 156: the whole PCM melted in 23 hours at a $T_{heater} = 65°$ C.
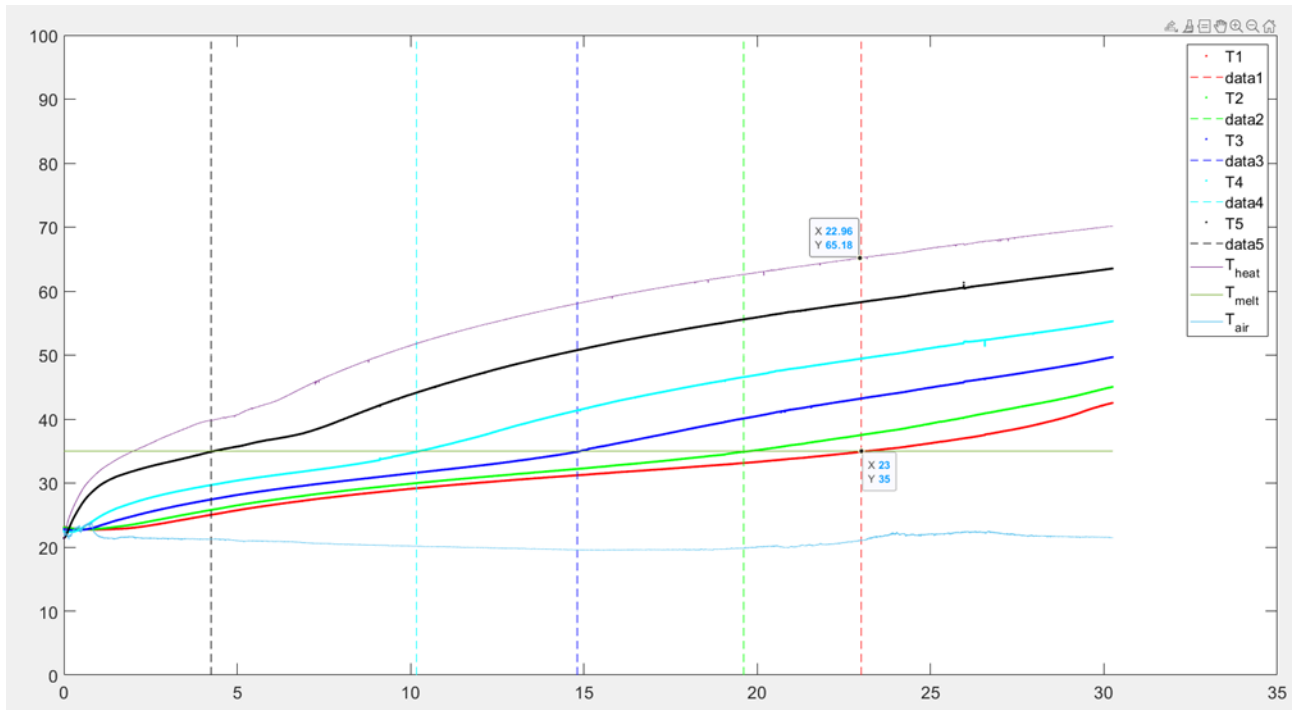
FIG. 156 EXPERIMENTAL RESULTS WITH 17.5 V.

2.3.3.3.2 COOLING WITH PURE RT35 PCM

To calculate the heat transfer coefficient it was considered the temperatures average in the area just before (Fig. 157). In Fig. 158 it is shown an extract of the Excel file in which the value of the heat exchange coefficient was calculated: it was equal to 0,045 W/m^{2}K and it perfectly matched the one calculated in Test 11.
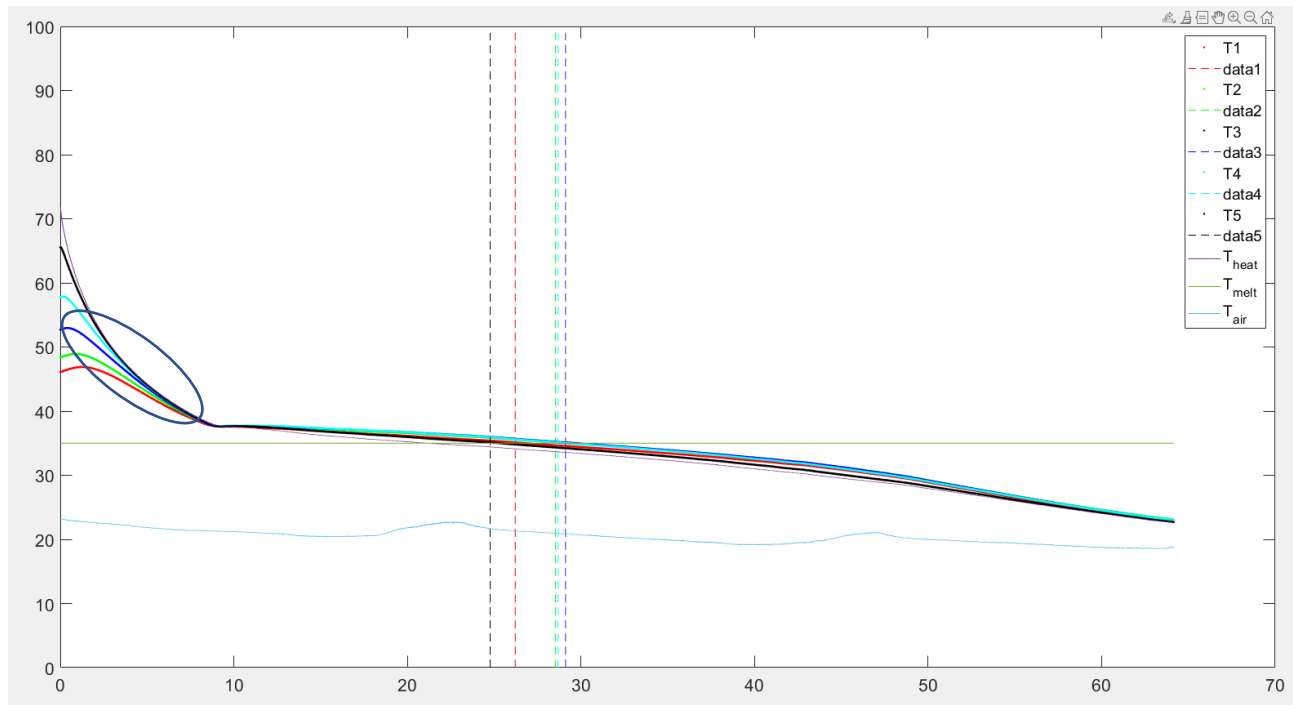
FIG. 157 EXPERIMENTAL RESULTS OF COOLING EXPERIMENT.

			LabVIEW Time	θ	Absolute Time	ln((θ)/(θ₀))	Interpolating line
			192520.33	33.04586	0	0	0
Σ (M*cp) [J/K]	1114.344		192522.091	33.06098	1.761	-0.000457536	4.28922E-05
			192523.856	33.05448	3.526	-0.000260741	8.58819E-05
B [s⁻¹]	2.43567E-05		192525.634	33.06152	5.304	-0.000473901	0.000129188
C	0		192527.389	33.03501	7.059	0.000328295	0.000171934
K [W/K]	0.027141783		192529.151	33.03521	8.821	0.000322196	0.000214851
			192530.917	33.03299	10.587	0.000389573	0.000257865
			192532.684	33.06177	12.354	-0.000481237	0.000300903
			192534.447	33.04833	14.117	-7.48028E-05	0.000343844
			192536.215	33.05051	15.885	-0.00014085	0.000386907
			192537.977	33.02432	17.647	0.000652122	0.000429823
			192539.725	33.02752	19.395	0.000555183	0.000472399
			192541.477	33.0078	21.147	0.001152501	0.000515072
			192543.228	32.99241	22.898	0.001618747	0.000557721
			192544.994	32.99284	24.664	0.001605798	0.000600735
			192546.763	32.9813	26.433	0.001955607	0.000643822
			192548.526	32.98615	28.196	0.001808599	0.000686763
			192550.294	32.97775	29.964	0.002063204	0.000729825
			192552.058	32.9883	31.728	0.001743275	0.000772791
			192553.824	32.97953	33.494	0.002009348	0.000815805
			192555.603	32.97879	35.273	0.002031637	0.000859135
			192557.373	32.99153	37.043	0.001645495	0.000902247
			192559.139	32.97296	38.809	0.002208439	0.000945261
			192560.904	32.96838	40.574	0.002347414	0.00098825
			192562.668	32.97251	42.338	0.002222189	0.001031215
			192564.434	32.9713	44.104	0.002258799	0.001074229
			192566.201	32.99242	45.871	0.001618352	0.001117268
			192567.963	32.99211	47.633	0.001627965	0.001160184
			192569.729	32.98864	49.399	0.001733152	0.001203198
			192571.498	32.97774	51.168	0.002063544	0.001246285

External heat exchanging surface [m²]	U [W/m² K]
0.6	0.0452363

FIG. 158 EXCTRACT OF THE EXCEL FILE WITH THE CALCULATION OF THE HEAT TRANSFER COEFFICIENT.

2.3.3.4 TEST 13: DEMONSTRATION OF EXPERIMENTS REPEATABILITY

2.3.3.4.1 MELTING OF PURE RT35 PCM - 17.5 V

The third experiment to demonstrate the experiments repeatability (with the same starting conditions of Test 11) gave the results shown in Fig. 159: the whole PCM melted in 22,4 hours at a $T_{heater} = 65,4 °$ C.°
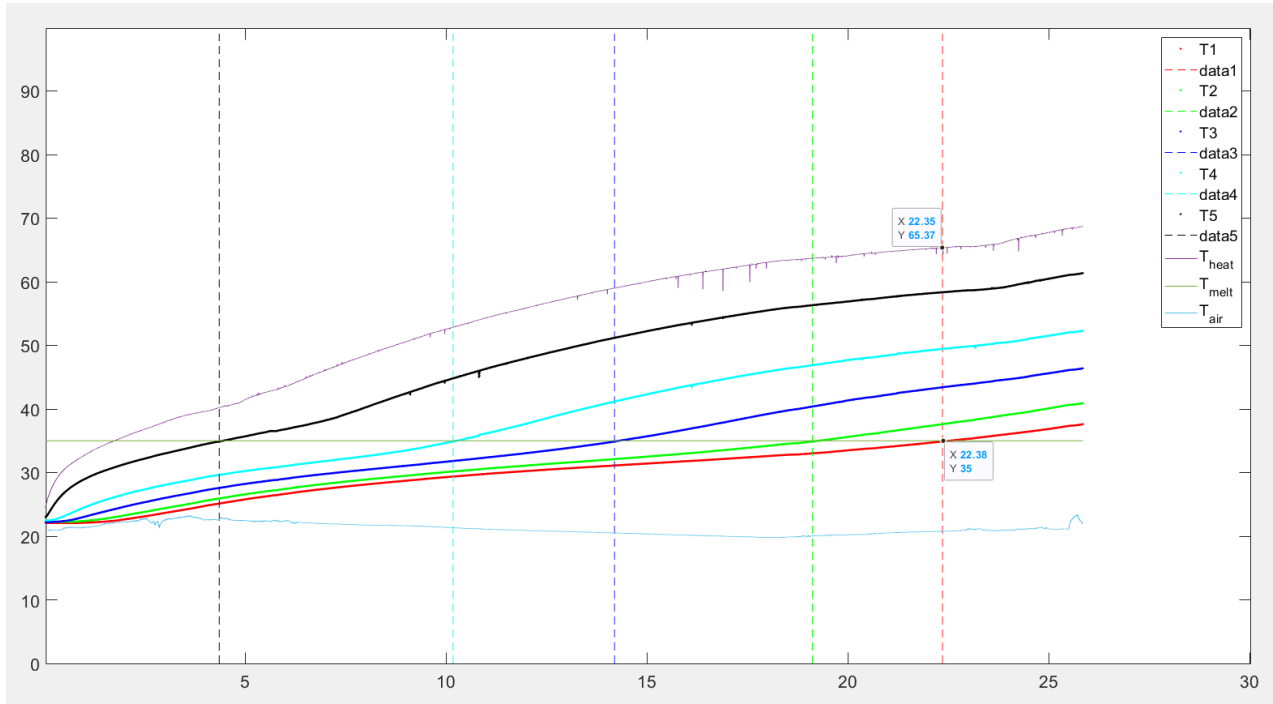
FIG. 159 EXPERIMENTAL RESULTS WITH 17.5 V.

2.3.3.4.2 COOLING WITH PURE RT35

To calculate the heat transfer coefficient, it was considered the temperatures average in the area just before the phase change (the blue circle in Fig. 160). In Fig. 161 it is shown an extract of the Excel file in which the value of the heat exchange coefficient was calculated: it was equal to 0,047 W/m^{2}K.
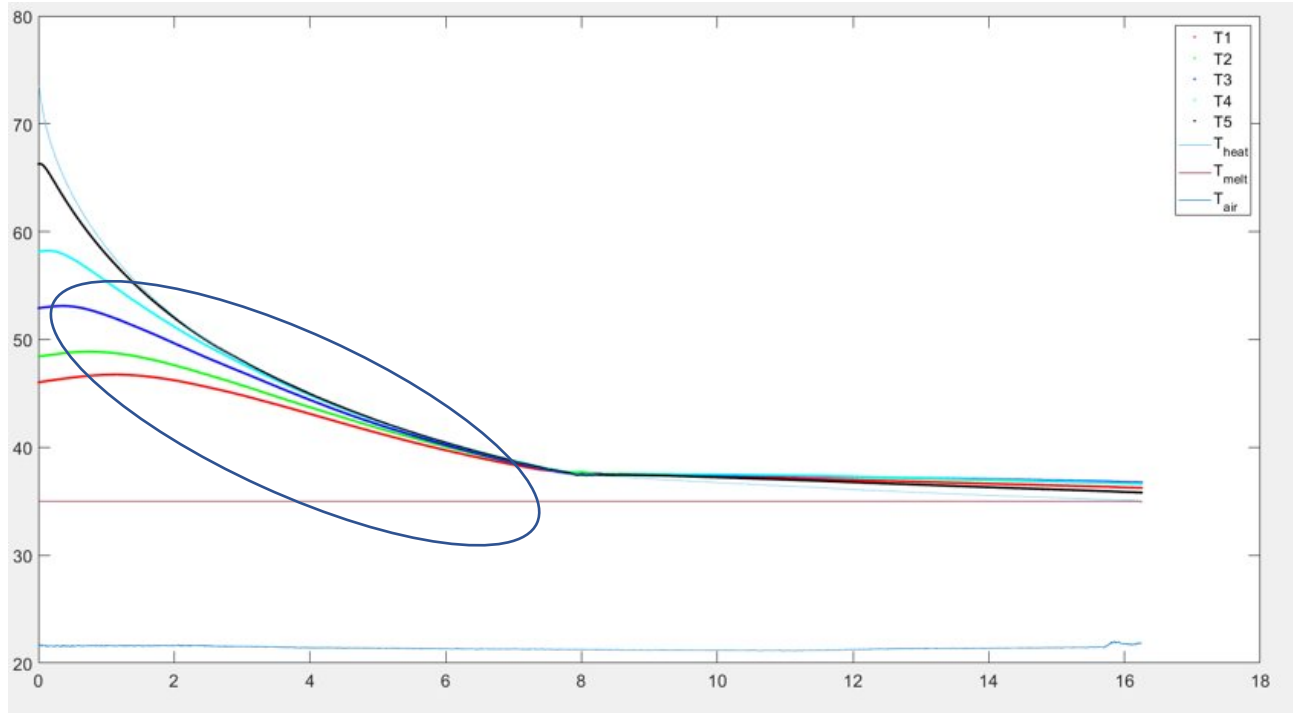
FIG. 160 EXPERIMENTAL RESULTS OF THE COOLING EXPERIMENT.

		825633.544	32.70726	0	0	0
Σ (M*cp) [J/K]	1114.344	825635.307	32.6908	1.763	0.000503518	4.46062E-05
		825637.072	32.6856	3.528	0.000662643	8.92629E-05
B [s⁻¹]	2.53013E-05	825638.821	32.68383	5.277	0.000716527	0.000133515
C	0	825640.574	32.69315	7.03	0.000431498	0.000177868
K [W/K]	0.028194329	825642.335	32.689	8.791	0.000558421	0.000222424
		825644.089	32.69209	10.545	0.000463912	0.000266802
		825645.851	32.68811	12.307	0.000585817	0.000311383
		825647.603	32.68381	14.059	0.000717383	0.000355711
		825649.357	32.69772	15.813	0.000291639	0.000400089
		825651.117	32.68588	17.573	0.000653852	0.000444619
		825652.867	32.67976	19.323	0.000841031	0.000488897
		825654.617	32.67231	21.073	0.001069301	0.000533174
		825656.371	32.68031	22.827	0.000824476	0.000577552
		825658.135	32.67278	24.591	0.001054912	0.000622184
		825659.903	32.674	26.359	0.001017568	0.000666916
		825661.664	32.66871	28.12	0.001179401	0.000711472
		825663.415	32.65574	29.871	0.001576386	0.000755775
		825665.165	32.66854	31.621	0.001184427	0.000800052
		825666.917	32.66896	33.373	0.001171748	0.00084438
		825668.681	32.66191	35.137	0.001387527	0.000889011
		825670.462	32.65952	36.918	0.001460816	0.000934073
		825672.232	32.65385	38.688	0.001634376	0.000978856
		825673.996	32.65956	40.452	0.001459559	0.001023487
		825675.762	32.65742	42.218	0.001524912	0.001068169
		825677.544	32.64986	44	0.001756538	0.001113256

External heat exchanging surface [m²]	U [W/m² K]
0.6	0.04699055

FIG. 161 EXCTRACT OF THE EXCEL FILE WITH THE CALCULATION OF THE HEAT TRANSFER COEFFICIENT.

2.3.3.5 COMPARISON BETWEEN TEST 11, TEST 12 AND TEST 13

In Fig. 162, Test 11, Test 12 and Test are compared overlapping the temperature trends: the match between the three experiments is good
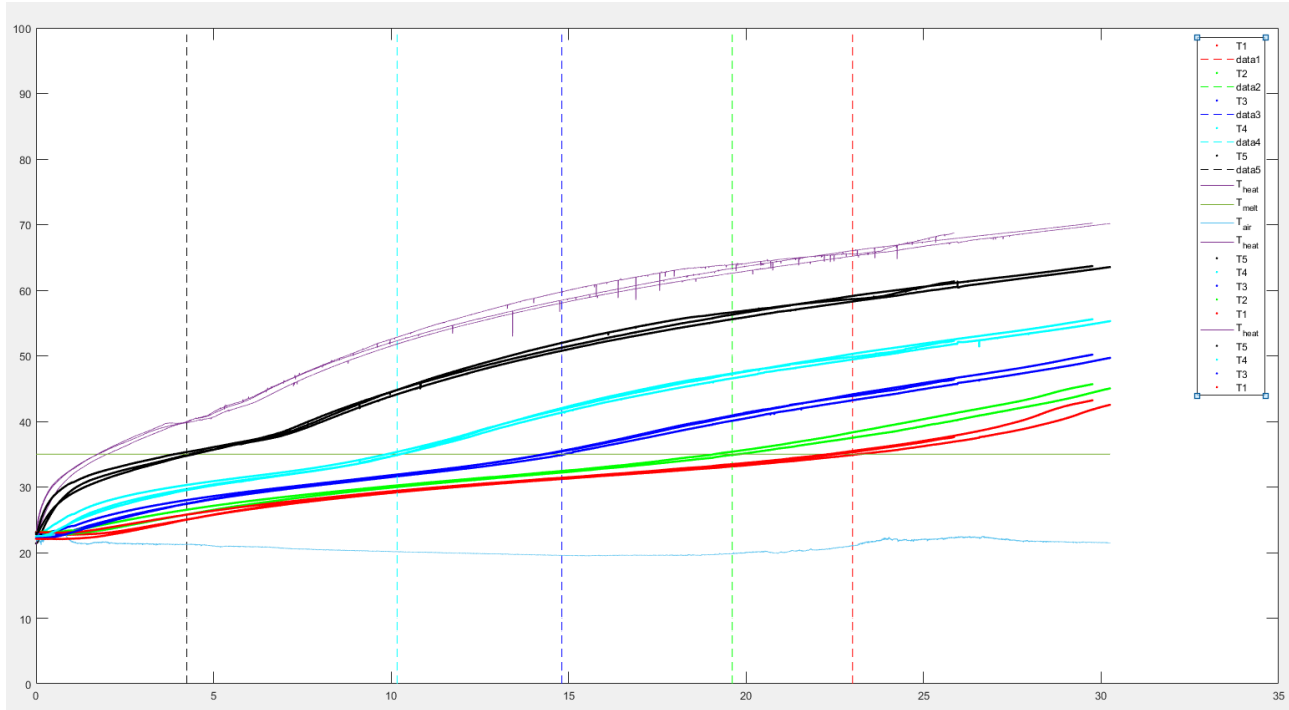
FIG. 162 COMPARISON BETWEEN THE TEMPERATURE TRENDS RECORDED BY THE THERMOCOUPLES IN TEST 11, 12, 13.

To confirm this observation, the temperature difference ΔT between two experiments was calculated for each TC. The uncertainties of TCs are 1° C, so the temperature range considered as acceptable in the comparison is 2° C. In Fig. 163, the comparison between Test 11 and 13 is illustrated: the values out of range were 0,06% for the heater temperature and 0,015% for the temperatures recorded from the TC at the top.164, there are no values out of the range of 2° C for all the TCs, except for the first TC at the top which had only 1,73% of values out of the acceptable range.
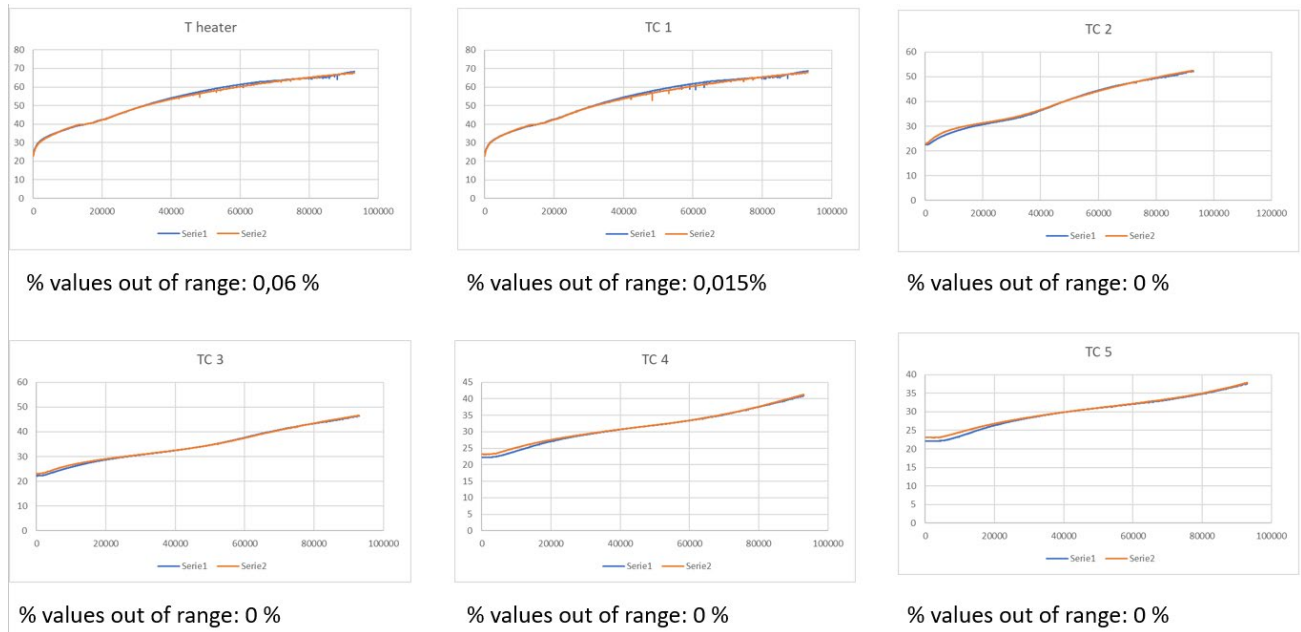
% values out of range: 0,06 %   % values out of range: 0,015%   % values out of range: 0 %

% values out of range: 0 %   % values out of range: 0 %   % values out of range: 0 %

FIG. 163 RESULTS OF ΔT CALCULATED FOR ALL THE THERMOCOUPLES, COMPARISON BETWEEN TEST 11 AND TEST 13.

% values out of range: 0 %   % values out of range: 1,73 %   % values out of range: 0 %

% values out of range: 0 %   % values out of range: 0 %   % values out of range: 0 %

FIG. 164 RESULTS OF ΔT CALCULATED FOR ALL THE THERMOCOUPLES, COMPARISON BETWEEN TEST 11 AND TEST 13.

2.3.3.6 TEST 14: DEMONSTRATION OF EXPERIMENTS REPEATABILITY

2.3.3.6.1 MELTING WITH COPPER FOAMS MELTING OF COPPER-FOAMS-LOADED RT35 PCM - 17.5 V

Copper foams were immersed into the PCM inside the polycarbonate case. Another experiment with the same initial voltage (17,5 V) was conducted. It can be seen from the Fig. 165 that the whole volume of PCM reached the melting temperature in 15,5 hours at a heater temperature of 42° C.
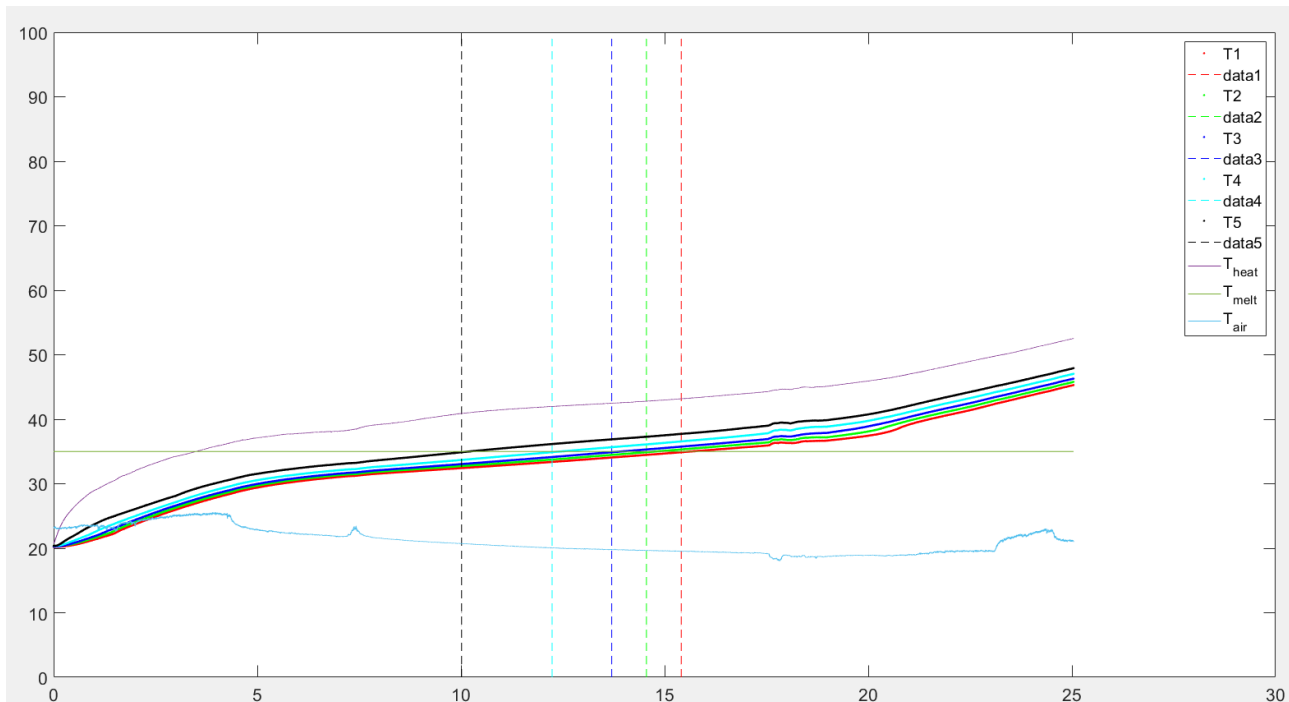
FIG. 165 EXPERIMENTAL RESULTS OF MELTING PURE RT35 PCM WITH COPPER FOAMS, V = 17,5 V.

To be sure about the repeatability of the experiment, another test had to be conducted and compared with this one.

2.3.3.7 TEST 15: DEMONSTRATION OF EXPERIMENTS REPEATABILITY

The last experiment was conducted with the same starting conditions of the previous one: from Fig. 166 it can be seen that the whole PCM melted in 15,8 hours at a heater temperature of 42,8° C.
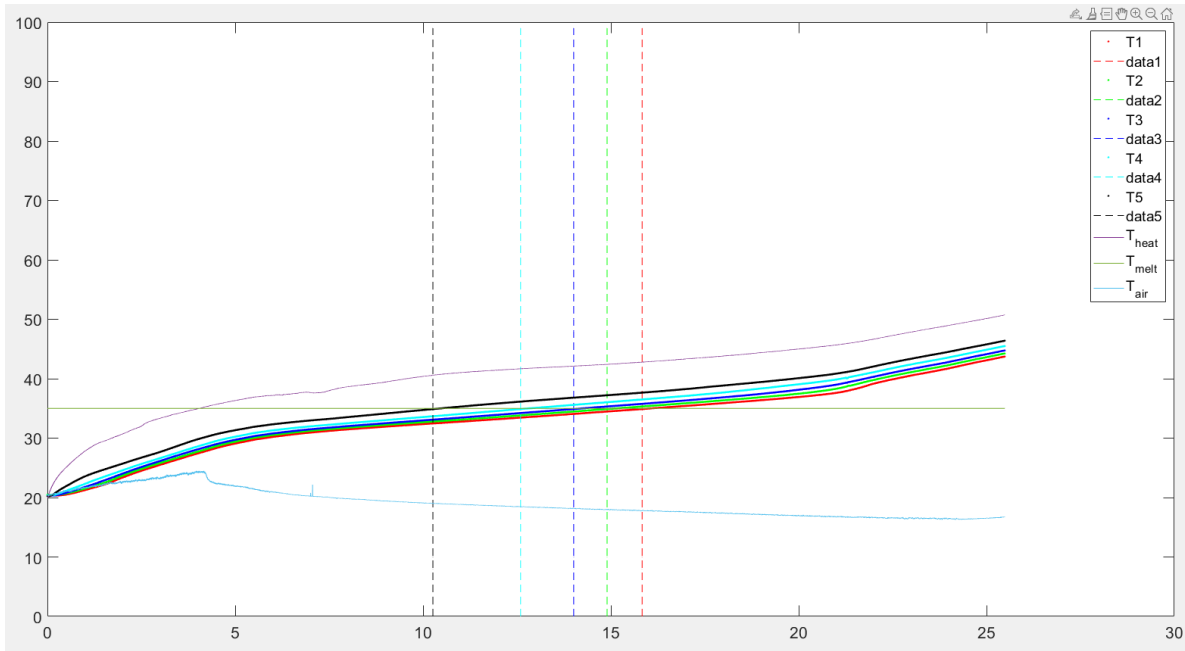
FIG. 166 EXPERIMENTAL RESULTS OF MELTING PURE RT35 PCM WITH COPPER FOAMS, V = 17,5 V.

Then, these experimental results were compared with Test 14 to demonstrate the experiments repeatability even with metallic foams. In Fig. 167 Test 14 and Test 15 have been overlapped. The uncertainties of TCs are 1° C, so the temperature range considered as acceptable in the comparison was 2° C. In Fig. 168, a comparison between Test 14 and 15 is illustrated: the values out of range were 4,15% for the heater temperature and about the temperatures recorded by the TC, from the top to the bottom part of the case, the percentages were respectively 1,14% 1,14%, 1,64%, 1,38%, 1,56%, 2%. From these values, the two experiments can be considered almost identical.
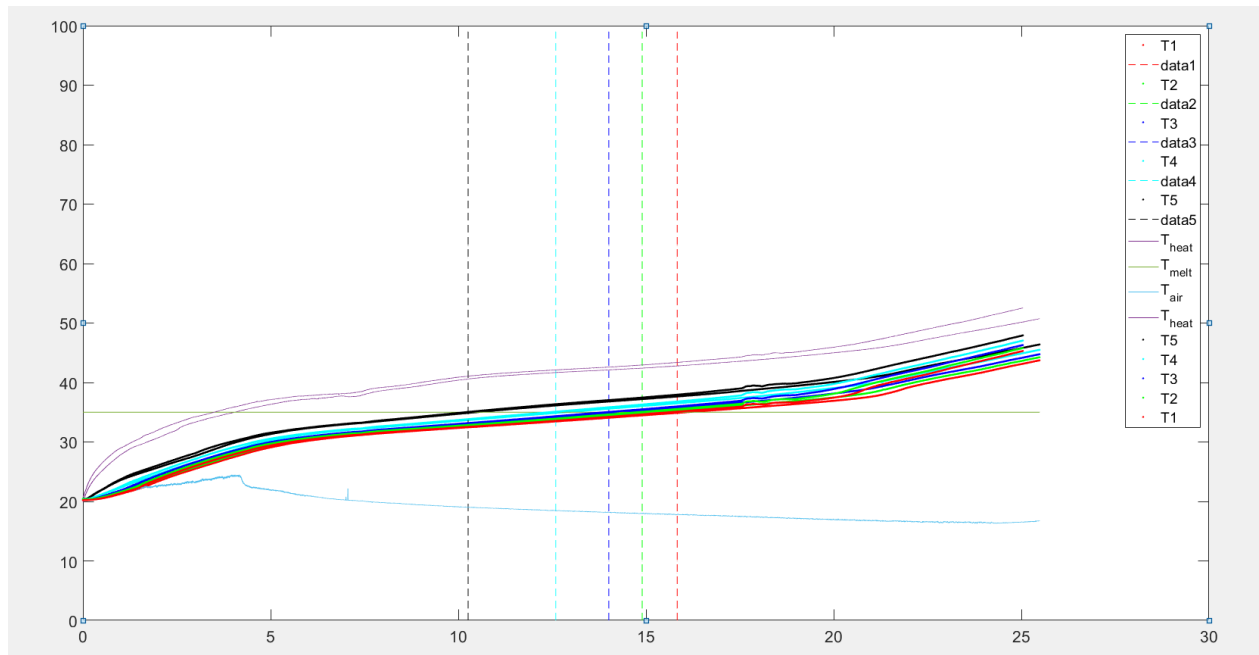
FIG. 167 COMPARISON BETWEEN THE TEMPERATURE TRENDS RECORDED BY THE THERMOCOUPLES IN TEST 14 AND TEST 15.

% values out of range: 4,15 %

% values out of range: 1,14 %

% values out of range: 1.64 %

% values out of range: 1,38 %

% values out of range: 1,56 %

% values out of range: 2 %
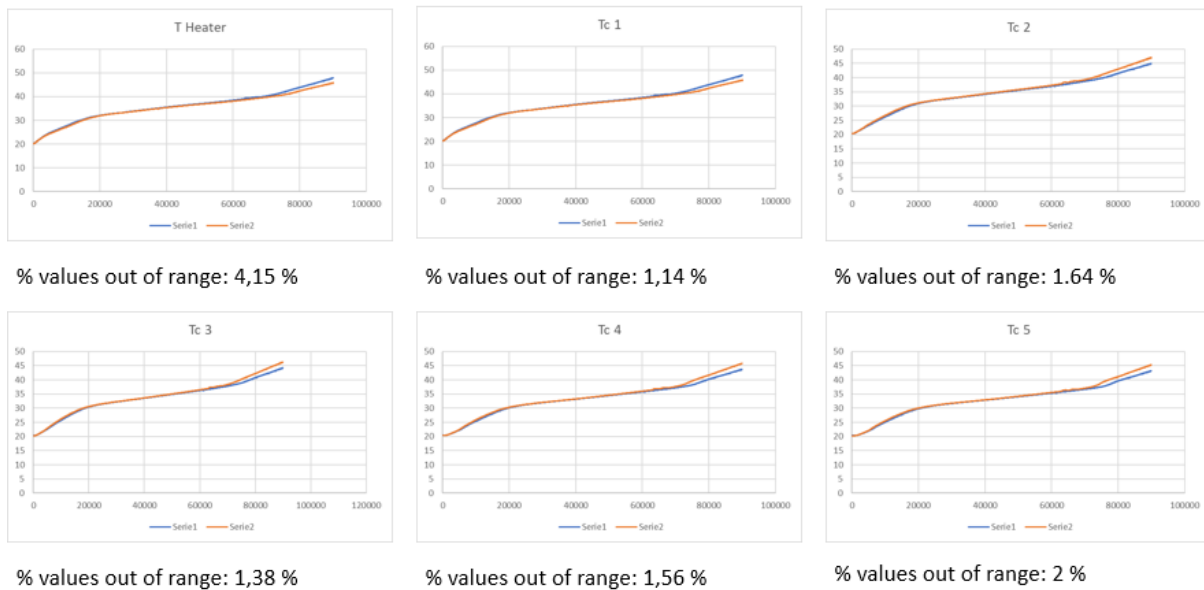
FIG. 168 RESULTS OF ΔT CALCULATED FOR ALL THE THERMOCOUPLES, COMPARISON BETWEEN TEST 14 AND TEST 15.

2.3.4 COMPARISON BETWEEN MELTING OF PURE AND METAL-FOAM-LOADED RT35 PCM

A comparison between the melting of pure PCM and copper-foam-loaded PCM is shown in Fig. 169 and Fig. 170. The difference in terms of melting time can be observed: with the addition of metal foams the PCM melts 8 hours earlier than in the cases of pure PCM. Another relevant aspect is the temperature of the heater which reaches temperatures 20° C lower than with pure PCM.

In Fig. 169 it is shown the typical temperature trend during the melting of pure RT35 PCM. The time needed to melt the whole PCM is 27 h. It is interesting to note the significant temperature difference among the TCs due to the low thermal conductivity of the PCM tested (0,2 W/m K).

In Fig. 170 it is reported the progress of the melting front in the case of copper-foam-loaded PCM (the copper foam chosen had a porosity of 94%) imposing the same heat flux used during the experiment with pure PCM (see Fig. 169).

It is evident how the presence of copper enhances the capability of PCM to transfer heat by internally conduction; the temperature difference among the 5 TCs is strongly reduced if compared with the case of pure PCM. In addition, a lower temperature is reached while the charging process. This is evident comparing the temperature recorded by the TC 1 placed immediately below the heater.

Metal-foams-loaded PCM can greatly enhance the thermal performance of these storage materials. Metal foams lead to an increase in the thermal conductivity of the composite PCM.
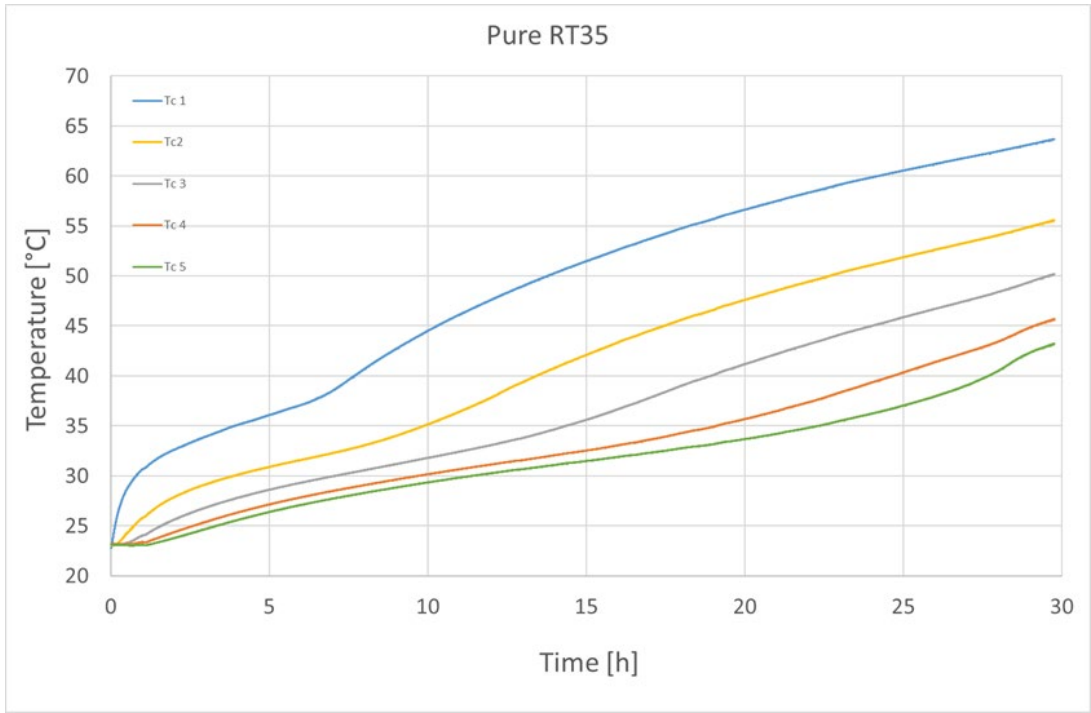
FIG. 169 PURE RT35 PCM HEATED WITH A FIXED HEAT FLUX ON THE TOP.
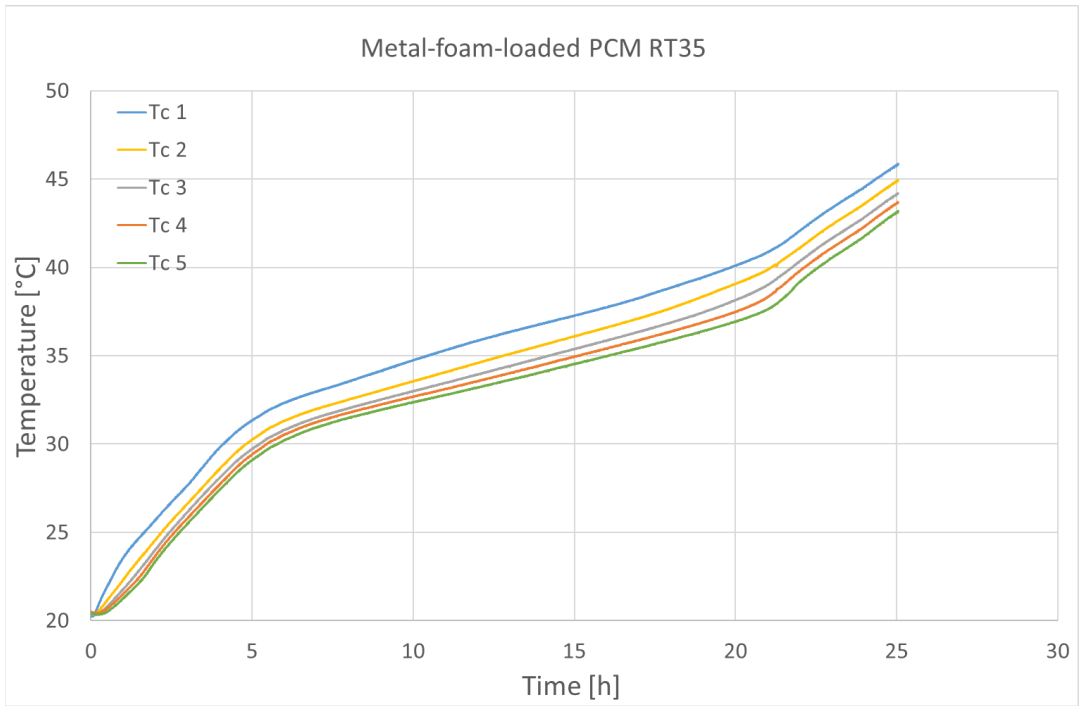
FIG. 170 COPPER-FOAM-LOADED RT35 PCM HEATED WITH A FIXED HEAT FLUX ON THE TOP.

2.3.5 COMPARISON WITH NUMERICAL SIMULATION RESULTS

Test 4, which appears to have the best insulation, was used to conduct a numerical simulation with COMSOL Multiphysics®. The trend of the experimental temperature and the calculated heat transfer coefficient were used as input data. The numerical simulation was firstly used to confirm the experimental data and later to validate the PCM properties.

2.3.5.1 NUMERICAL SIMULATION WITH MANUFACTURER DATA

The first numerical simulation was performed with the manufacturer input data. The comparison is illustrated in Fig. 171 in which the red curve represents the experimental data and the blue curve represents the simulation data. In this simulation a latent heat of fusion of 160 kJ/kg was used, although in the datasheet it is specified that this value is a combination of latent and sensible heat in a temperature range which goes from 26° C to 41° C. TC1, TC2, TC3, TC4, TC5 represent respectively the TCs named from top to bottom of the case. The first three experimental temperature trends recorded by TCs at the top result to be in good match with the simulation ones. The two TCs at the bottom do not show a good match with simulations, especially the temperature after the phase change which is much higher than the experimental one.
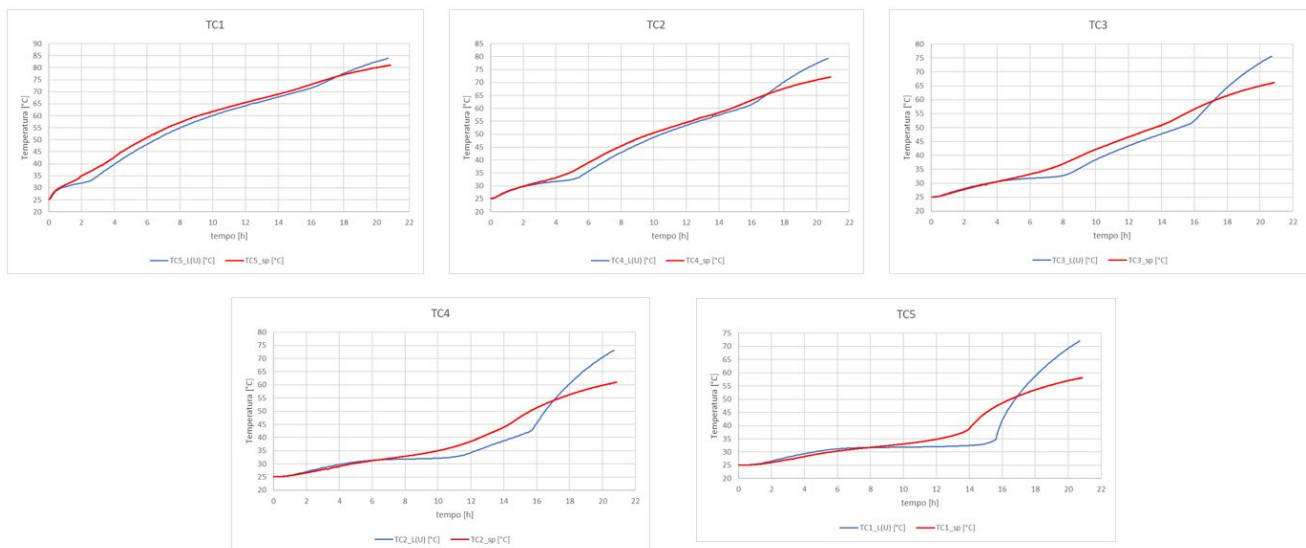
FIG. 171 COMPARISON BETWEEN EXPERIMENTAL RESULTS (RED CURVES) AND NUMERICAL ONES (BLUE CURVES).

2.3.5.2 Numerical simulation with manufacturer data, latent heat of fusion 120 kJ/kg

The first data that must be validated is the latent heat of fusion, which seems to be incorrect in the datasheet: it was decided to carry out a numerical simulation with a latent heat of fusion of 120 kJ/kg. A comparison between the experimental results and the numerical simulation is presented in Fig. 172. In this case it seems that the curves tend to get closer than before at the bottom of the case, but the numerical results still have a rapid increase in temperature after the phase change (after 14 hours).
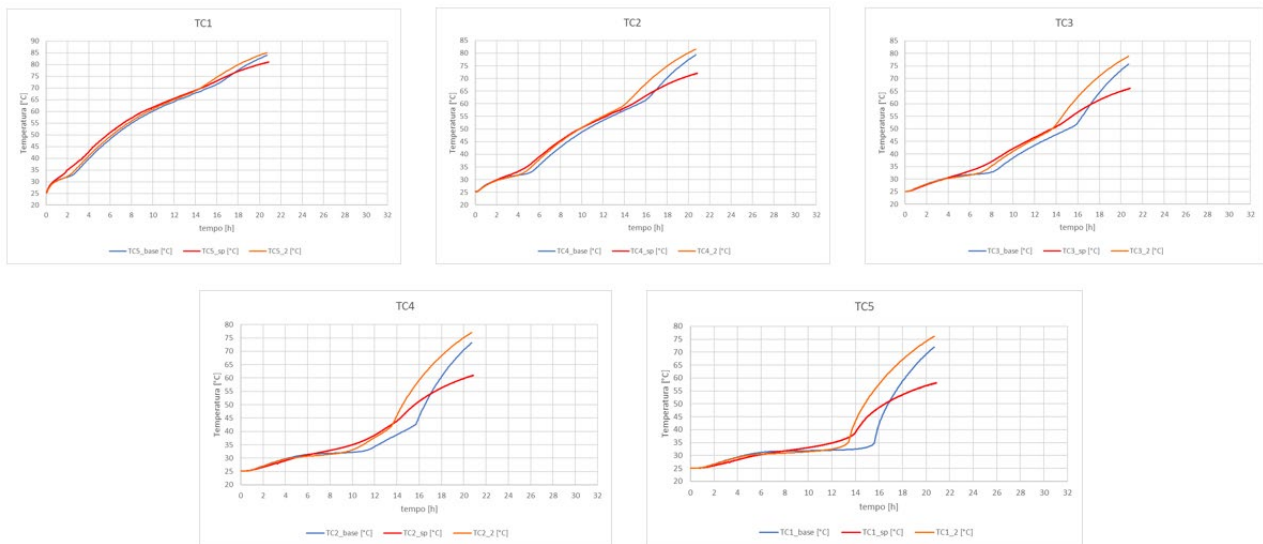
FIG. 172 COMPARISON BETWEEN THE EXPERIMENTAL RESULTS (RED CURVES) AND THE NUMERICAL ONES (ORANGE CURVES).

2.3.5.3 Numerical simulation with manufacturer data, latent heat of fusion 120 kJ/kg, melting point = 38° C, cp = 4 kJ/kg K

From the experimental data it has been realized that the actual phase change occurs at 38° C, while in the manufacturer datasheet it is declared 36° C. Furthermore, in the simulation, the rapid temperature increase after the phase change is very influenced by the variation of the heat capacity which, according to the datasheet, has an average value of 2 kJ/kg K. In reality, this value varies with the material phase. A last simulation was run using the previous latent heat value, a heat capacity of 4 kJ/kg K and a melting point value of 38° C. From the graphs in Fig. 173 it can be

seen how the new numerical simulations (green curves) are in agreement with the experimental results.
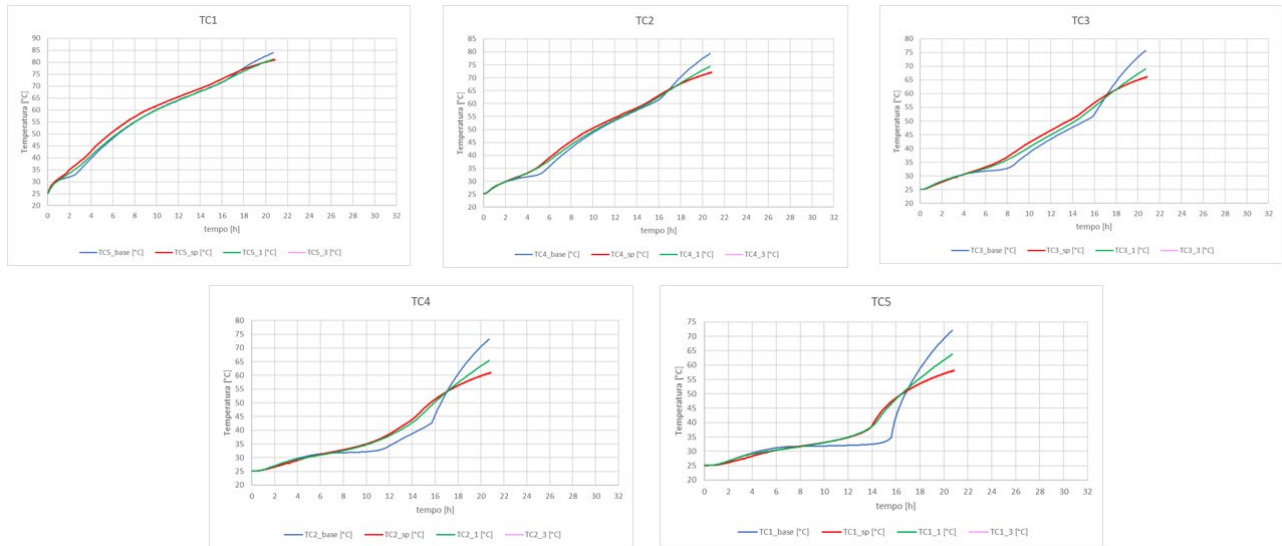
FIG. 173 COMPARISON BETWEEN THE EXPERIMENTAL RESULTS (RED CURVES) AND THE NUMERICAL ONES (GREEN CURVES).

These property changes, made thanks to the simulations, were necessary because in the manufacturer datasheet there were properties provided only for a narrow temperature range outside which there was not certainty about the physics behind the RT35 PCM. Another hypothesis of the non-optimal agreement between the numerical simulation and the experimental concerns with the boundary conditions which cannot be simulated well because the geometry of the insulation is not the same everywhere in the box, especially at the bottom part. Furthermore, the heat transfer coefficient calculated in the experiments was considered in the simulation as uniform for each wall of JIMMI. In reality, its value changes considering or not the the EUROBATEX ® layer (present on the base of JIMMI). Another reason for the non-optimal match with simulations, in particular considering TCs at the bottom, could be that the upper part of JIMMI is in contact with air, instead the lower part (its base) is supported by a plastic surface which could enhance the insulation of that wall. These observations will be surely useful for the next simulations that will be made by the University of Bologna.

CONCLUSIONS

The main conclusion of this thesis is that metal foams inserted inside the PCM can greatly enhance the thermal performance of these storage materials.

Metal foams lead to an increase in the thermal conductivity of the composite PCM. With JIMMI 1 it has been proved that it is reasonable to approximate the thermodynamics behind the tests to pure heat conduction experiments: during a complete charging (melting) and discharging (cooling) cycle of 65 hours, considering the maximum temperature differences between different thermocouples placed at the same heights, only 1,1% of the values are out of the acceptable range and the maximum temperature difference recorded is 2,4° C. The heat transfer coefficient has been calculated using the cooling curves and considering the lumped-parameter model: the global heat transfer coefficient of JIMMI 1 is estimated to be equal to U = 0,132 W/m^{2}K.

Starting from the case with no insulation (U = 2 W/m^{2}K) and passing through the partial insulated JIMMI 1 (U = 0,132 W/m^{2}K), with JIMMI 2 the global heat transfer coefficient improved up to 0,045 W/m^{2}K.

With JIMMI 3 the repeatability of the experiments was proved and a quantitative comparison between pure and metal-foam-loaded PCM was shown: with the addition of metal foams the PCM melting time is reduced by 8 hours. Another important aspect is that in presence of metal foams the heater works with a lower temperature (-20 K) with respect to the same tests made with pure PCM.

From the final comparison between experimental and simulations results, it can be seen that experimental curves are close to the numerical ones for almost any values of time except after the phase change happens. The reason is that the melting temperature range given by the datasheet (30÷36° C) is proved experimentally to be wrong since the melting range appeared to be 30÷39° C during the tests.

REFERENCES

[1] Thermal Energy storage using Phase Change Materials, fundamentals and applications, 2015, Amy S.Fleischer (1-93)

[2] Review on thermal energy storage with phase change materials and applications, 2007, Atul Sharma, V.V. Tyagi, C.R. Chen, D. Buddhi (318–345)

[3] Review of thermal energy storage for air conditioning systems, 2012 Abduljalil A. Al-Abidi, Sohif Bin Mat, K. Sopian, M.Y. Sulaiman, C.H. Lim, Abdulrahman Th (5802–5819)

[4] State-of-the-art for the use of phase-change materials in tanks coupled with heat pumps, 2017, Ángel Á. Pardin̄as, María Justo Alonso, Rubén Diz, Karoline Husevåg Kvalsvik, José Fernández-Seara (28–41)

[5] Heat and cold storage with PCM, An up to date introduction into basics and applications, 2008, Mehling Cabeza (1-305)

[6] Experimental Investigations on phase change material based thermal energy storage unit, 2013, M.J. Kabbara N.Ben Abdallah (694 – 701)

[7] Experimental and numerical investigation of the steady periodic solid–liquid phase-change heat transfer, 2002, G. Casano, S. Piva (4181–4190)

[8] Performance analysis of industrial PCM heat storage lab prototype, 2018, H.A. Zondag, R. de Boer, S.F. Smeding, J. Van der Kamp (402–413)

[9] Heat transfer enhancement in a latent heat storage system, 1999, R.Velraj,R.V.Seeniraj, B. Hafner. C. Faber, K. Schwarze (171-180)

[10] An experimental investigation of melting of RT44HC inside a horizontal rectangular test cell subject to uniform wall heat flux, 2019, Mohamed Fadl, Philip C. Eames (731–742)

[11] Thermal and fluid characteristics of a latent heat thermal energy storage unit, 2016, Xiaohu Yanga,b, Yang Lia, Zhao Luc, Lianying Zhanga, Qunli Zhangd, Liwen Jina (425 – 430)

[12] Experimental study on the thermal behavior of RT-35HC paraffin within copper and Iron-Nickel open cell foams: Energy storage for thermal management of electronics, 2020, Tauseef-ur-Rehman, Hafiz Muhammad Ali

[13] Termodinamica e trasmissione del calore, 2016, Yanus A. Cengel

[14] Air forced convection through metal foams: Experimental results and modeling Simone Mancin, Claudio Zilio, Andrea Diani, Luisa Rossetto

[15] Paraffin and paraffin/aluminum foam composite phase change material heat storage experimental study based on thermal management of LI-ion battery, 2015, Zichen Wang, Zhuqian Zhang, Li Jia, Lixin Yang (428-436)

[16] https://www.recemat.nl/specifications/

[17] https://www.arduino.cc/

[18] https://www.rubitherm.eu/

[19] https://www.electronics-tutorials.ws

[20] https://www.omega.com/en-us/resources/thermocouple-types

[21] https://www.britannica.com/

[22] https://www.ni.com/it-it.html

[23] https://platform.europeanmoocs.eu/